Zeitschrift: IABSE reports of the working commissions = Rapports des commissions de travail AIPC = IVBH Berichte der Arbeitskommissionen

Band: 34 (1981)

Rubrik: Session 3: Applications and experimental verifications

SESSION 3

June 4 th, 1981

Applications and Experimental Verifications

Applications et vérifications expérimentales

Anwendungsbeispiele und experimentelle Bestätigungen

Part 1
Morning Session

Chairman: **Prof. A.C. Scordelis, USA**

Introductory Reporters: **Prof. R.N. White, USA**
Prof. P. Gergely, USA
Applications and Experimental Verifications[1])

Part 2
Afternoon Session

Chairman: **Prof. Ir. B.W. van der Vlugt, The Netherlands**

Introductory Reporter: **Prof. Dr.-Ing. J. Eibl, F.R.G.**
Application and Experimental Verification of Advanced Mechanics in Reinforced Concrete[1])

[1]) Published in Introductory Report IABSE Colloquium, Delft 1981, Volume - Band 33

Leere Seite
Blank page
Page vide

Shear Failure of Beams: Experiments and Analysis

Rupture par effort tranchant de poutres: essais et analyse

Schubversagen von Balken: Versuch und Berechnung

A. VAN DEN BEUKEL
Research engineer
IBBC-TNO
Rijswijk, Holland

J. BLAAUWENDRAAD
Prof. dr. ir.
Rijkswaterstaat
Utrecht, Holland

P.J.G. MERKS
Research member
Rijkswaterstaat
Utrecht, Holland

TH. MONNIER
Senior Research engineer
IBBC-TNO
Rijswijk, Holland

SUMMARY
The results of experimental investigations into the ultimate strength of tunnels under combined action of bending and shear are used to verify the MICRO/1 program.
This program has been developed to analyze structures whose failure is strongly dominated by one or a few discrete cracks. The results of the analysis even enrich the insight which was gained by the experiments.

RÉSUMÉ
Les résultats de recherches expérimentales concernant la résistance à la rupture de tunnels soumis à l'action simultanée de flexion et de cisaillement sont utilisés pour vérifier le programme MICRO 1.
Ce programme a été développé pour l'analyse de structures dont la rupture est déterminée par quelques fissurres distinctes. Les résultats de l'analyse enrichissent d'ailleurs la compréhension du phénomène observé lors des essais en laboratoire.

ZUSAMMENFASSUNG
Die Ergebnisse von Traglastversuchen an Tunneln unter gleichzeitiger Wirkung von Biegung und Querkraft wurden zur Prüfung des Programms MICRO/1 benutzt. Dieses Programm wurde für die Berechnung von Konstruktionen entwickelt, deren Versagen sehr stark von Einzelrissen beeinflusst wird. Die Rechenergebnisse haben die Einsicht in das Verhalten beim Versuch sehr vergrössert.

1. INTRODUCTION

Reinforced concrete beams which fail in shear show at failure one or a few dominating cracks. Finite element programs using the concept of "smeared cracks" do not cover such types of problems in a proper way. The MICRO/1 program has been developed recently especially for such cases. At the same time Rijkswaterstaat, the Dutch State Public Works, and IBBC-TNO, the Institute TNO for Building Materials and Building Structures, co-operate in an investigation of the ultimate strength of tunnels for combinations of bending moment and shear force. This is a beam type problem for a uniformly distributed load. The first part of this paper reviews the experimental work of this study. The second part of the paper enters into the analysis of some of the tested beams and discusses the potentialities and results. It appears that the insight, which is gained from the experimental work, will get enriched by the detailed information of an analysis at a rather micro-level.

2. EXPERIMENTAL WORK

The experiments are part of a study on the shear-strength of reinforced concrete structures like tunnels, especially with the object to improve the design procedure. The load considered is uniformly distributed. Figure 2.1 being a picture of a tunnel-section on scale after testing, indicates one of the regions of special interest.

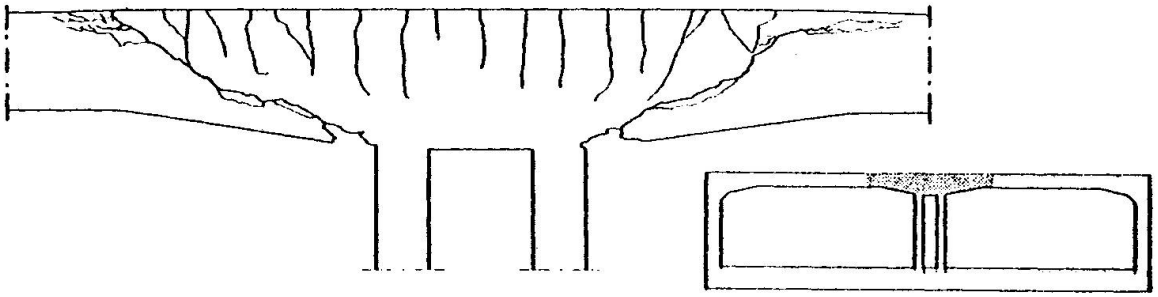

Fig. 2.1 Part of a tunnel-section after testing

The experimental investigation has rather a wide scope and concerns the influence on the shear-strength of reinforced concrete of:
- the ratio between moment and shear force;
- a low percentage of longitudinal reinforcement;
- varying depth of the structure;
- normal force;
- stirrup reinforcement.

An appropriate test-specimen has been developed for the experiments as shown in figure 2.2. In this set up of the tests a certain ratio between moment and shear force can be adjusted by choosing the right values for the sizes a, e and ℓ as indicated in figure 2.2. The test specimen were loaded uniformly distributed by means of hoses which were inflated by waterpressure. Loads, deformation and crack formation were recorded.

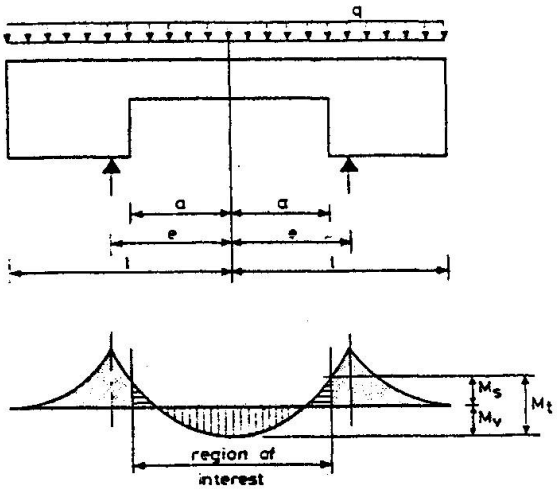

Fig. 2.2 Test-specimen

The decision on specific series of test-specimen was supported by the result of the study of data from literature. With that information an emperical formula has been developed for the shear strength as a function of the concrete strength f_c, the percentage of longitudinal reinforcement ω_o, the normal force N and the ratio between moment M and shear force T by means of the term $\frac{T\,h}{M}$ (h = effective depth of the cross-section).

Following literature, difference was made between diagonal tension failure (with shear T_1) and shear compression failure (with shear T_2), resulting in:

$$T_1 = \tau_1 . bh = (1 + 1.2\,\frac{T\,h}{M}) bh\,.\,f\{f_c,\ \omega_o,\ N\}$$

$$T_2 = \tau_2 . bh = \frac{T\,h}{M} . bh . g\{f_c,\ \omega_o,\ N\}$$

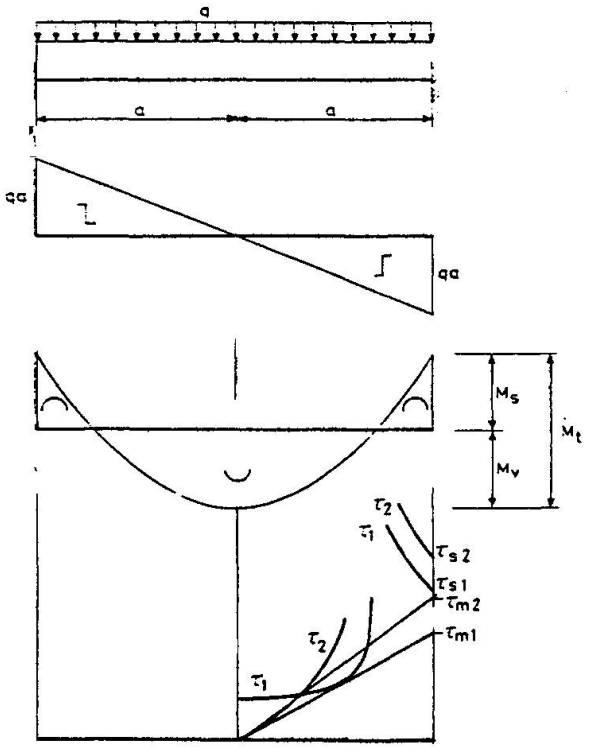

Fig. 2.3 Calculations of shear strength

Most of the experiments in literature are carried out with concentrated loads. In these cases the ratio $\frac{T\,h}{M}$ can be expressed in terms of sizes, the slenderness a/h in which a is the distance between the concentrated load and the nearest support.
By means of the formulas mentioned, the shear strength of an element can be evaluated as illustrated in figure 2.3.In this case τ_{m1} (the nominal shear stress), the extrapolation of the diagonal tension strength in the span determines the maximum shear force in the element at ultimate.
The series of test-specimen for the experimental investigation have been chosen in such a way that the area of practical interest would be covered.
As far as the study on the influence of the moment/shear force ratio is concerned, 3 series of test-specimen were designed:

serie A with a/h = 3
serie B a/h = 4,5
serie C a/h = 6

In each of the series 5 values of $\alpha = \frac{M_v}{M_t}$ have been investigated namely α = 0, 0.25, 0.50, 0.75 and 1.0. Those test-specimen had no stirrup-reinforcement, the percentage of longitudinal reinforcement amounts ω_o = 2%. Two of the results of those tests will be considered further here by means of calculations with the MICRO/1 program. It concerns the elements B2 and B4. The element B2 has a slenderness a/h = 4.5 and a moment distribution determined by α = 0.25. The shear strength near the clamped support governs the bearing capacity. Figure 2.4 shows the evaluation of the shear strength. The expected maximum shear force was T_u = 63.7 kN. Because a part of the uniformly distributed load will be carried down directly to the support, the line indicating T_2 at the support can be replaced over a certain distance x = 0.5 M_s/T_s as indicated in fig. 2.4 by a horizontal dotted line. The maximum shear force at ultimate in the test amounts 66.5 kN. After failure, this side of the element has been repaired and strengthened. At the other side of the element an ultimate maximum shear force of 78.4 kN was attainable. Failure occured after a gradual development of the crack pattern. At ultimate the concrete compression diagonal in the area of negative moments near the supports split suddenly.
The element B4 has a slenderness a/h = 4.5 and a moment-distribution determined by α = 0.75. The shear strength of this element in the region of the span governs the bearing capacity. Figure 2.5 shows the evaluation of the shear strength. The expected maximum shear force was T_u = 52.9 kN. The maximum shear force reached in the test was 52 kN. After failure on one side of the element this region has been repaired and strengthened and testing has been proceeded after that. The other side in this case showed the same strength giving a maximum shear force at ultimate of 52 kN. Failure occurred where that was expected; the mechanism appeared rather suddenly along a main crack more or less connecting cracks from lower load stages.

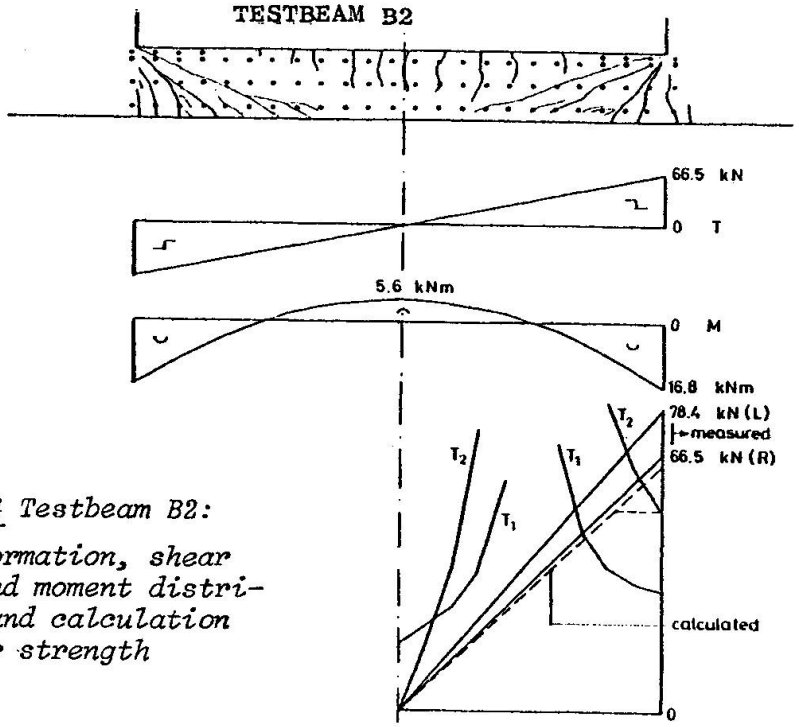

Fig. 2.4 Testbeam B2:
Crack-formation, shear force and moment distribution and calculation of shear strength

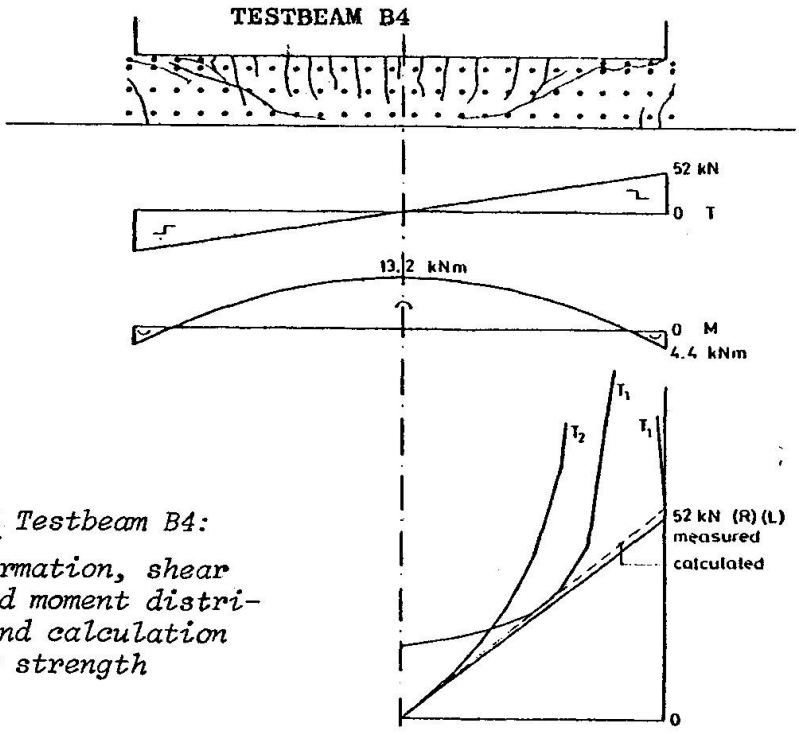

Fig. 2.5 Testbeam B4:
Crack-formation, shear force and moment distribution and calculation of shear strength

One of the conclusions from this study on shear strength is, that within the span of the member T_1 or T_2 is governing in accordance with prediction and shown. Near a clamped support a more favourable value T_2 is attainable in each case.

3. ANALYSIS

3.1. The MICRO/1 program

The program which is used for the analysis was developed in the frame-work of the Dutch joint research project 'Betonmechanica' [1]. The reader can find full details in HERON, 1981, nr. 1c by the authors H.J. Grootenboer, S.F.C.H. Leijten and J. Blaauwendraad. Here it is enough to recapitulate the following essential features:

- the program solves reinforced structures in plane stress.
- no 'smeared out' approach is used for cracking, but real discrete cracks can come into being and propagate, and may cross the element mesh irregularly.
- the aggregate interlock between the two faces of a crack is taken into account depending on the crack opening.
- bond and bondslip between concrete and reinforcement bars is taken into account. If a crack crosses a reinforcement bar, the discontinuous distribution of the bond stress is simulated.
- material data for concrete (crushing and cracking), reinforcement bond, aggregate interlock and dowel action account for nonlinearities, plasticity, hardening and softening, where applying.

The features listed here make this program particularly suited for the analysis of structures whose behaviour and failure is strongly influenced by one or a few dominating cracks. Beams which fail in shear typically belong to this category of problems.

3.2. Chosen beams and element mesh

The experimental investigations which have been discussed above, display a different type of failure in shear. Generally speaking two main types occur: the dominant crack at failure occurs somewhere along the span of the beam, or the dominant crack starts from the very end (the clamped end). In the latter case the crack is steeper than in the first case. The analysis reported here regards a simulation of each of the two main crack types. For this purposes the beams B2 and B4 have been selected (fig. 3.1) as described before. These beams have a similar slenderness but the ratio between the bending moment midspan and the total bending moment is different. The MICRO/1 program has been based on triangular elements for concrete and linear elements for the reinforcement bars. The modelling of the beams with aid of these elements is also shown in fig. 3.1, making use of symmetry. Supporting end blocks were added to the beam in order so to introduce the load, that the desired stress state in the beam will develop without disturbance. The analysis of beam B4 (ratio 0.75) had been started with the same mesh of beam B2 (ratio 0.25), but intermediate results of this analysis clearly indicated that the mesh should be refined in the compression zone at the clamped end, as is shown in the figure.

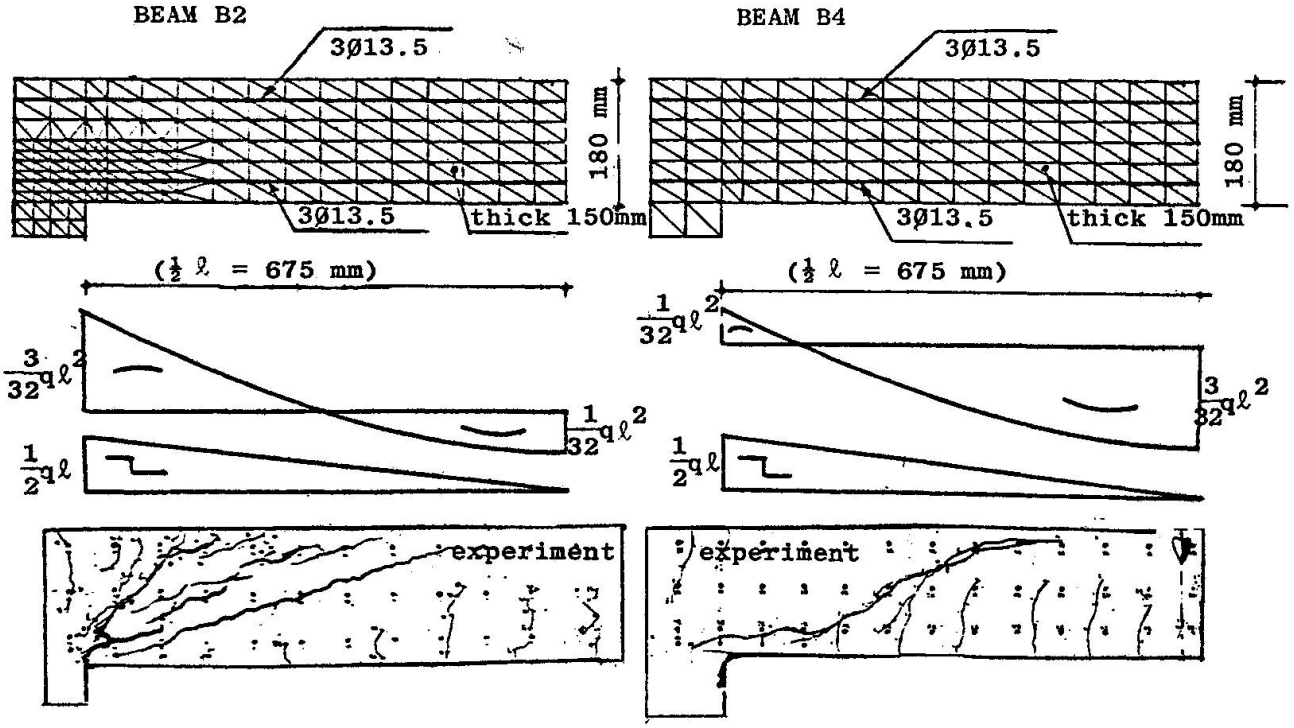

Fig. 3.1 Chosen beams and element mesh for verification of the MICRO/1 program

3.3. Material data

The material data listed in this section refer to the material models which have been presented in section 3.3 of [2].
Link's constitutive relations are used for the concrete, including crushing and cracking. The following data, taken from the relevant experiments, define the Link model and the cracking criterium:

Beam	E(N/mm^2)	f_c(N/mm^2)	f_{ct}(N/mm^2)
B2	27970	28.1	3.20
B4	27970	24.5	2.34

Aggregate interlock is accounted for in the following way. It is assumed that stresses normal to a crack will become zero, but shear stresses can occur in a crack. A rigid-plastic law is assumed for the relation between the shear stress τ and the parallel displacement of the two crack faces relative to each other $\Delta_{\parallel}$. The limit value τ_{max} in this rigid-plastic law is assumed to decrease for increasing crack opening $\Delta_{\perp}$ (dilatancy). The following relation is used (see [2]):

$$\tau_{max} = \frac{1}{k\,\Delta_{\perp}}$$

From earlier calculations it appeared that a good value for the coefficient k is:

k = 0.05 m/N

The reinforcement steel can be modelled as an ideal elasto-plastic material. The modulus of elasticity E_s and the yield strength f_y are:

$$E_s = 210\ 000\ N/mm^2$$

$$f_y = 415\ N/mm^2$$

The bond behaviour is modelled by a relation between the bond slip $\Delta_{||}$ and the bond stress τ. A linear relationship holds with stiffness G_b untill the bond stress reaches a limiting value f_b. A softening branch is defined using a factor k, see [2]. The following data yield from earlier comparisons:

$$G_b = 500\ N/mm^3$$

$$f_b = 5\ N/mm^2$$

$$k = 10\ mm^{-2}$$

The dowel action requires the specification of a relationship between normal stresses σ and a displacement $\Delta_{\perp}$ of the reinforcement bar relative to the concrete. An ideal elasto-plastic law is assumed, with a stiffness G_d and a limiting value f_d. The following data have been chosen:

$$G_d = 1\ N/mm^2$$

$$f_d = 20\ N/mm^2$$

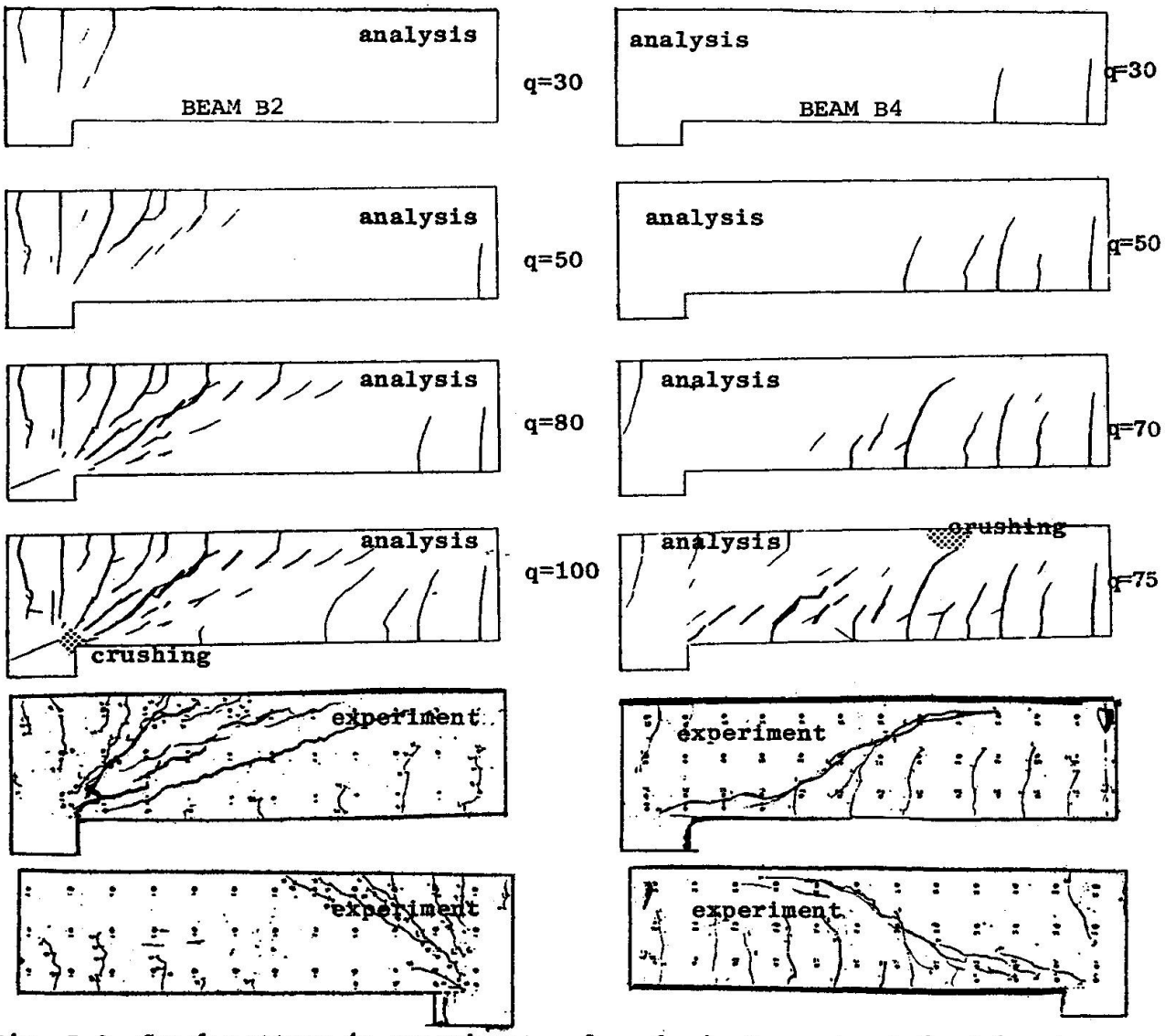

Fig. 3.2 Crack pattern in experiment and analysis for several load levels

3.4. Discussion of results

Crack pattern

The crack pattern for several load levels is shown in fig. 3.2. This figure is instructive as for the propagation of already existing cracks and the development of new ones. The thickness of lines in the analysis is a measure for the crack opening. It can be seen that initially all cracks start due to bending, but at higher load levels the cracks propagate or come into being under an inclination. Both beams start failing due to crushing in the compression zone. When we want compare the crack pattern in the analysis and the experiment, one should bear in mind that the final failure cracks spring up suddenly at the limit load level. For beam B2 these failure cracks accord pretty well with the crack pattern which had developed gradually during the loading process of the beam. In beam B4, however, a totally new crack comes into being in the very last second of the experiment which runs on top of all crack tips in the failure area. The MICRO/1 program is not able to calculate this very last crack phenomenon. Taking in account this fact, the agreement between the results of experiment and analysis is very satisfactory. We conclude: the two different patterns of cracking in beam B4 and beam B2, which showed up in the experiments, can be simulated by the MICRO/1 program.

Load-deflection curves

The agreement between experiment and analysis can be concluded also from the comparison of the load deflection curves in fig. 3.3. The displacement on the horizontal axis is the difference of the vertical displacement at midspan and at the support. In the experimental investigation this displacement was measured separately for the lefthand half of the span and for the righthand half of the span.

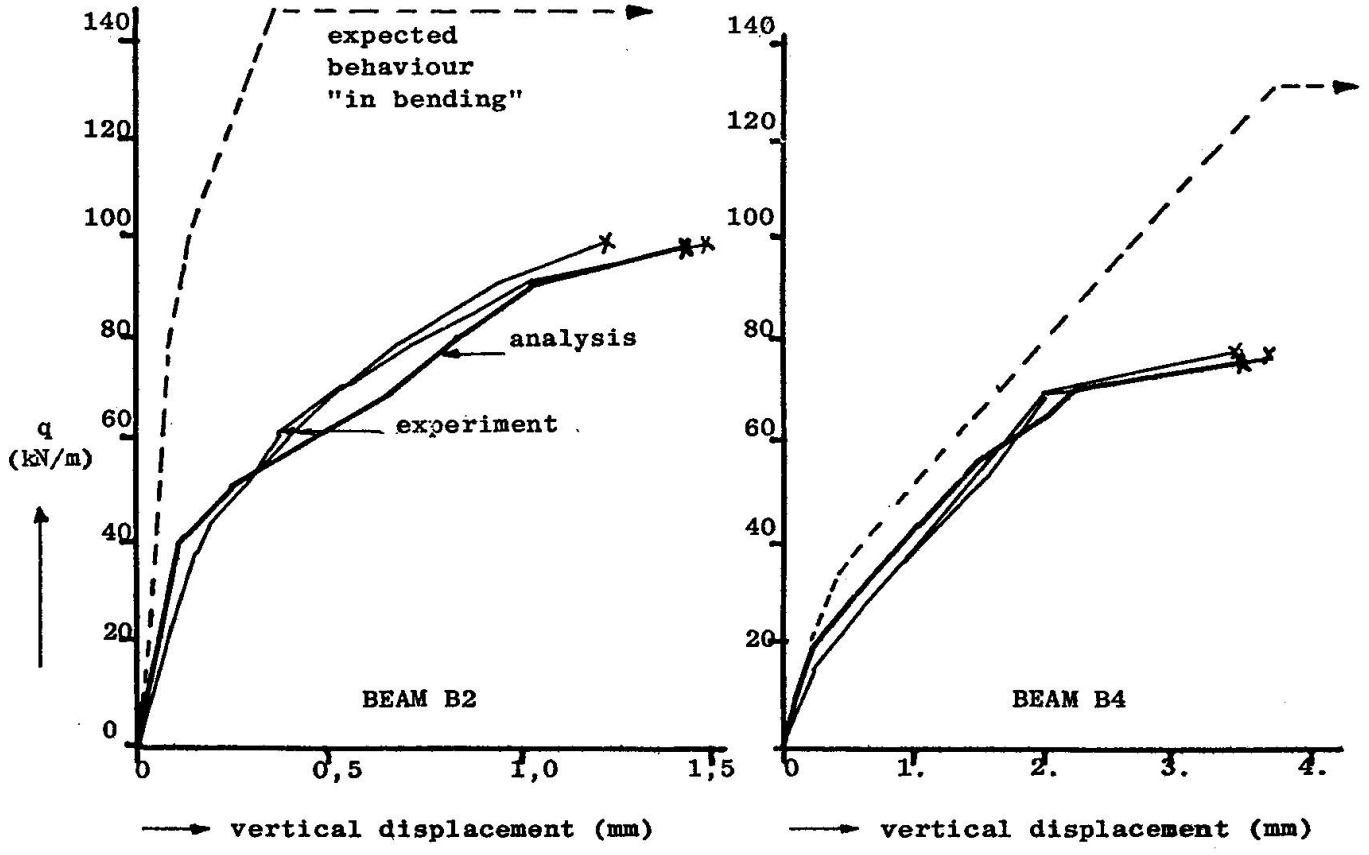

Fig. 3.3 Load deflection curves

The authors enjoyed the good agreement, especially for the ultimate value of the uniformly distributed load q in this figure. There is a noticeable difference between the behaviour of beam B2 and beam B4. The beam B2 shows a gradual decrease of stiffness during the loading process, whilest the beam B4 suddenly loses much stiffness in the last loading step. This difference also finds expression in the analysis. It can be explained with aid of the crack patterns of fig. 3.2. In beam B2 no new important cracks occur in the final loading stage between q = 80 kN/m and q = 100 kN/m, and the existing crack openings just grow something. In beam B4, however, a large number of new cracks develops in the final loading stage between q = 70 kN/m and q = 75 kN/m, one crack of which opens immediately very much. This explains the abrupt loss of stiffness.
The difference in behaviour of beam B2 and beam B4 appears once more when we compare the found load-deflection curves with the curve which is to be expected for the same beam in case sufficient web reinforcement was used to have the beam fail in bending. These curves have been calculated by the STANIL/1 program, which is described in [2] as well. Beam B4 behaves "in bending" and fails abruptly due to insufficient shear capacity. Beam B2 deviates from the "in bending" behaviour as soon as cracking starts occurring.

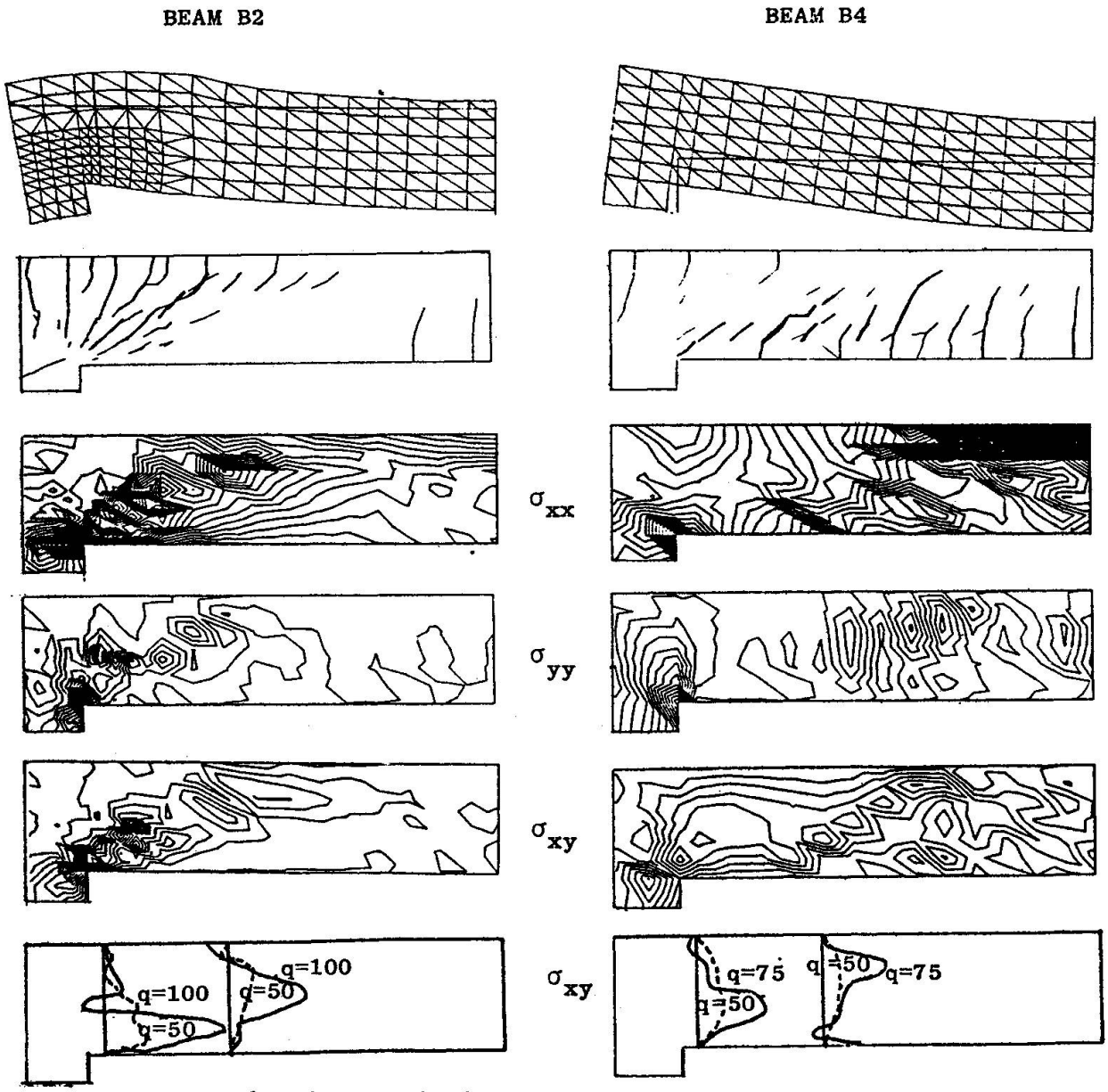

Fig. 3.4 Stress results from analysis

Stresses

In fig. 3.4 we show results for the stresses, together with the crack pattern and the deformed shape at the ultimate load. The stress plots are lines of constant value. Black areas occur for large gradients, which indicates stress concentrations. Such plots provide a quick view at the most interesting points. By hand we made a plot of the distribution of the shear stress at some interesting cross-sections which are self-explonatory in respect of the crack patterns. The stress in the reinforcement bars are plotted in fig. 3.5. The differences between the experimental results and the analysis results have been marked by a shaded area.

In both beams the point of zero stress value coincides for lower load levels with the position where the moment is zero. For higher loads this does not hold any longer, due to truss forming in the beam, which yields an increase of the reinforcement stress.

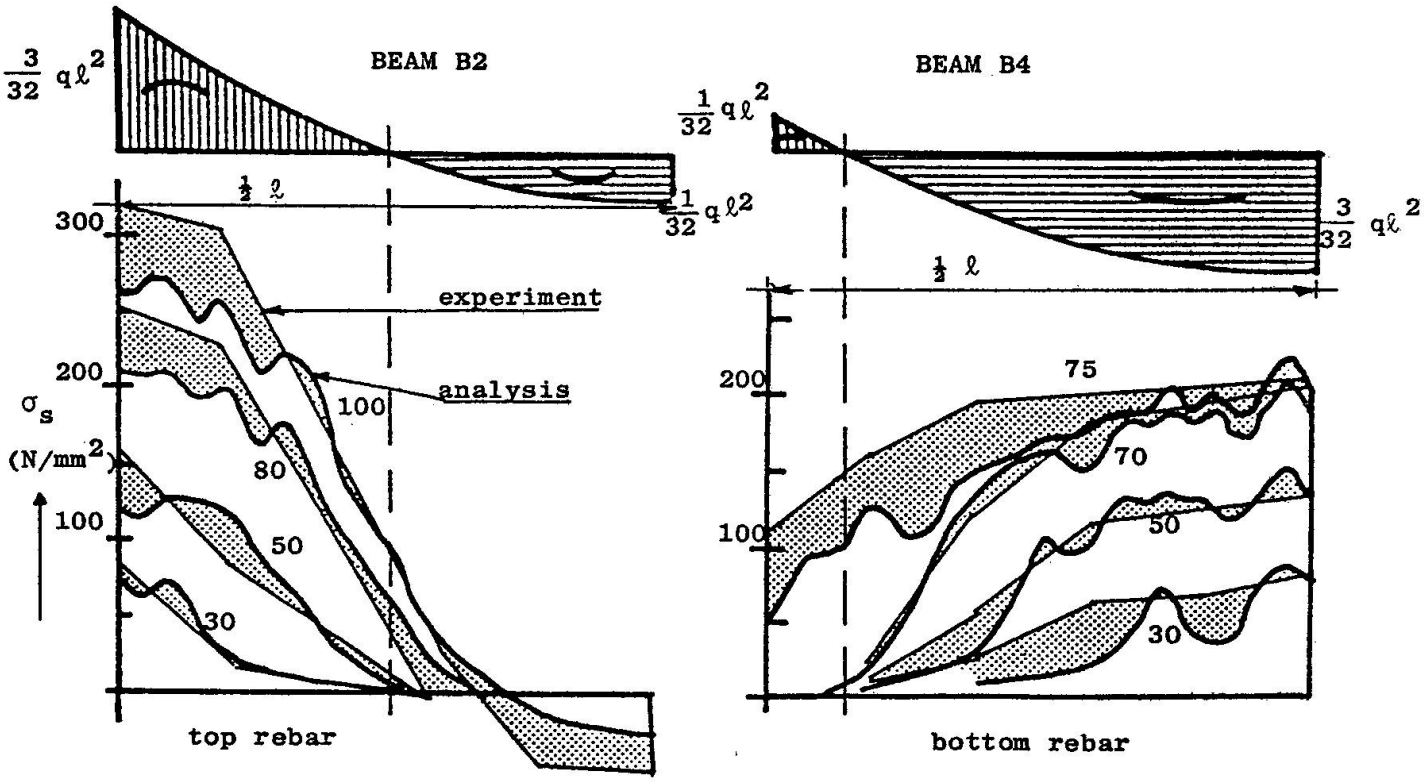

Fig. 3.5 Stresses in reinforcement bars for several load levels

4. CONCLUSION

The analysis of reinforced concrete beams without web reinforcement charged by uniformly distributed load yields results which are in close agreement with test results. The MICRO/1 program, handling discrete cracks, is capable of handling different types of shear failure in an appropriate way. If used complementary to experiments the analysis results will help understand the complete behaviour of the structure.

ACKNOWLEDGEMENT

The researchproject on shear capacity is jointly financed by Rijkswaterstaat and TNO-IBBC. The authors gratefully acknowledge the help and consult of ir. P. Kieft of Rijkswaterstaat, Department of Locks and Weirs, and of prof.Dr.Ing. H.W. Reinhardt and dr.ir. J.C. Walraven of Delft University of Technology, Department of Civil Engineering, in defining the research and in interpreting the results.

REFERENCES

1. Survey and Workplan of the joint project Betonmechanica, CUR-VB, 1977 Zoetermeer, The Netherlands.

2. GROOTENBOER, H.J.; LEIJTEN, S.F.C.H.; BLAAUWENDRAAD, J.: Concrete Mechanics; Numerical models for reinforced concrete structures in plane stress. Heron, 1980, no. 1c.

Plastic Rotations by Local Stress Analysis

Rotations plastiques etudiées par analyse locale

Lokale Berechnung von Fliessgelenken

ESTER CANTÙ
Researcher
University of Pavia
Pavia, Italy

GIORGIO MACCHI
Professor of Structural Engineering
University of Pavia
Pavia, Italy

SUMMARY
A local finite element analysis applied to the zone between two adjacent cracks can provide information about the extension of the zone of concrete in which limit conditions are reached in a triaxial state of stress. Such results can help in the definition of the "plastic length" and can therefore suggest a model for the localized plastic rotations.

RÉSUMÉ
Un calcul local aux éléments finis appliqué à la zone entre deux fissures adjacentes peut donner des informations sur l'extension de la zone de béton qui peut atteindre des conditions-limites en régime triaxial. De tels résultats peuvent être utiles dans la définition de la "longueur plastique" et suggérer un modèle pour les rotations plastiques localisées.

ZUSAMMENFASSUNG
Mit Hilfe einer Finite-Elemente-Berechnung der Zone zwischen zwei benachbarten Rissen können Erkenntnisse gewonnen werden über die Ausdehnung des Bereiches, in welchem der dreiachsige Spannungszustand des Betons den Erschöpfungszustand erreicht. Die Ergebnisse können für die Definition einer "plastischen Länge" in einem Berechnungsmodell mit örtlich konzentrierten plastischen Rotationen verwendet werden.

This research has been supported by grants from the Italian National Research Council (C.N.R.).

1. INTRODUCTION

Several cases of behaviour of r.c. structural members in the cracked stage have been successfully studied by means of finite element techniques. Most applications, nevertheless, concern cases in which the process of crack formation is studied |14| or the overall effect of cracking on the field of deformations or forces is considered |7| : the cracks are therefore considered to intervene at the edges of the elements or to be spread on the element itself.

A minor number of applications concerns the study of the stress field modifications caused in proximity of cracks by the presence of the cracks themselves; such studies require meshes having an higher degree of refinement, and their aim is limited to small areas, so that we can speak of a sort of a local analysis in comparison with the overall analysis of the structure.

The present paper aims to suggest the use of such local analyses by finite elements in the study of the rotation capacity of r.c. monodimensional members. This can be surprising: in fact, the research on the plastic rotations of flexural members has been basically performed on an experimental basis in the 60ies (under the urgent need of ductility conditions and of rotation values for non-linear analysis of frames); therefore, the results are very roughly expressed in simple empirical formulae, or based on a not well defined concept of "plastic length". But the authors treating the problem suggested since that time |1||10| · |4| that the phenomenon could find a satisfactory model only by a refined local analysis of the stress field near the cracks: the suggestion arose by the evidence of a concentrated nature of the local rotation, and by the belief that the formation of horizontal cracks may play an essential role in flexural failure |3|.

2. POSITION OF THE PROBLEM

Monodimensional flexural members can develop considerable plastic rotations θ_{pl} at the ultimate limit state. There are two ways of taking advantage of this property in current practice:

- by a nonlinear analysis of the structure;
- by taking account of the redistribution capacity that a ductile structure can develop, even if designed according to the usual linear assumptions.

An intensive experimental research provided safe values of the rotation capacity in function of several programmatas |1||2||4||5||6||9||11||12||23|, and empirical

formulations of permissible values for θ_{pl} in function of the relative depth x/d of the compression zone were introduced in design Codes. For CEB Code the empirical curve of Fig.10 has been proposed |11|, and consequently the ductility condition for a degree δ of moment redistribution was formulated |11| in the following way:

$$\delta \geq 0.44 + 1.25 \frac{x}{d} \quad ; \quad 0.75 \leq \delta \leq 1.00$$

Several efforts were done in order to derive the plastic rotation by integration of curvatures, but the tests showed that it was caused by a concentrated rupture mechanism .

A whish of consistency with the assumptions made for the analysis of the section led to assume the conventional ultimate strain of concrete ε_{cu} as extended on a "plastic length" L_p; but the plastic length appeared soon to be another conventional concept, and the tentatives of its rational derivation involved the assumption of variable values for ε_{cu} |1|.
On the other hand, many researchers agreed on two important observations:
- the measured strains on concrete were frequently considerably higher than the values of ε_{cu} which were standardized through prism tests;
- the concrete failure appeared often in the ways schematically shown in Fig.1, with formation of horizontal or inclined cracks, so that vertical or inclined tensile stresses seemed to play an essential role.

The present work is the beginning of a study intended to a better understanding of the phenomenon, taking into consideration the above experimental observations and the progress achieved in the meantime in the failure criteria in triaxial state of stress.

Preliminary studies done by Broms |3| and by the authors showed that (even in pure bending) the deviation of the neutral axis between adjacent cracks can cause sufficient tensile stresses in the zone of longitudinal compression to cause horizontal or inclined cracks.

The study is therefore performed along the following lines:
i) determination of the local state of stress in the region between two adjacent flexural cracks and particularly of the field of tensile stresses;
ii) determination of the region in which the failure is reached according to the triaxial criterion, and its interpretation as a physical plastic length;

iii) study of the variation of the plastic length as a function of the depth of the compression zone.

As a triaxial failure criterion, the formulation due to Ottosen |15||16| has been adopted: it is stated as

$$f\ (I_1,\ J_2,\ J) = 0$$

where I_1, J_2 and J are expressed in function of the principal stresses and of the principal stress deviators.

3. LOCAL STRESS ANALYSIS

The problem of determining the stress state is three-dimensional.
The element of a rectangular flexural member was studied by means of a plane finite element model. The beam element is represented through a slice of member of unit thickness, taking proper account of the contribution of concrete and steel areas.
Two-dimensional rectangular finite elements were used and the model was studied in plane strain conditions, with the aim of considering the confinement due to the three-dimensional behavior and to the transversal reinforcement.

The F.E. mesh (fig.2) represents a part of the beam between two cracks.
The element of flexural member, subject to simple bending, was studied in conditions close to the ultimate state; the mesh includes a predetermined crack of a given height.

A non linear constitutive law has been assumed for concrete according to Fig.3; the uniaxial nature of this law (not consistent with the triaxial assumptions) will require in the future a check of its influence on the results.

The reinforcement was represented by truss elements. The bond linkage was performed by using suitable spring elements with non-linear bond-slip relationship (Fig.4), according to |7| and |8| .

Five cases, characterized by different steel area, and therefore by different crack heights were studied in order to evaluate the influence of the crack height on the plastic length.

4. RESULTS

The case with $x/d = 0.56$ is described in detail.
Fig. 5 shows the distribution of longitudinal stresses σ_y and of the transversal stresses σ_z in six cross sections in proximity to the flexural crack. The fluctuation of the neutral axis depth along the beam is clearly shown, and therefore the cause of the considerable values of the transveral tensile stress σ_z.

The law of variation of the longitudinal stress in the reinforcing steel is shown in Fig.6, and Fig.7 gives the longitudinal distribution of the bond stress at the interface between concrete and reinforcement.

The blackened zone in Fig.8 is formed by the elements where the centroidal stress state causes failure according to the triaxial criterion; in this localization the transversal tensile stress and the invariants of the stress deviator play an essential role.

Similar results are obtained (Fig.9) in the other four cases, within the range of x/d from 0.12 to 0.56, covering most of the possible cases in pure bending. The location of the critical elements and the main cause of failure (the transversal tensile stress, and therefore the formation of horizontal cracks) seems to be in good agreement with the observed failure patterns of Fig.1.

From the comparison of various cases in Fig.9 the critical zone (considered as an effective plastic length) appears essentially constant: this could be hardly accepted when reasoning in terms of diffusion, and therefore expecting wider plastic lengths for higher x values. Nevertheless, a constant plastic length might lead to a satisfatory relationship between $\frac{L_p}{x}$ and the ratio $\frac{x}{d}$, if compared with the experimental results and the current empirical laws (Fig.10).

Caution must be used in interpreting the results of these exercises, only presented here with the aim of indicating a possible approach to the problem.

The study should be extended to cases with closer flexural cracks and with a shear action, situations in which the described phenomena should be emphasized. On the contrary, it has been checked that a linear constitutive law for concrete does not sensibly affect the amplitude of the critical zone.

The effect of different assumptions on the concrete confinement should be examined.

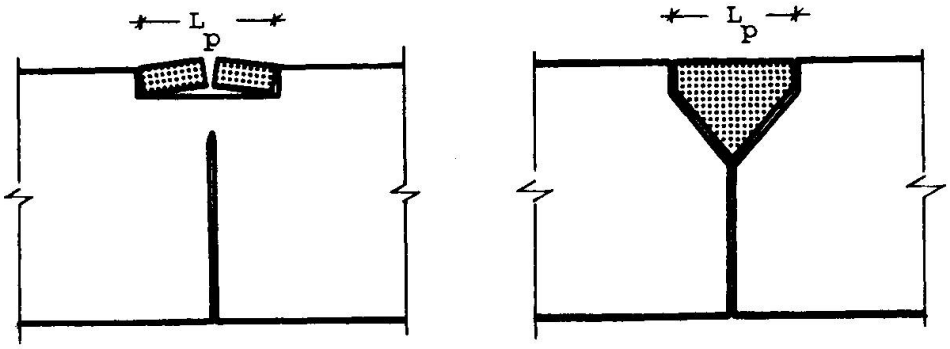

Fig. 1 - Typical failure patterns for different crack spacings.

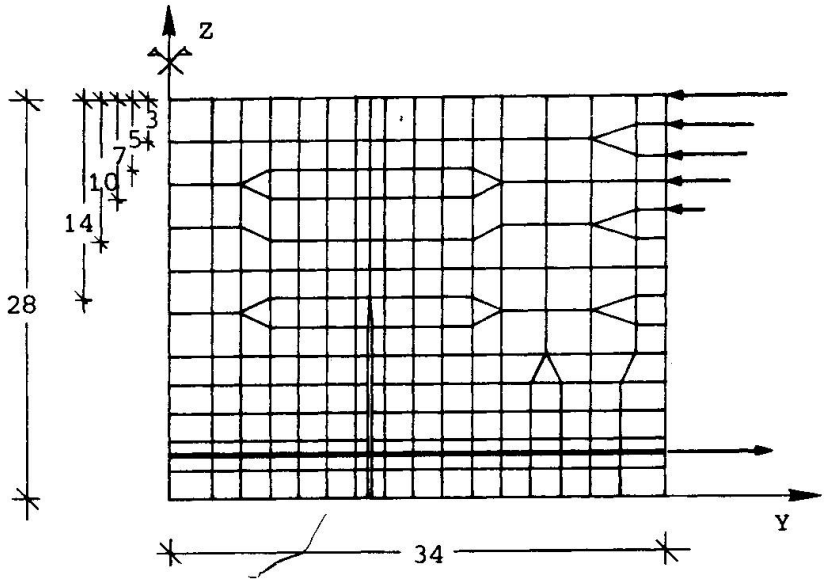

Fig. 2 - F.E. mesh for the five cases with different crack heights

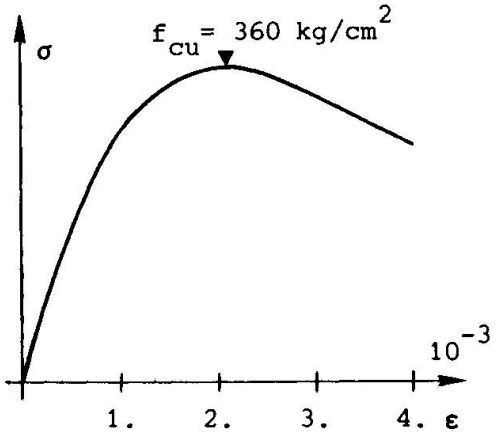

Fig. 3 - Assumed uniaxial stress-strain relationship for concrete

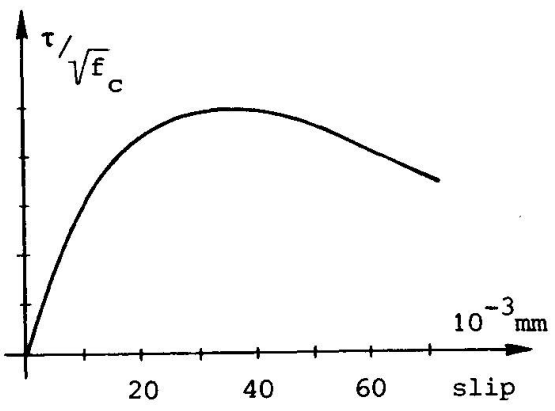

Fig. 4 - Assumed bond-slip relationship

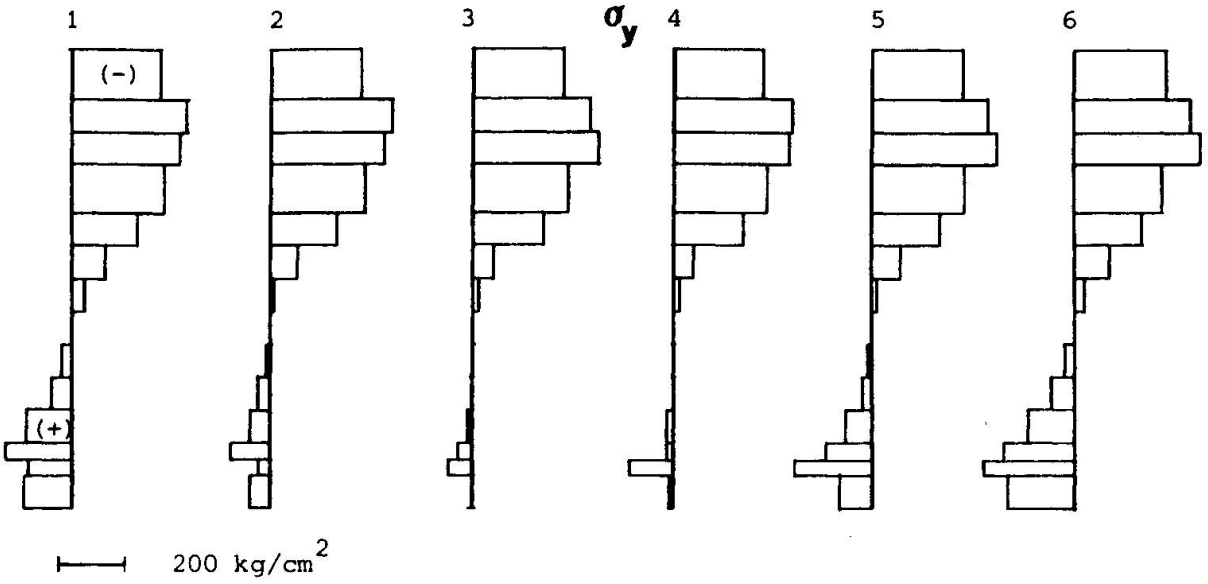

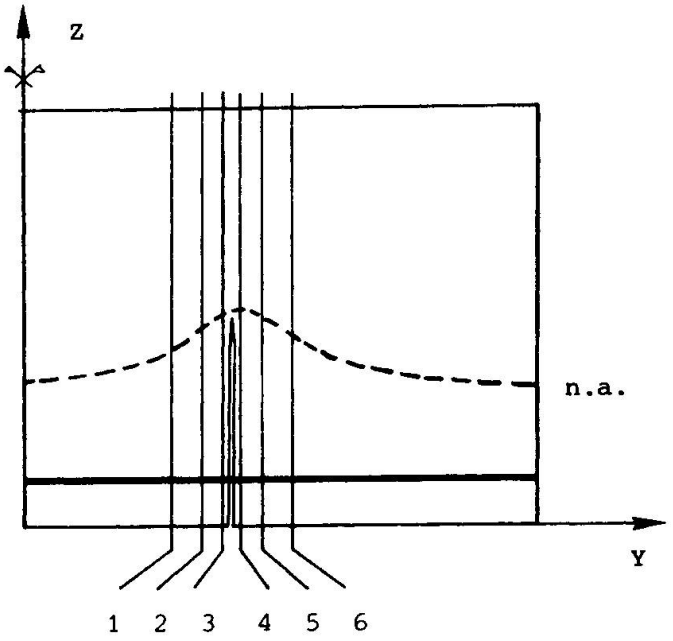

Fig. 5 - Longitudinal and transversal stress distributions close to the cracked section (case x/d = 0.56)

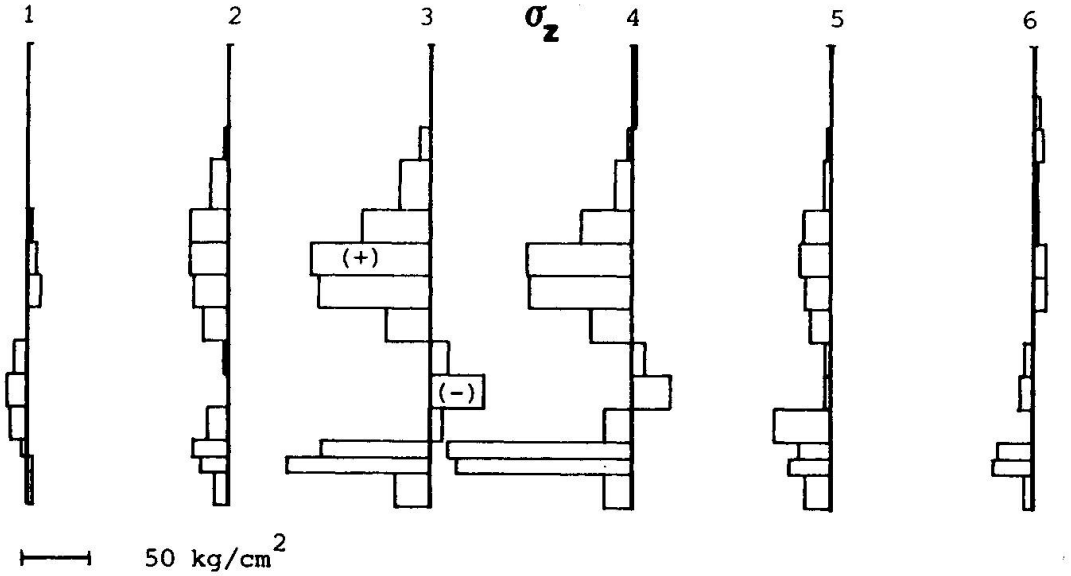

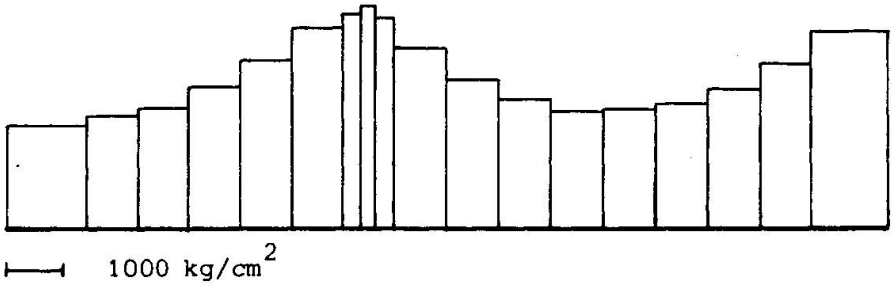

Fig. 6 - Longitudinal stresses along the reinforcement (case x/d = 0.56)

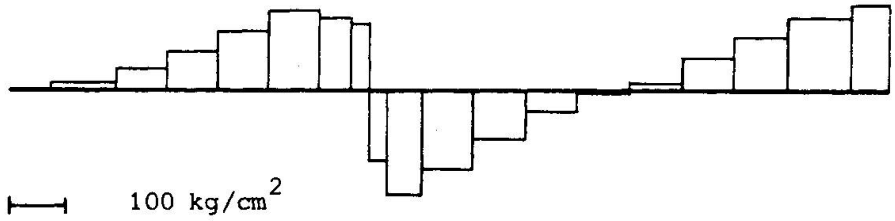

Fig. 7 - Bond stresses at the interface between concrete and steel (case x/d=0.56)

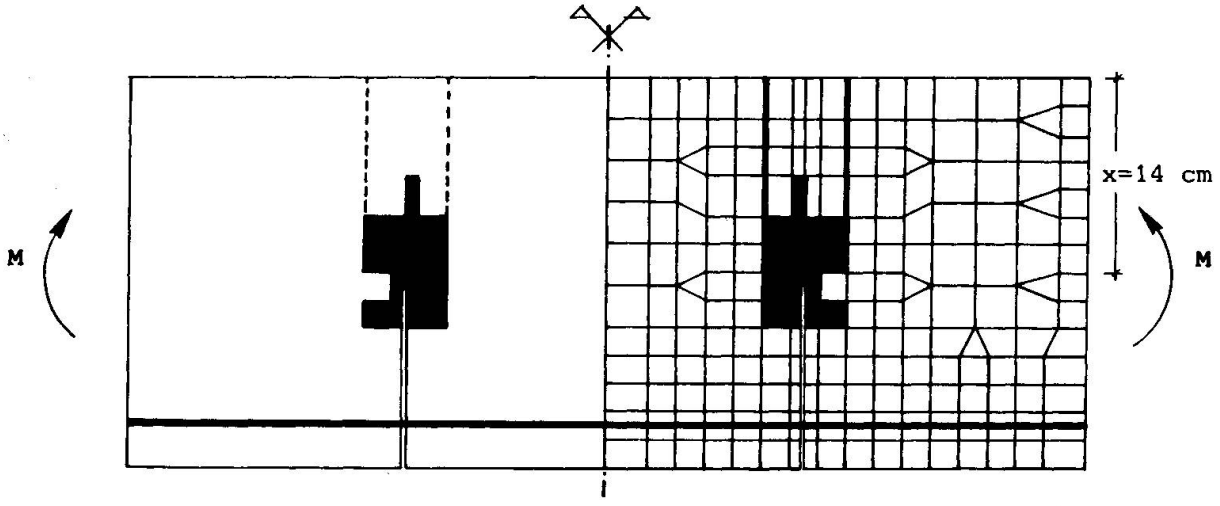

Fig. 8 - Failure zone found by applying the triaxial failure criterion (case x/d = 0.56)

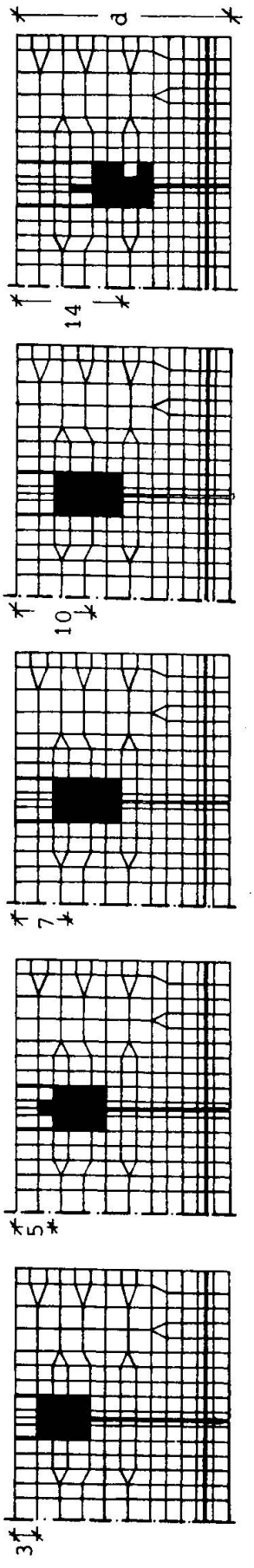

Fig. 9 - Failure zones for the five cases (x/d = 0.12; 0.20; 0.28; 0.40; 0.56)

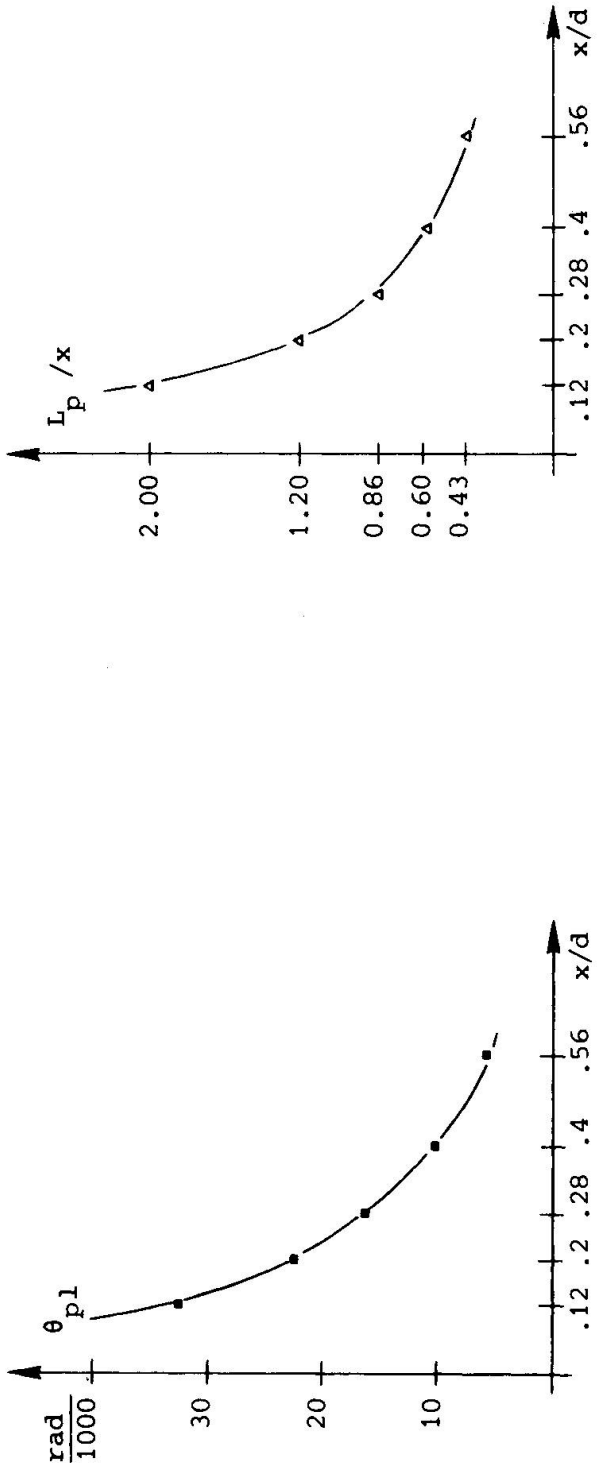

Fig. 10 a) - Plastic rotations versus x/d (empirical relationship)

Fig. 10 b) - $\frac{L_p}{x}$ ratio vs x/d (from finite element analysis)

REFERENCES

1. BAKER A.L.L., AMARAKONE A.M.N.: Inelastic Hyperstatic Frames Analysis, Proc. of the International Symposium, Miami, FLA, Nov. 10-12, 1964
2. MATTOCK A.H.: Rotational Capacity of Hinging Regions in Reinforced Concrete Beams - Ibidem
3. BROMS B.B.: Stress Distribution, Crack Patterns and Failure Mechanisms of Reinforced Concrete Members, ACI Journal, Dec. 1964
4. MALDAGUE J.C.: Contribution a l'étude des déformations instantanées des poutres en béton armé, Annales ITBTP, Sept. 1965
5. CORLEY W.G.: Rotational Capacity of Reinforced Concrete Beams, ASCE Journal, Oct. 1966
6. DILGER W.: Veränderlichkeit der Biege-und Schubfestigkeit bei Stahlbetontragwerken und ihr Einfluss auf Schnittkraftverteilung und Traglast bei Statich unbestimmter Lagerung, Deutscher Ausschuss für Stahlbeton, Heft 179, 1966
7. NGO D., SCORDELIS A.C.: Finite Elements Analysis of Reinforced Beams, ACI Journal, March 1967
8. NILSON A.H.: Non-Linear Analysis of Reinforced Concrete by the Finite Element Method, ACI Journal, Sept. 1968
9. BACHMANN H.: Influence of Shear and Bond on Rotational Capacity of Reinforced Concrete Beams, ETH, Zurich 1969
10. MACCHI G.: Limit-State Design of Statically Indeterminate Structures Composed of Linear Members, Corso di Perfezionamento, Politecnico di Milano, 1969
11. MACCHI G.: Ductility Condition for Simplified Design without Check of Compatibility, CEB, Commission XI, Oct. 1974, Innsbruck, CEB Bulletin n. 105
12. LENKEI P.: Local and Overall Specific Inelastic Rotation Capacities in Reinforced Concrete Beams, Acta Technica Academiae Scientiarum Hungaricae 79,1974
13. SIVIERO E.: Rotation Capacity of Monodimensional Members in Structural Concrete, CEB Bulletin n. 105, Feb. 1976
14. CEDOLIN L., DEI POLI S.: Finite Element Non-Linear Plane Stress Analysis of Reinforced Concrete, Studi e Rendiconti del Corso di Perfezionamento, Politecnico di Milano, 1976
15. OTTOSEN N.S.: A Failure Criterion for Concrete, Journal of the Mech. Division ASCE, August 1977
16. DEI POLI S.: Costruzioni in Cemento Armato, Politecnico di Milano 1978

Design of Reinforced Concrete Based on Mechanics

Calcul du béton armé basé sur la mécanique

Stahlbetonbemessung nach den Regeln der Mechanik

B. ERNANI DIAZ
Promon Engenharia S.A.
Rio de Janeiro, Brazil

MAURO SCHULZ
Federal University of Rio de Janeiro

SUMMARY

Design procedures for linear reinforced concrete members based on the principles of structural mechanics are presented. The general equations of the state of stress of a cracked reinforced concrete element and their solution at the cross section are given. Practical procedures and the consequences in usual design work are discussed. The section can be of general shape with a single symmetry axis. Axial force, bending moment and shear force can act on the concrete section. Numerical examples are presented and discussed.

RÉSUMÉ

Procédés pour le calcul des éléments linéaires en béton armé basés sur les principes de la mécanique technique sont presentés. Les équations générales de l'état de tensions d'un élément en béton armé fissuré sont données. Procédés pratiques et leurs conséquences dans le travail habituel de projet sont discutés. La section transversale peut avoir une forme géométrique quelconque avec un axe de symétrie. Force normale, moment fléchissant et effort tranchant peuvent exister dans la section transversale. Exemples numériques sont présentés et discutés.

ZUSAMMENFASSUNG

Gezeigt werden Bemessungsverfahren für Stahlbetonbauteile auf der Grundlage der technischen Mechanik. Die allgemeinen Gleichungen des Spannungszustandes in einem gerissenen Stahlbetonbauteil werden aufgestellt und die Lösung für einen Querschnitt angegeben. Die praktische Anwendung und die Konsequenzen für die Bemessung werden diskutiert. Die Form der Querschnitte ist beliebig, aber mit einer Symmetrieachse. Normalfräfte, Biegemomente und Querkräfte werden berücksichtigt. Rechenbeispiele werden gezeigt und diskutiert.

1. INTRODUCTION

Due to the possibility of the determination of stresses and strains of reinforced concrete members with the help of computers, taking into account many realistic features of the structural behaviour of reinforced concrete, it is possible nowadays to predict with good accuracy the load history of a reinforced concrete member. However,these calculations require a large amount of computer time and therefore they are not adequate to be applied in the everyday design work.To overcome these economic difficulties,a practical approach for design of reinforced concrete members will be presented herein. These design rules will be based on logical principles of the structural mechanics and at the same time they will demand small computer effort.

The criteria are based on the general equations of a cracked reinforced concrete element ,however considering neither dowell nor aggregate interlock action between the cracks. The consideration of the load history is not taken into account in the development of the equations.

The procedures are valid essentially for linear reinforced concrete members presenting a single symmetry axis. No restrictions are made to the shape of the concrete section and the reinforcement distribution along the section.

It shall be shown that some classic considerations of reinforced concrete design are not consistent with the usual longitudinal design of reinforced concrete members, such as the use of the lever arm of the internal forces in the calculation of the shear stresses,as well as the staggering rule of the tensile reinforcement.

In this paper the variation of the longitudinal reinforcement in the direction of the longitudinal member axis is not considered. The reason for doing that was to simplify the equations of the problem, presenting them in a shorter form.However,for practical problems,this variation of the reinforcement does exist and must be taken into ac unt (see DIAZ [2]).

The method of analyis presented handles the effects of the bending moment,axial force and shear force at the same time. Thus a full interaction of these effects is considered,requiring that the design in the longitudinal and transversal directions be made concurrently.

2. THE MATHEMATICAL MODEL FOR THE ANALYSIS

The structural member which will be investigated is a linear reinforced concrete member with a constant cross section presenting a single symmetry axis. A x-axis is defined along the longitudinal member axis. The cross section is symmetric in relation to the z-axis. The load effects at the given section are the axial force N ,the bending moment M and the shear force V . It will be assumed that in the member element of length dx no variations of N and V exist. The positive directions of the load effects are shown in Figure 1. The origin of the z-axis does not need to be at the centroid of the section.

The analysis will be performed considering a plane state of stress of an assembly formed by cracked reinforced concrete elements. The concrete will be considered formed by curved struts, which are not able to resist tensile stresses. The compressive stresses in the struts will be considered parallel to the directions of the cracks. The tranverse reinforcement placed in the

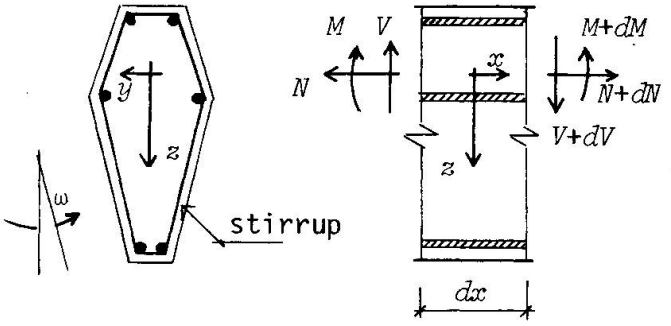

Fig. 1 Coordinate axis

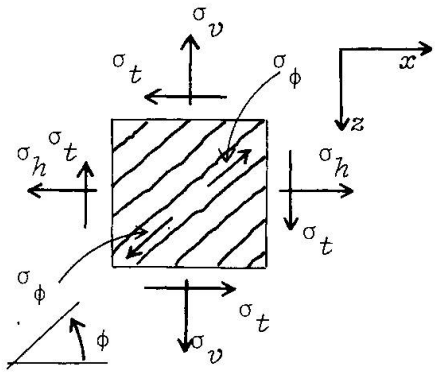

Fig. 2 Concrete stresses

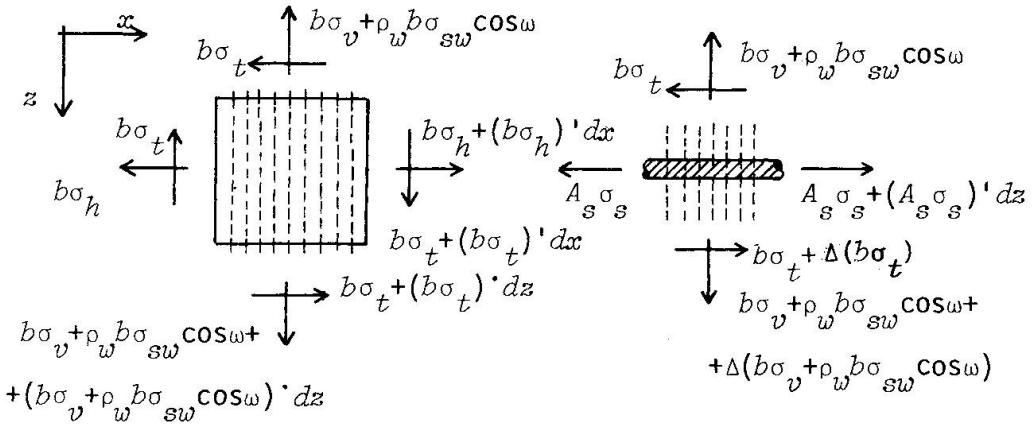

Fig. 3 Equilibrium conditions

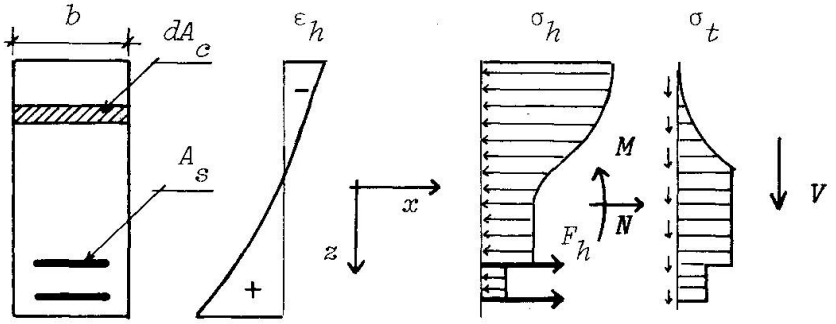

Fig. 4 Distribution of concrete stresses

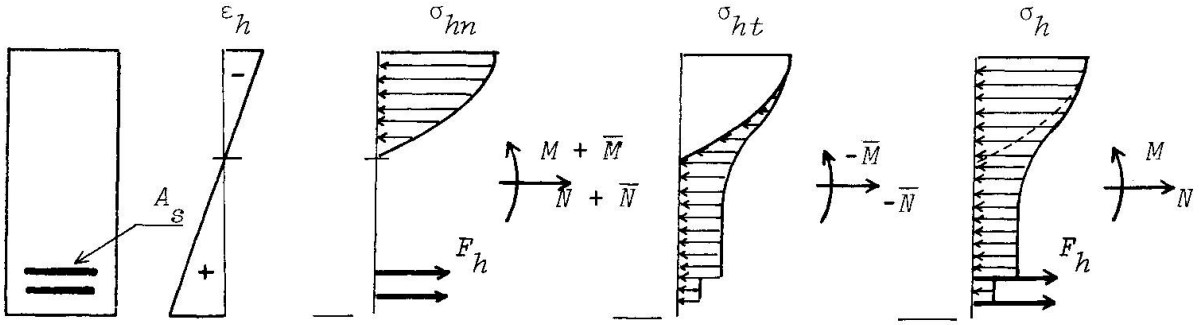

Fig. 5 Increments of loads effects

direction of the z-axis is supposed continuously distributed and variable along the x-axis. This reinforcement is actually formed by the stirrups. The longitudinal reinforcement will be assumed to be distributed in discrete quantities along the height of the member. This representation is required due to the usual practice of concentrating the longitudinal reinforcement at the top and bottom edges of the member. No shear transfer will be considered along the cracks due to aggregate interlock action of the cracked concrete. The dowell effects of the reinforcement going through the cracks will also be disregarded. In order to simplify the equations, the concrete corresponding to the volume occupied by the reinforcement will be considered as existing.

With the help of Figure 2 the following equilibrium conditions at a point of the concrete web of the member are obtained:

$$\sigma_t \tan\phi = -\sigma_v \tag{1}$$

$$\sigma_\phi \sin\phi \cos\phi = -\sigma_t \tag{2}$$

$$\sigma_t = -\tan\phi \, \sigma_h \tag{3}$$

in which σ_ϕ is the stress in the concrete strut, σ_h , σ_v , σ_t the stress components of σ_ϕ, and ϕ the slope angle of the cracks. It must be pointed out that the tensile stresses are denoted by positive signs.

The differential equations of equilibrium of a reinforced concrete element with transverse reinforcement as well as of a longitudinal reinforcement element (see Figure 3) are:

$$(b\ \sigma_t)^{\cdot} + (b\ \sigma_h)' = 0 \tag{4}$$

$$(b\ \sigma_t)' + (b\ \sigma_v + \rho_w\ b\ \sigma_{sw}\ \cos\omega)^{\cdot} = 0 \tag{5}$$

$$\Delta(b\ \sigma_t) + (A_s\ \sigma_s\ )' = 0 \tag{6}$$

$$\Delta(b\ \sigma_v + \rho_w\ b\ \sigma_{sw}\ \cos\omega) = 0 \tag{7}$$

in which b is the variable member thickness, ρ_w the relative amount of transverse reinforcement, σ_{sw} the stress in the transverse reinforcement, A_s the steel area of the longitudinal reinforcement at a certain height and σ_s the steel stress of the longitudinal reinforcement. The angle ω defines the slope of the stirrup in relation to the x-axis, as shown in Figure 1. In this paper f' will denote the partial derivative $\partial f/\partial x$ and $f^{\cdot}$ the partial derivative $\partial f/\partial z$. The symbol Δ will represent a discrete increment of the assigned function in the z-direction.

The overall equilibrium conditions over the entire height (see Figure 4) are:

$$N = \int \sigma_h \, dA_c + \Sigma\ \sigma_s\ A_s \tag{8}$$

$$M = \int z\ \sigma_h \, dA_c + \Sigma\ z\ \sigma_s\ A_s \tag{9}$$

$$V = \int \sigma_t \, dA_c \tag{10}$$

$$M' - V = 0 \tag{11}$$

in which dA_c is the elementary concrete area, calculated as $dA_c = b\ dz$. The force $A_s\ \sigma_s$ in Figure 4 is designated by F_h .

The state of deformation of the reinforced concrete plate is defined by the strains ε_h , ε_v in the longitudinal and tranversal directions and by the distortion γ . These strains are to be considered as average values of the strains and must encompass the crack openings between the concrete struts (see [5]).

Through geometric considerations and assuming that the strains in the y -direction are null, the following relationships are obtained:

$$\varepsilon_{sw} - \varepsilon_v \cos^2\omega = 0 \tag{12}$$

$$\varepsilon_\phi - \varepsilon_h \cos^2\phi - \varepsilon_v \sin^2\phi + \gamma \sin\phi \cos\phi = 0 \tag{13}$$

The principle of the complementary work yields the condition:

$$(\varepsilon_h - \varepsilon_v) \sin 2\phi + \gamma \cos 2\phi = 0 \tag{14}$$

The usual compatibility conditions must hold:

$$\varepsilon_h'' + \varepsilon_v'' - \gamma'' = 0 \tag{15}$$

At each reinforcement height the strains of concrete and steel must be equal:

$$\varepsilon_h = \varepsilon_s \tag{16}$$

The constitutive equations of concrete and steel are represented by:

$$\sigma_s = \sigma_s (\varepsilon_s) \tag{17}$$

$$\sigma_\phi = \sigma_\phi (\varepsilon_\phi) \tag{18}$$

$$\sigma_{sw} = \sigma_{sw} (\varepsilon_{sw}) \tag{19}$$

The set of 19 equations described above together with the prescribed boundary conditions define the problem of a stress state of a plane reinforced concrete member in a cracked condition.

The expression (14) was derived without consideration of the member load history. It is also assumed that the concrete is cracked everywhere, because no tensile stresses are to be supported by the concrete struts in their transversal direction.

3. THE SOLUTION OF THE ENTIRE SET OF EQUATIONS

The entire set of equations was solved numerically by SCHULZ [9] in the neighbourhood of a section, assuming for the strain in the x-direction the approximation:

$$\varepsilon_h = \sum_{p=1}^{n} \alpha_p z^{p-1} \tag{20}$$

The assumption (20) takes into account that the section warps after deformation. This solution will be named herein "the warping section solution". The method proposed by SCHULZ assumes variations for the stresses and strains in the x-direction in the form of 3rd grade polynomials. Four sections are examined in the neighbourhood of the given section by numerical methods. Due to the approximations involved in expression (20), the conditions (8), (9) and (15) are treated by numerical methods based on the method of weighted residuals (see [12]). A summary of the thesis [9], is presented in the paper [4] by SCHULZ and DIAZ.

Another set of solutions is possible to be made as long as the linear function for the longitudinal strain in a section is defined:

$$\varepsilon_h \cong \varepsilon_0 + \kappa z \tag{21}$$

in which ε_0 is the longitudinal strain ε_h for $z=0$ and κ the curvature of the deformed section.

COLLINS [6], as well as GUEDES and PRÉ [8] have chosen this way to give a rational approach to the problem. However due to the approximation inherently

present in expression (21) the complete set of equations can not be employed in numerical methods. Usually the conditions (13), (14) and (15) are eliminated from the problem and substituted by the condition:

$$\tan^2\phi = (\varepsilon_\phi - \varepsilon_h) \;/\; (\varepsilon_\phi - \varepsilon_v) \qquad (22)$$

which is obtained from (13) and (14).

Both numerical methods based on expression (20) or (21) need time consuming computer runs which turn the methods uneconomical for normal design work.

4. THE THEORY OF THE CRACKED REINFORCED CONCRETE PLATE AND THE USUAL DESIGN OF REINFORCED CONCRETE MEMBERS

In Figure 4 it can be seen that the distributions of the σ_h, σ_t stresses are different from those usually considered in the design of reinforced concrete members. Actually the design procedures in the design codes of reinforced concrete structures are based on considerations which are not logical in respect to structural mechanics ,but produce adequate results for normal design work. The approximations are necessary in order to allow the manual calculations in normal practice. It will be shown herein how far the discrepancies have gone.

In Figure 5 a reinforced concrete section is represented together with the distribution of the longitudinal deformations ε_h, which shall be assumed to be linear as given by the expression (21). It shall now be defined, as an approximation, that the longitudinal stresses denoted by σ_{hn} are determined as a function of the strain ε_h:

$$\sigma_{hn} \cong \sigma_\phi(\varepsilon_h) \qquad (23)$$

in which the stress-strain relationship σ_ϕ shall be the same as used before in the constitutive law (18). The stress resultants are now:

$$N_a = N + \overline{N} = \int \sigma_{hn}\, dA_c + \Sigma\, \sigma_s\, A_s \qquad (24)$$

$$M_a = M + \overline{M} = \int z\, \sigma_{hn}\, dA_c + \Sigma\, z\, \sigma_s\, A_s \qquad (25)$$

The acting load effects must now be incremented by $\overline{N}$ and $\overline{M}$ in order to reproduce the same longitudinal strains . It is important to note that the steel stresses of the longitudinal reinforcement are dependent upon the longitudinal strains , therefore the consideration of the force increments is extremely important to the design procedures of reinforced concrete members. Indirectly,the force increments are considered in the usual design practice through a procedure named staggering rule of the tensile force in the longitudinal reinforcement.

As shown in Figure 5 the stresses σ_h and σ_{hn} can define a new stress σ_{ht} with the help of:

$$\sigma_h = \sigma_{hn} + \sigma_{ht} \qquad (26)$$

Comparing expression (26) with the equilibrium conditions (24) and (25) , together with the conditions (8) and (9),it can be stated that the stress resultants of σ_{ht} are $-\overline{N}$ and $-\overline{M}$.

5. THE EQUIVALENT SECTION METHOD

As proposed by DIAZ in [1] , [2] and [3] it is possible to use the equivalent section method for the determination of the tangential stresses σ_t as long as the approximations (21) and (23) are taken together with the additional considerations:

$$\sigma_{ht}' \cong 0 \tag{27}$$

$$\sigma_t' \cong 0 \tag{28}$$

The conditions (27) and (28) state that the variations of σ_{ht} and σ_t can also be considered as null for the cases ,in which there is no variation of the shear force. These approximations have been shown to be adequate in the thesis [9] prepared by SCHULZ. Therefore their use in the design practice is possible. The discrepancies between the warping section solution,described in item 3 , and the method based on the equivalent section method are very small.

The derivative of expression (21) yields:

$$\varepsilon_h' = k_1 + k_2 z \tag{29}$$

Based on assumption (27) and with the help of the expressions (8), (9) , (11), (24), (25) and (26) together with the assumption $N'=0$, the following equilibrium equations are obtained:

$$(N + \overline{N})' = 0 \tag{30}$$

$$(M + \overline{M})' = V \tag{31}$$

Through sucessive derivation of (17) and (23) the following expressions are obtained:

$$\sigma_{hn}' = E_c \varepsilon_h' \tag{32}$$

$$\sigma_s' = E_s \varepsilon_s' \tag{33}$$

in which E_c and E_s are the derivatives $\partial\sigma/\partial\varepsilon$ at the points of the stress-strain curves for the deformations ε_h and ε_s . The values of E_c and E_s can be null as long as the curves are levelled , i.e. the yield point has been attained.

With the help of (24),(25),(29),(30),(31),(32) and (33) the following equations are derived:

$$k_1 \; A^e + k_2 \; S^e = 0 \tag{34}$$

$$k_1 \; S^e + k_2 \; I^e - V = 0 \tag{35}$$

in which:

$$A^e = \int E_c \; dA_c + \Sigma E_s \; A_s \tag{36}$$

$$S^e = \int z \; E_c \; dA_c + \Sigma \; z \; E_s \; A_s \tag{37}$$

$$I^e = \int z^2 \; E_c \; dA_c + \Sigma \; z^2 \; E_s \; A_s \tag{38}$$

The equations (34) and (35) allow the determination of the coefficients k_1 and k_2

The shear flow $v = b \; \sigma_t$ is determined with the help of the conditions (4) and (6), taking expression (27) into account:

$$v = \int_{z_s}^{z} E_c \; (k_1 + k_2 z) \, dA_c + \sum_{z_s}^{z} E_s \; (k_1 + k_2 z) \; A_s \tag{39}$$

in which z_s denotes the value of the variable z for the upper edge of the section.

The equivalent section is defined as the section formed by multiplication of the actual concrete and steel areas by the moduli E_c and E_s. Figure 6 shows how the equivalent section is obtained.

If the origin of the z-coordinate is chosen so that S_z^e is null, i.e. the origin is placed over the centroid of the equivalent section, the value of k_1 is also null, as can be seen from expression (34).

From (35) and (39) the following expression is derived:

$$v = (VS) / I \tag{40}$$

in which I is the moment of inertia of the equivalent section with respect to its centroid and S is the static moment of the elements of the equivalent section between z_s and z with respect to the centroid of the equivalent section.

Expression (40) allows the determination of the shear flow along the height of the member as long as the strains ε_h are known. Figures (7), (8) and (9) show some examples of this determination. It can be seen from these examples that, in the cases in which the yield stresses in the concrete and in the steel are attained concurrently, the shear stress at the edges must be null. This fact can be proved from expression (40), since the values of E_c and E_s are also null in these cases.

6. THE DESIGN PROCEDURES FOR THE TRANSVERSE REINFORCEMENT

If the shear flow is known, the design of the transverse reinforcement can be made using the rules of the codes as shown by DIAZ in [2].

Due to expression (28) the equilibrium condition (5) assumes the form:

$$\sigma_t \tan\phi = \rho_w \sigma_{sw} \cos\omega \tag{41}$$

In the modern design codes for reinforced concrete structures it is possible to obtain design rules which assume the following form:

$$\rho_w \sigma_{sw} \cos\omega = \text{function} (\sigma_t, \sigma_{hn}) \tag{42}$$

in which the function of the stresses σ_t , σ_{hn} is defined in the code itself.

For the calculation of the concrete stresses of the struts a simplified procedure can be derived from the expressions (41) and (42):

$$\sigma_t \tan\phi = \text{function} (\sigma_t, \sigma_{hn}) \tag{43}$$

Expression (43) allows the determination of the angle ϕ, which is consistent with the design rule (42). The stresses σ_ϕ are determined with the help of expression (2).

More details about these simplified design procedures are given in [1], [2] and [3].

7. AN ITERATIVE PROCEDURE TO DETERMINE THE SLOPE OF THE CRACKS

The determination of the angle ϕ in item 6 was based on an approach which has to be consistent with the design rules of the codes. However if these rules are disregarded a rational procedure can be found for the determination the angle ϕ (see SCHULZ [4] and [9]).

With the help of the expressions (1), (2), (7), (18), (19), (22), (23) and (41) the following equation can be obtained:

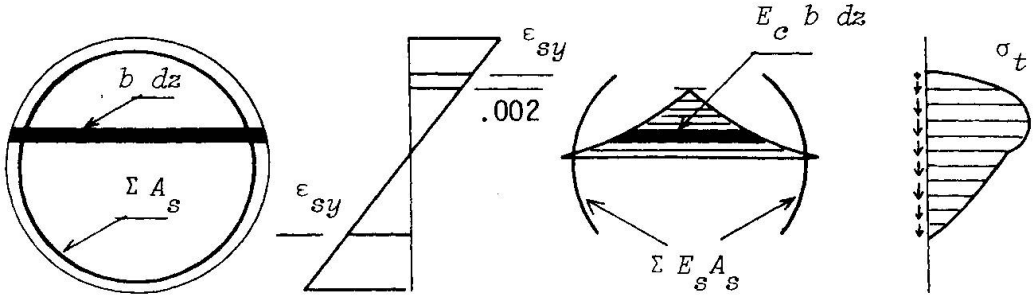

Fig. 6 The equivalent section

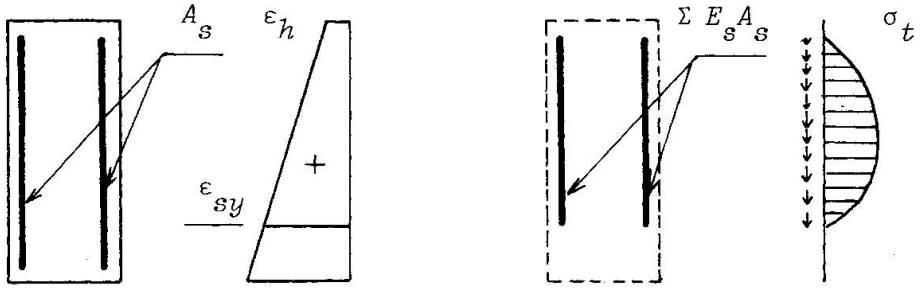

Fig. 7 Section subjected to M , V and positive N

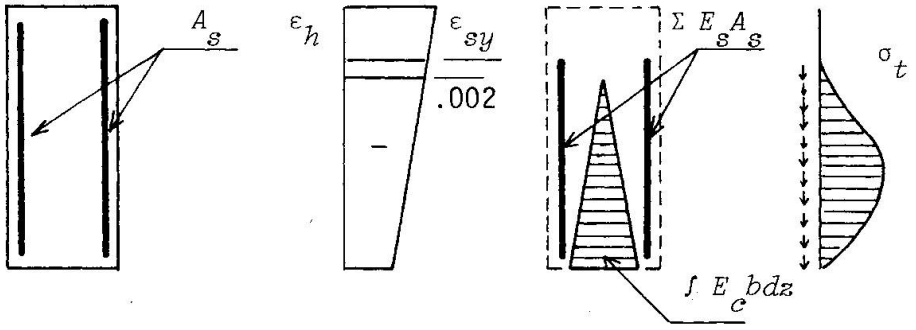

Fig. 8 Section subjected to M , V and negative N

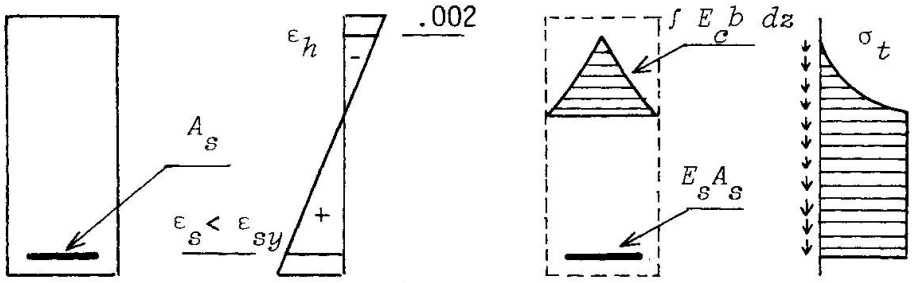

Fig. 9 Section subjected to M without yield of the reinforcement

$$\tan^2\phi = \frac{\varepsilon_\phi(\sigma_t, \phi) - \varepsilon_h}{\varepsilon_\phi(\sigma_t, \phi) - \varepsilon_v(\sigma_t, \phi)} \qquad (44)$$

The equation (44) allows the determination of the angle ϕ as long as the values of the functions σ_t and ε_h are known along the height of the member.

Before the iterative procedure begins a first set of approximate values of the deformation ε_0 and the curvature κ from expression (21) must be determined, with the help of the formulae of the structural mechanics,considering a linear behaviour of the materials. Afterwards the following steps are performed:

a-Based on the values of ε_h the characteristic values of the equivalent section are determined with the help of the expressions (36), (37) and (38).

b-The values of the coefficients k_1 and k_2 are determined through (34) and (35).

c-The values of σ_t along the height of the member are calculated with the help of expression (39).

d-The values of the angle ϕ are determined iteratively by means of equation (44). A Newton-Raphson procedure accelerates the convergence.

e-The values of σ_h are determined along the height with expression (3).

f-The stress resultants N^i and M^i are computed using the expressions (8) and (9). The stress resultants are compared with the given acting load effects N and M. If the difference between the approximate values of the stress resultants and the given load effects is small,the computation is finished. Otherwise a new set of values ε_0 and κ must be determined.

g-The estimate of the new values of ε_0 and κ is based on the calculation of the increments $\Delta\varepsilon_0$ and $\Delta\kappa$ which are obtained from the equations:

$$\Delta N = (\partial N/\partial\varepsilon_0)\,\Delta\varepsilon_0 + (\partial N/\partial\kappa)\,\Delta\kappa \qquad (45)$$

$$\Delta M = (\partial M/\partial\varepsilon_0)\,\Delta\varepsilon_0 + (\partial M/\partial\kappa)\,\Delta\kappa \qquad (46)$$

in which the partial derivatives are computed through expressions which are presented by SCHULZ in [9] . The increments ΔN and ΔM correspond to the difference between the given load effects N , M and the approximate values N^i , M^i determined in step f . After a new estimate of ε_0 and κ is made the whole set of steps must be repeated.

This numeric method represents a Newton-Raphson procedure due to the nature of the expressions (45) and (46). The iterative procedure converges quickly requiring small computer effort.

In Figure 10 a comparison between the results of the warping section method and the approximate method described herein is given. The agreement between the two methods has been excellent in all the examples which were calculated.

8. THE CONSEQUENCES OF THE PROPOSED PROCEDURES IN THE DESIGN OF REINFORCED CONCRETE MEMBERS

The design of reinforced concrete members has been made in the longitudinal direction with the values of the load effects N and M. The longitudinal tensile reinforcement is increased afterwards due to the staggering rule of the tensile force in the longitudinal reinforcement. It was shown in item 4 that a more adequate procedure is obtained when the acting load effects are incremented by the forces $\bar{N}$ and $\bar{M}$. These increments can be determined with the help of the expressions (24) and (25) as long as the values of ε_h are

M = 40 kN m ; N = -250 kN ; V = 70 kN ; A_{sw} = .0004 m^2/m

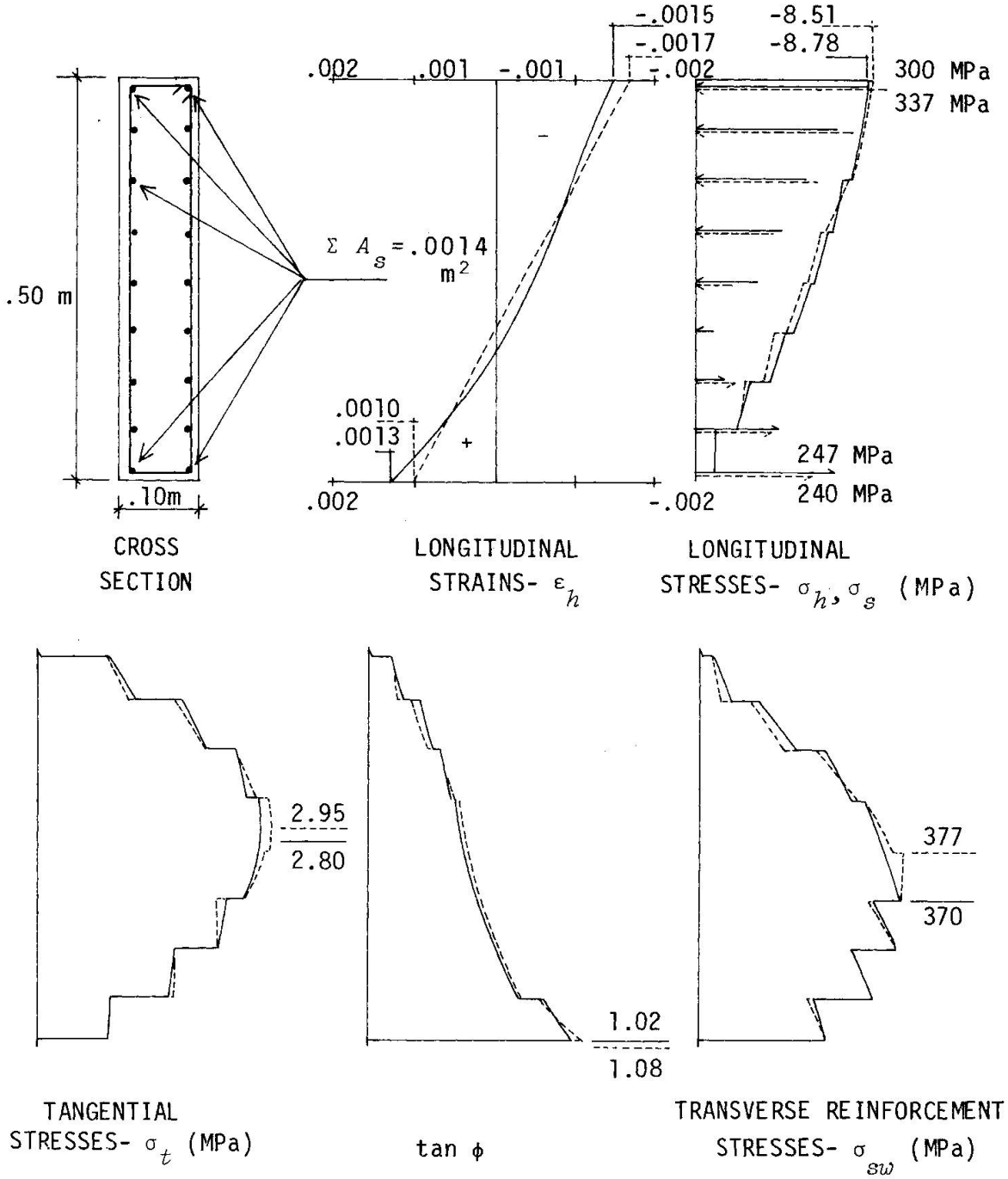

——— Warping Section Method

- - - - - - - - Equivalent Section Method

Fig. 10 Comparison between the warping section and the equivalent section methods

known. Consequently a computer procedure must be performed in the case of a section of general shape. It is possible to present approximate values for $\overline{N}$ and $\overline{M}$ which are adequate for normal design work (see [3]). TERRA has shown in [13] that the computer calculations can be performed in a programmable calculator such as the HP-41 C.

For members subjected to axial loads the staggering rule does not give the exact representation of what is really happening. It can happen in the cases of members subjected to tensile axial force, bending moment and shear force, that the usual design procedure fails to determine the necessary longitudinal tensile reinforcement at the "compressed" edge of the member, which actually can present positive strains. As shown by THUERLIMANN in [11], in those cases, it is necessary to increment the axial force N by $\overline{N} = |V|$ cotgϕ, which causes tensile stresses in the "compressed" edge of the member.

Another important point deals with the use of the lever arm in the calculation of shear stresses in reinforced concrete members. It has been shown in item 5 that the calculation of the tangential stresses can be performed with the usual formula $v = (V\,S)/I$. However when the materials are yielding at the edges the values of σ_t must be null. This fact is not really new, for in structural steel design it has always been considered that in the plastic state, the shear stresses must be absorbed in the central part of the member height. Therefore the lever arm of the internal forces can not give a correct evaluation of the actual shear stresses existent along the height. Only in the cases in which the compressive zone of the section is small the usual method for the determination of the shear stresses gives good results.

All the procedures presented herein are adequate to be used in almost all the cases encountered in practice. This includes the consideration of sections of general shape with a general distribution of longitudinal reinforcement. The set of acting forces at the section can be given in any combination of value and sign as long as the section has not attained the ultimate limit state. Only vertical stirrups are handled and the section must have at least a single symmetry axis. Due to the limitations in the development of the equations, the longitudinal reinforcement could not vary along the member axis. This limitation can be overcome as shown by DIAZ in [2].

The calculation of the problem variables in a single section, as shown in item 7, presents an additional advantage. The design procedures are entirely performed in a single section and the longitudinal reinforcement does not need to be further increased. For automatic design of a member along its axis this design procedure has enormous advantages because no use of the staggering rule is necessary. The automatic design of a reinforced concrete member along its axis until now requires the creation of a virtual tensile force diagram of the tensile reinforcement, which must be virtually staggered by the computer program. This cumbersome procedure is no long necessary.

9. CONCLUSIONS

The equations for the plane stress of a cracked reinforced concrete plate have been given. These equations can be employed in the solution of the problem of a reinforced concrete member subjected to axial force, bending moment and shear force.

The basic ideas for the solution of these equations with the assumption of the

warping of the section after deformation have been presented.

For practical calculations a new method was discussed for the determination of stresses and strains of a reinforced concrete member. This method is based on the concept of the equivalent section , which is obtained by multiplying the actual areas by the tangent deformation moduli of concrete and steel. This method needs little computational effort, which can be performed in programmable pocket calculators.

The method is valid for application to concrete sections of general shape presenting a single symmetry axis. The distribution of the longitudinal reinforcement can also be general. Only vertical stirrups are treated.

Some comments were made in connection with the shortcomings of the use of the lever arm of the internal forces in the determination of the shear stresses as well as to the staggering rule of the tensile force diagram .The latter is unable to predict the need of tensile reinforcement in some cases of members subjected to tensile axial force,bending moment and shear force.

The solution presented are consistent with the principles of structural mechanics, therefore they are entirely logical. The equilibrium equations are satisfied as well as the compatibility conditions for the strains.

Some examples have been presented showing the accuracy of the proposed approximate solutions.

The design of reinforced concrete members for shear force using the presented method does not require the design rules of the codes of reinforced concrete structures since the crack slopes are determined in the analysis.

REFERENCES

1. DIAZ,B.E.:Shear Design of Reinforced Concrete for General Shaped Member with a Single Symmetry Axis, Text of a lecture presented at the Clube de Engenharia on the 21th May 1980,Rio de Janeiro,1980.
2. DIAZ,B.E.:Dimensionamento a Esforço Cortante, Estrutura, Rio de Janeiro,Setembro 1980.
3. DIAZ,B.E.:Uma proposta prática para o dimensionamento à força cortante de uma seção de concreto armado de forma qualquer, XXI Jornadas Sulamericanas de Engenharia Estrutural, Rio de Janeiro,1981.
4. SCHULZ,M. e DIAZ,B.E.:Análise de tensões em vigas de concreto armado considerando o empenamento da seção transversal após a deformação, XXI Jornadas Sulamericanas de Engenharia Estrutural, Rio de Janeiro, 1981.
5. COLLINS,P.C.:Towards a Rational Theory for RC Members in Shear ,Journal of the Structural Division of the ASCE, New York, April 1978.
6. COLLINS,P.C.:Reinforced Concrete Members in Torsion and Shear,for presentation at the Colloquium on Plasticity in Reinforced Concrete,Kopenhagen, May 1979.
7. PRE,M.:Étude de la Torsion dans le Béton Précontrainte par la Méthode du Treillis Spatial Évolutif, Annales de l'ITBTP, Paris, Juillet, 1980.
8. GUEDES,A.C. e PRÉ,M.:Análise racional da influência do esforço cortante no comportamento de vigas de concreto armado e protendido,XXI Jornadas Sulamericanas de Engenharia Estrutural, Rio de Janeiro,1981.
9. SCHULZ,M.: Tese de mestrado em preparação na COPPE, Rio de Janeiro,1981.
10. GUEDES,A.C.:Tese de mestrado em preparação na COPPE, Rio de Janeiro,1981.

11. THUERLIMANN,B.,GROB,J. und LUECHINGER,P.:Torsion,Biegung und Schub in Stahlbetontraegern, Eidgenoessische Technische Hochschule Zuerich,1975.
12. FINLAYSON,B.A.: The method of Weighted Residuals and Variational Principles, Academic Press, New York, 1972.
13. TERRA,M.:Tese de mestrado em preparação na COPPE,Rio de Janeiro,1981.

Analysis of R.C. Bridge Columns under Imposed Deformations

Analyse de piles de pont en béton armé sous déformations imposées

Berechnung von Stahlbetonstützen unter aufgezwungenen Verformungen

JOSTEIN HELLESLAND[1]
Visiting Research Engineer
University of California
Berkeley, USA

ALEX C. SCORDELIS
Professor of Civil Engineering
University of California
Berkeley, USA

SUMMARY
A study of reinforced concrete columns under imposed end rotations and displacements is presented. Numerical solutions are obtained using a finite element computer program, PCFRAME, capable of performing nonlinear and time dependent analyses of reinforced and prestressed concrete frames Choice of element subdivision, nonlinear geometric effects, initially applied rotations and time dependent displacements are found to have significant effects on total displacement capacities.

RÉSUMÉ
Est présentée une étude de piles en béton armé sous l'effet de rotations et déplacements imposés aux extrémités. Les solutions sont obtenues en utilisant un programme aux éléments finis, PCFRAME, capable de calculer des structures en béton armé ou précontraint dans une analyse de type non-linéaire et dépendant du temps. Le choix de la décomposition des éléments, des effets du second ordre, des rotations appliquées initialement et des déplacements dépendant du temps se révèlent avoir des effets significatifs sur la capacité de la structure à résister aux déplacements donnés.

ZUSAMMENFASSUNG
Eine Untersuchung an Stahlbetonstützen unter aufgezwungenen Endrotationen und Stützenkopfverschiebungen is dargestellt. Das Finite-Elemente-Computerprogramm PCFRAME, das die nichtlineare Berechnung von Stahlbeton- und Spannbetonrahmen ermöglicht, wurde zur numerischen Auswertung verwendet. Es wird gezeigt, dass die Gesamtverschiebungskapazität der Stützen bedeutend von der Wahl der Elementeinteilung, den nichtlinearen geometrischen Effekten und von den aufgebrachten Vorverformungen, wie z.B. Rotationen und zeitabhängigen Horizontalverschiebungen, beeinflusst wird.

[1] On leave from Dr. Ing. A. Aas-Jakobsen A/S, Oslo Norway.

1. INTRODUCTION

A number of rigorous analytical procedures based on the finite element method have been developed in recent years that are capable of tracing the response of complex structures to varied loadings. One such procedure, developed by Kang and Scordelis [1], has been applied in the present study to examine the non-linear structural response of reinforced concrete columns, as found in bridges and other frame structures, due to imposed deformations.

Imposed deformations in columns are usually caused by relative lateral, Fig. 1a, movements of the column ends arising from length changes of the connecting girders due to prestressing, causing both short and long term (creep) deformations, shrinkage, and temperature changes. Also, girder rotations at the top of bridge columns, Fig. 1b, caused mainly by traffic loading, can generally be treated as imposed deformations on the columns since the superstructure girder usually has a much larger stiffness than the columns.

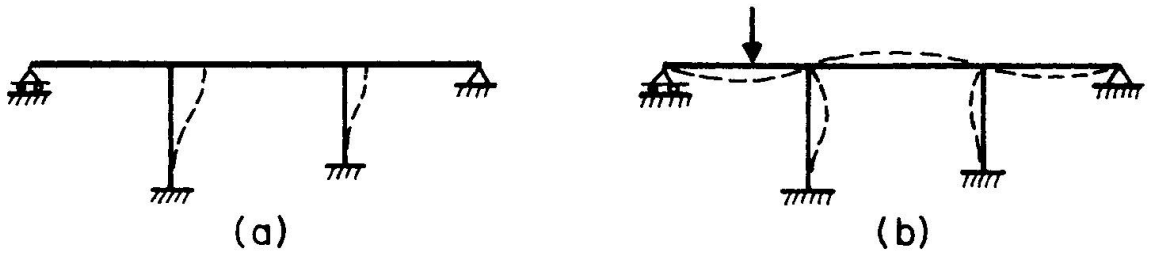

Fig. 1 Imposed Deformations in Bridge Columns

In the usual strength analysis the problem is generally that of determining the largest load the structure can carry. However, the problem in a pure imposed or controlled deformation analysis, in which the structure primarily must accommodate given rotations or displacements rather than carry loads, the problem is generally that of determining the maximum deformation the structure can be subjected to.

Imposed deformation studies of beams have been mainly related to short and long term settlements of supports and deal mainly with the linear [2] and the pre-yielding ranges [3]. Previous nonlinear studies of short and slender columns have been limited to short term end displacement aspects [4].

The main objectives of the present study are to determine end rotation and end displacement capacities of short and slender columns considering both single and combined action, and to study the effect of long term displacements and column creep on displacement capacities. The finite element analysis used for this purpose [1] takes both nonlinear material and geometric effects, i.e., the effects of axial loads on deflections, as well as time dependent concrete properties into account. Pure flexural solutions are sought, thus neglecting spread of inelastic zones due to extended concrete crushing, bond slip, inclined shear cracking, etc. Effects of element subdivision on such results are discussed. A comparison of theoretical predictions with test data is also presented.

Detailed results of the present investigation are given in [5], where the effect of previously imposed deformations on lateral load capacities of unbraced frames also has been studied. However, this aspect is not discussed herein.

2. METHOD OF ANALYSIS

The method of analysis employed in the present study is described in detail elsewhere [1,6]. Thus, only a brief review is given below.

2.1 Analytical Model and Solution Procedure

The analysis is based on the incremental form of the displacement formulation of the finite element method. Equilibrium equations for the total structure are set up and solved in a global coordinate system, which is fixed in space. The direct stiffness method is used to form the structure stiffness matrix.

The structure is divided into straight, one dimensional beam elements with the usual three degrees of freedom at each end, Fig. 2., and with the standard linear and cubic Hermitian shape functions describing the axial and transverse displacements between ends. Shearing deformations are not considered. The origin and direction of the local Cartesian coordinate system passing through the ends of the element, Fig. 2, follow the element, which is considered to be in a continuous quasi-static motion. Nonlinear geometric effects are accounted for by continuously updating the nodal point geometry and the transformation matrix between local and global coordinates.

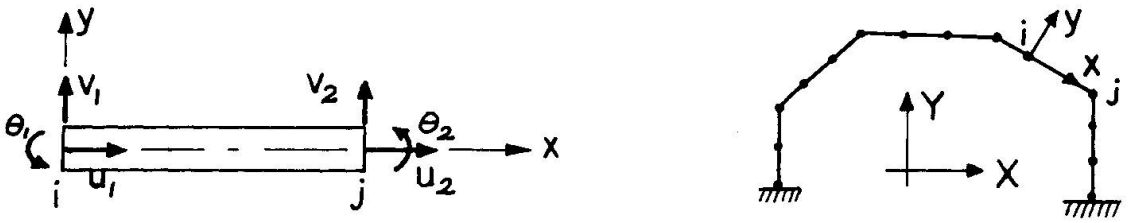

Fig. 2 Beam Element and Frame Structure

Different cross sections, symmetric about the local y-axis, but otherwise of arbitrary shape, and different material properties may be assigned to each element. Cross sections may be reinforced with both ordinary and prestressing steel, applied either in the pretensioned or post-tensioned sense. Cross sections are divided into a finite number of concrete and steel layers, each of which is assumed to be under uniaxial strain. Navier's plane section hypothesis is assumed to govern the distribution of total strains across sections. No bond slip is assumed to take place between rebars and concrete. Nonlinear material properties including cracking of the concrete are considered.

Time dependent load history and time dependent effects of material properties are considered using a step forward integration approach by dividing the time domain into a finite number of intervals of constant or varying length. External loads and equivalent loads due to nonmechanical strains (creep etc.) are applied in a specified number of load steps at each time step.

The nonlinear equilibrium equations are solved by an unbalanced load iteration method for each load step. Internal resisting loads are evaluated numerically by a 3-point Gaussian Quadrature over the current length of the element combined with a mid-point layer integration over the cross section. Stiffness matrices are evaluated at the center of each element only. Incremental solutions for each load step are added to previous totals to arrive at the current updated solution. In this manner, the structural response can be traced through the elastic, cracked, inelastic and ultimate ranges.

2.2 Material Properties

The total concrete strain ε at a given time and point in the structure is taken as the direct sum of mechanical (or instantaneous) strains ε_c and non-mechanical strains due to creep, shrinkage, aging and thermal effects. Incremental strains due to cyclic or repeated loading are not considered.

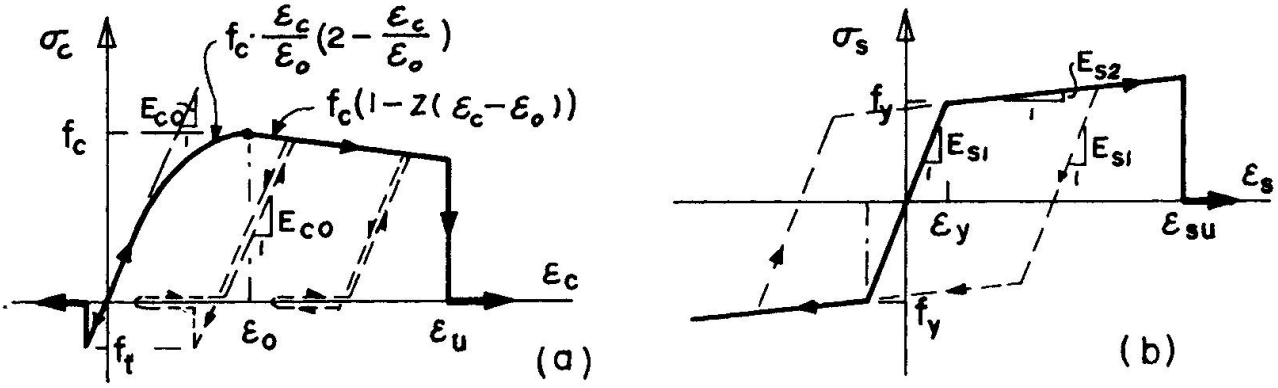

Fig. 3 Stress-Strain Relationships for Concrete (a) and Reinforcing Steel (b)

The nonlinear constitutive stress-strain relationships governing the response of the individual concrete and steel layers are shown in Fig. 3. The monotonic stress-strain curves are taken as envelope curves for the assumed nondegrading unloading-reloading response. Where the concrete tensile stress in a layer exceeds a specified tensile strength, f_t, cracking is assumed to occur. Once cracked, concrete can not again take tensile stress. The structural concrete compressive strength, f_c, taken as a function of the cylinder strength, f'_c, may vary with time.

Creep strain $\varepsilon_{cc}(t)$ of concrete is evaluated by an age and temperature dependent formulation based on the method of superposition. Thus,

$$\varepsilon_{cc}(t) = \int_0^t c\left(t', t-t', T\right) \frac{\partial \sigma(t')}{\partial t'} \tag{1}$$

$$c\left(t', t-t', T\right) = c_u(t') \sum_{i=1}^{m} a_i \left[1 - e^{-\phi(T)(t-t')/\tau_i}\right] \tag{2}$$

The creep compliance function, or specific creep $c(t',t-t',T)$, is the creep at time t' with temperature T. The values a_i (adding up to unity) and τ_i are constants selected to fit experimental or empirical data. $c_u(t')$ is the ultimate specific creep, which is a function of t', and $\phi(T)$ is a "temperature shift function". Temperaure effects on creep will not be considered in the present study. Consequently, $\phi(T)$ will be set equal to unity. Nonlinear creep effects at higher stress levels may be accounted for by replacing the actual stress by an "effective stress" according to specified input parameters.

2.3 Computer Program

The numerical solution described above for geometric, material and time dependent nonlinear analysis of reinforced or prestressed concrete planar frames has been incorporated into a computer program PCFRAME [6].

The input consists of: structure geometry and boundary conditions; element cross section and material properties; load history; time dependent properties and convergence tolerances.

The output, which can be requested for each iteration or each load increment at each time step, consists of the following: (1) joint displacements and rotations; (2) support reaction forces and moments; (3) unbalanced loads and moments; (4) element forces and moments (moments at the two end joints and the axial force); and (5) stresses, strains, and the material states on the stress-strain curve for each concrete and reinforcing steel layer and prestressing steel segment.

The computer program was used to obtain the numerical results described in the following sections.

3. EFFECT OF ELEMENT SUBDIVISION (MESH SIZE)

In linear elastic analyses, the finite element displacement method gives lower bound solutions for displacements. This may not be so for inelastic analyses. In order to study the effect of element subdivision, analyses of a symmetrically reinforced concrete cantilever column, Fig. 4, subject to constant axial load and increasing lateral displacement at the free end, were carried out for several element subdivisions, two of which are discussed below.

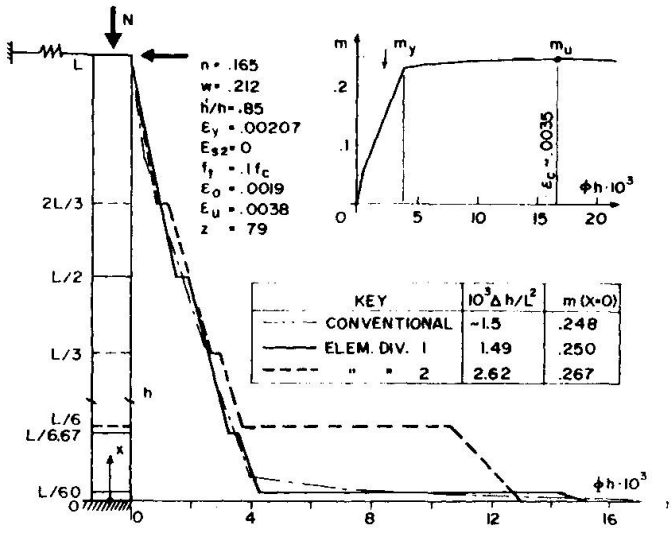

Fig. 4 Curvatures, Top Displacements and Base Moments for Different Element Subdivisions (First Order Analysis)

Element subdivisions "1" (full line) and "2" (broken line), material and section properties are given in Fig. 4. Elastic-perfectly plastic stress-strain properties are assumed for the rebars, and the concrete cross sections are divided into 20 equal layers. The sectional moment-curvature relationship, computed in conventional manner based on the monotonic stress-strain curves, is shown in the upper right hand corner of Fig. 4. It becomes very flat following yielding of the tensile steel, and is typical for low axial load levels. The axial load in the present analysis ($n = N/f_c bh = 0.165$) is 35% of the so-called "balanced" load. Maximum moment resistance M_u occurs in this case for a maximum concrete compressive strain of approximately 0.0035.

From a design point of view, it is of interest to compare finite element incremental load results with results based on conventional sectional M-ϕ considerations, corresponding to the above maximum concrete compressive strain (0.0035) at the column base.

Curvature distributions along the column length, displacements at the free end (Δ) and moments at the base ($m = M/f_c bh^2$) are given in Fig. 4. Geometric nonlinear effects are negligible, and are ignored in this example. Thus, the external moment distribution is linear. The "conventional" top displacement is obtained by a semigraphical integration of curvatures.

Element subdivision "1", with an element length of L/60 at the base, or approximately 1/3 of the conventional flexural plastic hinge length ($L_p = L(M_u-M_y)/M_u \simeq L/17.5$) gives results in satisfactory agreement with the conventional analysis, while element subdivision "2", where the shortest element at the base extends well into the elastic zone, overestimates displacement and moment by approximately 75% and 8% respectively.

As constrained by the assumed beam displacement functions used in the finite element analysis, which are exact for ideal elastic materials, the curvature distribution becomes linear within each element, and, due to the change in stiffness as cracking occurs, discontinuous at element nodes even in the pre-yield range. However, the results are not very sensitive to the size of elements entirely in the pre-yield range. If curvatures in the inelastic region as such were of interest, rather than displacements, a finer division using several small elements over the flexural plastic hinge length would be required.

With increasing constant axial load level, the stiffness will be reduced more gradually with increasing curvature, and also, the curvature corresponding to M_u will become smaller. The errors due to a coarse element subdivision in the inelastic region will thus be smaller than in the case considered above.

In a real structure, the inelastic deformations are usually larger than those predicted by the pure flexural hinge, as actual failure is spread over a finite zone rather than at a single section, due to such factors as spread of crushing, bond slip, etc., and also due to diagonal shear cracking in short, stiff members. Thus, a coarse element at the critical region, such as "2" in Fig. 4, which in a physical sense have extended the inelastic zone to the full length of the first element, might actually give displacements in better agreement with test results than would a finer subdivision.

Another aspect of interest related to element size is the response for moments on the descending branch of the $M-\phi$ relationship. In an actual structure, displacements may be increased beyond the point at which maximum moment resistance (m_u, Fig. 4) has been reached at the critical base region. However, in a conventional first order sectional analysis, as well as in a standard finite element analysis with a very small element at the critical region, the end displacement can not be increased beyond this stage. This can be explained by considering the response to an attempted increase in end displacement. At the critical section with maximum moment, the moment would decrease along the descending $M-\phi$ branch with increasing curvature. Moments at all other sections would have to decrease correspondingly, but by unloading with decreasing curvatures from the ascending branch. Since a curvature increase at a single critical section, or over a very short element in the critical region, does not contribute to the displacement, the reduced curvatures over the remainder of the column would imply a reduced displacement, i.e., an obvious contradiction. However, using a larger element at the critical region than envisioned above, the curvature increase over the element may more than balance the reduced curvatures over the remaining elements. Thus, additional displacements, increasing with increasing element size may be predicted. These might be in better agreement with test results than those of a finer subdivision, but may create inaccuracies in the computed internal forces due to the larger element size.

The problem of choosing an element size that would give a reasonable quantitative estimate of the above phenomena for the general case, would be, like the question of the true plastic hinge length itself, quite difficult to determine without careful study of solutions for several selected element subdivisions. The above discussion emphasizes the fact, often overlooked in nonlinear finite element analyses, that the mesh size selected may have an important influence on the results obtained compared to those from a real physical model.

4. COMPARISON WITH TEST DATA

The applicability of the present procedure has been demonstrated by comparison to a variety of test results of reinforced and prestressed beams and columns subjected to both short time and time dependent load histories [1,6,5].

A summary is given below of one of these comparisons [5] involving a hinged, symmetrically reinforced concrete column, subjected to an eccentrically applied axial load history consisting of a sustained service load for 131 days, 1444 load repetitions and subsequent loading to failure in a stroke controlled test, Fig. 5. The column is one of a test series reported in [7,8].

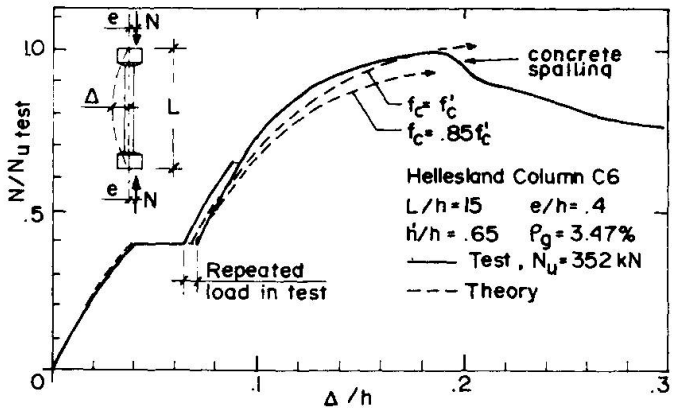

Fig. 5 Comparison with Test Data [7,8]

The material laws presently incorporated into the analysis do not account for effects on strength and strains of repeated loading. However, based on the above and other tests [9], it is believed that the relatively low number of repetitions and repeated load levels in the test may have had some, but only an insignificant, beneficial effect on stiffness and load capacity. Thus, a meaningful comparison can be obtained in this case in spite of the neglect of repeated loading in the analysis.

Column geometry and material data were as follows:

L = 1905 mm, $b \times h$ = 179 × 127.5 mm (average "as measured" in vicinity of midheight),

$A_s = A'_s$ = 396 mm^2 (1 #5 rebar in each corner),

h' = 82.6 mm, e = 50.8 mm, f'_c at initial (14 days) and final (145 days) loading 32.1 and 41.9 MPa respectively, f_y = 407 MPa,

E_{s1} = 211000 MPa (E_{s2} = 0, Fig. 3).

Over a length of 0.135L at column ends, the cross sections were enlarged to $b \times h$ = 229 × 406 mm.

Cylinder strength increases with time due to hydration, shrinkage (ε_{sh}), creep and effect on creep of age at loading (t'), as measured on plain concrete cylinders (152 × 304 mm), were approximated in the analysis as follows:

$$f'_c = f'_{c28} \cdot t/(4.32+0.845t); \quad f'_{c28} = 37.1 \text{ MPa}$$

$$\varepsilon_{sh} = 650 \cdot 10^{-6}(1 - e^{-t/60})$$

Creep: Eq. 2 with $c_u = 8.760 \cdot 10^{-5}\ (1.46 - 0.32 \log_{10} t')$ (per MPa)

$$a_1 = .386, \quad a_2 = .352, \quad a_3 = .262$$

The concrete σ-ε diagram used (Fig. 3) is defined by $E_{co} = 4735\sqrt{f_c}$ (MPa), $\varepsilon_o = 2f_c/E_{co}$, $\varepsilon_u = .0038$, $z = 79$ and $f_t = 0.5\sqrt{f_c}$. The structural concrete strength f_c is taken in terms of the time dependent cylinder strength as either 0.85 f'_c or 1.0 f'_c. The column, including the enlarged ends, was modelled using 8 elements for the half length. Each cross section was divided into 10 layers. The sustained load period was divided into 6 time intervals of increasingly larger duration.

Good agreement between test and theoretical load-deflection results can be noted, Fig. 5, with the better correspondence obtained with $f_c = 1.0\, f'_c$.

5. COLUMN DEFORMATION CAPACITIES

5.1 General

Controlled deformation and deformation capacity results from the analysis of several reinforced concrete columns with constant axial loads are presented below, and the effect on the results of important parameters are discussed.

The columns, representative of such as those in Fig. 1, are modelled as shown in Fig. 6. Apart from the controlled end deformations at the column top and shortening due to axial loading, the columns considered are fixed at both ends. This is achieved by assigning spring constants to the spring restraints (Fig. 6) that are several order of magnitudes larger than the rotational or translational column stiffness. External forces at the column top, required to produce a specified end rotation or displacement, are therefore a function of the spring constants alone.

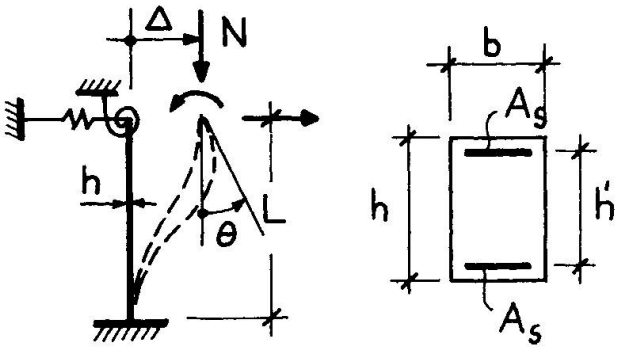

Fig. 6 Column Model and Cross Section

The columns all have constant, symmetrically reinforced cross sections, Fig. 6, with $h'/h = 0.85$. Cross sections are divided into 10 or 20 equal layers, with the finer layer division used for elements in the most strained regions of the column. Element lengths were chosen after careful study such that the pure flexural inelastic action was captured with reasonable accuracy.

While the results include both short and long term applications of controlled end displacements, end rotations are applied in a short term sense only.

Short term rotations and displacements are applied incrementally in 5 to 8 steps. Unless indicated otherwise the axial load is applied in the first step together with a small displacement or rotation. Long term displacements are applied incrementally over a period of 10,000 days (approx. 27 years) in two load increments at each time step as indicated in Fig. 7, where the time domain is divided into 8 intervals. Equivalent nonmechanical forces due to column creep are applied in one increment at each time step. Column shrinkage is not considered.

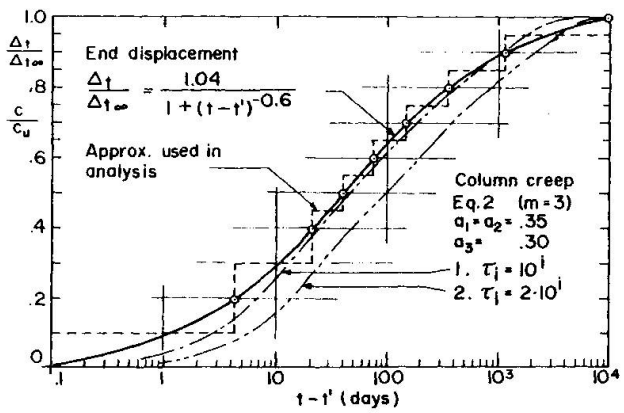

Fig. 7 Development of Time Dependent End Displacement and Column Creep with Time

Results presented below are based on creep curve "1", Fig. 7. Ultimate specific creep is taken as

$$c_u = 7.6 \cdot 10^{-5}\, (t'/t'_o)^{-0.118} \quad (MPa^{-1}) \quad (3)$$

with initial loading at $t_o' = 28$ days. This corresponds to a creep coefficient $\phi(t_o') = c_u E_{co} = 2.0$ for a concrete with $f_c = 25$ MPa and properties otherwise as given below. Only linear creep is considered.

Concrete strength and E-modulus is not assumed to increase with time, in order to be in line with common design practice. The constitutive stress strain relationships used, Fig. 3, are defined by

- $f_t = 0.1\, f_c'$, $\varepsilon_o = 0.0019$, $\varepsilon_u = 0.0038$ and $z = 79$

- $\varepsilon_{sy} = 0.00207$, $\varepsilon_{su} = 0.030$ and $E_{s2} = 0$.

Results are given in terms of the nondimensional axial load n, moment m and mechanical reinforcement ratios w and w';

$$n = N/f_c bh$$

$$m = M/f_c bh^2 \qquad (4)$$

$$w = w' = f_y A_s/f_c bh$$

Thus, within the constraints imposed by the assumed stress strain laws, the results are valid for any concrete (f_c) and steel strength (f_y).

Deformation capacities are limited by member failure caused by either primary material or section failure as maximum sectional moment resistance is reached, before or at a maximum concrete compressive strain of ε_u or steel strain of ε_{su} (does not govern), or by primary instability (buckling between column ends) due to nonlinear geometric effects at strains below the above limits.

5.2 Rotation and Displacement Results

Typical moment and maximum deflection (y_{max}) results versus controlled end rotations (θ) are shown in Fig. 8, and moment versus controlled end displacements in Fig. 9. Points at which rebars yield in compression (Y') or tension (Y) and where the concrete strain reaches ε_o (Fig. 3) are indicated on the figures. The reinforcement ratio in these figures ($w = 0.0828$) corresponds to a total steel percentage of approx. 1% for $f_c = 25$ MPa and $f_y = 400$ MPa.

Typical deflection and moment distributions along the length are indicated schematically in Fig. 10. Maximum moments (m_{max}) may occur at column ends, or, with increasing nonlinear geometric effects, at an increasing distance from column ends. Also shown (Fig. 10) is the additional deflection due to nonlinear geometric effects, computed as the difference in results ($y_2 - y_1$) of second and first order analyses for a given end rotation or end displacement. Essentially, these shapes correspond to the first and second Euler buckling mode for fixed ended columns with sway prevented. Results associated with controlled end displacements of initially straight columns, as in the present study, are anti-symmetric about midheight. For such cases it is sufficient to analyze one half of the column.

Some moment-deformation aspects, typical for slender columns, may be discussed with reference to the columns with end rotation in Fig. 8. The top moment m_t increases with increasing rotation θ until it reaches a maximum prior to column failure. This maximum moment, which would be the one of main interest in a strength analysis, is for the more slender column ($L/h = 45$) considerably smaller than the sectional moment resistance due to the nonlinear geometric effects.

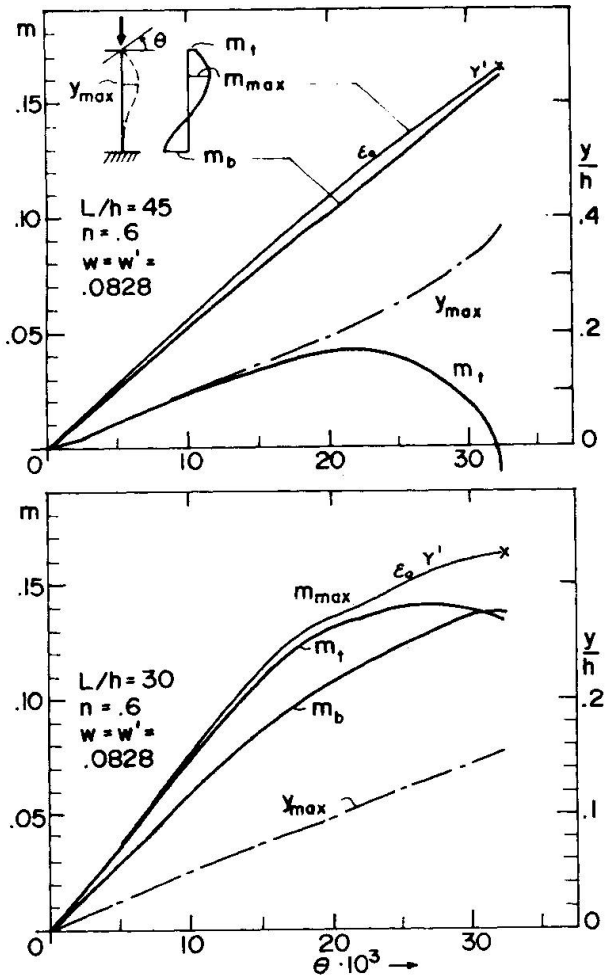

Fig. 8 Typical Moment versus Rotation Results

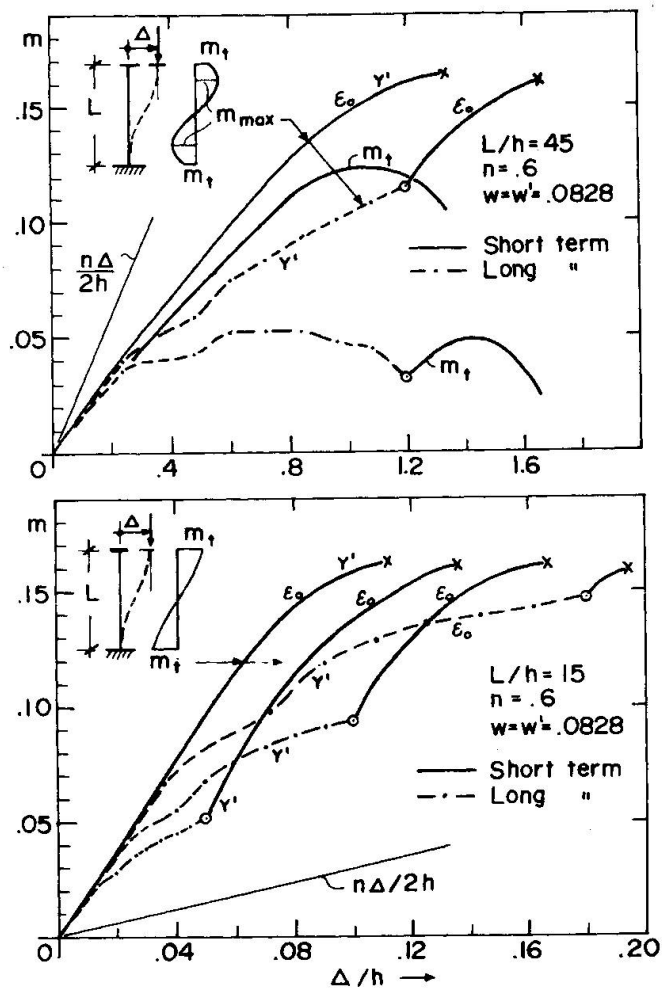

Fig. 9 Typical Moment versus Displacement Results

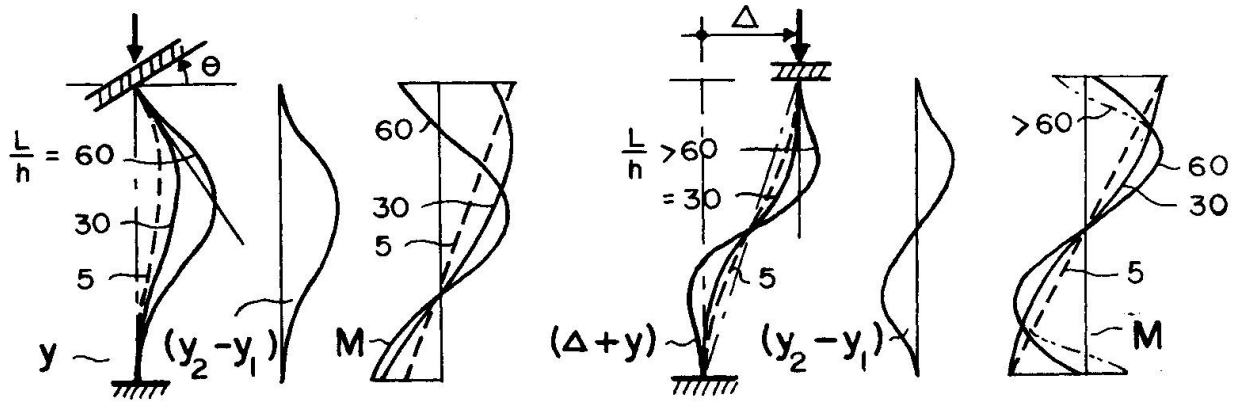

Fig. 10 Schematic Short Term Deflection and Moment Distributions at Failure (n~0.6; w~.08)

With further increase in θ, m_t decreases until at some point it may become zero and thereafter change direction. Thus, rather than resist the imposed rotation from this point on, the column needs moment support in order not to collapse. In an actual structure, this moment support must be provided by the girder. However, the column may still be able to carry axial loads and accommodate further imposed rotations, until material failure or buckling (between ends) occur.

Similar behaviour can be observed for columns with controlled end displacements. The lateral column resistance or support under increasing end displacements is given by the shear force V in the column,

$$V = \frac{2}{L}\left(m_t - \frac{N\Delta}{2}\right) \tag{5}$$

The second term in Eq. 5 is shown (nondimensionalized) in Fig. 9. For the column with L/h = 45 it is always larger than m_t. Consequently, this column needs lateral support from the onset of imposed displacements.

The slenderness or axial load at which a column needs moment or lateral support already at the onset of imposed deformations, can be determined from the usual Euler load expression. For this computation a stiffness (EI) corresponding to the tangent at the origin of the respective M-ϕ relationships should be used.

5.3 Short Term Deformation Capacities

Short term end rotation and end displacement capacities, θ_{uo} and Δ_{uo} respectively, obtained by increasing θ and Δ incrementally as shown in Figs. 8 and 9, are given in Fig. 11 for various slenderness ratios and two axial load levels that comprise load levels of practical interest. Points at which results have been calculated are indicated by circled values. The variation drawn in between these values is approximate only. Also shown are results from first order analyses which neglect geometric nonlinearities.

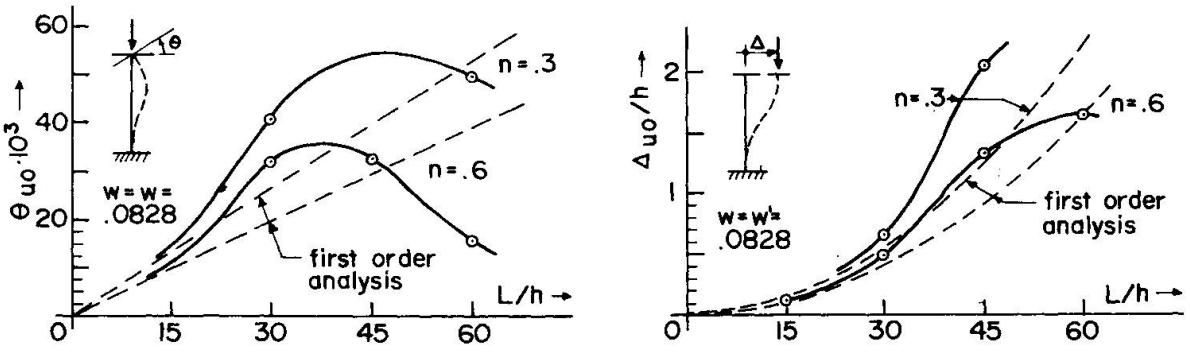

Fig. 11 Short Term Rotation and Displacement Capacities

Material failure was the primary cause of failure for columns subjected to controlled end rotations and n = 0.3 for all L/h ratios up to about 60. This was also the case for n = 0.6 for L/h values less than about 50. Thereafter, failure was by primary instability (buckling associated with rapid deflection increases between the column ends). Columns with controlled end displacements are less sensitive to nonlinear geometric effects due to the smaller "buckling" length, Fig. 10, and thus all failed by primary material failure. For n = 0.6 and L/h = 60, end moments were approximately zero at this point.

Conventional computation of moment-curvature curves and integration of curvatures based on linear moment distribution over the column length, gave results in good agreement with the first order computer results, Fig. 11 (broken lines). First order rotation and displacement capacities vary linearly and parabolically respectively w.r.t. the column slenderness for a given n and w,

$$\theta_{uo}/h = a\ L/h \tag{6}$$

$$\Delta_{uo}/h = b\ (L/h)^2 \tag{7}$$

where, for $w = 0.0828$, the following approximate constants were found for $n = 0.3$ and $n = 0.6$: $a = 0.880 \cdot 10^{-3}$ and $0.650 \cdot 10^{-3}$; $b = 0.625 \cdot 10^{-3}$ and $0.455 \cdot 10^{-3}$. These expressions may be used to compute deformation capacities for small L/h values where the geometric nonlinearity effect is negligible, Fig. 11.

For most L/h values of practical interest, the first order capacities are on the safe side. As long as maximum moment and failure is obtained at the column ends, the discrepancy between second and first order analysis results increases at an increasing rate with increasing slenderness due to the additional moments brought about by the geometric nonlinearity (axial load on deflections) in the second order solution. As maximum moments start forming at an increasing distance from column ends at larger slenderness values, and as end moments reduce, Fig. 10, this discrepancy gradually tapers off and may eventually change sign as seen in Fig. 11 as the second order curve crosses over the first order curve.

In a real structure columns will usually be subjected to both end rotations and end displacements. The effect on displacement capacities of a previously imposed end rotation; θ, applied simultaneously with the axial load, can be seen in Fig. 12. All values are given in terms of the short term (single action) capacities in Fig. 11 for the respective slendernesses. Of interest in Fig. 12 are also the first order results which are seen to be on the safe side.

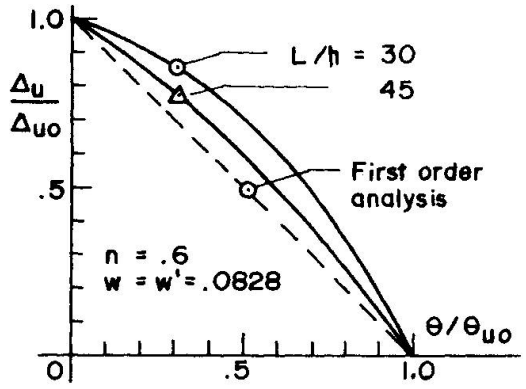

Fig. 12 Effect of Previously Imposed Rotation on Displacement Capacity

Short term deformation capacities appear to increase with increasing reinforcement, decreasing axial load, and, as seen in Fig. 12 with increasing slenderness ratios up to a certain point. Similar results have been found in other investigations for single action end displacements [4].

The flexural deformation capacity results computed above are on the safe side, in particular for shorter columns with insignificant nonlinear geometric effects. The additional deformation potential of such columns due to the spread of the inelastic zone caused by lateral tie or hoop confinement, longitudinal strain gradients, strain hardening of the steel, bond slip, inclined shear cracking, extended concrete crushing, etc., may be estimated for an actual column using procedures described in available code or code related publications, summarized in [10].

5.4 Time Dependent Effects

When end displacements are applied gradually over a period of time, creep in the column tends to relieve the development of internal column moments as seen, Fig. 9, when comparing moments obtained in a short term and long term (broken lines) application of the same end displacement. The dips in the long term moment curves are partly due to the discretization in time in the analysis, and partly, due to the differences in variation with time assumed for end displacement and specific creep (Fig. 7).

The effect of a given time dependent displacement on final displacement capacities, Δ_u, was obtained by incrementing the end displacement in a controlled short term application after the given total time dependent displacement $\Delta_{t\infty}$ had been attained. It is seen, Fig. 9a, that the magnitude of the total time dependent displacement $(\Delta_{t\infty})$, which is always applied over the same period of

time (27 years) and in the same manner (Fig. 7), may have a significant effect. Similar studies were carried out for other columns. Typical results for columns with relative high axial load levels, with most of the cross section in compression, and small reinforcement ratios are summarized in Fig. 13, which is non-dimensionalized in terms of short term capacities Δ_{uo} that can be obtained from figures such as 9 and 11b (second order).

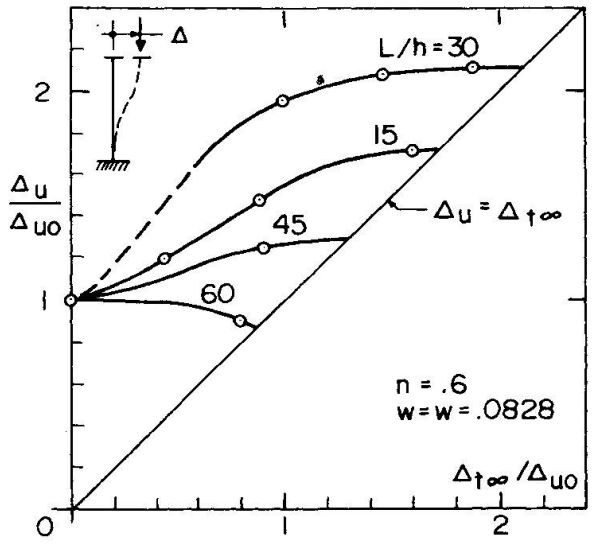

Fig. 13 Total Displacement Capacity versus Long Term Displacement

Figure 13 clearly shows the effect of an initial imposed long term displacement $\Delta_{t\infty}$ and slenderness ratio on the total displacement capacity Δ_u. For high slenderness ratios in combination with high axial loads and small reinforcement ratios, as in the present case for L/h = 60, large creep deflections measured from the chord through the column ends may cause premature failure through instability at end displacements less than Δ_{uo}. However, for small and intermediate slenderness ratios, and load levels and reinforcement ratios of practical interest, an increase in displacement capacity beyond Δ_{uo} will usually result when part of the displacement is applied gradually over a period of time.

The increase may not be as large as that shown in Fig. 13 for other n and w values. For example, by either reducing n in Fig. 13 to 0.3 or by increasing w to 0.25, increases of 41% and 50% respectively were found for $\Delta_{t\infty}/\Delta_{uo} = 0.77$ as compared to approximately 80% above, for L/h = 30.

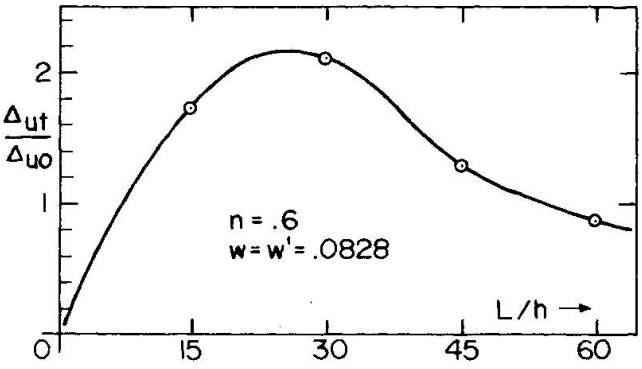

Fig. 14 Long Term Displacement Capacity versus Slenderness Ratio

Figure 14 shows the largest long term displacements that can be applied for a given slenderness for failure to take place just at the end of the time period considered. These values are given by the intersection of the curves in Fig. 13 and the 45° line in the same figure.

A non-exhaustive comparative study of the effects on displacement capacities of nonlinear creep, slower creep development with time (curve "2" in Fig. 7) and of replacing parts (about 40%) of the time dependent displacement ($\Delta_{t\infty}$) above with a short term initial displacement, was also carried out. The latter two factors do not appear to affect capacity results significantly. Nonlinear creep may increase total displacement capacities of shorter columns due to increased creep "relief", while slender columns with large geometric nonlinearity may be affected adversely. Similar results can be expected for larger creep values than that used in the present study (Eq. 3).

6. SUMMARY AND CONCLUSIONS

A study of reinforced concrete columns under imposed end rotations and displacements has been presented. Numerical solutions were obtained using a finite element computer program, PCFRAME, capable of performing nonlinear and time dependent analyses of reinforced and prestressed concrete frames. Choice of element subdivision, nonlinear geometric effects, initially applied rotations and time dependent displacements were found to have significant effects on total displacement capacities.

Additional nonlinear analytical studies are planned to develop sufficient data from which improved design recommendations may be made for reinforced concrete bridge columns under imposed deformations.

ACKNOWLEDGEMENTS

This research was partially sponsored by the National Science Foundation by Grant No. CME-7918057. Additional support was provided to the first author from the Royal Norwegian Council for Industrial and Scientific Research (NTNF), Janson's Legat and Dr. Ing. A. Aas-Jakobsen A/S. The Computer Center at the University of California, Berkeley, provided the facilities for the numerical work.

REFERENCES

1. KANG, Y.-J., and SCORDELIS, A. C., "Nonlinear Analysis of Prestressed Concrete Frames," Journal of the Structural Division, ASCE, Vol. 106, No. ST2, Febr. 1980.

2. GHALI, A., DILGER, W., and NEVILLE, A. M., "Time-Dependent Forces Induced by Settlement of Supports in Continuous Reinforced Concrete Beams," ACI Journal, Nov. 1969.

3. BISHARA, A. G., and JANG, S.-Z., "Settlement-Induced Forces in Concrete Bridges," Journal of the Structural Division, ASCE, Vol. 106, No. ST7, July 1980.

4. GRENACHER, M., "Einfluss von Verschiebungen und verschiedenen Lagerungen auf das Traqverhalten von Stahlbetonstützen," Bericht Nr. 61, Institut für Baustatik und Konstruktion, ETH, Zürich, Febr. 1976.

5. HELLESLAND, J., "Nonlinear, Time Dependent Analysis of R. C. Bridge Columns under Imposed Deformations and Lateral Loads," UC-SESM Report (in preparation), Univ. of California, Berkeley.

6. KANG, Y.-J., "Nonlinear Geometric, Material and Time Dependent Analysis of Reinforced and Prestressed Concrete Frames," UC-SESM Report No. 77-1, Univ. of California, Berkeley, Jan. 1977.

7. HELLESLAND, J., "A Study into the Sustained and Cyclic Load Behaviour of Reinforced Concrete Columns," Ph.D. Dissertation, Dept. of Civil Engineering, Univ. of Waterloo, Waterloo, Ont., Canada, Aug. 1970.

8. HELLESLAND, J., and GREEN, R., "Sustained and Cyclic Loading of Concrete Columns," Journal of the Structural Division, ASCE, V. 97, No. ST4, Apr. 1971.

9. GREEN, R., and HELLESLAND, J., "Repeated Loading Tests of Reinforced Concrete Columns," ACI Publication, SP-50, 1975.

10. PARK, R., and PAULAY, T., "Reinforced Concrete Structures," John Wiley & Sons, 1975.

NOTATIONS

b - width of concrete section
h - depth of concrete section
h' - distance between compression and tension steel
L - column length
A_s - tensile steel area
A'_s - compression steel area
f_c - structural concrete compressive strength
f'_c - cylinder concrete compressive strength
f_t - structural concrete tensile strength
f_y - yield stress of reinforcing steel
E_{s1} - initial elastic modulus of reinforcing steel
E_{s2} - post yield elastic modulus of reinforcing steel

ε - total strain
ε_c - mechanical (instantaneous) concrete strain
ε_{cc} - concrete creep strain
ε_{sh} - concrete shrinkage strain
ε_o - concrete strain at maximum stress
ε_u - concrete crushing strain
ε_y - steel strain at yield
ε_{su} - steel strain at fracture

Δ - imposed (controlled) end displacement
Δ_u - end displacement capacity
Δ_{uo} - single action short term end displacement capacity
Δ_{ut} - single action long term end displacement capacity
θ - imposed (controlled) end rotation
θ_{uo} - single action end rotation capacity
$\Delta_{t\infty}$ - long term end displacement applied gradually over a period of approximately 27 years

Leere Seite
Blank page
Page vide

Nonlinear Analysis of a Prestressed Concrete Bridge

Analyse non-linéaire d'un pont en béton précontraint

Nichtlineare Berechnung einer Spannbetonbrücke

MARK A. KETCHUM
Research Assistant
University of California
Berkeley, California, USA

ALEX C. SCORDELIS
Professor of Civil Engineering
University of California
Berkeley, California, USA

SUMMARY

A nonlinear material and time dependent analysis is applied to a three span continuous post tensioned single cell concrete box girder bridge. The analytical procedure, based on the finite element method, considers the nonlinear stress strain relationships of the materials as well as the time dependent effects of creep, shrinkage, relaxation of prestress, and load history. The time dependent behavior of the bridge is traced through a period of 27 years from the time of construction. Overload behavior and ultimate strength under increasing vehicular load are investigated at two times in the service life of the bridge. The bridge is shown to have a large overload capacity.

RÉSUMÉ

Une analyse de type non-linéaire et dépendant du temps est appliquée à un ouvrage à trois travées continues formé d'un caisson en béton précontraint. L'analyse, basée sur la méthode des éléments finis, prend en compte la relation non linéaire contrainte-déformation des matériaux ainsi que les effets du fluage, du retrait, de la relaxation des aciers et du processus de chargement. Le comportement de l'ouvrage est suivi sur 27 années s'écoulant après sa finition, en particulier sous charges ultimes, appliquées deux fois pendant cette période. Il se révèle que l'ouvrge a une large résistance résiduelle vis-à-vis des surcharges.

ZUSAMMENFASSUNG

Eine dreifeldrige, durchlaufende, einzellige Hohlkastenspannbetonbrücke wird unter Berücksichtigung von nichtlinearem Material- und zeitabhängigem Verhalten berechnet. Das Berechnungsmodell, das auf der Finiten-Elemente-Methode basiert, berücksichtigt sowohl das nichtlineare Spannungs-Dehnungsverhalten des Materials als auch die zeitabhängigen Einflüsse der Belastungsfolge, des Kriechens und Schwindens des Betons und der Relaxation des Spannstahls. Das zeitabhängige Verhalten der Brücke wird über einen Abschnitt von 27 Jahren nach der Bauwerksfertigstellung verfolgt. Das Verhalten unter Überlastung und die maximale Tragfähigheit infolge zunehmender Verkehrslasten sind für zwei Zeitpunkte innerhalb des Nutzungszeitraums der Brücke untersucht. Es wird gezeigt, dass die Brücke eine grosse Überlastkapazität besitzt.

1. INTRODUCTION

Post tensioned concrete box girders are frequently used as structural elements in modern bridge construction. Such highway structures in the United States are currently subjected to increasing truck loads and traffic densities. Design procedures, however, do not always reflect this situation. Some standard design specifications are still based on light weight trucks and outmoded bridge structure types [1]. Recent studies within the California Department of Transportation [2] have indicated a need for explicit consideration of increasing traffic loads and an improved understanding of overload behavior of modern highway structures. Such understanding is also complicated by the time dependent nature of the problem.

In this paper, a post tensioned concrete box girder highway bridge is investigated using a material and time dependent nonlinear analysis, in order to determine its response to time dependent effects and to increasing truck overloads up to ultimate failure. The objectives of the investigation were to use a special purpose finite element computer program for the material, geometric and time dependent analysis of prestressed concrete frames to (1) make a comparison of time dependent response as analytically predicted with that predicted using typical design assumptions and (2) to study the ultimate strength of the structure under increasing truck overloads, both before and after consideration of time dependent response. Results are presented which demonstrate bridge response parameters which include deflections, stresses and their resultants, and strains and curvatures, under these conditions.

2. THE ANALYSIS PROCEDURE

2.1 General

The analytical formulation used for this study has been developed by Kang [3] to trace the material and geometric nonlinear response of reinforced and prestressed concrete planar frames through the elastic, cracking, inelastic, and ultimate ranges. The formulation is implemented in the finite element computer program PCFRAME which is capable of the analysis of planar frames with arbitrary geometry, consisting of beam elements of arbitrary cross section but with a plane of symmetry common to the plane of the structure, Fig. 1. Major goals in the preparation of the computer program included the development of simple but realistic material models for the concrete and steel, their implementation in an efficient discretization of the structural system which captures the significant response of a range of structures of interest, and the development and testing of a reliable and cost effective nonlinear solution algorithm. The detailed theoretical formulation, as well as a comparison of results with those of experimental studies has been reported elsewhere by Kang [4], demonstrating the validity of the nonlinear material, geometric, and time dependent response of concrete beams and planar frames. A brief summary of the theory will be presented here.

2.2 Material Models

The constitutive relationship for concrete includes the effects of creep, shrinkage, aging, and temperature strains. Total uniaxial concrete strain $\varepsilon(t)$ at a time t is assumed to be composed of the following contributions:

$$\varepsilon(t) = \varepsilon^{m}(t) + \varepsilon^{c}(t) + \varepsilon^{s}(t) + \varepsilon^{a}(t) + \varepsilon^{T}(t) \qquad (1)$$

The mechanical strain $\varepsilon^m(t)$ is the instantaneous strain caused by the loads. The nonmechanical strain is assumed to consist of creep strain $\varepsilon^c(t)$, shrinkage strain $\varepsilon^s(t)$, aging strain $\varepsilon^a(t)$ and temperature strain $\varepsilon^t(t)$. Implicit in this formulation is the assumption that the principal of superposition is valid, and that each component of strain can be considered separately. The meanings of these strain components are shown in Fig. 2.

The stress-strain curve for concrete is assumed to be independent of the nonmechanical strain but is influenced by the change with time of the strength and initial elastic modulus of the concrete. This stress-mechanical strain curve considers unloading and reloading but does not consider dynamic cyclic effects. The following assumptions are made in the development of the stress-mechanical strain law: (1) stress is uniaxial; (2) the ascending initial curve is a parabola as proposed by Hognestad [5]; (3) unloading modulus equals the initial modulus; (4) tensile cracking occurs at a limiting value of stress; (5) compression failure occurs at a limitng value of mechanical strain; (6) once cracked, concrete can not again resist tensile stress, but can resist compressive stress upon crack closure and reloading. The resulting stress-strain curve is shown in Fig. 3, and eleven distinct material states are identified.

All concrete properties may vary with time according to the recommendations of ACI Committee 209 [6], based on the work by Branson et al. [7]. In addition, other guidelines such as those of CEB/FIP [8] or Bazant and Panula [9] may be separately input into the computer program if desired.

Creep strains are evaluated based on an age and temperature dependent integral formulation. Creep strain is expressed as a functional of stress σ according to the integral

$$\varepsilon^c(t) = \int_0^t c\left(\tau, t-\tau, T\right) \frac{\partial \sigma(\tau)}{\partial \tau} \, d\tau \tag{2}$$

in which the kernel function $c(\tau, t-\tau, T)$ is the age and temperature dependent specific creep, defined as the creep strain at time t due to a unit sustained stress applied at time τ and temperature T. This kernel is expressed as a series

$$c\left(\tau, t-\tau, T\right) = \sum_{i=1}^{3} \alpha_i(\tau) \left[1 - e^{-\lambda_i \phi(T)(t-\tau)}\right] \tag{3}$$

in which $\alpha_i(\tau)$ and λ_i are coefficients determined by a least squares fit to experimental data, or to specified empirical design curves [7,8,9], and $\phi(T)$ is a temperature shift function [10]. Nonlinear creep at high stress levels is accounted for by the concept of effective stress [11].

Shrinkage strain increments, as well as current concrete strength, are provided as program input explicitly at each stage of the analysis. Shrinkage and aging strains are evaluated on the basis of this information.

Reinforcing steel is represented by a simple bilinear nondegrading hysteretic stress-strain curve, Fig. 4. Four distinct material states can be identified: (1) primary tension or compression; (2) yielded, (3) in load reversal; (4) failed. Thermal strain is the only nonmechanical strain considered for reinforcing steel.

Prestressing steel is represented by a multilinear stress-strain curve, and is assumed to act only in tension. The load reversal modulus is assumed equal to

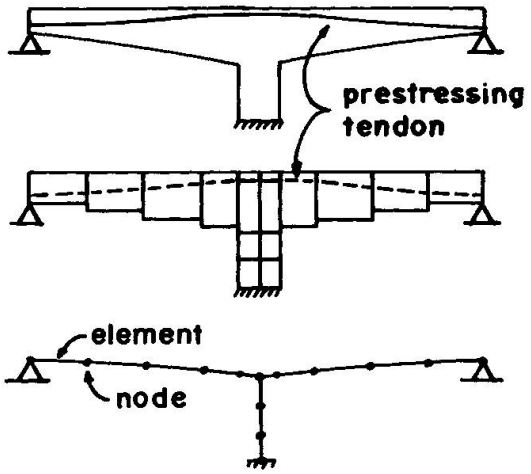

FIG. 1 ACTUAL AND IDEALIZED PRESTRESSED CONCRETE FRAME

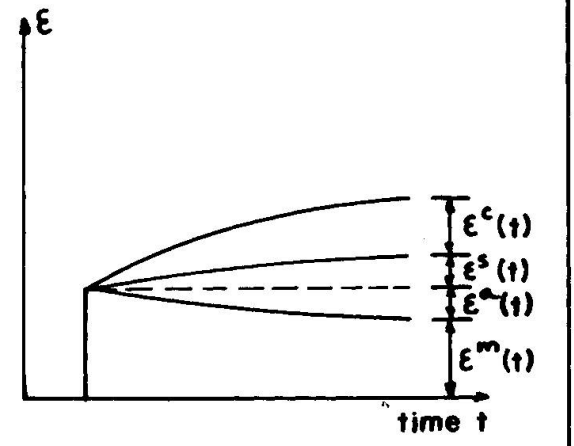

FIG. 2 STRAIN COMPONENTS OF CONCRETE

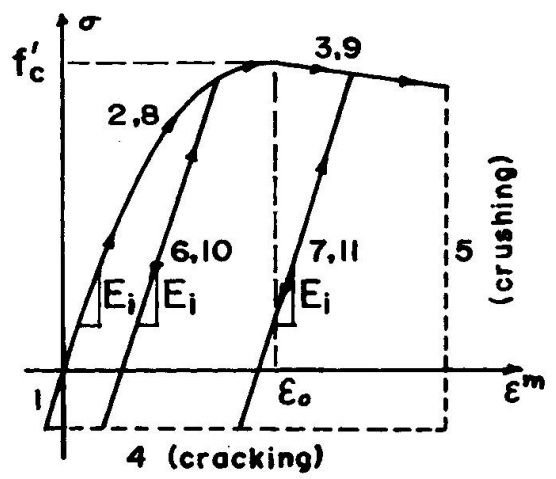

FIG. 3 STRESS-STRAIN CURVE OF CONCRETE

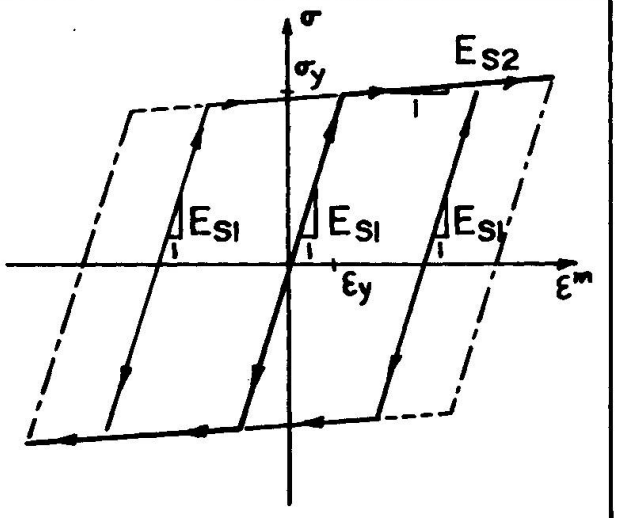

FIG. 4 STRESS-STRAIN CURVE OF MILD STEEL

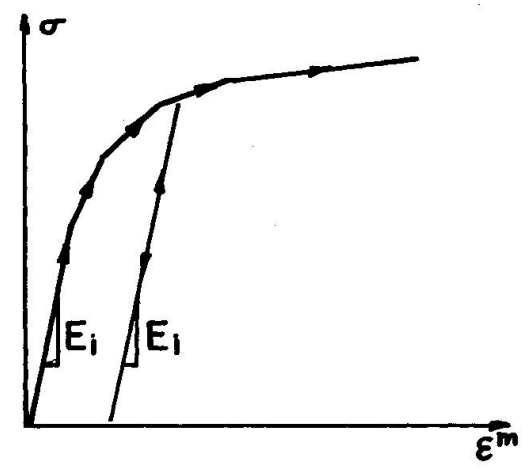

FIG. 5 STRESS-STRAIN CURVE OF PRESTRESSING STEEL

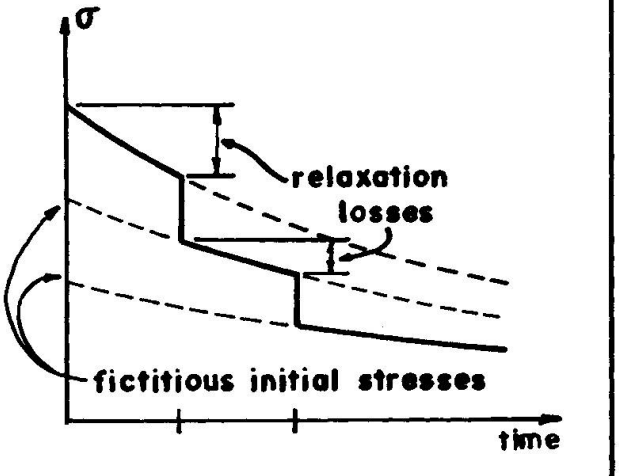

FIG. 6 STRESS RELAXATION OF PRESTRESSING STEEL

the initial modulus, Fig. 5. Stress relaxation is computed utilizing a formula developed by Magura, Sozen, and Seiss [12] and modified for time dependent strains by Hernandez and Gamble [13]. Based on the known time dependent strain variations, a fictitious initial tensioning stress is calculated so that the logarithmic relaxation curve may be applied and result in the correct current stress and relaxation rate. This is shown conceptually in Fig. 6.

2.3 Structural Model

Structural discretization is based on the displacement finite element method, in which the planar structure is idealized as an sssemblage of one dimensional beam finite elements interconnected by nodes, Fig. 1. The cross section is divided into layers, Fig. 7. Element property matrices are evaluated in local element coordinate systems, transformed to the common global system, and then assembled by the direct stiffness method. In a geometrically nonlinear analysis, the local coordinate systems are assumed to change according to the current deformed state of the structure.

The layered finite element, Fig. 7, is assumed to be prismatic, and must have an axis of symmetry in the plane of the structure. This six degree of freedom element represents the entire width and a portion of the length of the bridge girder or other structural element, thus shear lag, as well as torsion and associated warping and distortion of the box girder cross section are neglected in this study. The composite layer system consisting of a finite number of discrete concrete and steel layers is adopted to account for the varied materials and material states across the depth of an element. Each layer is assumed to be in a state of uniaxial stress, and its geometry is completely described by its area and local y-coordinate. A prestressing steel segment is defined by its end eccentricities, area, and initial force. Friction is considered in the calculation of the initial force. After bonding of a tendon, it is represented by a steel layer to account for its contribution to structural stiffness.

The displacement field within an element is developed by assuming a linear variation of axial displacements and a cubic variation of transverse displacements between the nodes. Thus the classical elementary beam functions are used. Then, adopting Navier's plane section hypothesis, the axial displacement and thus the strain in any layer may be determined. Integration of the terms in the element characteristic matrices is performed on a layer by layer midpoint rule basis over the element depth, and with three point Gauss quadrature along the element length. This and the element shape functions constrain the element to linear curvature. Nonlinear geometry effects, when included, are based on the updated Lagrangian approach.

2.4 Time Dependent Nonlinear Analysis Procedure

The time dependent nonlinear analysis is performed by dividing the time domain into a discrete number of time steps, and discretizing the load, temperature, and shrinkage history accordingly. Then a step forward integration is performed in which incremental solutions are superposed to obtain the current solution. To progress from a solution at time t_{n-1} to time t_n, the nodal load increment is summed from the equivalent loads due to nonmechanical strains, the external joint load increment, and the unbalanced load left over from previous steps. The nonlinear equilibrium equations are solved for this load vector based on an incremental load technique combined with tangent stiffness iteration. Three criteria are used for termination of iteration: (1) unbalanced load tolerance, (2) incremental displacement ratio tolerance, and (3) maximum number of iterations. Output may be printed at each iteration, or only at the end of iteration within the load increment. At the end of the last load increment for

a given time step, the procedure continues to the next time step, or else terminates.

3. DESCRIPTION OF THE BRIDGE STRUCTURE

3.1 Structural Design

The bridge structure considered in this investigation, Fig. 8, is a three span, straight, continuous, post tensioned single cell box girder. Its span arrangement is 48.8 m, 61 m, 48.8 m (160 ft, 200 ft, 160 ft) and its roadway width is 10.4 m (34 ft). Cast-in-place construction is assumed to proceed for the entire structure simultaneously. This is typical for a moderate span two lane highway bridge built in California. Simple support conditions are assumed at the ends of the structure, and vertical bearing supports (not monolithic construction) are assumed at the intermediate columns.

For the sake of simplicity the cross-section, Fig. 8, is assumed constant from end to end of the structure, although design practice often calls for thickening of the bottom slab or the webs in regions near supports. The top slab design is based on the use of transverse post tensioning, although its effects are not considered in this analytical investigation. For ease of discretization of the box girder section into the discrete layer system required for the nonlinear analysis, the top and bottom slabs have been simplified to the uniform thicknesses shown.

Structural design of the girder is based on State of California standard criteria. Concrete strength, mild steel strength, and post tensioning strand strength are assumed to be 27.6 MPa (4000 psi), 413.7 MPa (60,000 psi), and 1861.7 MPa (270,000 psi) respectively. Post tensioning force is proportioned on the basis of a traffic load consisting of a chain of 320 kN (36 ton) trucks in each lane, an impact factor based on span length, and no tension allowed in the concrete after all prestressing force losses have occurred. A total of 8, 31 strand tendons are required, for a total steel area of 244.8 cm^2 (37.94 in^2). Ultimate strength load factor design additionally considers the overload of a 952 kN (107 ton), 33 m (108 ft) long permit vehicle with 13 axles. Mild steel reinforcement, having a total area of 542 cm^2 984 in^2) was uniformly distributed over the cross section. This steel, not required for strength is provided for construction purposes.

3.2 Finite Element Model

For the purpose of this analysis, the bridge is divided into 16 elements, making use of symmetry so that only one half of the length of the bridge is considered. The finite element mesh is shown in Fig. 9.

The cross section is discretized into ten concrete layers as shown in Fig. 10. Since torsion is not considered in the planar frame analysis, the two webs of the box girder are combined into one web with six layers in the model. The top and bottom slabs are each divided into two layers so that partial cracking or crushing can be traced.

This model is utilized to study both the time dependent behavior and the overload behavior of the bridge structure. The time dependent analysis traces the response of the bridge from its initial prestressing through a period of 27 years. The effects of variation of time step size, and the influence of the presence of nominal mild steel reinforcement are studied. Time dependent variation of deflections, curvatures, moments, and stresses as well as prestressing forces are traced. The ultimate load analysis traces the response of the bridge

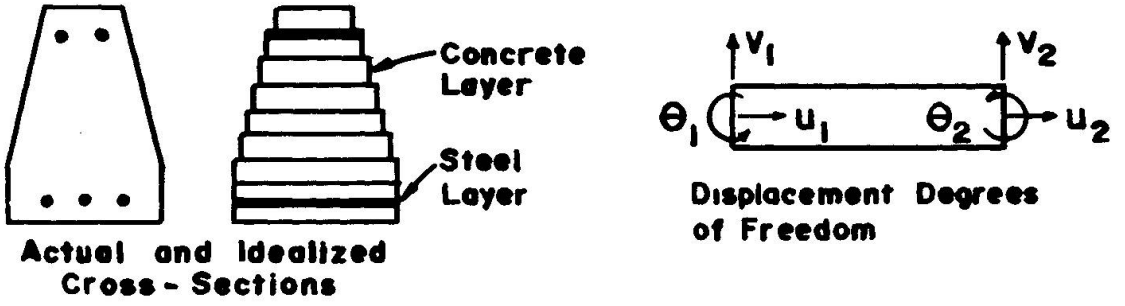

FIG. 7 LAYERED PLANAR BEAM FINITE ELEMENT

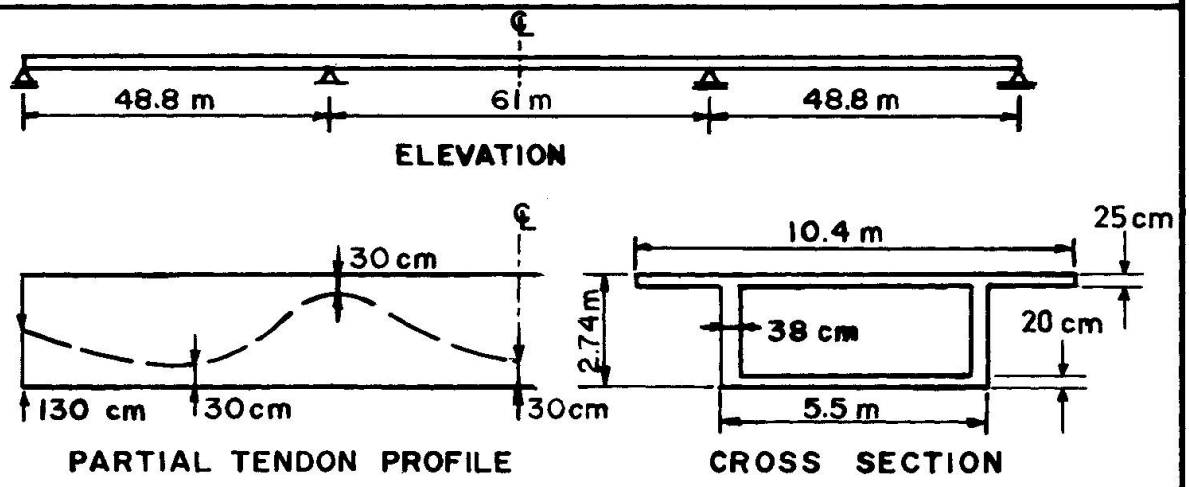

FIG. 8 CONTINUOUS POST TENSIONED CONCRETE SINGLE CELL BOX GIRDER BRIDGE

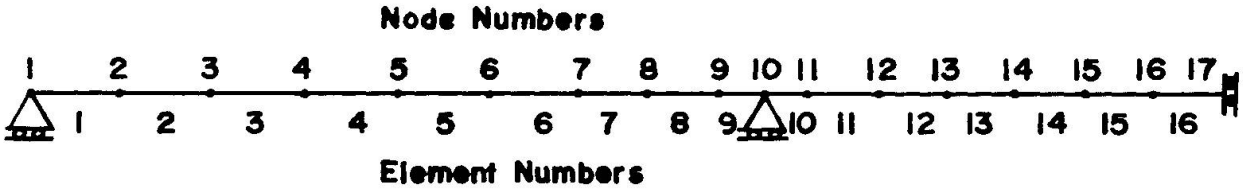

FIG. 9 FINITE ELEMENT MESH OF BRIDGE GIRDER

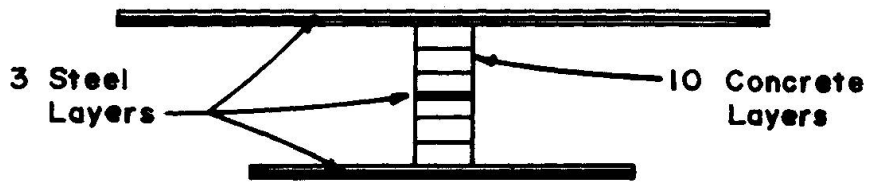

FIG. 10 CROSS SECTION DISCRETIZATION

under increasing loads in the pattern of the California standard overload vehicle previously described. Response curves are presented for increasing loading to ultimate both early in the life of the structure, and after 27 years of time dependent effects have taken place.

4. TIME DEPENDENT ANALYSIS

4.1 Description of Problem

A time dependent analysis of the bridge was performed to determine its response over a 10,000 day (27 year) period with initial loading at 28 days. Intermittent live loads are assumed to play an insignificant role in the time dependent behavior of the structure, therefore the self weight of the girder, and additional dead load due to concrete guard rails, etc. are the only external loads applied to the analytical model. Prestressing is included, considering friction and anchor set losses, generated within the program. Two analytical models are considered, one neglecting the nominal mild steel construction reinforcement, the other including this steel in three discrete layers.

The 10,000 day time period is divided into eight time steps in order to trace the variation of response with time and to provide a basis for a precise solution with the previously described algorithm. The relative lengths of the unequal time steps were chosen in order for creep strains to be of similar magnitude in each time step. Initial creep strain rates are high, so time steps during this period are quite short. Later time steps are made quite long with little or no effect on the solution. Time step size and the creep function are shown in Fig. 11. Longer initial time steps significantly changed the computed response due to the rapid change in the creep function in this time period. Further refinement of the time step size had only a small effect.

Material properties are assumed to be time invariant, thus aging strains are neglected. Strength and initial elastic modulus are taken as 27.6 MPa (4000 psi) and 24856 MPa (3605000 psi) respectively, in accordance with ACI recommendations [6]. An ultimate creep coefficient of 2.5 and ultimate shrinkage strain of 0.001 are utilized, based on a dry climate. Shrinkage is taken as uniform across the depth of the girder.

4.2 Results for Displacement

Figures 12, 13 and 14 present the time variation of displacement response at several locations along the girder. In each figure, response is shown for the two different structural models, one including the nominal mild steel reinforcement, the other neglecting this steel. Time variation of vertical displacement at the middle of the center span of the bridge (Fig. 12), horizontal displacement at the interior support (Fig. 13), and rotation of the interior support (Fig. 14) all show similar trends. Notably evident is the significantly stiffer response of the model including the nominal mild steel reinforcement, both in terms of initial displacement as well as increase in displacement with time. The stiffer initial response agrees well with predictions from an elastic beam theory analysis, based on gross section properties or transformed section properties respectively. Additionally, the model including nominal mild steel reinforcement shows a ratio of 10000 day displacement to initial displacement which is about 20 to 25 percent lower than that for the model without mild steel reinforcement, depending on the displacement component considered. The decrease in creep and shrinkage strain rate as time progresses is also evident in these figures. Displacement increases by a factor of about 3 within the first 100 days, while at 10000 days the response has levelled off so that little additional displacement occurs.

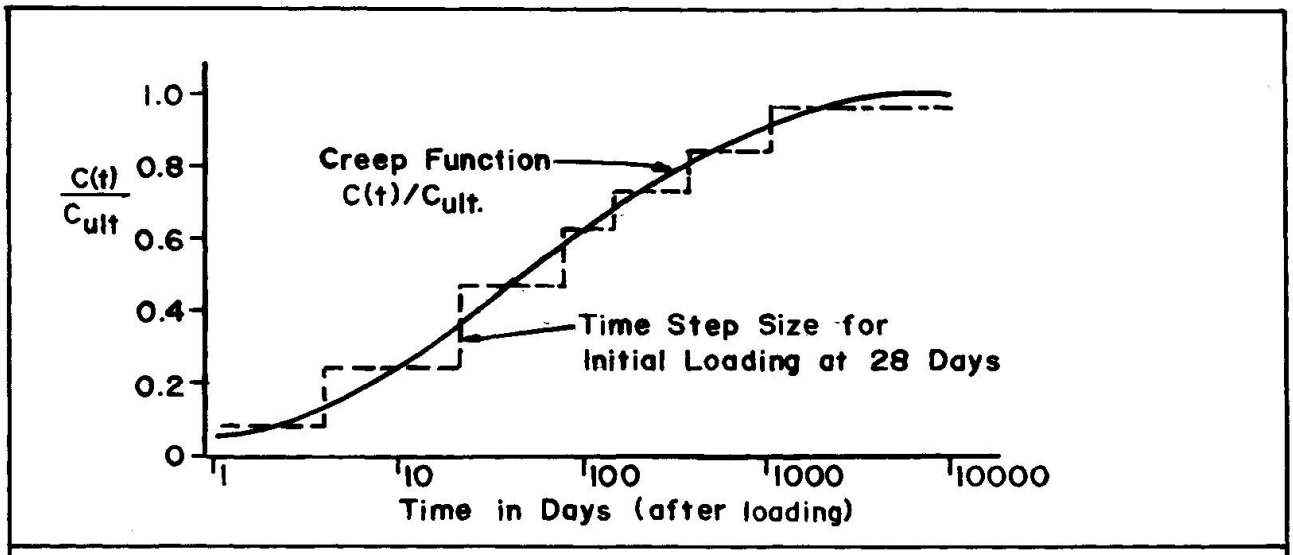

FIG. 11 CREEP FUNCTION AND TIME STEP SIZE

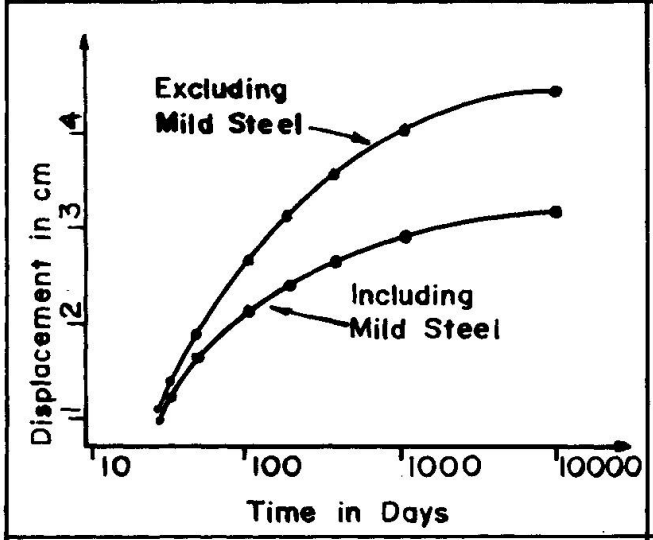

FIG. 12 VERTICAL DISPLACEMENT AT CENTER SPAN VS TIME

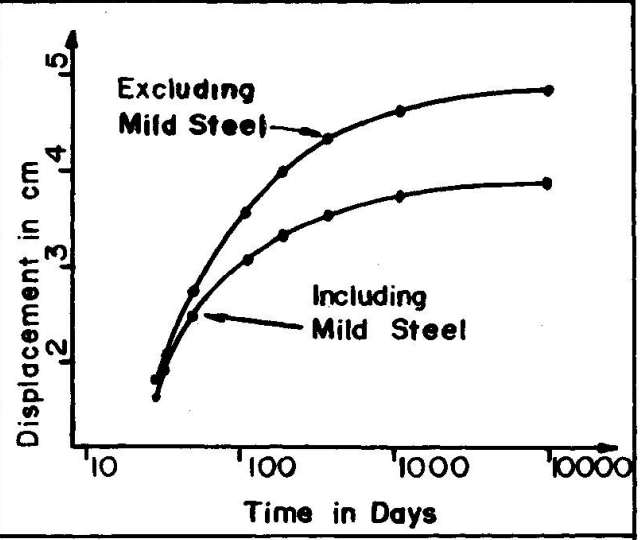

FIG. 13 HORIZONTAL DISPLACEMENT AT INTERIOR SUPPORT VS TIME

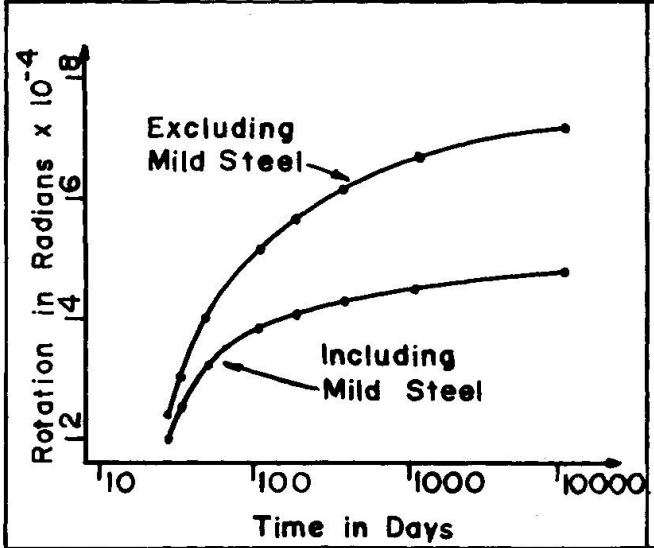

FIG. 14. ROTATION AT INTERIOR SUPPORT VS TIME

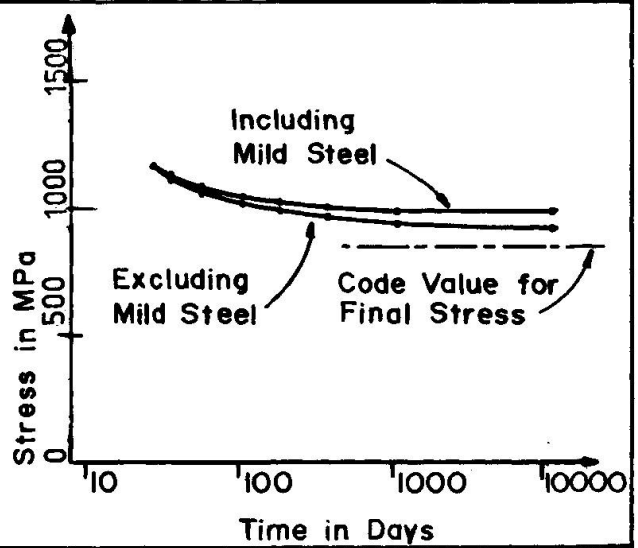

FIG. 15 TENDON STRESS AT CENTER SPAN VS TIME

4.3 Results for Prestressing Tendon Stress

Figure 15 shows variation of stress in the post tensioning strand with time, for the bridge model including nominal mild steel reinforcement as well as the model neglecting this steel. Comments pertaining to the displacement response are also applicable to this stress variation with time: most of the stress loss occurs within the first 100 days, and after 10000 days, little additional loss occurs. The figure also shows the significant discrepancy between the losses predicted by this analysis and those arrived at through AASHTO design specification [1] procedures. The finite element analysis predicts losses 25 and 40 percent lower than the AASHTO procedure, respectively, for the model without and with mild steel reinforcement. This is probably because the design specification is based on an extrapolation of data from shorter time periods and is intended to be a conservative guide to design.

4.4 Results for Curvatures

Figure 16 depicts the change in curvatures with time along the half length of the prestressed bridge model without mild steel reinforcement. Trends here are again similar to those in the displacement response: curvatures increase much more between 28 days and 300 days than in the period between 28 days and 10000 days. Note that the points of zero curvature (inflection points) move with time. Since the girder stresses remain in the elastic range throughout the time period, and since the loads on the girder do not change, the change in the distribution of curvature along the span can be attributed to the variation in loss of prestress. This is of only minor significance in the overall response.

4.5 Results for Moments

The moment diagram along the half length of the bridge is shown in Fig. 17. Moments shown include those due to applied dead load plus the so-called "secondary" prestressing moments. "Primary" prestressing moments are not included. There is only a very small redistribution of moment during the time period considered, with a slight shift of the total static moment away from the center of each span toward the interior support. This is due to the net reduction in prestressing force, and the associated reduction of the "secondary" moment.

4.6 Summary for Time Dependent Analysis

The results of this material and time dependent nonlinear analysis are in general agreement with the observed behavior of continuous post tensioned concrete box girder bridges. Time dependent deformations occur rapidly in the early stages of the history of the bridge, and then decrease markedly after several years. The presence of mild steel reinforcement stiffens the bridge, restrains creep and shrinkage deformations and reduces the associated loss of prestress. Curvatures increase in a fairly uniform fashion over the length of the girder, so that the final deflected shape of the structure is similar to the initial deflected shape, but with a greater magnitude. Prestressing losses are predicted in this time dependent and material nonlinear analysis to be smaller than the estimate of the design specification, but this does not adversely effect the safety of the structure.

5. OVERLOAD ANALYSIS AND LOADING TO ULTIMATE FAILURE

5.1 Description of Problem

In order to study the response of the bridge girder to increasing load levels up to ultimate failure, the analytical model of the bridge was subjected to

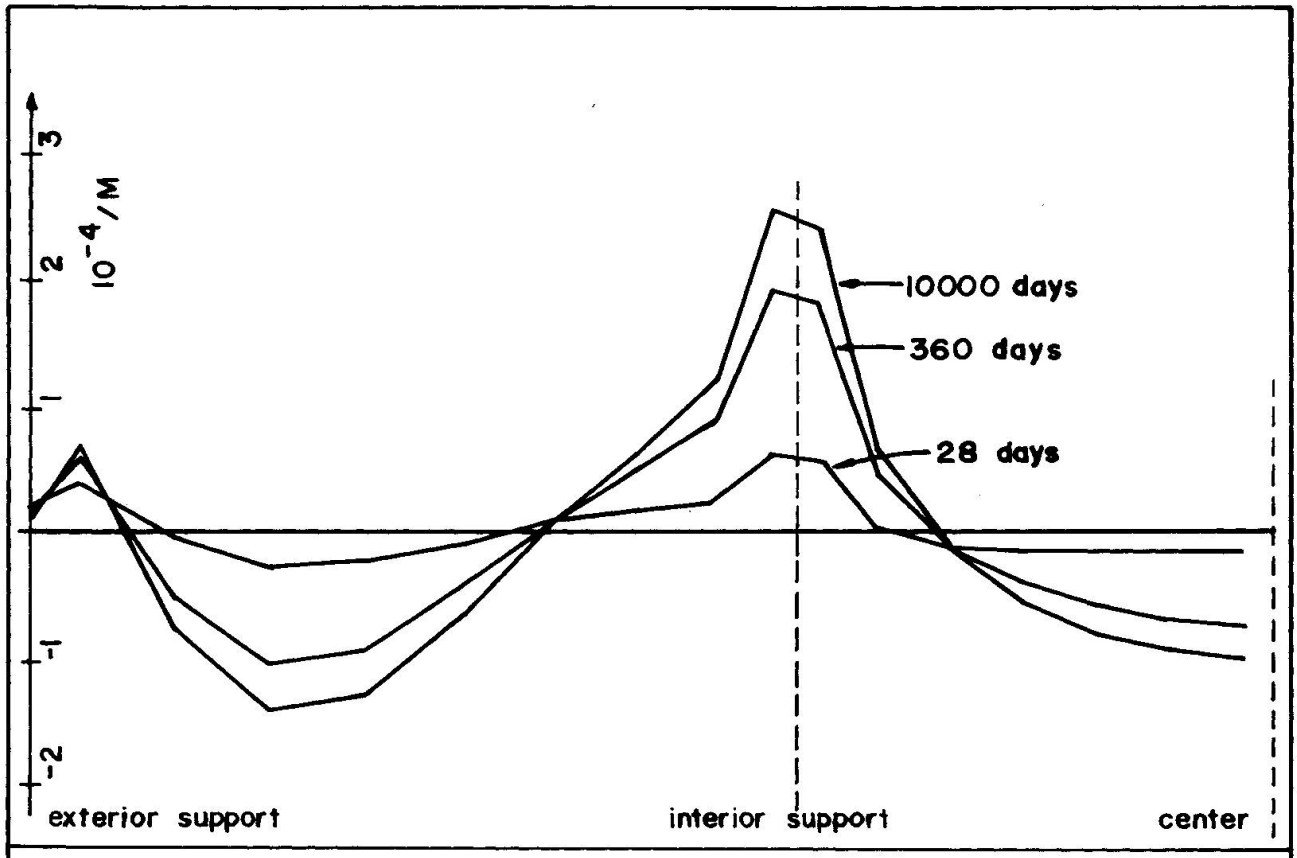

FIG. 16 CHANGE WITH TIME OF CURVATURES ALONG THE SPAN

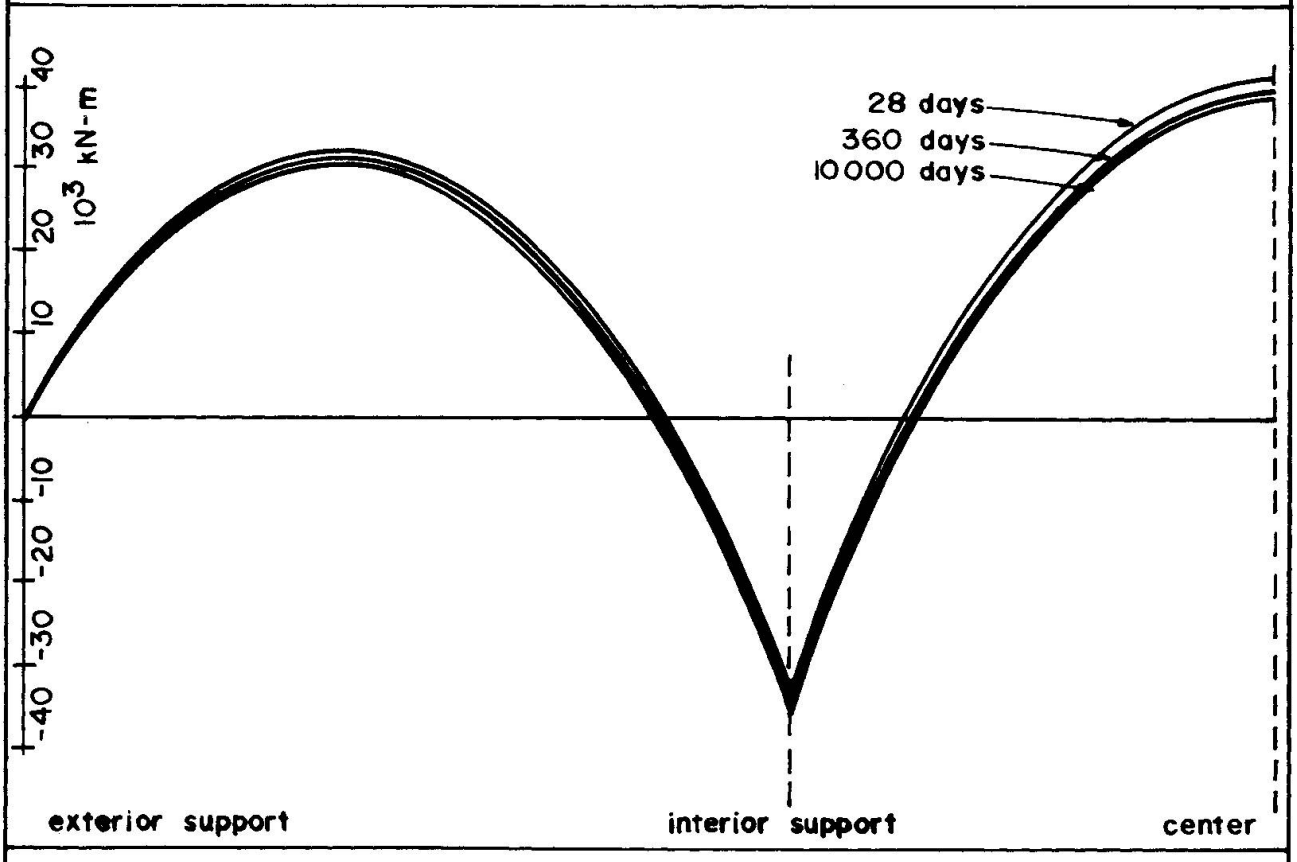

FIG. 17 CHANGE WITH TIME OF MOMENTS ALONG THE SPAN

increasing levels of vehicle overload up to ultimate failure. This analysis was carried out at two different times in relation to the time dependent analysis, once early in the history of the structure (30 days) and again late in its history (10000 days). Each analysis considers a structure previously not subjected to high overload levels. Overall response of the girder at the two loading ages proved to be quite similar, however certain differences were identified.

The overload vehicle used as a basis for the input to the analysis is typical of the heaviest vehicles found on California highways. A special road use permit is required before the vehicle is allowed on a highway, and it must travel at reduced speed. Total length of the vehicle is 33 m (108 ft), total weight is 952 kN (107 tons) and it is carried by 13 axles. In this overload analysis the truck is positioned in the middle of the center span of the bridge, and the structural load vector due to its weight is incremented until ultimate failure occurs.

The nominal mild steel reinforcement considered in the time dependent analysis is not considered in this analysis. Its ultimate capacity is very small compared with that of the post tensioning and concrete, since it is provided for construction purposes and its area is very small. The various stages of overload response are only slightly affected by the presence of this steel, and are more readily identified when it is neglected.

Multiples of the load due to one overload vehicle are incrementally applied to the analytical model in order to trace its response up to ultimate failure. At small overload levels the response of the structure is very nearly linear, so that the load increments are equal to the load due to one overload vehicle. When the total load is near the ultimate capacity of the structure, its response becomes increasingly nonlinear so that a smaller load increment equal to one fifth of the load due to one vehicle is used. This is evident in the following figures.

5.2 Results for Displacements

Figure 18 shows vertical displacement response at the center of the main span under increasing overload, for loading at both 30 days and 10000 days. The curves are of similar shape, however the structure is slightly stiffer when loaded at 30 days than when loaded at 10000 days. This is a result of the reduction in prestressing force due to time dependent effects, and the resulting decrease in cracking load of the bridge. The large overload capacity of the bridge is clearly evident in this figure. Even though service load design of the bridge is based on a load smaller than that due to one overload vehicle, so that this vehicle overstresses portions of the bridge, ultimate failure occurs at a load equal to Dead Load plus about 7.2 times the load due to one vehicle. This ultimate load level does not vary significantly with time. Simple analysis methods can be used to arrive at upper and lower bounds on the ultimate load. A lower bound solution, based on an inelastic analysis of the cross section and an elastic analysis of the girder, results in an ultimate load estimate of Dead Load plus 5 times the load due to one vehicle. An upper bound solution, based on an inelastic analysis of the cross section and an inelastic analysis of the girder assuming large plastic hinge rotation capacities, results in an ultimate load estimate of Dead Load plus 8 times the load due to one vehicle. The computer solution predicts an ultimate load capacity between these two values.

Figure 19 depicts horizontal displacement of the bridge at the interior support under increasing vehicle overload. Note that as the vehicle load increases, the center span of the bridge increases in length, due to increasing tensile strains over a large portion of the girder depth. Initial cracking loads may be identified in this figure as the load at which the response curve first becomes nonlinear: at Dead Load plus about 3 times the load of one vehicle when loaded

at 30 days, and at Dead Load plus about 2 times the load of one vehicle when loaded at 10000 days.

5.3 Results for Prestressing Tendon Stress

Figure 20 plots tendon stresses at two critical locations along the girder under increasing vehicle overload. Response is shown only for loading at 30 days. Loading at 10000 days results in curves that are similar but shifted slightly. The initiation of cracking at the critical locations is readily identified in this figure. After Dead Load plus 3 times the load of one vehicle, cracking is initiated at the center of the main span, resulting in a large increase in tendon stress at that location. After Dead Load plus 5 times the load of one vehicle, cracking is initiated over the interior support, resulting in a similarly large increase in tendon stress at that location, and a further increase in tendon stress at center span due to a redistribution of moment. Tendon stress continues to increase under increasing overload until ultimate failure of the bridge occurs due to rupture of the tendons at the center of the main span.

5.4 Results for Cross-Section Stress Distributions

Figure 21 shows stress distributions across the depth of the bridge girder at center span and at the interior support under loading to failure at 30 days. Almost all stages of structural response can be identified in this figure. The stress distribution at each location is almost linear up to a load of Dead Load plus 3 overload vehicles. Then cracking occurs at center span, the neutral axis at that location shifts upwards, and stresses increase significantly at the interior at the interior support. After a load of Dead Load plus 5 vehicles, cracking occurs over the interior support, and both sections start to respond inelastically. Further loading causes the compressive forces to be localized in the flanges of the girder, particularly at center span, until the structure fails due to rupture of the prestressing steel. The concrete never reaches its crushing strength, since in this structure with a relatively small area of prestressing steel, the steel yields first.

5.5 Summary for Overload and Ultimate Load Analysis

This nonlinear analysis demonstrates that this bridge has a large time invariant overload capacity and an ultimate failure mechanism of the same type as predicted by a typical designer's analysis. During loading to ultimate failure the individual critical cross sections of the girder experience significant inelastic deformations. Therefore the ultimate load level is higher than that predicted by present design methods used in the United States in which redistribution of moment along the length of the bridge is neglected. Thus this fully prestressed bridge designed according to standard specifications has a high overload capacity.

6. SUMMARY AND CONCLUSIONS

A nonlinear material and time dependent analysis of a three span continuous post tensioned concrete box girder bridge has been presented. The special purpose finite element computer program PCFRAME, for the nonlinear and time dependent analysis of prestressed concrete frames, was used to obtain the numerical solutions. The time dependent response of the structure was studied over a time period of 10000 days (27 years) from the time of construction. Prestressing losses were shown to be significantly lower than predicted by conventional methods. Overload response up to ultimate failure was studied both before and after the passage of time, demonstrating that the structure has a large time

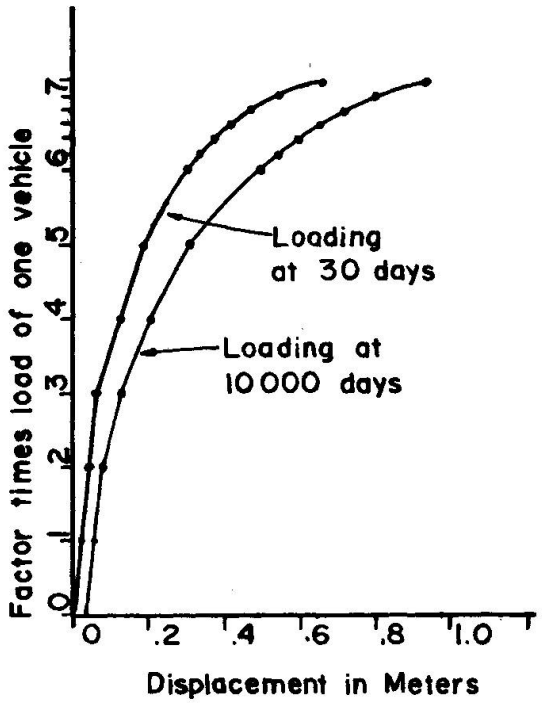

FIG. 18 VERTICAL DISPLACEMENT AT CENTER SPAN UNDER OVERLOAD

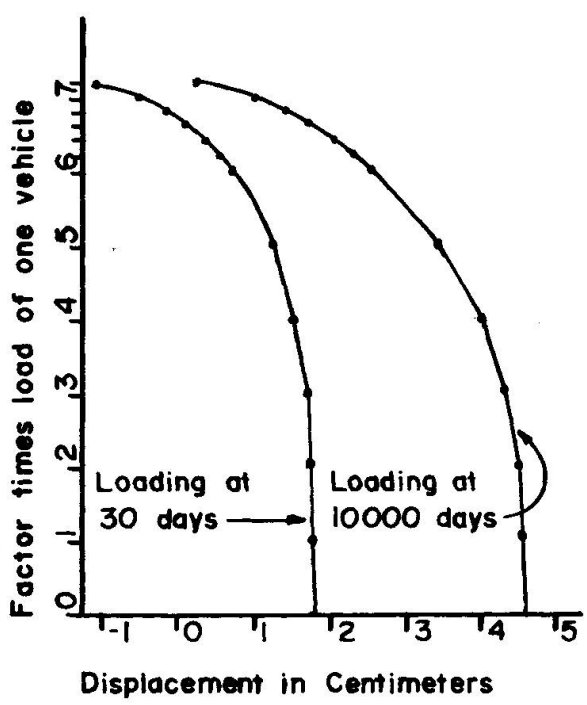

FIG. 19 HORIZONTAL DISPLACEMENT AT INTERIOR SUPPORT UNDER OVERLOAD

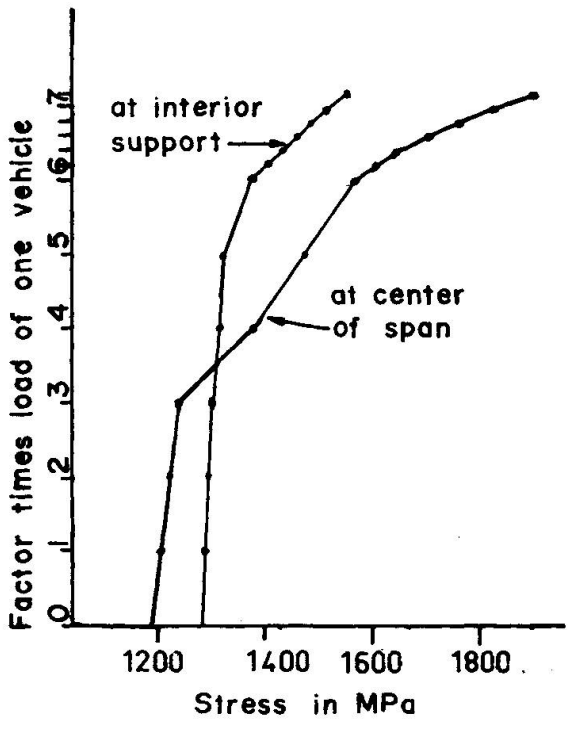

FIG. 20 TENDON STRESS AT CRITICAL SECTIONS UNDER OVERLOAD

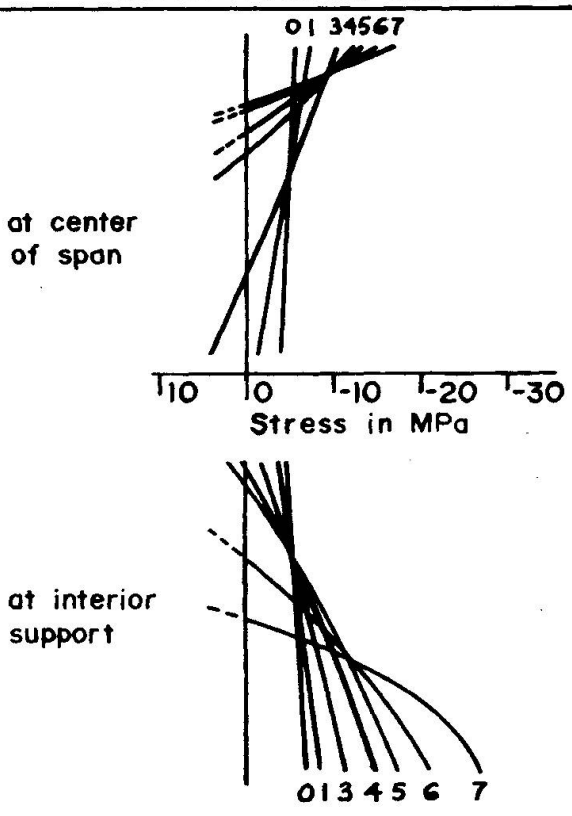

FIG. 21 STRESS DISTRIBUTION AT CRITICAL SECTIONS UNDER OVERLOAD

invariant overload capacity. Conventional methods of estimating ultimate capacity were shown to provide reasonable bounds on the total load capacity of the bridge.

Additional developments in the material, geometric, and time dependent analysis of concrete bridge structures considering segmental construction schemes as well as the three dimensional nature of the box girders are currently being carried out.

ACKNOWLEDGEMENTS

This research was partially sponsored by the U. S. National Science Foundation by Grant No. CME 7918057. The Computer Center of the University of California, Berkeley, provided the facilities for the numerical work.

REFERENCES

1. Standard Specifications for Highway Bridges, 11th Edition, American Association of State Highway and Transportation Officials, Washington, D.C., 1977.

2. CASSANO, R. C., LE BEAU, R. J., "Correlating Bridge Design Practice with Overload Permit Policy," Transportation Research Record 664, National Research Council, Washington, D.C., 1978.

3. KANG, Y. J., "Nonlinear Geometric, Material, and Time Dependent Analysis of Reinforced and Prestressed Concrete Frames," thesis presented to the University of California, Berkeley, in 1977, in partial fulfillment of the requirements for the degree of Doctor of Philosophy in Civil Engineering.

4. KANG, Y. J., SCORDELIS, A. C., "Nonlinear Analysis of Prestressed Concrete Frames," Journal of the Structural Division, ASCE, Vol. 106, No. ST2, Proc. Paper 5886, Feb. 1980.

5. HOGNESTAD, E., "A Study of Combined Bending and Axial Load in Reinforced Concrete Members," University of Illinois Engineering Experiment Station, Bulletin Series No. 399, Bulletin No. 1, 1951.

6. ACI Committee 209 (Chaired by D. E. Branson), "Designing for Effects of Creep, Shrinkage, and Temperature, ACI-SP27, American Concrete Institute, Detroit, 1971.

7. BRANSON, D. E., CHRISTIASON, M. L., "Time-Dependent Concrete Properties Related to Design Strength and Elastic Properties, Creep, and Shrinkage," SP-27, Designing for Effects of Creep, Shrinkage, and Temperature, American Concrete Institute, Detroit, 1971.

8. CEB-FIP Model Code for Concrete Structures, Commité Eurointernational du Béton-Fédération Internationale de la Précontrainte, CEB Bulletin No. 124/125-E, Paris, 1978.

9. BAZANT, Z. P., PANULA, L., "Creep and Shrinkage Characterization for Analyzing Prestressed Concrete Structures," PCI Journal, May/June 1980.

10. MUKADDAM, M. A., BRESLER, B., "Behavior of Concrete under Variable Temperature and Loading," ACI SEminar on Concrete for Nuclear Reactors, ACI-SP27, American Concrete Institute, 1972.

11. BECKER, J., BRESLER, B., "FIRES-RC, A Computer Program for the Fire Response of Structures-Reinforced Concrete Frames," Report No. UCB FRG 74-3, University of California, Berkeley, August 1974.

12. MAGURA, D. D., SOZEN, M. A., SIESS, C. P., "A Study of Stress Relaxation in Prestressing Reinforcement," PCI Journal, Vol. 9, No. 2, April 1964.

13. HERNANDEZ, H. D., GAMBLE, W. L., "Time Dependent Prestress Losses in Pretensioned Concrete Constructions," Structural Research Series No. 417, Civil Engineering Studies, University of Illinois, Urbana, May 1975.

Partially Prestressed Concrete Beams under Pure Bending

Poutres partiellement precontraintes en flexion pure

Teilweise vorgespannte Träger in reiner Biegung

MICHEL LORRAIN MICHEL PINGLOT RIDWAN SUHUD
Professeur Maître-Assistant
Laboratoire de Génie Civil de l'U.P.S. et de l'I.N.S.A.
Toulouse, France

SUMMARY
Prestressing permits economical design of structures, particularly when the live loads attain a high level. Some lack of knowledge, however, still exists, especially about the permissible crack-width. A series of tests was carried out in order to obtain more information in this field. The beams were tested in pure bending; they had ractangular cross-sections and were prestressed by pretension at variable reates.

RÉSUMÉ
La précontrainte des structures en béton permet d'obtenir des éléments économiques, surtout dans le cas où les charges variables sont élevées. Cependant, cette technique n'est pas toujours utilisée au mieux de ses possibilités en raison des incertitudes qui subsistent sur son comportement, principalement de la fissuration que l'on doit accepter. Nous avons effectué des essais permettant de préciser ce comportement en flexion pure, dans le cas de poutres de section rectangulaire, précontraintes à des degrés divers à l'aide de fils adhérents.

ZUSAMMENFASSUNG
Die Vorspannung von Betonkonstruktionen wird nicht den Möglichkeiten entsprechend voll benutzt wegen der Unsicherheit, die über ihr Verhalten besteht, vor allem was die Rissbildung betrifft. Wir haben Versuche angestellt, bei denen wir das Verhalten bei reiner Biegung bestimmen, im Falle von Trägern mit rechteckigem Querschnitt bei gleichem Bruchmoment, aber verschieden stark vorgespannt.

INTRODUCTION

An experimental research program on the behaviour of partially prestressed beams with rectangular shaped cross section has been undertaken [1] [2]. This paper presents the results obtained under pure bending of such beams prestressed by pre-tension.

In the case of pre-stressing by post-tension, important economies can be made by replacing the wires with their casings and anchorages with ordinary reinforcing bars.

In the case of prestressing by pre-tension, the savings are essentially due to the simplification of the design because the prestress forces, when the beam is unloaded, are lower. Besides, the pre-tension technique permits to submit the prestressed beams to alternate bending and, consequently, it makes easier the design of continuous beams loaded with heavy mobile loads (rolling loads particularly). This process moreover seems to be properly fitted for seismic effects.

1. TESTING PROGRAM

1.1. Characteristics of the beams

The characteristics and dimensions of the tested beams are schematically shown in figure n° 1 and table n° 1.

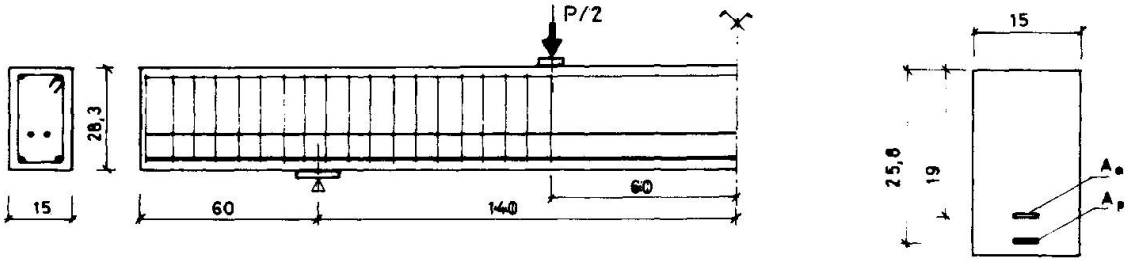

Figure 1

Nbr beam	prestressing rate P %	A_a cm^2 prestressed reinf.	A_p cm^2 ordinary reinf.
A	0	0	5,08
B	40	1,0	3,14
C	60	1,5	2,26
D	80	2,0	1,0
E	100	2,5	0

Table 1

Table n° 1 indicates for each beam :

- the cross-section of the prestressing steel, A_a,
- the cross-section of the ordinary reinforcing bars (hardened high-bond steel, type TOR), Ap,
- the rate of prestressing defined as the part of the failure bending moment equilibrated by the prestressing steel only.

The elastic conventional limit stress of ordinary reinforcing steel is equal to 412 MPa , the one of prestressing steel equals 1470 MPa. The corresponding actual mean values are, respectively, 460 MPa and 1520 MPa.

The mean strength of concrete in compression was equal to 43,5 MPa, the mean strength in pure tension was equal to 33 MPa and the ultimate compressive strain was $2,5\ 10^{-3}$.

The beams were prestressed after 14 days hardening, the loading tests were performed on the 28 th day.

1.2. Loading program

The beams were submitted to a four points bending. The loads were applied in two successive steps :

- from zero to the service-load for flexure (P = 7 500 daN)
- from the service-load to the failure with a constant deflection-rate (0,2 mm/mn).

1.3. Measurements

The strains on the upper fiber of the beam were measured with inductive transducers (active length 0,10 m ; total length of measurement area 0,40 m). The same process was used before cracking on the lower fiber.

After cracking, the mean deformation of the reinforcing unstressed bars, was obtained with transducers placed in the center of uncracked blocks. The width of the cracks was measured with other transducers placed over the crack-lines.

The deflection and edge-rotations were also recorded during the loading test.

The position of the cracks was detected as soon as they appeared by the aid of a microscope with magnifying power varying from 10 to 100.

1.4. Initial strains

The initial strains developing in the concrete and the bars during the hardening have been determined owing to the measurement of the deformation of the beams since the unmoulding. We have calculated the stresses in the concrete and in the reinforcement from the so obtained strains. The results are shown in table n° 2.

Beam P %	Lower fiber stress daN/cm^2	Upper fiber stress daN/cm^2	Ordinary bars stress daN/cm^2	Prestressing bars stress daN/cm^2
A (0 %)	- 6	+ 2	+ 147	-
B (40 %)	+ 38	+ 6	+ 647	- 11150
C (60 %)	+ 68	+ 5	+ 768	- 11190
D (80 %)	+ 96	+ 4	+ 1110	- 10910
E (100 %)	+ 130	0	-	- 10860

Table 2

(Compressive stresses are considered as positive)

2 - STRAIN STATE AT SERVICE LOAD STAGE

2.1. Theoretical calculation

The theoretical calculation of strains has been performed for a cracking cross-section. The results were then corrected to take into account the effect of the uncracked stretched concrete between the crack-lines. This first calculation assumed the Navier's hypothesis and a perfect bond between steel and concrete. We have also assumed that cracks appear when the tensile stress of concrete reaches its tensile strength. The elastic modulus in compression was choosen in correlation with the stress level, as the secant modulus.

The values of the strains were then corrected according to the CEB-FIP Model Code [3] which allows to take into account the decrease of the strain due to the existence of stretched concrete between the crack-lines.

2.2. Comparison between theoretical and experimental results

It appears that before cracking the experimental and theoretical values of strains are almost equal. Beyond, experimental strains are slightly higher than the calculated ones. It is essentially a creep-effect because we have waited ten minutes before measuring the strains at each step of loading, to let the deformation of concrete be stabilized. On the contrary the experimental strains in the rods are lower than the theoretical values, even after correction, as shown on figures n° 2, 3, 4 and 5. The difference between the experimental and theoretical values of strains in the rods tends to vanish when the load increases. This difference seems to be due to under-estimation of the effect of the stretched concrete at the casing of the rods and at the

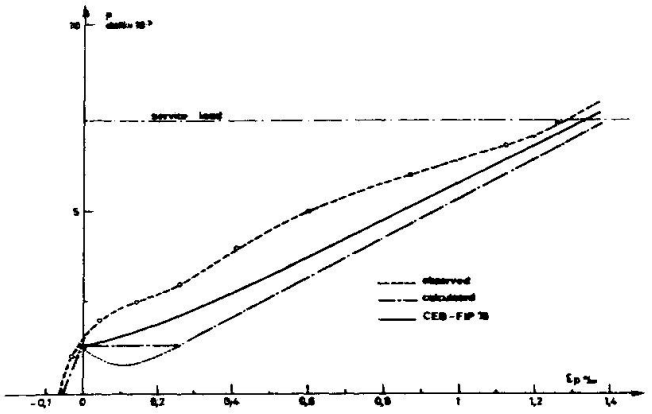

Figure n° 2
beam A

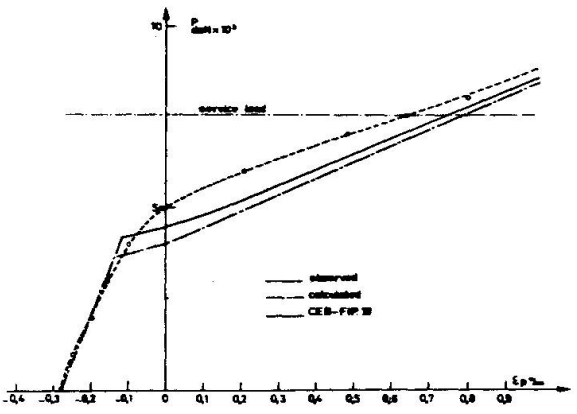

Figure n° 3
beam B

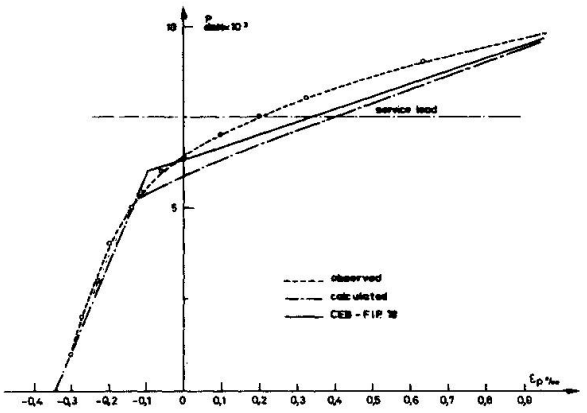

Figure n° 4
beam C

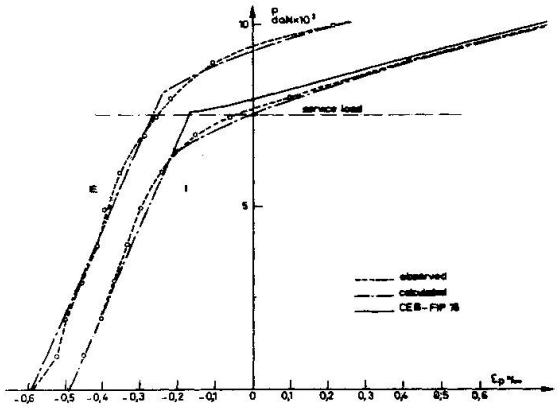

Figure n° 5
beam D and beam E

Figures 2, 3, 4, 5 – Ordinary renforcement stresses

crack-tips. Other authors [4] assume indeed that in that last case the stretched concrete could be submitted to high unelastic strains without cracking.

In conclusion, the calculation of curvatures from theoretical values of strains in a cracking cross-section, after the CEB-FIP Model Code correction, gives a very satisfactory approximation of the experimental actual values. In the case of totally reinforced beams and under low loads, there still exists a higher gap.

2.3. Comparison of the behaviour of beams with different prestressing rates.

As shown on figure n° 6 the curvatures of the beams decrease strongly when the prestressing rate increases. So, at the service load, the curvature of the beam totally reinforced is almost 2,5 higher than the one of the totally prestressed beam. For a prestressing rate of 40 % there is no very appreciable improvement. For 60 % and especially 80 % the beams get an interesting stiffness. In this last case, indeed, we can see that the curvatures of beams D (80 %) and E (100 %) are almost equal till a load level in the neighbourhood of 90 % of the service load, without noticeable change beyond this load level. As the service load P is scarcely reached and as the area in which the bending moment would be higher than 0,9 x service moment is probably very small, it does not seem necessary to prestress the beams beyond a rate equal to 80 %. A rate lower than 60 %, on the contrary, does not seem to be sufficient.

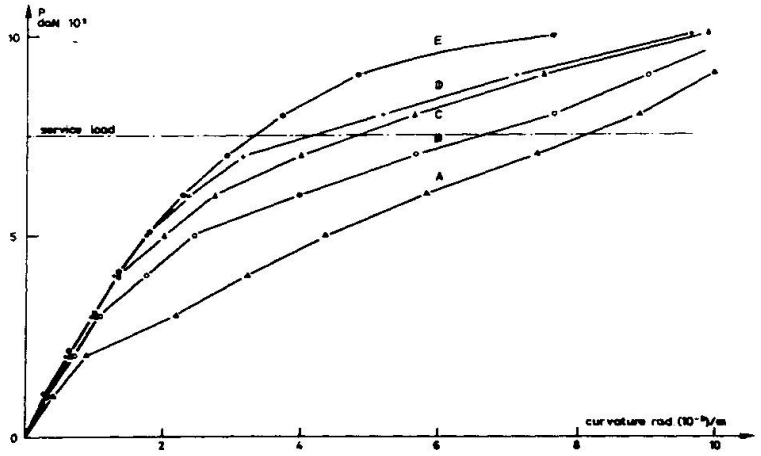

Figure n° 6
Curvature of beams versus prestressing rate

3. CRACKING CONDITIONS

3.1. Cracking bending moment

The formation of cracks appears as a sudden change in the response of the transducers which are placed, on the Lower fiber, over a crack-line. The microscope allows, with a magnifying power equal to 50, to locate the crack more precisely. At this moment the crack cannot be seen with the naked eye : it becomes possible for a noticeably higher load.

Table n° 3 shows the comparison between the values of the cracking bending moment, actual, determined with the naked eye and theoretical. The latter has been calculated according to the previous assumptions, about the limit stress cracking criterion.

Moment daNxm / Beam	Actual value	Naked eye determined value	Theoretical value	σ_{br} actual (°)	σ_{br} apparent (°)
A	910	1110	630	39	53
B	1710	2110	1580	39	57
C	2110	2510	2200	29	47
D	2510	2910	2680	25	44
E	3110	3310	3270	25	35

Table 3 (°) σ_{br} daN/cm^2

It appears clearly that the experimental values are very close to the theoretical ones, calculated under the previous hypothesis. The σ_{br} corresponding stresses (1st crack) are very close to the mean value calculated for the failure under pure tension (33 daN/cm^2).

The differences that can be observed, in comparison with this mean value are of the same importance than the summation of the incertitudes about the strength of the concrete in tension and about the initial values of the strains.

The lower values observed for the beams D and E, however, let us to think that the concrete which has been highly compressed and submitted to creep-effects could be less resistant in tension.

The value of the bending moment determined with the naked eye is, on the contrary, always very higher than the actual value. The corresponding stress, calculated assuming the cross-section uncracked, should be 50 % higher than the tensile strength.

For these reasons, we think that the cracking of stretched concrete has not followed some measurable unelastic strains.

3.2. Decompression bending moment (craked beams)

This value of the bending moment plays an important part because it corresponds to the re-opening of the craks. If, indeed, cracking is permitted in partially prestressed concrete, the cracks must not open, generally, before a certain loading level defined as a part of the live loads. In such conditions the risks of corrosion of the prestressed wires remain low enough.

The decompression bending moment has been theoretically calculated assuming that the stresses when un loaded are the same that before the first loading and, besides, that the concrete behaves elastically even after cracking as long as the cracked cross-sections are compressed.

The experimental value of this bending moment has been calculated from the recording of the transducers placed on the stretched fiber.

Table n° 4 allows the comparaison between the experimental and theoretical values of the decompression bending moment Mdec.

Moment daNxm / Beam	Exp.	Theor.
B	810	844
C	1230	1486
D	1710	1996
E	2110	2612

Table 4

One can see that the experimental value of the decompression bending moment is always lower than the theoretical one ; the difference increases with the prestressing rate and is equal to 20 % of the theoretical value. Hence it seems necessary to take this difference into account in the design, if the condition of closing of the cracks has to be respected.

The difference we have observed, seems to be due to the role of the bonding wires. Indeed, when the cracks open, a sliding appears near the crack-lines, between the concrete and the wire, although prevented by the bonding forces (friction). During unloading, the bonding forces, acting in the opposite way, compress the prestressed wire. The consequence will be a loss of prestress for the wires or an increase of compressive stress in the ordinary reinforcing bars, which implies a decrease of the value of the decompression bending moment.

In our case, this phenomenon seems to appear for the two kinds of bars, since for the beam E totally prestressed the decrease is important.

3.3. Progression of cracking.

In totally reinforced or slightly prestressed concrete, when a crack appears in the lower fiber, it reaches immediatly the upper part of beam. MALDAGUE [5] showed that there occurs, under constant or increasing loading, a momentary instability, because the tensile strength in the reinforcement increases at a lower rate than the one relaxed by the cracking concrete.

In partially prestressed beams, on the contrary, this phenomenon does not exist beyond a prestressing rate equal to 40 %. The cracking progression is then very regular for the tensile strength progressively relaxed is balanced by a modification of the compressive stresses diagram (in the concrete).

This characteristic behaviour favours the use of partially prestressed concrete : one can be sure that the prestressed wires remain in an uncracked area even after cracking.

3.4. Opening of cracks

a) Comparison between experimental and theoretical values

The theoretical values have been calculated from the code model CEB-FIP 1978 [3].

The mean, experimental and theoretical (1978 CEB-FIP Model Code) values are nearly coincident, although the calculation from CEB under-estimates the cracking bending moment. Theoretical value of the maxima width presents an important safety allowance for 0 %, 40 %, 60 % rate beams. This safety allowance is lower for important loads but remains satisfactory for loads close to the service-level. (Figure n° 7)

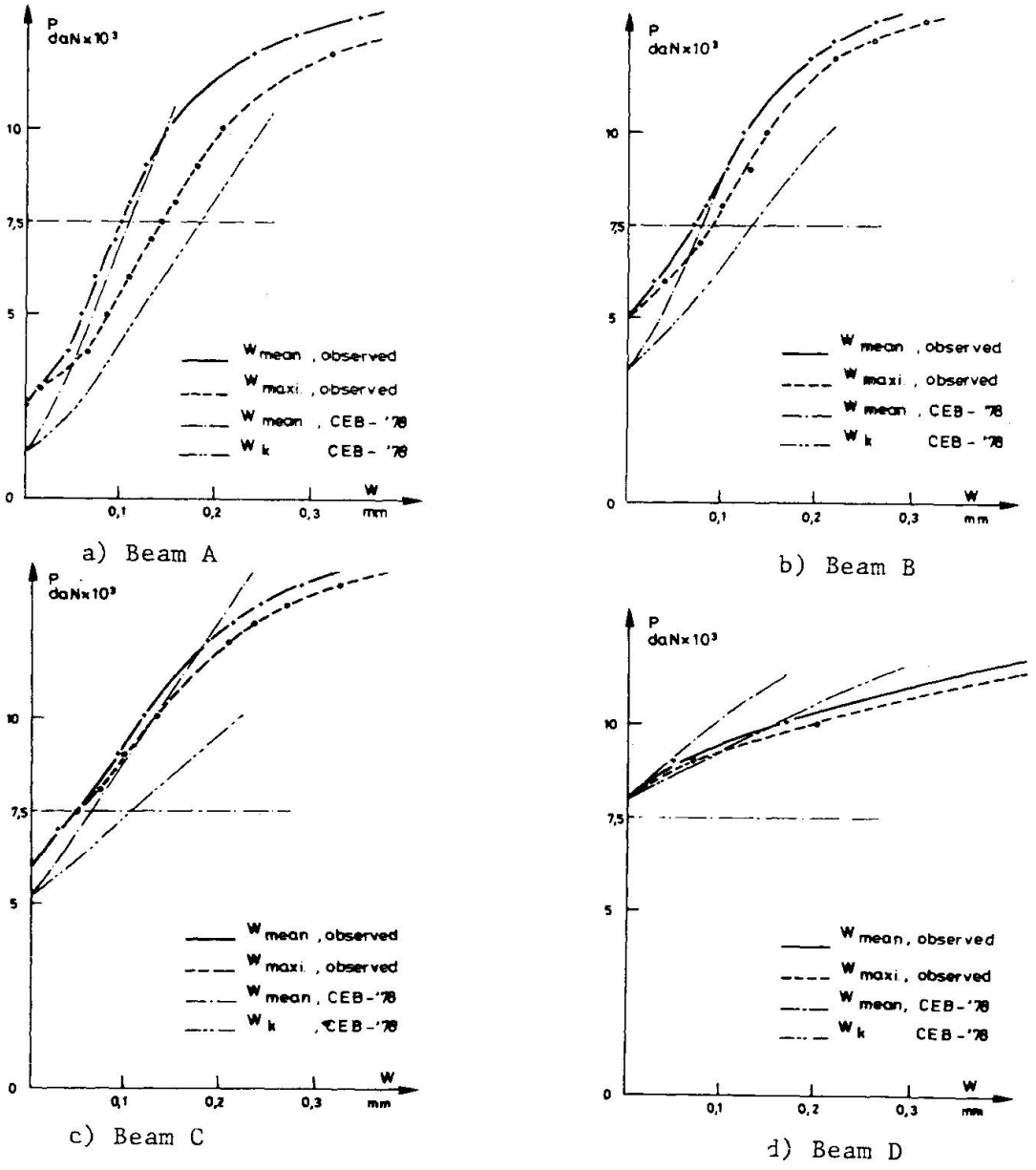

Figure n° 7 - Observed and calculated width of cracks.

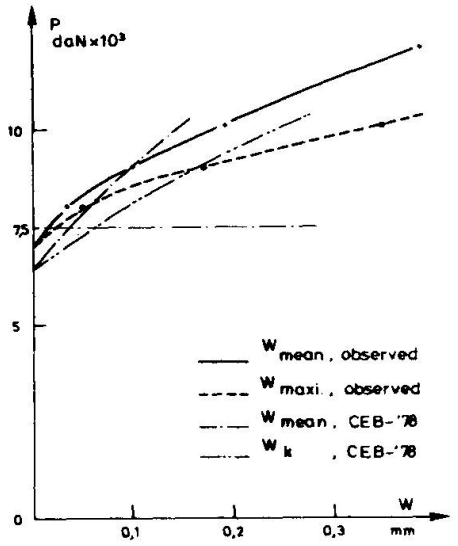

Figure n° 7 (e)

Observed and calculated width of cracks

beam E

b) Comparison between beams with different prestressing rates

The cracking-load increases with the prestressing rate as well as the cracks progression.

Figure n° 8 shows that till 0,5 M_R, the width of the cracks decreases when the prestressing rate increases; on the contrary, beyond 0,6 M_R the cracks of the most prestressed beams are the widest. We think that this phenomenon is due to the decrease of the total steel cross section, the increase of the bonded concrete section and the decrease of the bonding properties, when the prestressing rate increases.

In our case, for the service-load, the improvment obtained becomes perceptible beyond a prestressing rate equal to 60 %. Below, the decrease of the crack-width in comparison with the totally reinforced beam is not sensitive. This remark does not, however, make us forget that the decompression bending moment increases noticeably with the prestressing rate. So, a prestressing rate can be choosen only according to the duration of live-loading and the surrounding aggressiveness. Particularly, if the service-load is scarcely applied, 80 % prestressing rate is sufficient enough in aggressive surroundings, for the cracks will almost never open.

We can notice, besides, that the measured openings of the cracks under service-load are lower than the limit value (0,1 mm) proposed by Code Model CEB-FIP for frequent cases.

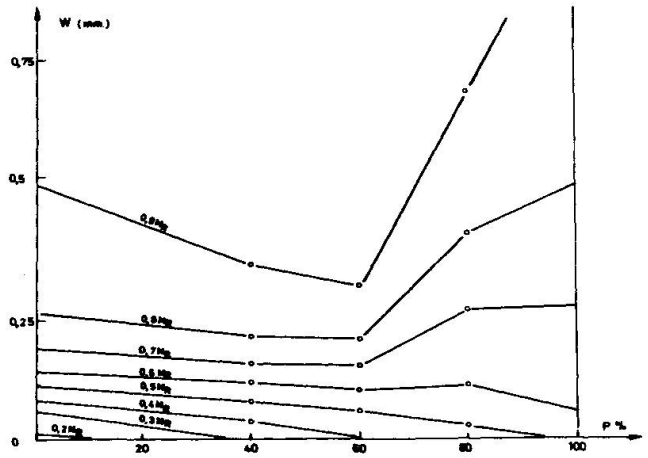

Figure n° 8
Openning of cracks
Versus prestressing rate

4. FAILURE CONDITIONS

4.1. Comparison between the experimental and theoretical values of the failure bending moment and the ultimate limit moment

The theoretical calculation has been performed with the common hypothesis, assuming therefore that failure of compressed concrete occurs when its compressive strain reaches 5 10^{-3} (experimental value obtained by preliminary tests) for the determination of the failure bending moment.

The ultimate limit moment was calculated with a failure compressive strain value equal to 3.5 10^{-3} (CEB-FIP Model Code).

Table n° 5 shows the obtained results and allows the comparison. (The experimental value of the failure moment corresponds to the maximum of loading).

Beam	A	B	C	D	E
Prestressing rate	0	40	60	80	100
Experimental value	5,91	6,15	6,35	6,07	5,99
Theoretical value	5,93	6,20	6,46	6,34	6,18
Ultimate value	4,65	4,55	4,57	4,35	4,27
Exp./Ult.	1,27	1,35	1,39	1,40	1,40

Table 5

We can see that theoretical calculation gives a good approximation but is shightly higher. We think that this difference is due to the slidings between concrete and steel.

Besides, the CEB-FIP calculation offers a safety allowance independent from the prestressing rate (but slightly lower for the totally reinforced beam). The safety of these structures can however be different according for instance to the scatter of mechanical characteristics of prestressed or ordinary reinforcements.

4.2. Failure strains

Table n° 6 shows the experimental and theoretical values of the failure strains.

Beam	prestressing rate (%)	experimental				Theoretical strain variation 10^{-3}	
		mean strain (1) variation 10^{-3}		max. strain (2) variation 10^{-3}			
		$\Delta\varepsilon_b$	$\Delta\varepsilon_s$	$\Delta\varepsilon_b$	$\Delta\varepsilon_s$	$\Delta\varepsilon_b$ (hypoth.)	$\Delta\varepsilon_s$ (cal.)
A	0	4,07	13,37	4,21	15,4	5	20,1
B	40	4,25	12,07	4,63	14,9	5	16,1
C	60	4,48	10,75	4,54	13,8	5	14,2
D	80	4,73	9,44	5,11	12,5	5	13,6
E	100	5,15	9,52	5,26	10,3	5	11,9

Table 6

(1) mean value calculated from the recording of four transducers (measurement area length $\simeq$ 40 to 50 cm)

(2) maxima value of the recordings.

The slight differences which appear between theoretical and experimental strain values correspond to those previously noticed about the bending moments. They are probably due to the non-planearity of the cross-section and to the measurement method.

We have then calculated the ultimate curvatures plotted on the figure n° 9, versus the prestressing rate. The curvature decreases slightly with the prestressing rate but the variation is not very important which shows the low influence of the prestressing rate upon the unelastic deformations of the beams. This result is essentially valid for partially prestressed beams by pre-tension. In the case of post-tension it won't be so favourable.

Figure n° 9
Ultimature curvature
versus prestressing rate

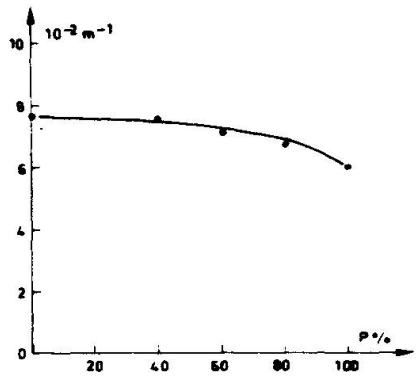

CONCLUSIONS

The obtained results show that the behaviour of partially prestressed by pretension beams can be foreseen owing to the theoretical calculation in a satisfactory way on condition that the estimation of the initial stage stresses takes into account the mechanical effects of the ordinary reinforcement.

The cracking load seems to decrease when the lower fiber has previously been highly compressed (beams with 80 % os 100 % prestressing rate). The width or the cracks obeys to the 1978 CEB-FIP Model Code previsions. The prestressing rate near of 70 % - 80 % seems necessary to limit efficiently the width of the cracks at the service-load, but if the design conditions allow a maximum width equal to 0,1 mm the optimum prestressing rate may be lower than 70 %.

There is no fondamental difference in the failure behaviour of the beams with respect to the prestressing rates. The safety allowance in relation with the CEB-FIP Model Code does not seem dependent on the prestressing rate, nor the failure strains values.

BIBLIOGRAPHIE

1 - M. PINGLOT - G. PONS
Contribution à l'étude du béton partiellement précontraint - Congrès de la FIP - New York 1974.

2 - NEUMAN
Contribution à l'étude de l'influence de l'effort tranchant sur le comportement de poutres en béton armé précontraint. Thèse Docteur Ingénieur - Toulouse, Juillet 1980.

3 - CEB-FIP Model Code - Bulletin d'information n° 124-125 - février 1978.

4 - TUSET
"Modélisation du comportement des structures en béton armé par prise en compte de la résistance en traction du béton" - Thèse Docteur Sciences Lyon, mai 1980.

5 - J.C. MALDAGUE
Détermination expérimentale des lois moments courbures de poutres en béton armé - Annales I.T.B.T.P., mai 1965.

Leere Seite
Blank page
Page vide

A Calculation of Reinforced Concrete Beams Under Bending and Torsion Using Three-Dimensional Finite Elements

Le calcul des poutres en béton armé soumises à la flexion et à la torsion, utilisant les éléments finis tridimensionnels

Berechnung von Stahlbetonbalken unter Biegung und Torsion mit dreidimensionalen Finiten Elementen

GERHARD MEHLHORN
Professor of Civil Engineering

GÜNTER SCHMIDT-GÖNNER
Research Assistent

Institut für Massivbau, Technische Hochschule Darmstadt
Darmstadt, Federal Republic of Germany

SUMMARY

The problem of solid prestressed or reinforced concrete members under pure torsion or under combined loading is pointed out. The solution with the help of three-dimensional finite elements and a coordinating 3d-concrete-material model is shown. A comparison of calculation with a test result is given.

RÉSUMÉ

L'auteur a examiné le problème d'éléments massifs en béton précontraint ou béton armé, soumis à la torsion pure ou à un chargement combiné. Il montre la solution utilisant des éléments finis tridimensionnels et le modèle polyaxiale pour le matériau béton. Il donne une comparaison de calcul avec le résultat d'un essai.

ZUSAMMENFASSUNG

Die Problemstellung von massiven Bauteilen aus Stahlbeton oder Spannbeton unter reiner Torsion oder kombinierter Beanspruchung mit Torsion sowie die Lösungsmöglichkeit mittels räumlichter finiter Elemente werden aufgezeigt. Ein hierzu erforderliches Materialmodell auf der Grundlage schrittweiser elastischer Ansätze wird vorgestellt. Die Vergleichsrechnung eines Testbeispiels wird ebenfalls gezeigt.

1. A SURVEY OF PREVIOUS WORK DONE AT THE TECHNISCHE HOCHSCHULE DARMSTADT CONCERNING PROBLEMS OF BENDING AND TORSION ON REINFORCED CONCRETE BEAMS

In his thesis [1] the first named author of this paper examined the influence of material behavior on the lateral buckling of reinforced and prestressed concrete beams. With regard to concrete pressure zones, the torsional stiffness was determined with the help of the Boundary Element Method (BEM). The influence of warping torsion on reinforced concrete was referred to, and for the I-cross-section, a simple method for determining the warping stiffness was given. It was also shown, however, that for the combined stresses of bending, shear and torsion on a reinforced concrete beam, with a arbitrary cross-section, no suitable calculating method was available. For this reason, researchers of the Institut für Massivbau at the Technische Hochschule Darmstadt have been working on this problem for the past ten years.

Bertram [2] following the tests of Lampert and Thürlimann [3], which used reinforced concrete beams with rectangular cross-sections and T-sections, developed a method for calculating the ultimate moment and the interaction between the ultimate bending moment and torsional moments. Information was also given for determining the torsional stiffness. However, the procedure proved to be too cumbersome and not general enough. (For example, determining torsional stiffness, influenced by the position of the neutral axis, using only the bending moment).

In his thesis [4], Rützel developed a procedure for thin-walled reinforced concrete beams, with and without prestressing, with which one could ascertain the stresses and deformations caused by bending, normal force, shearing force and torsion in relation to material non-linearity. He showed that for thin-walled beams, especially in State II, the portion of the warping torsion at the torsion carrying behavior should not be neglected. Rützel took into consideration the alteration of the torsion resistance after cracking by changing the position of the neutral axis. Since the strains from the various loads were determined separately - and after the superposition - there had to follow in each case a reconsideration of the assumptions, which resulted in subsequent revisions and improvements in them. Because of this, the procedure is also relatively cumbersome.

Bertram's [2] and Rützel's [4] methods, in addition, are not well suited for implementation into a general computer code, because the numerical processing is too costly and the prior assumptions used are too specific. Therefore, a new way had to be sought out, and the Finite Elemement Method (FEM) proved to be especially suitable for this purpose.

With the help of the FEM, Maurer [5] developed a computational procedure for box girders under random loads. He used layered plate elements. With it, the stresses of the cross-section could be determined; distinct not only from the overall loads, but also from the cross-sectional deformation or the transverse bending. The FEM-program has manifold applications: it is able to take into account the non-linear stress-strain relationship of the concrete in compression, the cracking in tension, the influence of prestressing, as well as the yielding of the reinforcement. In his thesis, Maurer showed that with his program, there was good conformity between his calculation results and test results.

Subsequently, following the course set by [1], Sauer [6] developed the theoretical fundamentals for applying the BEM to the solution of shear and torsion problems for elastic beams, and wrote a computer code for determining St. Venant's torsional stiffness, warping resistance and position of the shear center as well as the shear stresses, that could be used for beams with arbitrary, polygonal-sided cross-sections.

Röder's thesis [7] investigated the lateral buckling of reinforced and prestressed concrete beams in consideration of non-linear material behavior: non-linear stress-strain behavior of the concrete in compression, cracking in tension and the yielding of the reinforcement. In contrast to [1], where the bifurcation problem was dealt with, Röder treated the investigation of stability as a problem in accordance with "Sedond Order Theory", but to do so, he had to presume there were imperfections in the beam or excentricity of the loading. For the given loads, the state of strain was determined for various points on the beam and verified with the conditions of equilibrium. From the state of strain, the stiffness was figured, and the calculations were performed repeatedly. This iterated method of calculation was terminated if the deformation did not differ essentially from the preceding step. The torsion stiffness was determined by the procedure for the concrete area under compression, in accordance with Sauer [6], and for the cracked area, he used a truss model. The procedure used various prior assumptions about the cracked area, and because of this it was not suitable for making calculations concerning beams primarily loaded by torsion.

Finally, it should be mentioned that a combination of the FEM and the BEM promises distinct advantages, especially with regard to computation time.

2. CALCULATIONS WITH THREE-DIMENSIONAL FINITE ELEMENTS

As the preceding discussion illustrates, the calculation of torsion carrying behavior has led those of us at the Technische Hochschule Darmstadt along a path of steady progression from simple "beam statics", through a consideration of geometric and material non-linearity in the beams toward spatial models of box girders, with plate elements considering realistic material behavior. The last cited procedure, however, provides no method for analyzing solid beams. Since under pure torsion the carrying mechanism is fairly clear (and assuming "hollow cross-sections, with presumed wall thicknesses, useful results are derived not only relative to the ultimate load, but also to deformation behavior for State II), one could say the research is extensively finished. However, under combined stress (torsion, bending, shear, normal force), especially as related to deformation behavior, there is still a gap to be closed. Because the afore mentioned problem generally concerned with conditions of three-dimensional stress and deformation, three-dimensional (spatial) finite elements should be used.

After test computations, we decided upon using hexahedral elements, with a variable number of nodes (8 to 21 nodes) and isoparametric displacement function.

For calculations with non-linear material specifications, however, relatively simple elements appeared to us to be the most suitable (we use the element-type mainly with eight nodes (corner nodes)), and thereby we reached a linear displacement function.

In essence, the questions to be asked, subsequent to the idealization of the reinforcement, are about the bond behavior and non-linear stress-strain relationship of the concrete, here too, cracking must be taken into consideration. To consider a practical and realistic comprehension of beam behavior for reinforced concrete structural members under torsion there are still several detailed problems to be examined:

a. Questions of load carrying in.
b. Local tension problems at the stirrup corners.
c. Splitting of the concrete layers outside the reinforcement.

2.1 Idealization of the Reinforcement

For calculating the beam segments, the reinforcement rods were individually idealized using truss elements with linear displacement function, only normal force are considered. The possible yielding of the reinforcement was taken into account by considering a bi-linear stress-strain relationship.

2.2 Idealization of the Bond

To calculate the bond behavior, a bond element was developed [9] for the computer code ADINA. The theoretical work and experimental certification was performed largely by Dörr [10] and [11]. The element is compatible with the concrete and steel elements used. It possesses no geometrical dimensions, but the element connects the concrete and steel, so that the forces parallel and perpendicular to the reinforcement can be transmitted.

A bi-linear relationship between the relative displacement (concrete-reinforcement) Δ and the bond stress τ was supposed. This procedure represented an approximation and neglected the dependence of the bond stress upon the transverse pressure Q. (Fig. 2).

2.3 Idealization of the Concrete

2.3.1 Elements

Three-dimensional continuum elements were used in cubic form (hexahedron), with eight nodes and three degrees of freedom per node. The element in this form is based on the linear displacement function.

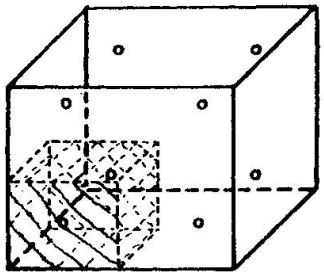

Test calculations with elastic material behavior and with cross-sectional types frequently found in real structures, gave us information about the necessary refined grid for the required precision. Figure 1 shows a few of the F.E. idealizations utilized. (The comparative precision was calculated according to Sauer [6]).

Since we want to confine ourselves, relatively short parts of real structures are to be modelled and analyzed, and the required computer time remains, even with grid refinement, justifiable. Using short structural members, in which the loadings along the beam axis is constant, we want to analyze the influence of torsion carrying behavior under normal force and bending moments. The calculations are done using the computer code ADINA [8].

For our presumptions to be valid, and compatible with the previous test results, we have to use realistic material models.

The material models used were selected and developed not only with regard to the problem to be analyzed, but also relative to F.E. idealization.

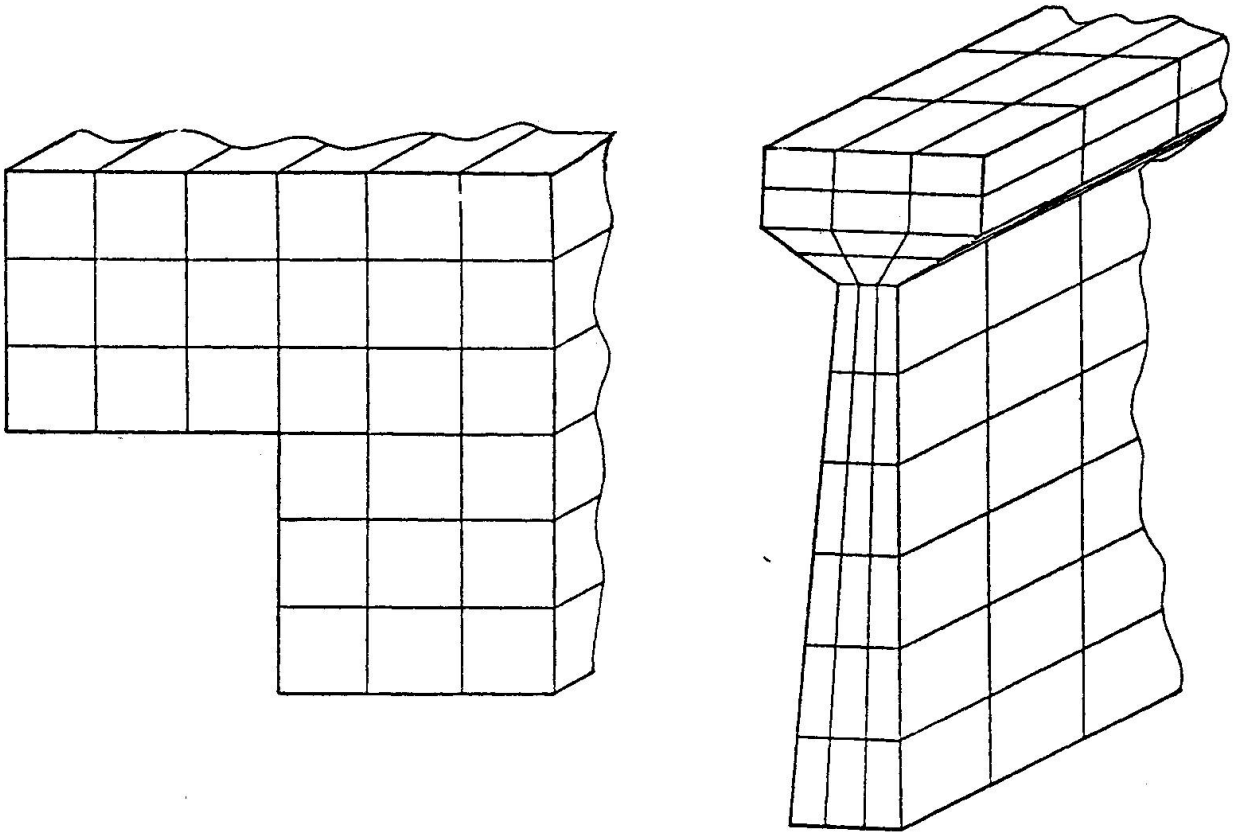

Fig. 1 F.E. Mesh for solid beams

The stiffness of the elements was formed of at least eight integration points. On these integration points, the state of stress and strain was also determined. In the event of cracking, the cracks were not supposed to be discrete, but rather "smeared" over the integration area. In this way, the conditions of stress or cracking at the integration point were determined, and the formation of element stiffness ascertained by using the integration points. Such a methodology can produce a great amount of information about the non-linearity of material.

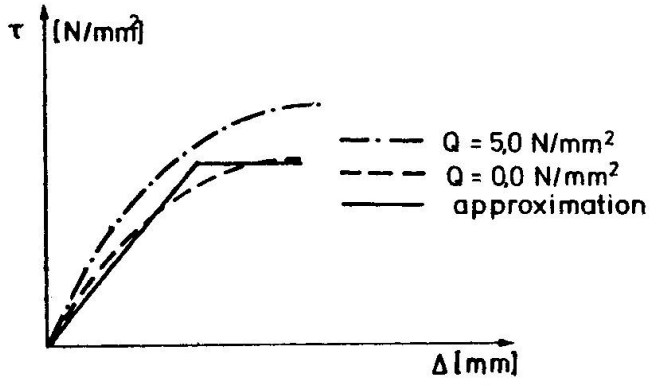

Fig. 2 Bond-Behavior

2.3.2 Multi-Axial Strength

The dependence of the concrete's strength on the state of stress was taken into consideration. We used a principle-stress-related representation of multi-axial strength. Figure 3 shows the multi-axial compression strength, which is normalized by the uni-axial compression strength (σ_c).

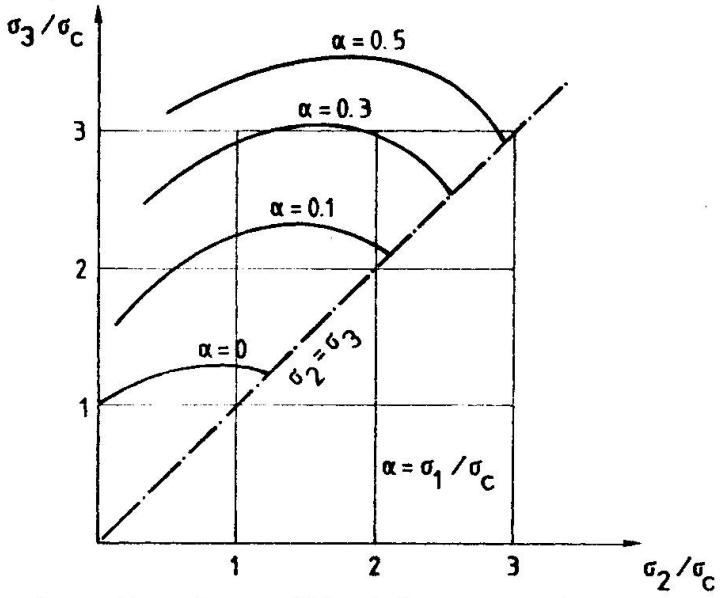

Figure 3 Concrete strength under multiaxial compression

The sets of curves, whose lowest (σ_1 = 0) represents the bi-axial strength, shows quite visibly the increase of the compression strength with increasing transverse pressure (the smallest principle compressive stress). In the program, the sets of curves were replaced by six polygons, between which we interpolate in the linear form. Current values for the multiaxial compressive strength were determined by the results of the international comparative test program, for example [12], and already published in [13]. For a specific condition of stress (σ_2, σ_1), a value γ was determined, that gave us the greatest bearable compressive strength σ_3 for these conditions of stress, in comparison to a uni-axial compressive strength: $\min \sigma_3 = \sigma_c \cdot \gamma$.

For the tensile strength with regard to the conditions of stress, a simple prior assumption, corresponding to Figure 4, was used. It means: in tri-axial tension, everywhere the uni-axial tensile strength is valid; in the compression-tension regions, dependent upon σ_2 and σ_3, the value for the tensile strength was determined through linear interpolation. If the greatest compressive stress approaches the compressive strength, then the tensile strength is set to zero.

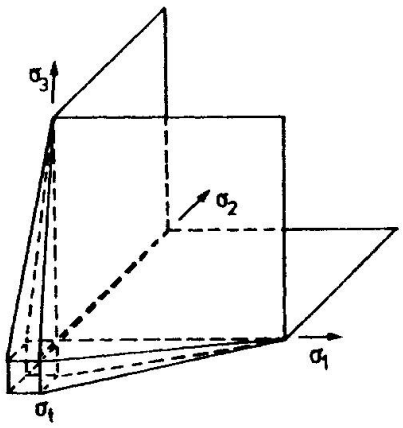

Figure 4 Tensile strength under multiaxial conditions

2.3.3 Multi-Axial Stress-Strain Behavior

The material model is compiled in an incremental form; that means: we considered the non-linear material relationship during a load step as a linear-elastic material relationship. However, it was ensured through a process of iteration, that for the respective states of strain, the corresponding tangents and secant stiffness were used.

We employed an orthotropic, linear-elastic material model, by which the material characteristics varies correspondingly to the strains. The directions of the orthotropic axes are identical with those of the principle stress axes. The values of the tangents or secant moduli of the orthotropic axes were determined from the distorted uni-axial stress-strain relationship. For the uni-axial case, we used the simple relationship:

with

$$\sigma_{(\varepsilon)} = \tilde{\sigma}_c \left[1 - \left(1 - \frac{\varepsilon}{\tilde{\varepsilon}_c}\right)^{\alpha}\right]$$

$$\alpha = E_o \cdot \tilde{\varepsilon}_c / \tilde{\sigma}_c$$

$$\rightsquigarrow \quad E_{(\varepsilon)} = E_o \cdot \left(1 - \frac{\varepsilon}{\tilde{\varepsilon}_c}\right)^{\alpha - 1}$$

For the multi-axial region, the curve was distorted for all principle stress axes, with the factor γ defined by using the multi-axial strength. Its value $\sigma_c = \gamma \cdot \tilde{\sigma}_c$, $\varepsilon_c = \gamma \cdot \tilde{\varepsilon}_c$ etc.

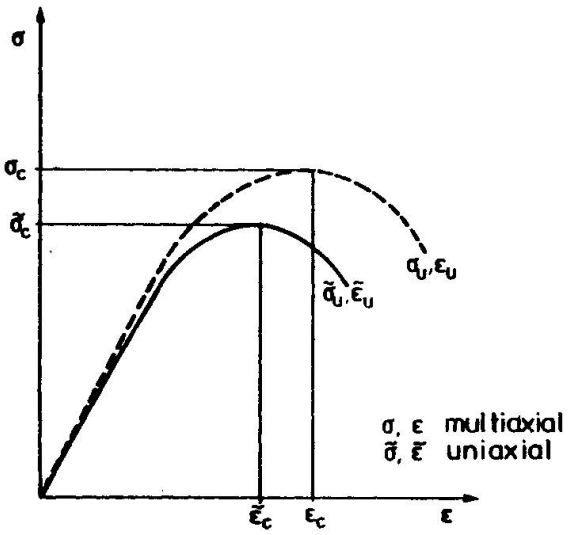

Figure 5 Uniaxial and multiaxial stress-strain-relation

2.3.4 Post-Cracking Behavior

From a reinforced concrete test, the total stiffness, after the development of the first cracks, is still clearly greater than the stiffness of the reinforcement alone, meaning: the concrete between the cracks is still carrying a load. If the carrying effect of the concrete after cracking is not considered in a computational model, then one mathematically obtains, after the appearance of the first cracks, incontinuity in the deformation plot - although in reality this is not clearly observed. In order to avoid this after cracking we set the remaining concrete tension perpendicular to the crack not to zero, but reduced the stresses step-wise, as indicated in Figure 6, with regard to the unit elongation perpendicular to the crack.

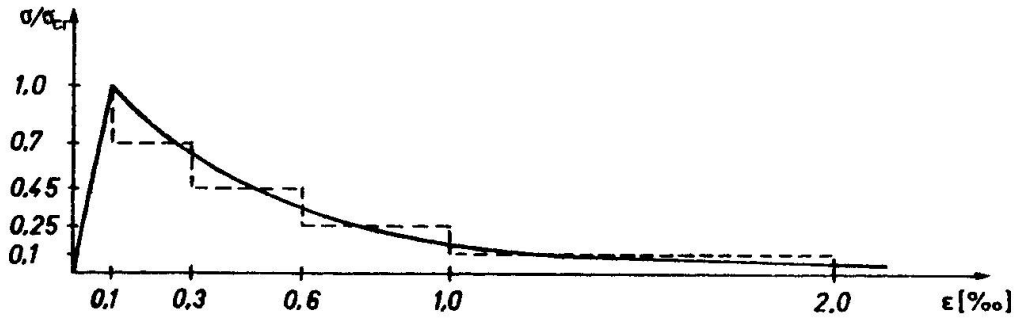

Figure 6 Stresses in the concrete after cracking

At the beginning of cracking, the stresses parallel to the crack are zero, because the crack was defined as perpendicular to the principle tensile stress. Through load re-arrangement and alteration, however, deformations parallel to the crack can occur. As a consequence, the crack inter-lock can, dependent upon the width, still transfer shear forces. Defining the resistance against the displacement parallel to the crack (corresponding to the elastic shear modulus (G_o)) as G_r, and plotting the relationship G_r/G_o, depending upon the width of the crack, results in a plot like that shown in Figure 7. The dependence upon the width of the crack was approximated in the computer code in a step-wise manner.

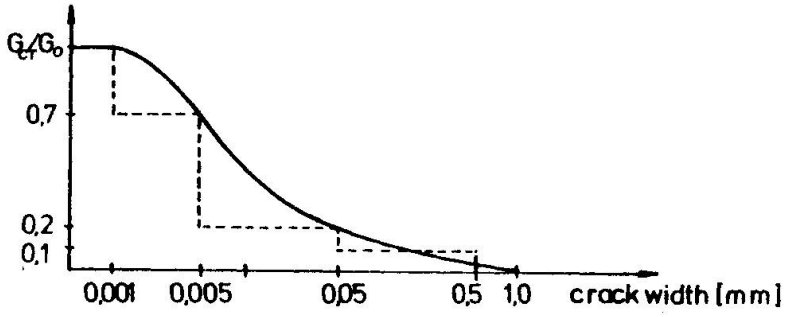

Figure 7 Shear-stiffness of cracked concrete

2.3.5 Loading - Unloading

The stress-strain behavior described in 2.3.3 was only used for the virginal load (1). For unloading (2) and re-loading (3) - as long as the structure still showed no cracks - the original stiffness was used (see Fig. 8). If re-loading reached a point over the first load (4), then the virginal loading curve again was taken.

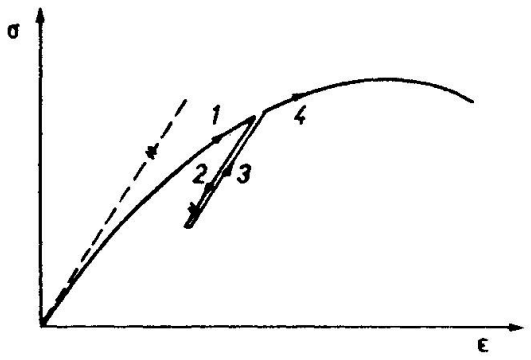

Figure 8 Loading - Unloading

2.4 Special Problems

With regard to local stress concentration at the corner of the stirrups, and the problem of splitting of the concrete layer outside of the reinforcement, we are now working on a detailed, computational analysis, also with a 3-D-model. With such an analysis, the corner of a stirrup, the longitudinal reinforcement truss and the surrounding concrete can be represented. We expect from it information about the carrying behavior of this area. Furthermore we would like to mention the results of the analysis in the overall computational models.

2.5 Example

With the aforementioned procedure, the various cross-sections and varying loads should be able to be analyzed. At the present time, we have the first results of the calculation for the tests [14].

Fig. 9 illustrates an F.E. idealization with 3 x 4 x 5 elements for concrete. The reinforcement is modelled by means of truss elements at the beam surface.

The comparison of the distortion and the stirrup stress from calculations and a test is shown in Fig. 9.

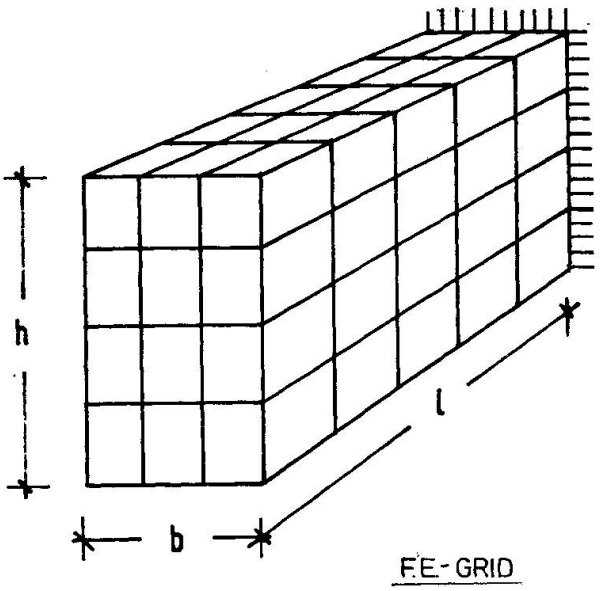

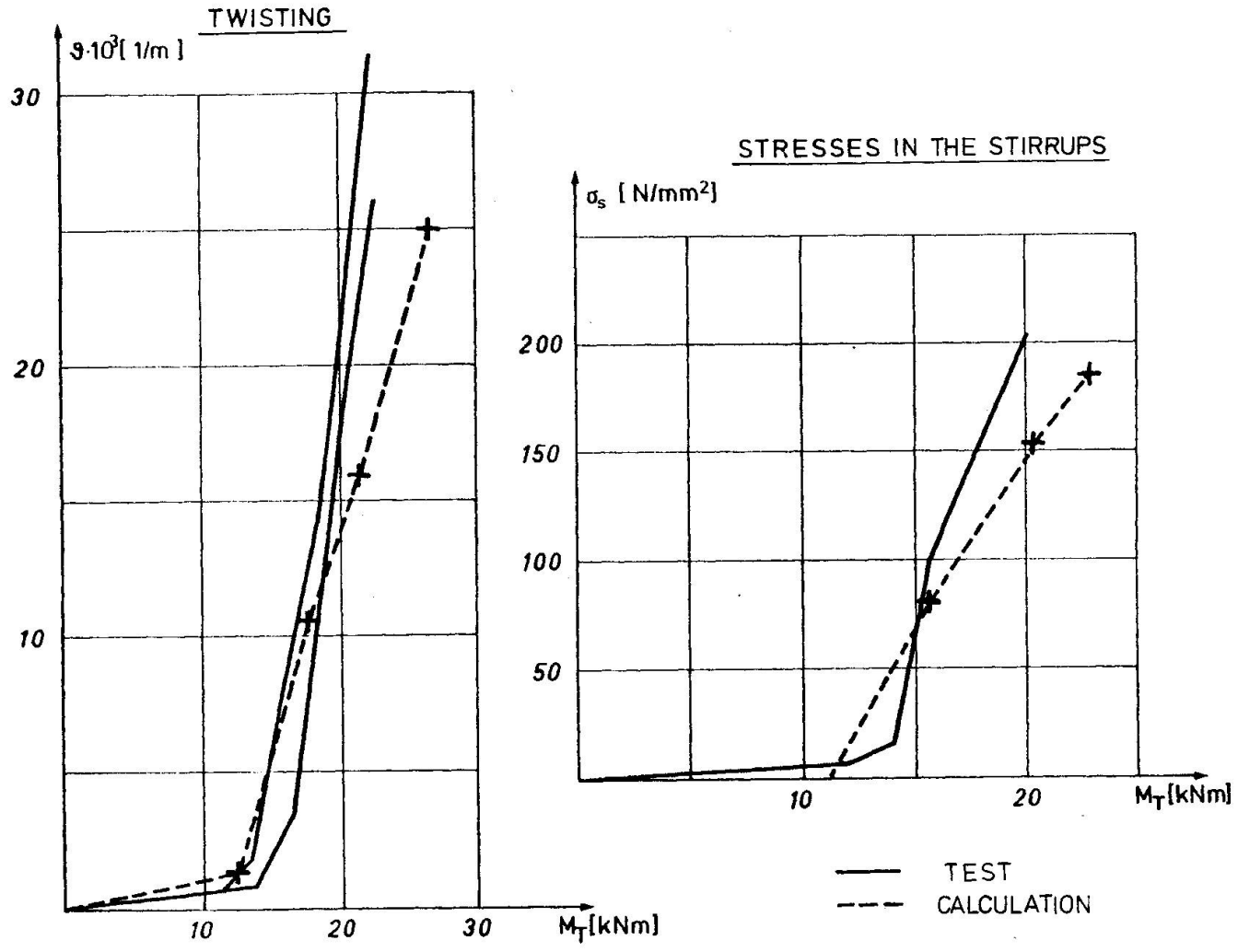

Figure 9 F.E.-Model and a comparison of calculation and test results

3. OUTLOOK

Through parametric studies of concrete members, under combined loadings, using the described computational models, the interaction between the individual types of loading should be able to be determined and demonstrated.

We believe, however, that the computational model can also be a useful tool for analyzing a series of wider problems concerning reinforced concrete structures – especially for the researcher.

ACKNOWLEDGEMENT

The work was supported by the Deutsche Forschungsgemeinschaft. This support is gratefully acknowledged.

REFERENCES

1 Mehlhorn, Gerhard: Ein Beitrag zum Kipp-Problem bei Stahlbeton- und Spannbetonträgern. Dissertation TH Darmstadt 1970.

2 Bertram, Dieter: Ein Beitrag zur Berechnung von Stahlbetonträgern unter Biegung und Torsion. Dissertation TH Darmstadt 1973.

3 Lampert, Paul; B. Thürlimann: Torsions-Biegeversuche an Stahlbetonbalken. Bericht Nr. 506-3 (1969). Institut für Baustatik ETH Zürich.

4 Rützel, Hubert: Zur Berechnung biege- und torsionsbeanspruchter dünnwandiger Stahlbeton- und Spannbetonträger. Dissertation TH Darmstadt 1975.

5 Maurer, Gerhard: Zum Tragverhalten des einzelligen Spannbetonkastenträgers. Dissertation TH Darmstadt 1979.

6 Sauer, Ernst: Schub und Torsion bei elastischen prismatischen Balken. Dissertation TH Darmstadt 1979.

7 Röder, Friedrich-Karl: Berechnungen von Stahlbeton- und Spannbetonträgern nach Theorie II. Ordnung. Dissertation TH Darmstadt (to be submitted 1981).

8 Bathe, Klaus-Jürgen: ADINA, A Finite Element Program for Automatic Dynamic Incremental Nonlinear Analysis. Report 824481. Massachusetts Insitute of Technology.

9 Cornelius, Volker; G. Mehlhorn: Tragfähigkeitsuntersuchungen im Verankerungsbereich von Verpreßankern und Pfählen mit kleinem Durchmesser für den Anwendungsbereich Lockergestein: 1981. Abschlußbericht eines vom Institut für Bautechnik, Berlin, geförderten Forschungsvorhabens.

10 Dörr, Karlfried: Ein Beitrag zur Berechnung von Stahlbetonscheiben unter besonderer Berücksichtigung des Verbundverhaltens. Dissertation TH Darmstadt 1979.

11 Dörr, Karlfried; G. Mehlhorn, W. Stauder, D. Uhlisch: Berechnung von Stahlbetonscheiben im Zustand II bei Annahme eines wirklichkeitsnahen Werkstoffverhaltens. Deutscher Ausschuß für Stahlbeton, Heft 238, Berlin, 1974.

12 Linse, Diethelm; H. Aschl: Versuche zum Verhalten von Beton unter mehrachsiger Beanspruchung, Versuchsbericht der TU München 1976.

13 Schmidt-Gönner, Günter; K. Gerstle, G. Mehlhorn: A Comparison Between ADINA Concrete Model and Experimental Concrete Behavior. Proceedings of ADINA-Conference August 1979, Report 82448-9, Mass. Institute of Technology.

14 Leonhardt, Fritz; G. Schelling: Torsionsversuche an Stahlbetonbalken. Deutscher Ausschuß für Stahlbeton, Heft 239, 1974.

Leere Seite
Blank page
Page vide

Rational Analysis of Shear in Reinforced Concrete Columns

Analyse rationnelle de "la contrainte de cisaillement" des poteaux en béton armé

Zweckmässige Berechnung der Querkraft in Stahlbetonstützen

KOICHI MINAMI
Lecturer
Department of Architecture
Osaka Institute of Technology
Osaka, Japan

MINORU WAKABAYASHI
Professor
Disaster Prevention Research Institute
Kyoto University
Uji, Japan

SUMMARY
Proposed in this paper is an evaluation method of the strength of reinforced concrete columns under combined axial, bending and shear stresses by an easy and convenient analysis. In the analysis, shear resistances of the beam- and the arch -mechanisms, which satisfy a statically admissible stress field, are first obtained and the ultimate shear strength of the column is computed applying a modified and extended additive strength theory.

RÉSUMÉ
On propose ici une méthode d'évaluation de la résistance des poteaux en béton armé sous l'effet des contraintes axiales, fléchissantes et de cisaillement, suivant une analyse simple et commode. Dans cette analyse, les résistances de "la contrainte de cisaillement" du mécanisme de la poutre et de l'arc, qui satisfont un champ de force statiquement admissible, sont obtenues en premier, et la résistance limite de "la contrainte de cisaillement" du pilier est estimée, en appliquant une théorie des forces d'addition modifiées et étendues.

ZUSAMMENFASSUNG
In dieser Abhandlung wird eine Methode vorgeschlagen, die durch eine einfache und passende Analyse die Tragfähigkeit von Stahlbetonstützen unter der kombinierten Axial-, Biege- und Querkraft evaluiert. In der Analyse werden zuerst die Querwiderstände der Balken- und Bogenmechanismen, die einem statisch zulässigen Spannungsfeld Genüge leisten, festgestellt; dann wird der äusserste Schubwiderstand der Stützen berechnet, indem man eine modifizierte und erweiterte Widerstandsadditionstheorie anwendet.

1. INTRODUCTION

Extensive studies have been made to estimate shear strength of concrete members, including ordinary reinforced concrete, prestressed concrete, mixed steel and concrete members, by means of plastic analysis[1-9]. There already is an established method of determining the flexural strength of reinforced concrete members when subjected to compression and bending. Also, it was proved that an extended additive strength theory, which is analytically very simple and clear, is practically applicable to the same problem.

Described in this paper is a trial to provide analytical approach to obtain the strength of reinforced concrete members with ordinary or diagonal main reinforcement under combined state of compression, bending and shear by applying the extended additive strength theory, and to systematically know the correlation among compressive, flexural and shear strengths of reinforced concrete members, which has often been discussed individually. Following are the method of analysis and the feature of the analytical solutions. Finally, the comparisons of theoretical prediction with experimental results are shown.

2. ORDINARY REINFORCED CONCRETE COLUMNS

2.1 Basic Assumptions in the Analysis

Generally, there are two types of shear transmitting mechanisms in reinforced concrete members ; beam mechanism and arch mechanism. To solve the shear problem, it is important to determine the shear resistance of each mechanism corresponding to elastic state to ultimate state. In this paper, however, two types of shear transmitting mechanisms are assumed on the basis of ultimate state of stress, as illustrated in Fig.1 ; the beam mechanism consists of longitudinal and shear reinforcements, and concrete with the width of $_rb$, and the arch mechanism consists of reinforcement-less concrete with the width of $(b-{}_rb)$. Once a set of strength, $({}_rM,{}_rN,{}_rQ)$ and $({}_cM,{}_cN,{}_cQ)$, is determined, which satisfies the static admissible stress field for each resistant mechanism, the member strength, (M,N,Q), is assumed to be given by,

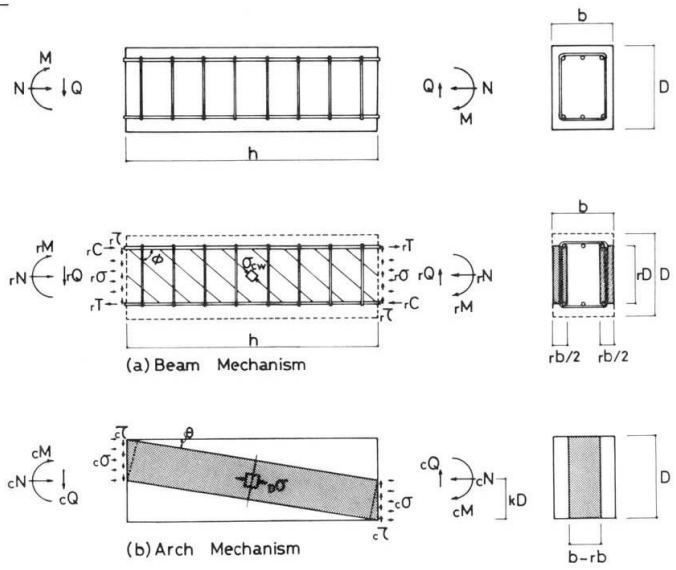

Fig.1 Resistance Mechanism of Reinforced Concrete Members

$$M = {}_rM + {}_cM \ , \ N = {}_rN + {}_cN \ , \ Q = {}_rQ + {}_cQ \tag{1}$$

based upon the extended additive strength theory. Here, the stresses at the member ends are assumed to be in anti-symmetric flexural-shear state and the following relation is assumed to hold.

$$M / Q = {}_rM / {}_rQ = {}_cM / {}_cQ = h / 2 \tag{2}$$

Also, it is assumed for both beam and arch mechanisms, that plastic deformation is allowed to the extent where the component steel and concrete strengths can be added. Concrete material causes compressive deformation at and maintaining the stress equal to the cylinder compressive strength, F_c, and steel material

causes either tensile or compressive plastic deformation at and maintaining the steel yield stress, ${}_r\sigma_y$ or ${}_{rw}\sigma_y$.

The analytical technique adopted in this paper is similar to those described in Ref.[3]. The difference is that this paper considers concrete without any reinforcements as arch mechanism, hence the advantage of this technique over others lies in its simplicity in treating truss nodal points in application.

2.2 ${}_rn$-${}_rq$ Equations for Beam Mechanism

As shown in Fig.1(a), the beam mechanism is assumed to consist of the three elements; longitudinal reinforcements that resist tension or compression, shear reinforcements that resist tension, and concrete blocks with the width of ${}_rb$, whose axis is twisted by the angle of ϕ from the member axis. The condition that the maximum shear resistance is attained for the beam mechanism gives $\phi = \pi/4$, then the non-dimensional shear strength of the beam mechanism, ${}_rq$ can be obtained by Eq.(3) when the shear resistance is determined by tensile yielding of the shear reinforcements, and by Eqs.(4) and (5) when determined by either tension or compression of the longitudinal reinforcements, respectively.

$$-2_r\mu_t + {}_r\mu_w\cdot({}_rD_1 + \eta) \leqq n \leqq 2_r\mu_t + {}_r\mu_w\cdot({}_rD_1 - \eta)$$
$$rq = {}_r\mu_w\cdot{}_rD_1 \tag{3}$$

$$-2_r\mu_t \leqq {}_rn \leqq -2_r\mu_t + {}_r\mu_w\cdot({}_rD_1 + \eta)$$
$$n = -2_r\mu_t + (1 + \eta / {}_rD_1)\cdot rq \tag{4}$$

$$2_r\mu_t + {}_r\mu_w\cdot({}_rD_1 - \eta) \leqq {}_rn \leqq 2_r\mu_t$$
$$n = 2_r\mu_t + (1 - \eta / {}_rD_1)\cdot rq \tag{5}$$

The maximum shear resistance of the beam mechanism is attained when both the top and the bottom longitudinal reinforcements yield simultaneously, and the resistant shear, ${}_rq_o$, is given by,

$${}_rq_o = 2_r\mu_t\cdot{}_rD_1 / \eta \tag{6}$$

and the required amount of shear reinforcements for the above shear resistance, ${}_r\mu_{wo}$, is given by,

$${}_r\mu_{wo} = 2_r\mu_t / \eta \tag{7}$$

This is the amount of shear reinforcements necessary to produce flexural-compression failure of the member. The concrete width required to constitute the beam mechanism, ${}_rb_1(={}_rb/b)$, varies depending on the magnitude of resistant shear of the same mechanism, that is, ${}_rb_1=2_r\mu_w$ when the capacity is determined by the tensile yielding of shear reinforcements (Eq.(3)), ${}_rb_1=4_r\mu_t/\eta$ when determined by the simultaneous yielding in tension and compression of the longitudinal reinforcements (Eq.(6)), and ${}_rb_1=2_rq/{}_rD_1$ when determined by Eqs.(4) and (5). Therefore, the width of resisting concrete for the arch mechanism, ${}_cb_1(={}_cb/b$, ${}_cb=b-{}_rb)$ can be expressed as,

$$\begin{aligned} {}_cb_1 &= 1 - 2_r\mu_w \\ {}_cb_1 &= 1 - 4_r\mu_t / \eta \\ \text{and} \\ {}_cb_1 &= 1 - 2_rq / {}_rD_1 \end{aligned} \tag{8}$$

depending, in the same order, on the above three cases.

2.3 $_cn$-$_cq$ Equations for Arch Mechanism

It is assumed that the arch mechanism is constituted when the resultant uniaxial compressive stress, $D\sigma$, of the nomal stress, $_c\sigma$, and the shear stress, $_c\tau$, both uniformly distributed over the compression region at both ends of the reinforcement-less concrete with the width $_cb$ which is the remaining width used for the beam mechanism, are produced in the direction that is off from the member axis by the angle of θ. Further, the maximum shear resistance of the arch mechanism is assumed to take place when the above-mentioned resultant stress, $D\sigma$, reaches F_c, when the shear strength, $_cq$, can be expressed by Eq.(9).

$$_cq = {}_cb_1 \{\sqrt{4\cdot {}_cn / {}_cb\cdot(1 - {}_cn / {}_cb_1) + \eta^2} - \eta \} / 2 \qquad (9)$$

in which, $\quad 0 \leq {}_cn \leq {}_cb_1$

Therefore, by substituting the corresponding values of $_cb_1$ given above into Eq. (9), the shear strength of the arch mechanism can be computed depending on those values of the beam mechanism. Note that Eq.(9) can also be written in the form shown below.

$$({}_cq + {}_cb_1\cdot\eta / 2)^2 + ({}_cn - {}_cb_1 / 2)^2 = {}_cb_1^2\cdot(1 + \eta^2) / 4 \qquad (10)$$

2.4 Application of Extended Additive Strength Theory

Next step of the analysis is computation of the strength of reinforced concrete member as a whole (n-q equation) by applying the additive strength theory using the above-obtained strengths of the beam mechanism ($_rn$-$_rq$ equation) and the arch mechanism ($_cn$-$_cq$ equation). However, the conventional theory of adding component strengths is not directly applicable to the shear problem under consideration. Illustrated in Fig.2 is the scheme of the strength addition for the current problem, where $_rI$ represents $_rn$-$_rq$ interaction curve of the beam mechanism, and $_cI_a$, $_cI_b$ and $_cI_c$ represent $_cn$-$_cq$ interaction curves of the arch mechanism associated with the change in concrete width, $_cb_1$. In the current analysis, the member strengths are to be calculated under the condition of, $_rb_1$+$_cb_1$=1. Therefore, the additive strength can be obtained considering that the arch mechanism varies with the condition of the beam mechanism strength. For instance, in Fig. 2, the strength of the beam mechanism represented by the point "a" (Eq(3))

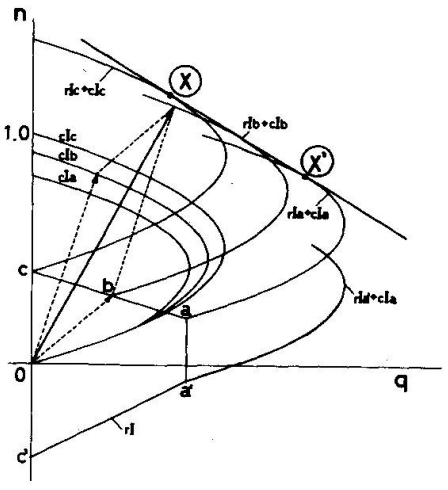

Fig.2 Extended Concept of Superposition

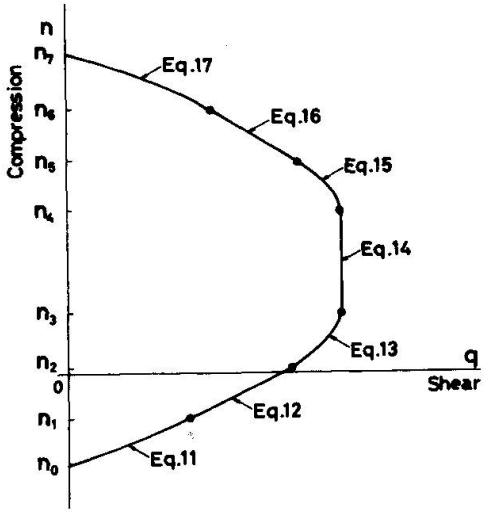

Fig.3 Interaction Cruves between Compression and Shear

should be added to that of the arch mechanism given by the curve ${}_cI_a$. Similarly, the strength of the point "b" (Eq.(5)) should be added to the curve ${}_cI_b$ and the point "c" to ${}_cI_c$. Therefore, the n-q interaction curve of the entire reinforced concrete member is given by the envelope of the curves obtained by the above-mentioned technique. The envelope is then expressed by the n-q equations, in which the shear strength, q, is given by Eqs.(11) through (17) depending on the magnitude of working compression, n(see Fig.3). In the current analysis, it is assumed that there exists linear relationship between the reduction ratio of the concrete width of the beam mechanism and the increase ratio of that of the arch mechanism. Therefore, the interaction curve between X and X' of the envelope in Fig.2 is represented by a straight line.

$$\text{(a) } n_0 \leqq n < n_1 \quad q = \{ \sqrt{4 (n + {}_r\mu_t)(1 - n - {}_r\mu_t) + \eta^2} - \eta \} / 2 \tag{11}$$

$$\text{(b) } n_1 \leqq n < n_2 \quad q = \lambda_1 (n - n_1) + q_1 \tag{12}$$

$$\text{(c) } n_2 \leqq n < n_3 \quad q = \delta \{ \sqrt{4 n_a (1 - n_a) + \eta^2} - \eta \} + {}_r\mu_w \cdot {}_rD_1 \tag{13}$$

$$\text{(d) } n_3 \leqq n < n_4 \quad q = \delta (\sqrt{1 + \eta^2} - \eta) + {}_r\mu_w \cdot {}_rD_1 \tag{14}$$

$$\text{(e) } n_4 \leqq n < n_5 \quad q = \delta \{ \sqrt{4 n_b (1 - n_b) + \eta^2} - \eta \} + {}_r\mu_w \cdot {}_rD_1 \tag{15}$$

$$\text{(f) } n_5 \leqq n < n_6 \quad q = \lambda_2 (n - n_6) + q_6 \tag{16}$$

$$\text{(g) } n_6 \leqq n \leqq n_7 \quad q = \{ \sqrt{4 (n - {}_r\mu_t)(1 - n + {}_r\mu_t) + \eta^2} - \eta \} / 2 \tag{17}$$

in which, $n_0 = - {}_r\mu_t$

$$n_1 = \{ \beta_1 \cdot \gamma - \sqrt{(\beta_1 \cdot \gamma)^2 - \omega_1 \cdot \rho} \} \gamma / \omega_1 + (1 - {}_r\mu_t) / 2$$

$$n_2 = 2\delta \cdot (n_1 + {}_r\mu_t) - {}_r\mu_t + {}_r\mu_w \cdot ({}_rD_1 + \eta)$$

$$n_3 = \delta - {}_r\mu_t + {}_r\mu_w \cdot ({}_rD_1 + \eta)$$

$$n_4 = \delta + {}_r\mu_t + {}_r\mu_w \cdot ({}_rD_1 - \eta)$$

$$n_5 = 2\delta \cdot (n_6 - {}_r\mu_t) + {}_r\mu_t + {}_r\mu_w \cdot ({}_rD_1 - \eta)$$

$$n_6 = \{ \beta_2 \cdot \gamma + \sqrt{(\beta_2 \cdot \gamma)^2 - \omega_2 \cdot \rho} \} \gamma / \omega_2 + (1 + {}_r\mu_t) / 2$$

$$n_7 = 1 + {}_r\mu_t$$

$$q_1 = \{ \alpha \cdot \gamma + \sqrt{(\alpha \cdot \gamma)^2 - \omega_1 \cdot \rho_1} \} \gamma / \omega_1 - \eta / 2$$

$$q_6 = \{ \alpha \cdot \gamma + \sqrt{(\alpha \cdot \gamma)^2 - \omega_2 \cdot \rho_2} \} \gamma / \omega_2 - \eta / 2$$

where,

$$\lambda_1 = \frac{\alpha \cdot \omega_1 - \{ \alpha \cdot \gamma + \sqrt{(\alpha \cdot \gamma)^2 - \omega_1 \cdot \rho_1} \} \gamma}{\beta_1 \cdot \omega_1 - \{ \beta_1 \cdot \gamma - \sqrt{(\beta_1 \cdot \gamma)^2 - \omega_1 \cdot \rho} \} \gamma}$$

$$\lambda_2 = \frac{\alpha \cdot \omega_2 - \{ \alpha \cdot \gamma + \sqrt{(\alpha \cdot \gamma)^2 - \omega_2 \cdot \rho_2} \} \gamma}{\beta_2 \cdot \omega_2 - \{ \beta_2 \cdot \gamma + \sqrt{(\beta_2 \cdot \gamma)^2 - \omega_2 \cdot \rho} \} \gamma}$$

$$n_a = \{ n + {}_r\mu_t - {}_r\mu_w \cdot ({}_rD_1 + \eta) \} / 2\delta$$

$$n_b = \{ n - {}_r\mu_t - {}_r\mu_w \cdot ({}_rD_1 - \eta) \} / 2\delta$$

$$\omega_1 = \alpha^2 + \beta_1^2 , \quad \omega_2 = \alpha^2 + \beta_2^2$$

$$\rho = \gamma^2 - \alpha^2 , \quad \rho_1 = \gamma^2 - \beta_1^2 , \quad \rho_2 = \gamma^2 - \beta_2^2$$

$$\alpha = ({}_rD_1 + \eta) / 2 , \quad \beta_1 = ({}_rD_1 + \eta - 1) / 2$$

$$\beta_2 = ({}_rD_1 - \eta - 1) / 2, \quad \gamma = \sqrt{1 + \eta^2} / 2, \quad \delta = (1 - 2_r\mu_w) / 2$$

$$m = M / bD^2F_c , \quad n = N / bDF_c , \quad q = Q / bDF_c$$

2.5 n-q Interaction Curves for Reinforced Concrete Columns

Schematic example of the n-q interaction curves of reinforced concrete members obtained by the forementioned analysis are illustrated in Fig.4 for various amount of shear reinforcements, $_r\mu_w$. In the figure, the interaction curves for the case of $_r\mu_w=0$ and for $_r\mu_{wo}$(Eq.(7)) are shown in dotted lines, and those for the case of $\eta=\infty$, which corresponds to the case where the shear strength is computed from end moments of the member that fails in flexure under compression and bending, are shown in chained lines. When a reinforced concrete member is subjected to combined compression, bending and shear, it is learned that the strength of the member does not reach flexural failure strength under compression and bending because of the effect of shear, even if the member is provided with the amount of shear reinforcements enough to cause simultaneous yielding of the longitudinal reinforcements both in compression and tension. It is also noted that the region where the shear strength maintains the constant ratio to the compression increases with the decrease in the amount of shear reinforcements. This proves that the influence of compression upon the shear strength reduces as the amount of shear reinforcements decreases.

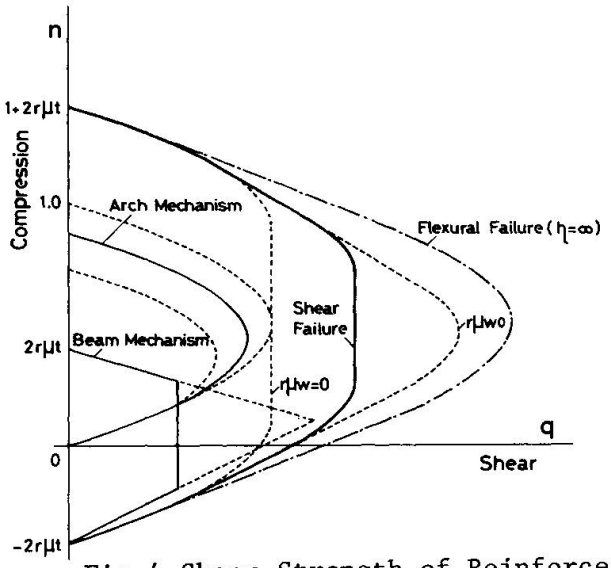

Fig.4 Shear Strength of Reinforced Concrete Column

Shown in Fig.5 are the n-q interaction curves of the reinforced concrete members with $_r\mu_t=0.2$, $_r\mu_w=0.05$ and $_rD_1=0.8$, computed for variable η . It is indicated that, for a constant value of $_r\mu_w$, the effect of compression on shear strength tends to become smaller as η becomes smaller. Hence, it is supposed that the compression tends to affect less in reinforced concrete members that fails in flexure than those that fails in shear.

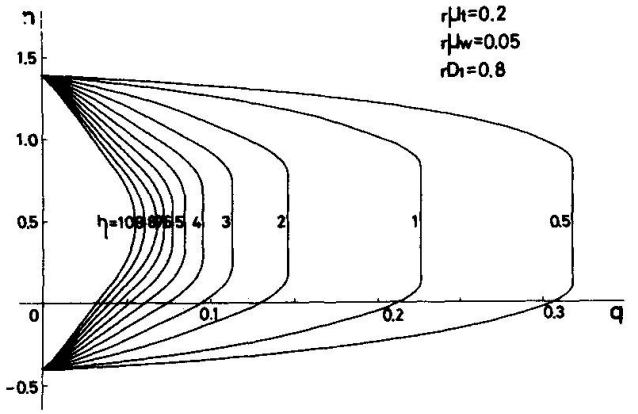

Fig.5 Nondimensional Interaction Curves between Compression and Shear

2.6 m-n-q Relationship of Reinforced Concrete Columns

Shown in Fig.6 are the m-q interaction relationship, transformed from the interaction curves given in Fig. 5, with n and η as variables. It is learned that, in the vicinity of the compression n=0.5 where either flexural or shear strength is the maximum, the m-q interaction curves are of concave configuration. In other words, the m-n-q interaction surface that represents the strength of a reinforced concrete member which predominantly fails in shear under combined compression, bending and shear does not show convex configuration.

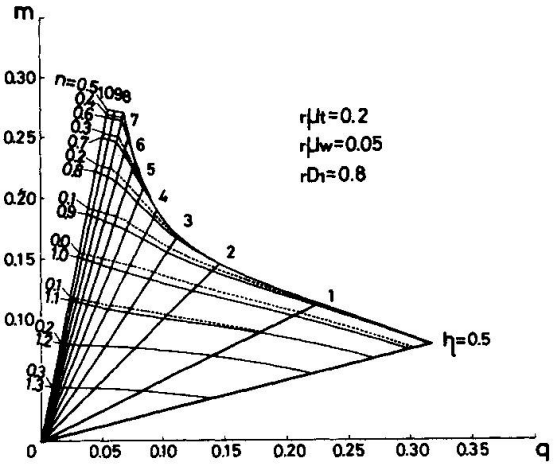

Fig.6 Nondimensional Interaction Curves between Bending and Shear

As an example of m-n-q interaction surface which contains a portion showing convex configuration, the interaction surface of the reinforced concrete members with $_{r}\mu_{t}$=0.2, $_{r}\mu_{w}$= 0.05 and $_{r}D_{l}$=0.8 are shown in Fig.7.

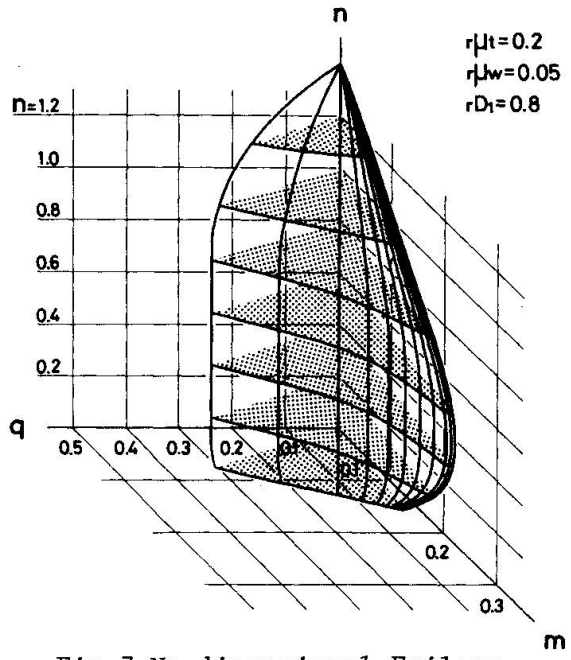

Fig.7 Nondimensional Failure Interaction Surface

Shown in Fig.8 is the m-q interaction curves for n=0.5, $_{r}D_{l}$=0.8 and $_{r}\mu_{t}$=0.25 with η and $_{r}\mu_{w}$ as variables. The outermost curve among these corresponds to the case where n=0.5 and the longitudinal reinforcements yield simultaneously in both tension and compression and shows that the m-n-q interaction surface is convex in all region when flexural failure predominates. Also, it is implied that the ratio of the flexural failure strength to the shear failure strength is greatly affected by the values of η and $_{r}\mu_{w}$, and the contribution of shear reinforcements to the strength capacity increase is smaller when η is smaller.

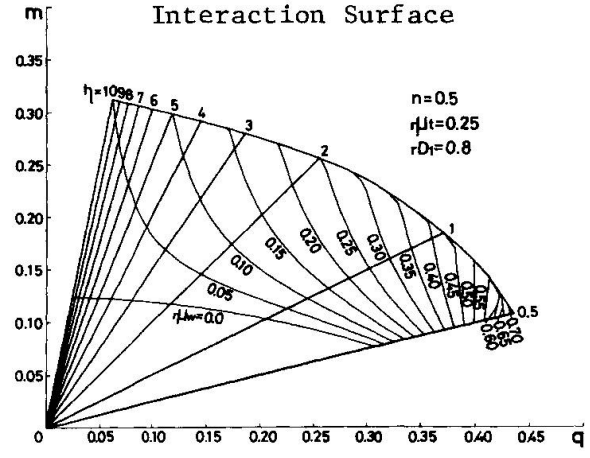

Fig.8 Nondimensional Interaction Curves between Bending and Shear

3. Diagonally Reinforced Concrete Columns

3.1 Failure Mechanism

Illustrated in Fig.9 is the ultimate state of columns with diagonal reinforcements resisting compression, bending and shear. The strength of a reinforced concrete column can be given by the sum of concrete strength and the strength of the system of diagonal reinforcements. Concrete, without reinforcement, only works against diagonally introduced com-

pression and prevents compressed reinforcements from buckling. Therefore, no shear failure takes place in concrete although eccentric compressive failure may occur. One set of main reinforcements is subjected to uniform compression, and the other set to uniform tension. When they reach their yield stress, plastic deformation progresses. At this state, bondage between concrete and main reinforcements is not necessary to resist the external load, and no bond failure should take place.

3.2 Equilibrium Analysis

Using a simple model of statical equilibrium of concrete and system of reinforcements as shown in Figs.8(a) and 8 (b), their strengths are obtained. The strength of a reinforced concrete member is then calculated by the extended concept of adding component strength of concrete and reinforcements. Computed shear strength of reinforced concrete columns with diagonal reinforcements in a non-dimensional expression are given below, depending on the non-dimensional magnitude of working compression, n as indicated in Fig.10.

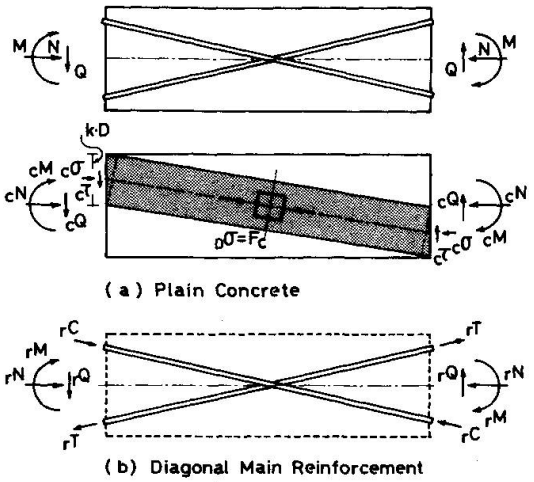

Fig.9 Equilibrium Analysis.

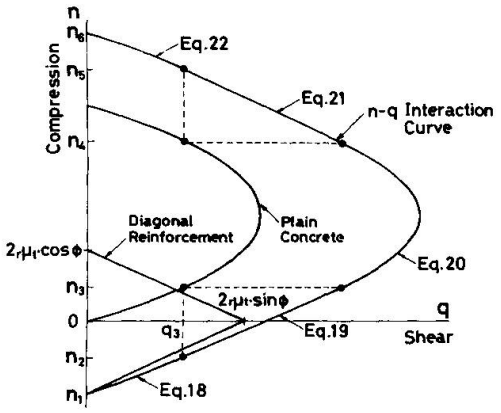

Fig.10 Method of Superposition.

(a) $n_1 \leqq n < n_2$ $\quad q = \frac{1}{2}\cdot\{ \sqrt{\eta^2 + 4\cdot(n - n_1) - 4\cdot(n - n_1)^2} - \eta \}$ (18)

(b) $n_2 \leqq n < n_3$ $\quad q = (n - n_3)\cdot\tan\phi + 2\cdot\mu_t\cdot\sin\phi + q_3$ (19)

(c) $n_3 \leqq n < n_4$ $\quad q = 2\cdot\mu_t\cdot\sin\phi + \frac{1}{2}\{ \sqrt{\eta^2 + 4\cdot n - 4\cdot n^2} - \eta \}$ (20)

(d) $n_4 \leqq n < n_5$ $\quad q = -(n - n_4)\cdot\tan\phi + 2\mu_t\cdot\sin\phi + q_3$ (21)

(e) $n_5 \leqq n \leqq n_6$ $\quad q = \frac{1}{2}\cdot\{ \sqrt{\eta^2 + 4\cdot(n + n_1) - 4\cdot(n + n_1)^2} - \eta \}$ (22)

in which $n_1 = -2\cdot\mu_t\cdot\cos\phi$, $\quad n_2 = -2\cdot\mu_t\cdot\cos\phi + (1 - \lambda) / 2$,

$n_3 = (1 - \lambda) / 2$ and $\geqq 0$, $\quad n_4 = (1 + \lambda) / 2$ and $\leqq 1$,

$n_5 = 2\cdot\mu_t\cdot\cos\phi + (1 + \lambda) / 2$, $\quad n_6 = 1 + 2\cdot\mu_t\cdot\cos\phi = 1 - n_1$,

and $\quad q_3 = \frac{1}{2}\cdot\{ \sqrt{\eta^2 + 4\cdot n_3 - 4\cdot n_3^2} - \eta \}$

where $n = N / bDF_c$ (positive for compression) , $\quad q = Q / bDF_c$,

$\mu_t = T_o / bDF_c$, $\quad \lambda = \sqrt{\tan^2\phi\cdot(1 + \eta^2) / (1 + \tan^2\phi)}$, $\eta = h / D$

b : column width , D : column depth , h : column length ,

F_c : compressive strength of concrete ,

T_o : tensile yield strength of diagonal reinforcement ,

ϕ : angle between column axis and diagonal reinforcement ,

N : applied axial compression , Q : shear strength of column .

4. COMPARISON OF ANALYSIS WITH EXPERIMENTS

Followings are the comparisons of analytical prediction to the experimental results. As shown in Fig.11, the experiments of 184 column specimens with ordinary main reinforcements were performed by the authers and these tests were composed of four series, Series I to IV, and refered to references [10][11][12] and [13] respectively.

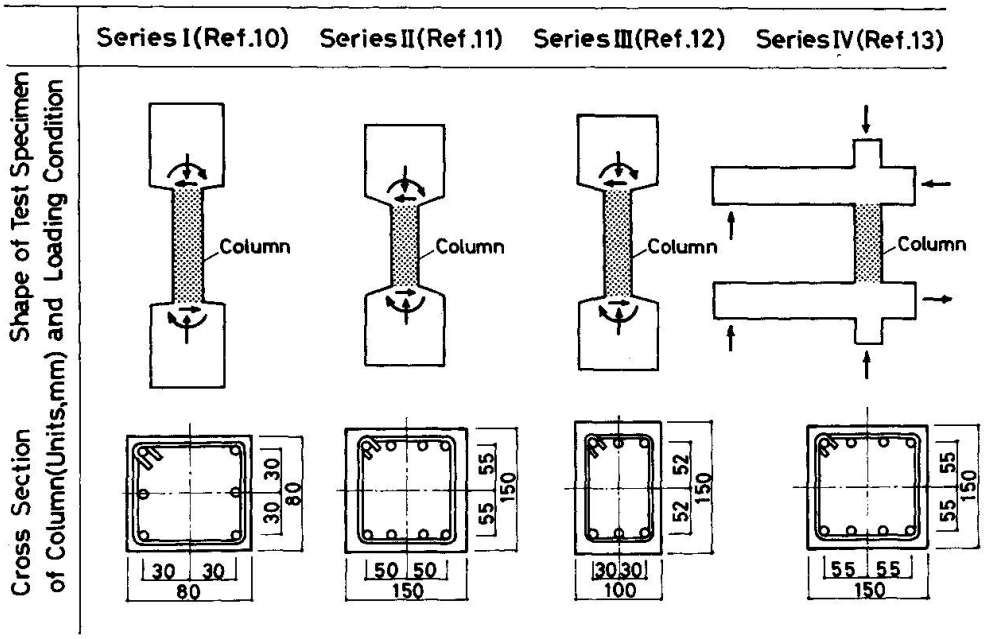

Fig.11 Shear Tests of Ordinary Reinforced Concrete Columns and Frames

Experimentally obtained failure interaction surface and that obtained by the analysis are compared in Fig.12, where the former was systematically made up from the experimental results on 100 test specimens of reinforced concrete members both with and without reinforcements of Series I[10]. In each of Fig. 12, three axes represent non-dimensional axial force (n), bending moment (m) and shear (q), and the figures on the left are drawn from the experimental results while those on the right show the analytical prediction. Series I-1(Fig.11(a)) is for the member without any reinforcement, that is, $r\mu_t=0$ and $r\mu_w=0$, and Series I-2 to I-4(Fig.12(b) to (d)) are for those of $r\mu_t=0.1$ with $r\mu_w$ being equal to 0, 0.05 and 0.1 respectively.

General trend common in all the series is that the analytically obtained failure interaction surfaces are slightly smaller than those obtained by the experiments. However, the configurational characteristics of both surfaces are alike each other. Here again, the failure interaction surface shows concave shape in the region where shear failure is predominant over flexural failure while the surface is convex for members with much shear reinforcements and larger values of η, hence the shear failure is unlikely to take place. Also, it is indicated that the influence of working axial force upon the shear capacity is less in those members with less amount of shear reinforcements and smaller value of η.

Figure 13 shows the histogram of the ratios of experimental results to analytical prediction obtained from Series II to IV. The mean value of the ratio is 1.08 and the standard deviation is 0.228.

(a) Series I-1
Plain
Concrete
$r^{\mu}t = 0$
$r^{\mu}w = 0$

(b) Series I-2
Reinforced
Concrete
$r^{\mu}t = 0.1$
$r^{\mu}w = 0$

(C) Series I-3
Reinforced
Concrete
$r^{\mu}t = 0.1$
$r^{\mu}w = 0.05$

(d) Series I-4
Reinforced
Concrete
$r^{\mu}t = 0.1$
$r^{\mu}w = 0.10$

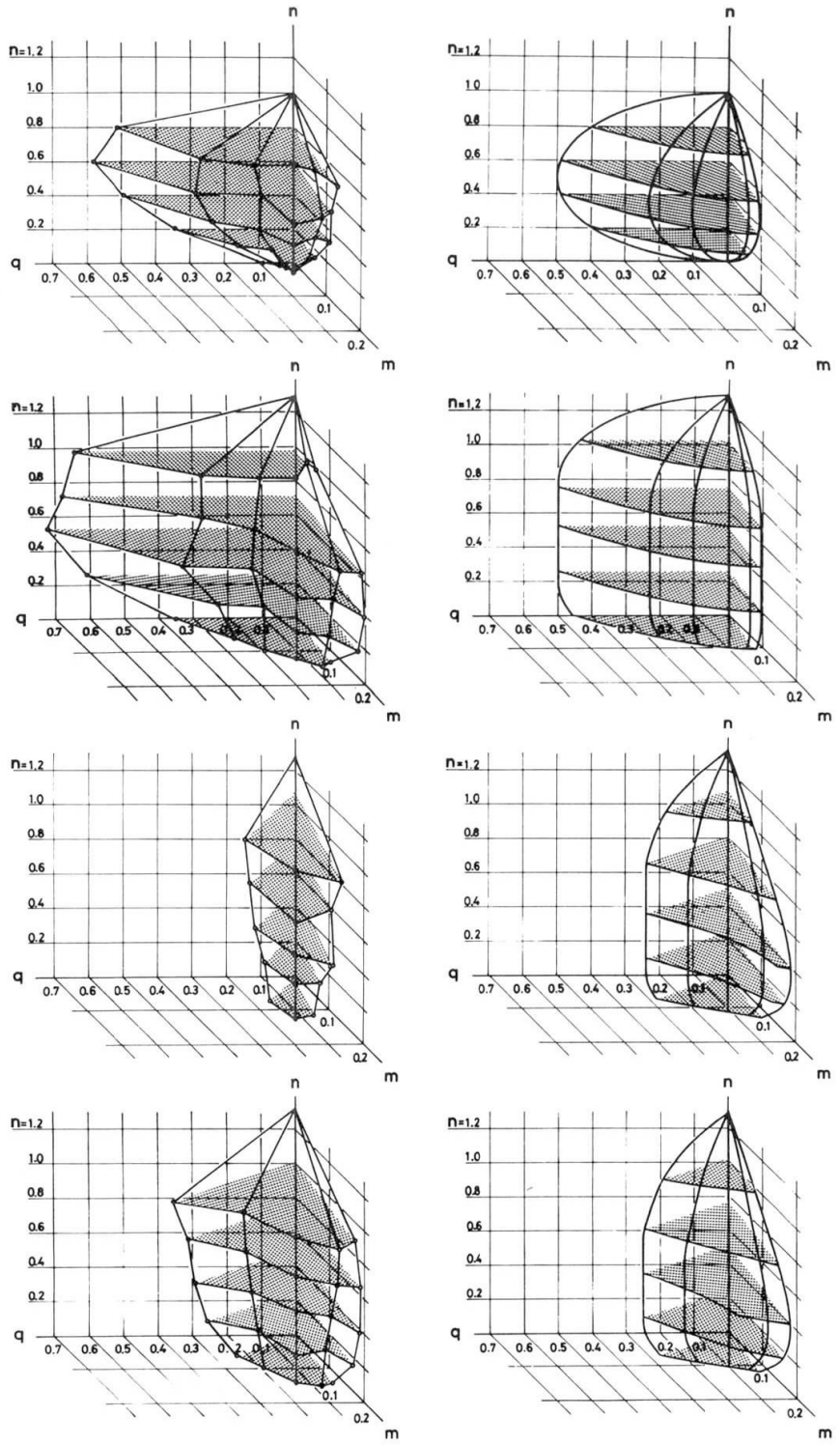

Experimental Results Analytical Prediction

Fig.12 Comparison of Analytical Prediction to Experimental Results

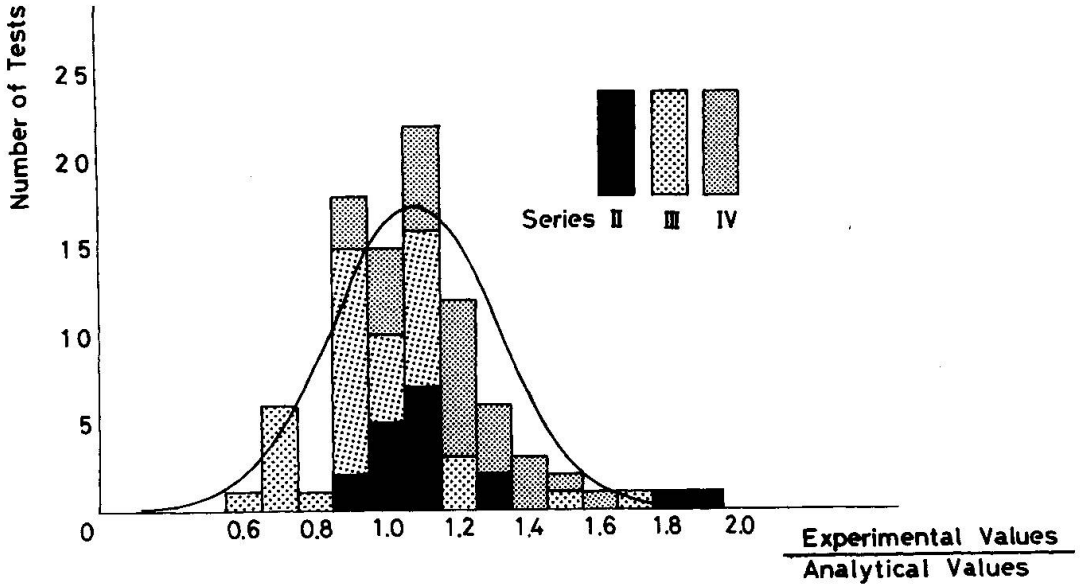

Fig.13 Histogram of the Ratios of Experimental Values to Analytical ones

5 CONCLUSION

Proposed in this paper was an analytical approach to determine the shear capacity of reinforced concrete members subjected to combined compression, bending and shear. The analysis made use of the so-called extended additive strength theory based upon beam and arch mechanism concept. In the case of diagonally reinforced concrete columns, the additive strength theory is based on diagonal reinforcement and arch mechanism.

The resulting analytical solution for ordinary reinforced concrete columns were expressed in terms of the magnitude of compression, the length-to-depth ratio of column, the amount of longitudinal and shear reinforcements, material strength, cross-sectional dimensions and others. For reinforced concrete columns, m-n-q failure interaction surface was obtained which enables one to know the effect of axial force and bending upon shear strength of columns. It is indicated that failure surface is concave in the region where shear failure is predominant, and that the ultimate strength of reinforced concrete member that is supposed to fail in shear is hardly affected by axial force.

The configurational characteristics of theoretically and experimentally obtained interaction surfaces are alike each other and the mean value of the ratios of the experimental values to analytical ones are 1.08.

NOTATION

b = width of rectangular section
D = depth of rectangular section
$_rD$ = distance between top and bottom longitudinal reinforcement
$_rD_1$ = distance ratio of longitudinal reinforcement ($_rD/D$)
F_c = concrete cylinder strength
h = column length
M = bending moment in general
m = non-dimensional bending moment (M/bD^2F_c)
N = axial force in general

n = non-dimensional axial force (N/bDFc)
Q = shear force in general
q = non-dimensional shear force (Q/bDFc)
r_{pt} = longitudinal reinforcement ratio
r_{pw} = shear reinforcement ratio
T_o = tensile yield strength of diagonal reinforcement
$r\sigma_y$ = yield stress of longitudinal reinforcement
$r_w\sigma_y$ = yield stress of shear reinforcemtnt
η = column length-to-depth ratio (h/D)
μt = diagonal reinforcement parameter (T_o/bDF_c)
$r\mu t$ = longitudinal reinforcement parameter ($r_{pt}\cdot r\sigma_y/F_c$)
$r\mu w$ = shear reinforcement parameter ($r_{pw}\cdot r_w\sigma_y/F_c$)
ϕ = angle between column axis and diagonal reinforcement

REFERENCES

1. HATTORI, T., T. SHIBATA and K. ONO, "On the Mechanism of Shear Failure of Reinforced Concrete Members", Trans. Architectural Institute of Japan, No. 200, Oct., 1972, pp.35-44 (in Japanese).
2. SUENAGA, Y. and R, ISHIMARU, "Kinematic Analysis of Concrete Members under Combined Stresses-Part 4 — A Theoretical Study on the Ultimate Shear Strength of Reinforced Concrete Beams and Columns", Trans. Architectural Institute of Japan, No.221, July, 1974, pp.9-16 (in Japanese).
3. KATO, B, and R. SHOHARA, "Strength of Steel-Reinforced Concrete Members", Trans. Architectural Institute of Japan, No.266, Apr., 1978, pp.19-29 (in Japanese).
4. BRAESTRUP, M. W., "Plastic Analysis of Shear in Reinforced Concrete", Magazine of Concrete Research, Vol.26, No.89, Dec., 1974, pp.222-228.
5. GROB, J. and B. THURLIMANN , "Ultimate Strength and Design of Reinforced Concrete Beams under Bending and Shear", Publication, IABSE, 1976, pp.105-120.
6. NIELSEN, M. P., M. W. BRAESTRUP and F. BACH, "Rational Analysis of Shear in Reinforced Concrete Beams", IABSE Periodical, No.2, May, 1978, IABSE Proceedings P-15/78.
7. NIELSEN, M. P. and M. W. BRAESTRUP, "Shear Strength of Prestressed Concrete Beams without Web Reinforcement", Magazine of Concrete Research, Vol.30, No. 104, Sept., 1978, pp.119-128.
8. THURLIMANN, B., "Plastic Analysis of Reinforced Concrete Beams", Introductory Report of IABSE Colloquium KOPENHAGEN 1979, Plasticity in Reinforced Concrete, 1979, pp.71-90.
9. CAMPBELL, T. I., L. CHITNUYANONDH and B. dev BATCHELOR, "Rigid-Plastic Theory B. Truss Analogy Method for Calculating the Shear Strength of Reinforced Concrete Beams", Magazine of Concrete Reseach, Vol.32, No.110, Mar., 1980, pp. 39-44.
10. WAKABAYASHI, M., K. MINAMI and S. TOKURA, "Experimental Studies on Failure Surface of Reinforced Concrete Columns under Axial Force, Bending and Shear", Annuals, Disaster Prevention Research Institute, Kyoto University, No.18-B, April 1975, pp.125-141 (in Japanese).
11. WAKABAYASHI, M., K. MINAMI, T. NAKAMURA, R. SASAKI and S. MORINO, "Some Tests on Elastic- Plastic Behavior of Reinforced Concrete Frames with Emphasis on Shear Failure of Column", Annuals, Disaster Prevention Research Institute, Kyoto University, No.17-B, Oct. 1974, pp.171-189 (in Japanese).
12. WAKABAYASHI, M. and K. MINAMI, "An Experimental Study on Hysteretic Characteristics of Reinforced Concrete Columns Failing in Shear", Proc. of the Symposium on Resistance and Deformation of Structures and Their Components, 18th National Symposium on Bridge and Structural Engineering, Japan Society for the Promotion of Science, Tokyo, 1972, pp.97-112.
13. MINAMI, K. and M. WAKABAYASHI, "Seismic Resistance of Reinforced Concrete Beam-and-Column Assemblages with Emphasis on Shear Failure of Column", Proc. of 6th WCEE, New Delhi, Jan. 1977, Vol.III, pp.3101-3106.

Evaluation of Tension Stiffening Effects in Reinforced Concrete Linear Members

Détermination des effets de "tension stiffening" dans des éléments linéaires en béton armé

Reststeifigkeit von stabförmigen Stahlbetonbauteilen

WOLFGANG MOOSECKER
Dr.-Ing., M.Sc.
Technische Universitat München
München, Fed. Rep. of Germany

currently at: Istituto di Scienza
e Tecnica delle Costruzioni
Universita di Pavia, Italy

EMIL GRASSER
Professor Dr.-Ing.
Technische Universitat München
München, Fed. Rep. of Germany

SUMMARY
The stiffness of reinforced concrete beams is increased by tensile concrete stresses between cracks. Methods to evaluate this stiffening effect are described and results obtained using these methods are compared with test results. A satisying agreement is found using several methods for first loading. For the case of reloading a calculation procedure is proposed.

RÉSUMÉ
Entre les fissures dans une poutre en béton armé existent des contraintes de traction. Ces contraintes contribuent à la raideur. Cette communication a pour objet la considération et le calcul de l'augmentation du raideur. Les résultats ont montré une bonne concordance avec les essais.

ZUSAMMENFASSUNG
In Stahlbetonbalken bestehen zwischen den Rissen Betonzugspannungen, die einen Beitrag zur Steifigkeit liefern. Methoden zur Berücksichtigung dieser Steifigkeitserhöhung werden beschrieben und die mit ihnen ermittelten Resultate mit Versuchsergebnissen verglichen. Dabei kann mit verschiedenen Methoden gute Übereinstimmung für Erstbelastung erzielt werden. Für den Fall der Wiederbelastung wird ein Berechnungsverfahren vorgeschlagen.

1. INTRODUCTION

Reinforced concrete sections are usually designed for bending moments and axial forces neglecting any resistance of concrete to tensile stresses. This approximation can well be made for cracked sections. Between cracks, tensile stresses are transferred to the concrete by means of bond stresses between reinforcement and adjacent concrete. Thus, the steel stresses are reduced between cracks and the stiffness is increased with respect to the cracked state without any contribution of concrete in tension. This effect which has been called the "tension stiffening effect of concrete" is of considerable interest in members with a small amount of reinforcement.

Numerous methods have been proposed in the literature for the treatment of tension stiffening effects, many of them being fundamentally different from each other. Since there have been at least ten new proposals ([1] to [9] , [17]) in the last three years, it is now necessary to study the results of the existing procedures and to compare them with test results in order to determine whether further refinements and new proposals are still necessary.

2. METHODS FOR THE EVALUATION OF TENSION STIFFENING EFFECTS FOR FIRST LOADING

2.1 Complete description of steel stress distribution

By integrating the differential equation of bond with the help of an appropriate bond-slip relationship and boundary conditions, a complete description of steel and concrete stresses and strains along the axis of reinforcement can be developed. NOAKOWSKI [3] has used this procedure for the determination of effects due to temperature gradients, where it can be assumed that between cracks remain undisturbed regions.

PLAUK [8] has developed an iterative procedure to determine the steel stress distribution by assuming a parabolic distribution of bond stresses. According to his proposal the maximum value of bond stress depends on a bond-slip relationship derived from pullout tests.

2.2 Determination of average steel stress

The average steel stress σ_m is calculated from

$$\sigma_m = \sigma_s - \Delta\sigma_s \tag{1}$$

where σ_s is the steel stress in a cracked section without any contribution of concrete tensile stresses and $\Delta\sigma_s$ is the average reduction of steel stress due to tension stiffening effects. From equilibrium considerations, $\Delta\sigma_s$ can be determined as

$$\Delta\sigma_s = c\, f_{tc}\, \frac{A_{ct}}{A_s} \tag{2}$$

with: c = empirical factor
f_{tc} = concrete tensile strength
A_{ct} = area of concrete in tension
A_s = area of reinforcement cross-section

YU, WINTER [1o] have expressed the tensile strength of concrete in eq.(2) in terms of the compressive strength and propose the equation

$$\Delta\sigma_s = o,o2\ f_c^{2/3}\ \frac{b\ h\ (h - x)}{A_s\ z} \qquad (3)$$

where: f_c = compressive strength of concrete
b = width of cross-section in the tension zone
h = total height of section
x = height of compression zone
z = lever arm of internal forces

In eq. (3), $\Delta\sigma_s$ and f_c must be expressed in MN/m^2.

By studying the experimental evidence, RAO [11] has found that the reduction $\Delta\sigma_s$ due to tension stiffening is reduced when the applied forces increase. A good fit of experimental data was found with the expression

$$\Delta\sigma_s = o,18\ \frac{\sigma_{sr}}{\sigma_s}\ f_{tc}\ \frac{bd}{A_s} \qquad (4)$$

where: σ_{sr} = steel stress in a cracked section immediately after cracking
σ_s = steel stress in a cracked section at the load level considered
d = effective height.

Eq. (4) was further modified for the CEB-FIP Model Code for Concrete Structures [12] :

$$\Delta\sigma_s = c\ \frac{\sigma^2_{sr}}{\sigma_s} \qquad (5)$$

where c is a factor depending on bond characteristics and type of loading.

2.3 Fictitious stress-strain relationship for steel

Already in 195o, MURASHEV proposed to multiply the elastic modulus of steel by an empirical factor to take into account the stiffening effect of concrete in tension. The appropriate factor was determined from experiments in function of concrete strength, percentage of reinforcement, steel stress and loading characteristics.

Recently, GILBERT, WARNER [2] have made a refined proposal for a fictitious stress-strain relationship to be used in the analysis of slabs (fig.1).

2.4 Fictitious stress-stain relationship for concrete in tension

In analogy to the consideration of average steel stresses along the beam axis, also average concrete stresses in the tension zone of reinforced concrete beams can be considered. In the last few years, there have been several proposals to relate these to the average tensile strains in the tension zone. In figure 2, such fictitious relationships used by SCANLON, MURRAY [13] , LIN, SCORDELIS [15], CHITNUYANONDH et al. [5] and COPE et al. [7] are compared. It can be concluded that there is very little agreement on the shape of such a stress-strain function. Other proposals have been made by MACCHI, SANGALLI [6] (constant concrete tensile stress in the tension zone), QUAST [9] (analogous stress-strain relationship as in compression), and GILBERT, WARNER [2].

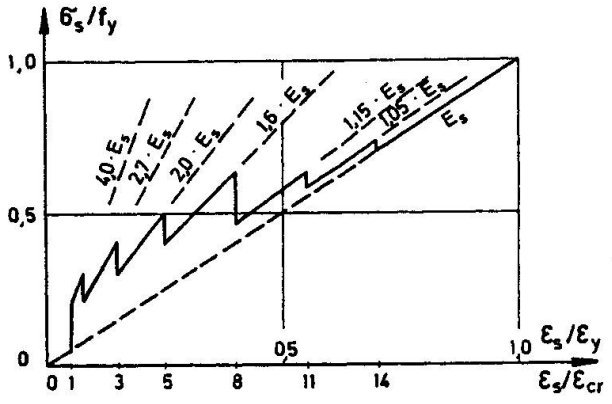

Fig.1: Fictitious stress-strain relationship for steel proposed by GILBERT, WARNER [2]

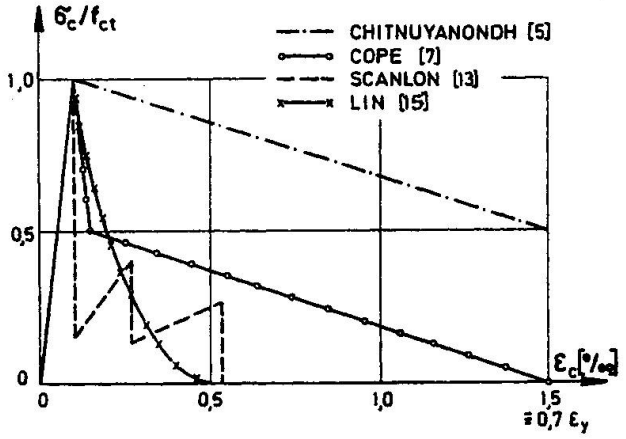

Fig.2: Comparison of fictitious stress-strain relationships for concrete in tension

2.5 Fictitious additional reinforcement

The average tensile force in the concrete between cracks can also be represented by a fictitious reinforcement to be added to the real reinforcement. The German concrete code (DIN 1045) recommends to enlarge the tensile reinforcement by 10 %. Another approach is followed by CAUVIN [4] who has derived the equation

$$\Delta A_s = c \frac{f_{tc} \cdot b \, (d - x)}{\sigma_s} \qquad (6)$$

where: ΔA_s = area of fictitious reinforcement
c = factor, can be taken as 1/6
σ_s = stress in reinforcement $(A_s + \Delta A_s)$

This proposal can be regarded as a special case of the methods discussed in chapter 2.2.

2.6 Determination of effective stiffness

The stiffness of reinforced concrete beam elements can also be determined directly without explicit evaluation of the average stress and strain state in the tension zone by means of moment-curvature relations.

KRAEMER, THIELEN, GRASSER [14] have used piecewise linear moment-curvature functions which are characterized by the points:
- cracking moment and corresponding stiffness of uncracked section,
- yield moments of tension and compression reinforcement and corresponding stiffness of cracked section
- ultimate limit state.

The fact that the formation of cracks in reinforced concrete beams is influenced by the random nature of the concrete tensile strength is considered by RAUE, TUNG [17].

For the calculation of deflections, the ACI Building Code (318-71 and 318-77) gives a simple expression for the effective moment of inertia to be used (originally developed by BRANSON):

$$I_{eff} = \left(\frac{M_{cr}}{M_{max}}\right)^3 I_g + \left[1 - \left(\frac{M_{cr}}{M_{max}}\right)^3\right] I_{cr} \qquad (7)$$

where: I_{eff} = effective moment of inertia
I_g = gross moment of inertia
I_{cr} = moment of inertia of cracked transformed section
M_{cr} = cracking moment
M_{max} = maximum moment

3. COMPARISON WITH TEST RESULTS

The results which are obtained using some of the methods described in chapter 2 are compared with test results. For the calculations, a parabolic-rectangular stress-strain relationship for concrete in compression is used as defined in the CEB-FIP Model Code [12] . The maximum concrete stress is taken as 85 % of the concrete cube strength f_c. The tensile strength f_{tc} of concrete is evaluated from

$$f_{tc} = 0{,}30\ f_c^{2/3} \qquad (8)$$

It must be noted that the behaviour of reinforced concrete beams is subject to random variations even if they are produced under laboratory conditions. Therefore, small deviations between test results and calculated values cannot be regarded to be essential.

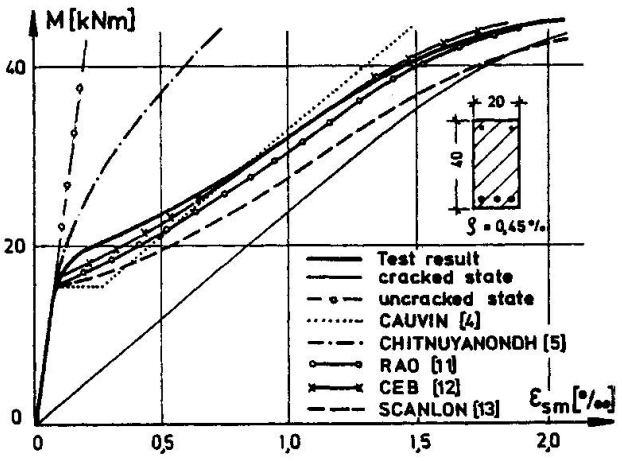

Fig.3: Mean strain of tension reinforcement as a function of bending moment for beam 4 of CLARK, SPEIRS [1]

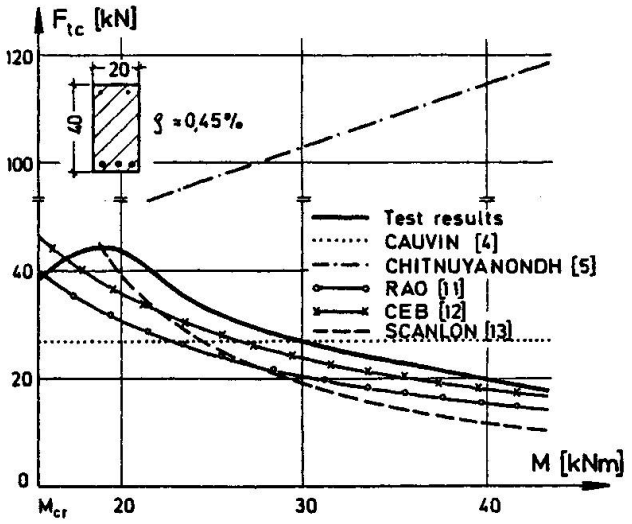

Fig.4: Tension stiffening force as a function of bending moment for beam 4 of CLARK, SPEIRS [1]

In fig. 3, the average strains ε_{sm} in the tensile reinforcement calculated with different procedures are compared with test results obtained by CLARK, SPEIRS [1] . The strains in an uncracked section and in a cracked section without any contribution of concrete in tension are also shown. The fact

that the reduction of average tensile strains with respect to the cracked state is diminishing when the applied bending moment is increased, is well reflected by most methods. Only the fictitious stress-strain relationship for concrete in tension proposed for prestressed concrete wall segments by CHITYUNDANONDH et al [5] leads to unrealistic results in this case. The results of the procedures of RAO [11] and the CEB-FIP Model Code [12] show excellent agreement with the test results.

The tension stiffening effect can also be described by a tensile force F_{tc} in the concrete, which is shown in fig. 4 as a function of the applied moment for the same beam of CLARK, SPEIRS. For the test results and the methods which do not explicitly define the average tensile stress state of concrete, the concrete tensile force is assumed to act at the level of the reinforcement and can be defined by

$$F_{tc} = (\sigma_m - \sigma_{II}) \cdot A_s$$

where: σ_m = average stress in the reinforcement
σ_{II} = stress in a cracked section under the same bending moment
A_s = area of reinforcement cross-section

It can be stated that the tension stiffening force is well approximated by most methods.

For the evaluation of deformations, it is necessary to determine the stiffness of beam elements. The stiffness is in most cases defined by means of moment-curvature relations. In fig. 5, curves which are derived theoretically are compared with the values determined by CLARK, SPEIRS from average strain measurements. For the methods which do not define the tensile stress state of concrete, it is assumed that the maximum concrete strain can be taken as the value calculated for a cracked section. It can be seen that the results of different procedures agree quite well and that the stiffness is, for the example considered, somewhat underestimated.

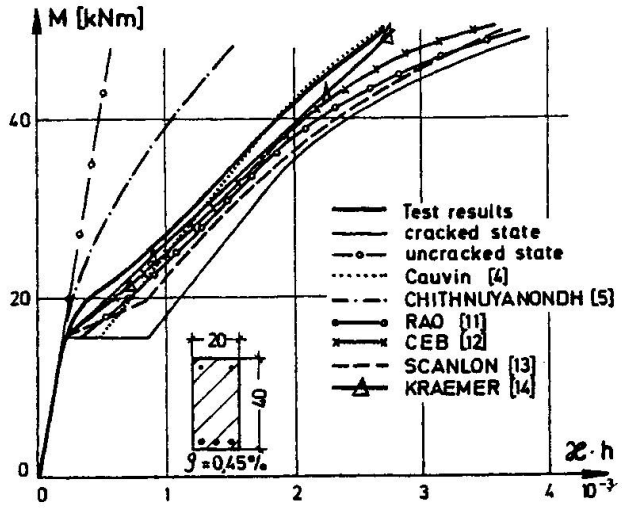

Fig.5: Moment-curvature relationship for beam 4 of CLARK, SPEIRS [1]

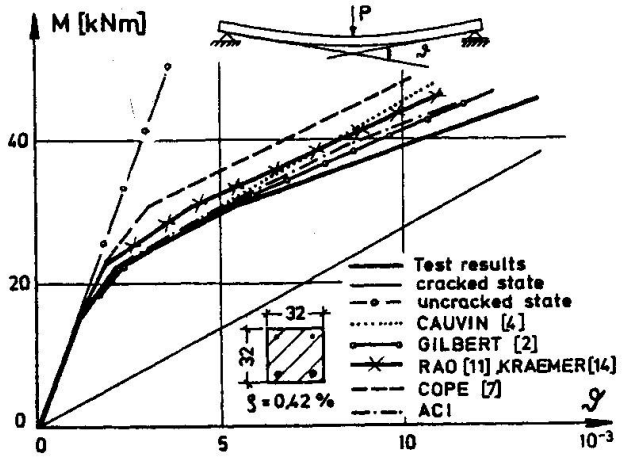

Fig.6: Rotation of support sections as a function of maximal moment for beam 1.13 of EIFLER, PLAUK [16]

Since there are no deformations recorded in [1] , measured and calculated deformations are compared in fig.6 for a beam tested by EIFLER, PLAUK [16] . To determine the deformations, moment-curvature relations have been derived in an analogous way as for fig.5. Also, the effective stiffness method of the ACI code (eq.7) is included in the comparison. For all calculations, shear deformations have been disregarded. It can again be stated that the calculated deformations agree reasonably well with the test results for most methods, but are in this case somewhat smaller than the recorded values indicating an overestimation of stiffness.

The distribution of internal forces in reinforced concrete beams is in general not very much affected by tension stiffening effects. But this influence can be large for internal forces due to actions which dependdirectly on stiffness such as imposed deformations. If imposed deformations are dominant, it must be considered that the crack pattern may not be complete (NOAKOWSKI [3] , MACCHI, SANGALLI [6])

Since there are very few experiments with imposed deformations, a theoretical example is considered. A fixed end beam is acted upon by a constant temperature gradient $\Delta t = 20^{o}$, which produces negative moments almost of the magnitude of the cracking moment. Fig.7 shows the maximum support and span moments of the beam as a function of an applied distributed load p. It can be seen that there is a large difference between the moments calculated for the uncracked and cracked state, the latter being determined without taking into account concrete tensile stresses. The tension stiffening effect of concrete influences the distribution of bending moments up to a load level where the maximum support moment reaches half of the yield moment M_y. For larger loads, the distribution of bending moments is very close to the fully cracked state.

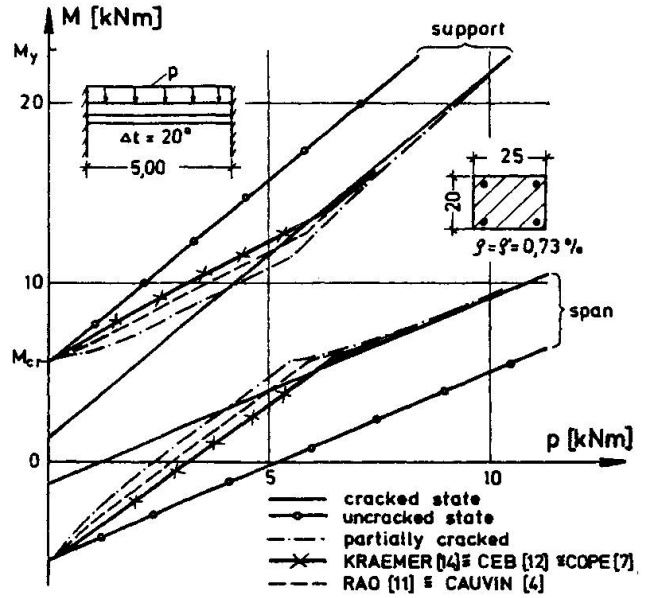

Fig.7: Calculated maximum support and span moments for distributed load p and temperature gradient Δt

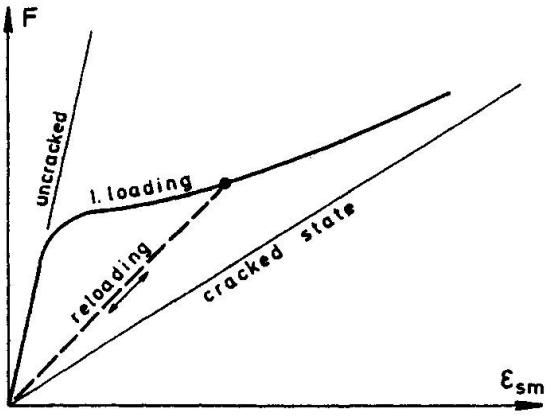

Fig.8: Mean steel stress at reloading according to SCHLAICH et al [18]

4. INFLUECNE OF LOAD REPETITIONS

It is a well known fact, that the influence of concrete tensile stresses on the stiffness of reinforced concrete beams is reduced by load repetitions, but there have been much less efforts to evaluate this reduction. KRIPANARAYANAN, BRANSON [2o] have modified the ACI formula (eq.7) to account for the influence of load repetitions

$$I_{rep} = \psi I_{eff} + (1 - \psi) I_g \qquad (1o)$$

with: $\psi = (P_{ult}-P_{rep})/(P_{ult}-P_{cr})$

I_{rep} = effective moment of inertia for load repetions
I_{eff} = effective moment of inertia without load repetions (eq.7)
I_g = gross moment of inertia
P_{ult} = ultimate load estimated with ACI code procedures
P_{rep} = maximum load of load repetition
P_{cr} = load at initial cracking

SCHLAICH, SCHOBER, KOCH [18] have performed tests on reinforced concrete tubes under axial load and bending. They have studied the stiffening effect of concrete in tension also during 3o load cycles of the transverse force with the upper load limit being the working load according to the German concrete code (DIN 1o45). From their experiments they deduce that the mean steel strain in the tensile reinforcement can be determined from a straight line connecting the strain at the maximum preload (fig.8) with the origin.

The tension stiffening effect is only considerable in beams with a small amount of reinforcement. In such beams the maximum steel strain is much larger than the maximum concrete strain in the compression zone. Considering these facts, it can be assumed that an analogous approximation can also be made for the moment-curvature relationship (fig.9). It must be noted that the reloading branch can only be assumed to go back to the origin, if the reinforcement has not exhibited plastic deformations. In the latter case, the curvature $\varkappa_{pl}$ due to plastic strains must remain after unloading.

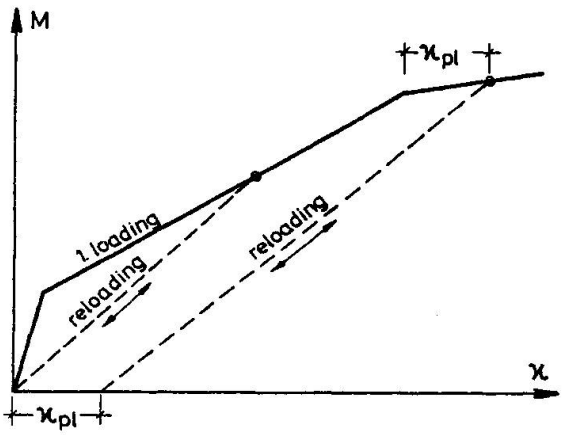

Fig.9: Moment-curvature relations for reloading

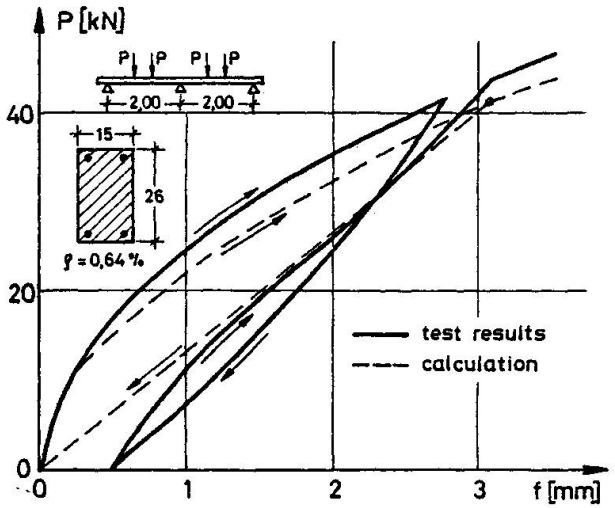

Fig.1o: Calculated and measured deflections at first loading and reloading of beam B 2 of MONNIER [19]

This approximation of the curvature at unloading together with a trilinear moment-curvature relationship for the first loading are used to calculate the maximum deflection of a test beams of MONNIER [19] . It can be seen, that the deflections are also reasonably well determined during unloading and reloading except for very small loads (fig.1o).

5. CONCLUSIONS

Methods to evaluate the stiffening effect of concrete tensile stresses between cracks for first loading and reloading have been described and their results have been compared with test results. It can be concluded that the influence of concrete tension at first loading on mean steel stresses, moment-curvature relations and deformations can be well approximated with most methods. Some of the proposed fictitious relationships between average concrete tensile strains and stresses cannot be used for reinforced concrete beams. It has been found that tension stiffening effects influence considerably the distribution of internal forces in statically indeterminate beams due to imposed deformations when additional external loadings are not dominant.

The stiffening effect of concrete in tension is reduced at reloading and can be evaluated approximately using a modified moment-curvature relationship.

REFERENCES

1. CLARK, L.A., SPEIRS, D.M.: Tension stiffening in reinforced concrete beams and slabs under short-term load, Cement and Concrete Ass., Rep.42.521, 1978
2. GILBERT, R.I., WARNER, R.F.: Tension stiffening in reinforced concrete slabs, ASCE, J.Str.Div. 1o4 (1978), ST 12
3. NOAKOWSKI, P.: Die Bewehrung von Stahlbetonbauteilen bei Zwangbeanspruchung infolge Temperatur, Deutscher Ausschuß für Stahlbeton, H.296, 1978
4. CAUVIN, A.: Analisi nonlineare di telai piani in cemento armato, Giornale del Genio Civile, 1978, p. 47-66
5. CHITNUYANONDH, L., RIZKALLA, S., MURRAY, D.W., MACGREGOR, J.G.: Effective tensile stiffening in prestressed concrete wall segments, 5th SMIRT, Berlin 1979
6. MACCHI, G., SANGALLI, D.: Effect of crack formation process and tension stiffening on thermal stress relaxation in reinforced concrete containments, 5th SMIRT, Berlin 1979
7. COPE, R.J., RAO, P.V., CLARK, L.A.: Nonlinear design of concrete bridge slabs using Finite Element procedures, Int.Symp.Nonlinear Design of Concr.Str., Waterloo 1979
8. PLAUK, G.: Ermittlung der Verformungen biegebeanspruchter Stahlbetonbalken mit der Methode der Finiten Elemente, Bundesanstalt für Materialprüfung, Bericht 59, 1979
9. QUAST, U.: Rechenansätze in Form einer Spannungsdehnungsbeziehung für das Mitwirken des Betons in der gerissenen Zugzone von Stahlbetonquerschnitten, TU Braunschweig, 198o
1o. Yu, W., WINTER, G.: Instantaneous and long-time deflections of reinforced concrete beams under working loads, ACI Journal 57, No.1, July 196o
11. RAO, P.S.: Die Grundlagen zur Berechnung der bei statisch unbestimmten Stahlbetonkonstruktionen im plastischen Bereich auftretenden Umlagerungen der Schnittkräfte, Deutscher Ausschuß für Stahlbeton, H. 177, 1966
12. CEB-FIP: Model Code for Concrete Structures, 3rd Edition, 1978
13. SCANLON, A., MURRAY, D.W.: Discussion to paper of GILBERT, WARNER, ASCE, J.Str.Div. 1o6 (198o), ST 1

14. KRAEMER, U., THIELEN, G., GRASSER, E.: Berechnung der Durchbiegung von biegebeanspruchten Stahlbetonbauteilen unter Gebrauchslast, Beton- und Stahlbetonbau 7o (1975), H.4
15. LIN, C., SCORDELIS, A.C.: Nonlinear analysis of r.c.shells of general form, ASCE, J.Str.Div. 1o1 (1975), ST 3
16. EIFLER, H., PLAUK, G.: Drehfähigkeit plastischer Gelenke in biegebeanspruchten Stahlbetonkonstruktionen, Teil A, Bundesanstalt für Materialprüfung, 1974
17. RAUE, E., TUNG, T.T.: Ermittlung der Formänderungen und Schnittkräfte in zwangbeanspruchten Stahlbetonbalken bei Biegung unter Berücksichtigung des Zufallscharakters der Betonzugfestigkeit, Bauplanung-Bautechnik 26 (1979)
18. SCHLAICH, J., SCHOBER, H., KOCH, R.: Versuche zur Mitwirkung des Betons in der Zugzone von Stahlbetonröhren, Universität Stuttgart, 1979
19. MONNIER, T.: The behaviour of continuous beams in reinforced concrete, TNO, Delft 1969
2o. KRIPANARAYANAN, K.M., BRANSON, D.E.: Short-time deflections of beams under single and repeated load cycles, ACI Journal 69, Feb. 1972

Non-linear Finite Element Analysis of Deep Beams

Analyse non-linéaire par éléments finis de poutres de petite portée

Nichtlineare Finite-Elemente-Berechnung von hohen Trägern

JUNICHIRO NIWA
Graduate Student
University of Tokyo
Tokyo, Japan

KOHICHI MAEKAWA
Graduate Student
University of Tokyo
Tokyo, Japan

HAJIME OKAMURA
Associate Professor
University of Tokyo
Tokyo, Japan

SUMMARY
A non-linear finite element method of analysis was applied to predict the behavior of reinforced concrete deep beams. The behavior of concrete including strain softening tendency and anisotropy was modelled by the total strain theory and combined with non-linear analysis. The analytical results were compared with the experimental results. The techniques for the non-linear method of analysis and the capability to predict the behavior of deep beams were investigated.

RÉSUMÉ
Le comportement non-linéaire de poutres en béton armé de petite portée est analysé par éléments finis. Le comportement du béton, comprenant l'anisotropie et le "strain-softening", est simulé par la théorie de la déformation totale combinée à l'analyse non-linéaire. Les résultats analytiques furent comparés aux résultats expérimentaux. Les techniques d'analyse non-linéaire et la capacité de prédiction du comportement de poutres à petite portée sont analysées.

ZUSAMMENFASSUNG
Eine nichtlineare Finite-Elemente-Methode wurde auf die Berechnung von hohen Tägern aus Stahlbeton angewandt. Das Verhalten mit Einschluss von Steifigkeitsabnahme und Anisotropie wurde mit einer nichtlinearen Berechnung kombiniert. Theorie und Experiment an hohen Trägern wurden verglichen.

1. INTRODUCTION

The behavior of reinforced concrete structures under applied loads is complex due to numerous internal load paths. Such load paths vary a great deal due to the distribution of stiffness in the structure, and that variation in stiffness arises from variable pattern and sequence of crack occurrence and plastification of materials. On the other hand the whole picture of the constitutive law of concrete is not yet apparent particularly when the combination of applied stresses changes as they are increased. The various factors influencing the behavior of reinforced concrete structures are interlaced and therefore, any devised methods of analysis need be scrutinized in the lights of experimental observations [1].

A finite element method of analysis with a few techniques to overcome the difficulties characteristic to nonlinearlity was presented to predict the behavior of reinforced concrete deep beams and the analytical results were compared with the experimental results specially tested for this purpose.

2. NUMERICAL METHOD

In the analysis step iterative procedure for non-linear finite element method was used. In applying the analysis to deep beams, enforced displacements were imposed because of the easier evaluation of the ultimate strength. The general flow of the main routine is as shown in Fig.1.

At the first iteration of each step, the equivalent nodal forces, which appear when constraint displacements are applied to the structures, are calculated using the updated stiffness matrix in the preceding step. During iterative routine, the stiffness matrix was formed at each iteration. The increments of nodal displacements are then calculated.

$$u = K^{-1}\Delta F \qquad (1)$$

$$\Delta F = F - \iiint B^T \sigma \, dv \qquad (2)$$

K : global stiffness matrix , F : equivalent nodal force
F : total external nodal forces, F=0 in this analysis
B : strain displacement matrix , σ : stresses

In each iteration, the unbalanced forces are calculated by equation 2. If unbalanced forces are not as small as required, the next incremental displacements are calculated by setting the equivalent nodal forces as the unbalanced forces. When the value of unbalanced force differs from that of previous iterative routine significantly or the direction of the force changes, the nodal force increment for correction is made one half the corresponding unbalanced force. The selection of one half is arbitrary, but by this procedure, the risk of divergence or a great leap beyond equlibrium points was avoided to some extent.

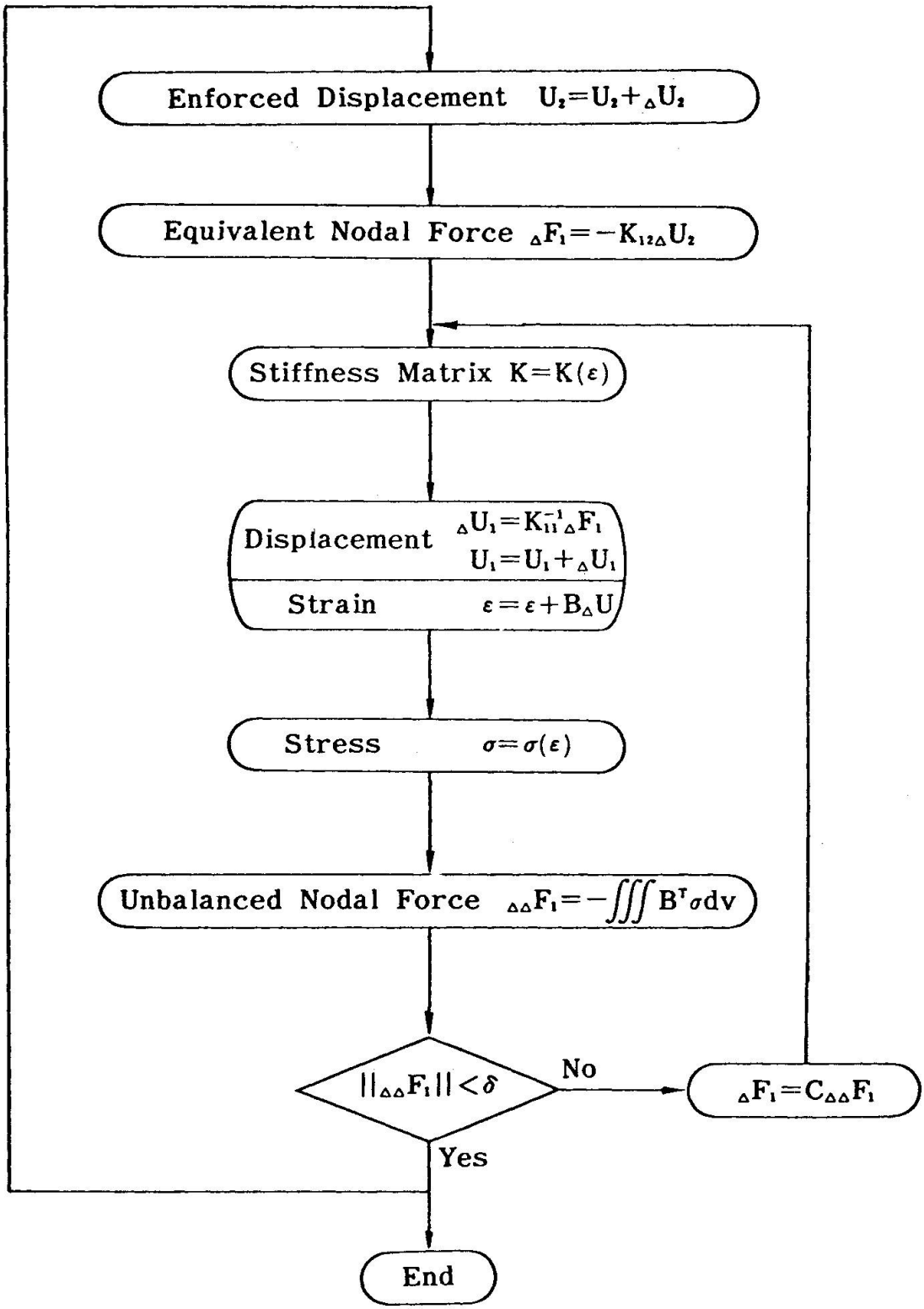

Fig. 1 General Flowchart of Non-linear Iterative Routine

3. CONSTITUTIVE EQUATIONS OF CONCRETE

3.1 Stress strain relationship of concrete

There exist two families of constitutive formulations according to the method of stress evaluation, namely differential and total strain formulation. The former evaluates stresses by integrating stress increment at each step. The total strain formulation calculates stresses by total strains and constitutive equations which contain invariants with regard to coordinate transformations as parameters. In the analysis the total strain formulation was used for evaluating stresses for the following reasons.
(a) Strain softening tendency under multiaxial stress states is easily modeled.
(b) No accumulation of errors in estimating the stresses occurs so that the step size can be set relatively large.
(c) Experimental data are directly used for making the constitutive equations.

The constitutive law used for the analysis of deep beams is two dimentional, and the following scalar values named equivalent stress and equivalent strain which are indicated by stress and strain invariants with regard to coordinate transformations are defined.

$$s = s(\sigma_{ij}) = s(\sigma_1, \sigma_2) = \sqrt{\left(\frac{\sigma_1+\sigma_2}{2.32fc}\right)^2+\left(\frac{\sigma_1-\sigma_2}{1.108fc}\right)^2} \qquad (3)$$

$$e = e(\varepsilon_{ij}) = e(\varepsilon_1, \varepsilon_2) = \sqrt{\left(\frac{\varepsilon_1+\varepsilon_2}{9.6\times10^{-4}}\right)^2+\left(\frac{\varepsilon_1-\varepsilon_2}{6.2\times10^{-4}}\right)^2}\Big/\sqrt{fc} \qquad (4)$$

where s : equivalent stress, e : equivalent strain
fc : uniaxial compressive strength, assumed as 90% of the cylinder strength [2]
σ_1 σ_2: principal stresses ($\sigma_1 > \sigma_2$), ε_1 ε_2: principal strains

These two invariants represent the degree of stress and strain level respectively, and are introduced in order to allow the actual biaxial stress-strain curves to be expressed in an one-to-one relationship as in the case of uniaxial conditions, so that a family of uniaxial concepts of stress-strain relationships is to be used. This equation was determined by a least squares fit of biquadratic polynomial from the reported experimental data [2,3,4,5].

$$s = f(e) \qquad (5)$$

$$= 1.042\ e - 2.083\ e + 0.42\ e + 2.0\ e \quad : e < e2$$

$$= -0.25\ e + 1.25 \quad : e > e2$$

The relationship of each stress and strain components in the local coordinate system whose axes coincide with the principal stress axes is developed, in consideration of anisotropic characreristics of concrete due to microcracking and void formation. These characteristics of concrete are dependent on the strain level, and

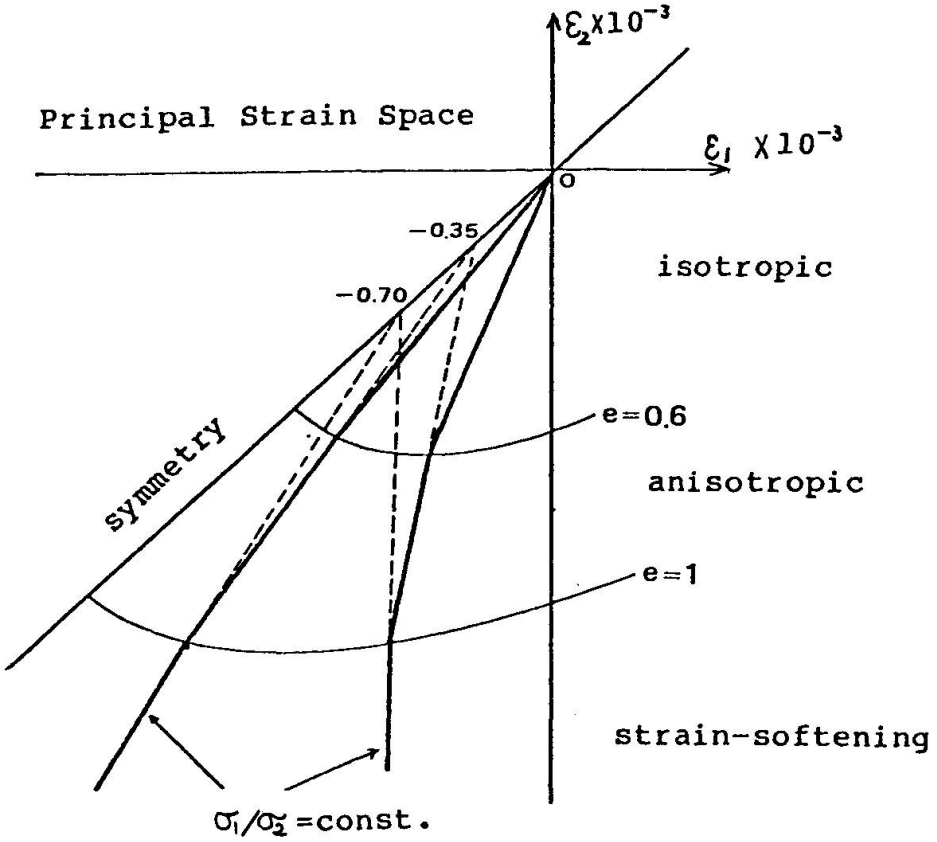

Fig. 2 Proportional Loading Pathes on Principal Strain Surface

the relationship of two principal strains under constant principal stress ratio is modeled as tri-linear one as shown in Fig.2. The relation is developed based on the reported experimental data [2], [3],[4].

In the low level of strain, concrete can be assumed an isotropic material [5] and the relation of two principal values, stresses and strains, is reasonablely assumed as the one for elastic materials.

$$p = (q + \nu)/(1 + \nu * q) \qquad (6)$$

where p : stress ratio = σ_1/σ_2 ,q : strain ratio = $\varepsilon_1/\varepsilon_2$
ν : Poisson's ratio

On increasing the strain to a high level, a stage is reached where the microcracking between aggregates and mortar starts to propagate and the anisotropic behavior appears gradually. This boundary between the isotropic and the anisotropic is assumed to depend on the value of the equivalent strain, and is assumed as 0.6 in the calculation (see Fig.2). After this stage the slope of the line which shows the relationship of the two principal strains is changed to express the anisotropic behavior of concrete. When the strain-softening level is attained (e=1), the effect of

anisotropic behavior and drastic void formation becomes significant, and the slope is changed again.

When two principal strains are given, the corresponding strain ratio at the isotropic stage is obtained by using the tri-linear relation as shown in Fig.2. Then, the stress ratio is calculated by equation 6. Using this stress ratio and the equivalent stress, which can be calculated by equation 5, each principal stress is calculated by using equation 3.

s.2 Cracking

In non-linear finite element method of analysis, there are two methods for representing the behavior of cracked concrete; discrete crack and smeared crack model. The former simulates a crack by releasing the connection of each element. The latter represents a crack by modifying the constitutive equations. The smeared crack model can simulate the total responses of structural systems in which crackings occur, and was used for the analysis of deep beams.

Criterion of cracking is determined by stresses, and cracking is defined to occur when the principal stresses make the following crack index equal to unity.

$$\begin{aligned} Ci &= (\sigma_1/ft) - \sqrt[3]{(1 + \sigma_2/fc)} \text{ : under compression-tension} \\ &= (\sigma_1/ft) - 1 \text{ : under biaxial tention} \end{aligned} \quad (7)$$

where ft : uniaxial tensile strength

The orientation of crack is considered to be normal to the major principal stress, and the stress component normal to a crack is reduced to zero. The condition, where the crack index is zero, represents the failure envelope at compression-tension and tension-tension stress states. When the value of crack index is between zero and one, stress normal to the direction of a crack is maintained constant although the stress calculated by the above mentioned method exceeds the value corresponding to zero of crack index.

Shear transfer across the crack is simply simulated by changing the shear stiffness along the crack as shown in equation 10. Calculations were made by zero stiffness in general and half of the uncracked stiffness in some case. When the strain normal to the crack is compressive, the crack is closed and the condition is assumed to be the same as that of uncracked concrete. If concrete at an evaluation point has previous experiences of cracking, the stress component normal to the crack is calculated and the crack is assumed to open again when the stress is tensile.

3.2 Stiffness of iterative calculation

In the non-linear iterative procedures a stiffness for each evaluation point is necessary. The stiffness matrix is formed by superposing the isotropic stiffnesses of uncracked concrete and

the anisotropic stiffnesses of cracked one. The assumption of quivalent stress-strain relationship permits the evaluation of incremental elastic moduli as in equation 8.

$$E = E0 \frac{ds/de}{ds/de|e=0} \tag{8}$$

where E0 is the initial tangent stiffness moduli

With the tangent moduli and effective Poisson's ratio, the isotropic tangent stiffness matrix of uncracked concrete is obtained by equation 9. The anisotropic tangent stiffness of cracked concrete is written in equation 10, using the tangent moduli parallel to crack direction. The effective Poisson's ratio is also assumed as in equation 12 in consideration of the equivalent strain level.

$$\frac{E}{1-\nu^2}\begin{bmatrix} 1 & \nu & 0 \\ \nu & 1 & 0 \\ 0 & 0 & \frac{1-\nu}{2} \end{bmatrix} \tag{9}$$

$$\begin{bmatrix} 0 & 0 & 0 \\ 0 & E & 0 \\ 0 & 0 & \alpha G \end{bmatrix} \tag{10}$$

where $\alpha = 0$ or 0.5, $G = E/(2(1+\nu))$ (11)

$$\begin{aligned} \nu &= 0.2 && e < e1 \\ &= 1.75\, e - 0.85 && e1 < e < e2 \\ &= 0.9 && e > e2 \end{aligned} \tag{12}$$

A lower limit is set for the possitive tangent stiffness, because the global tangent stiffness matrix becomes numerically unstable when diagonal terms approach zero. One hundredth of the initial tangent stiffness was used for the lower limit, after some trial calculations were executed.

4. APPLICATION TO THE ANALYSIS OF DEEP BEAMS

Reinforced concrete deep beam is one of the problems which need the help of a suitable non-linear finite element method of analysis for understanding the behavior. The applicability of the analytical method to deep beams is investigated. Deep beams used in the comparison with the analytical results were particularly tested for this purpose. The characteristics of eight specimens are shown in Table 1. The parameters such as concrete strength (13 MPa - 67 MPa), reinforcement ratio (3 % - 6 %), shear span (150 mm - 200 mm) and height of beam (300 mm - 600 mm) are widely and systematically varied. To ensure the anchorage, main reinforcing bars were bent up as shown in Fig.4. No shear reinforcement is used.

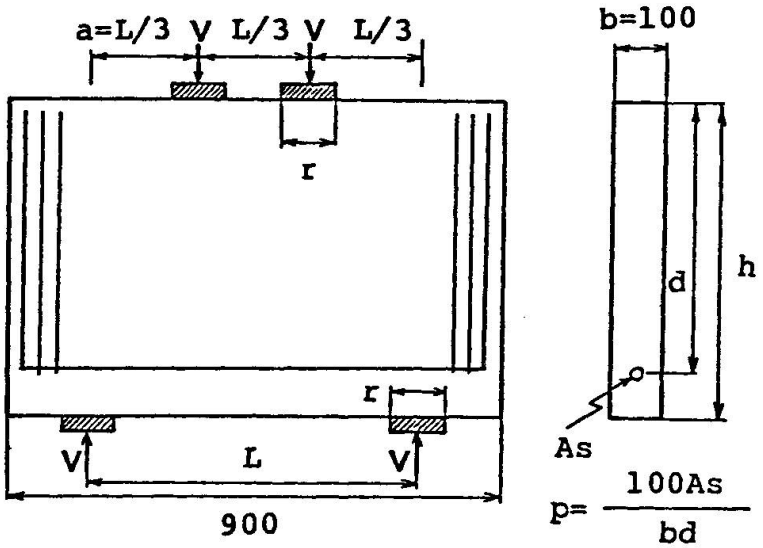

Fig. 4 Deep Beam Specimens Tested

Table 1 Characteristics of Deep Beam Specimens

Beam	a(mm)	d(mm)	a/d	r(mm)	h(mm)	p(%)	fy(MPa)	fc'(MPa)
T1	200	228	0.88	140	300	6.0	364	35.8
T2	200	507	0.39	100	600	3.0	389	54.7
T3	200	228	0.88	100	300	3.0	364	13.1
T4	150	507	0.30	140	600	3.0	389	13.1
T5	200	507	0.39	140	600	6.0	389	66.6
T6	150	507	0.30	100	600	6.0	389	35.8
T7	150	228	0.66	100	300	6.0	364	59.9
T8	150	228	0.66	140	300	3.0	364	58.8

Considering the flow of stresses in the beam, a finite number of skew quadrilateral elements as shown in Fig.5 were used for the analysis of plane stress conditions. The same topological shapes and number of elements were used for all the eight beams.

The assumption of the plane stress is considered to be reasonable for most portions of the beam. But, concrete near the bearing plate is obviously stressed triaxially and the effect on the behavior of the beam is not negligibly small, especially in the concrete mainly stressed in compression by bending moment. Therefore, five elements hatched in Fig.5 were to have an apparent higher compressive strength 1.8 times that for other elements. However, the concrete strength for the element at the span center was made normal, so that the increase of concrete strength

in triaxial compression zone might not affect the flexure dominant strength of the beam.

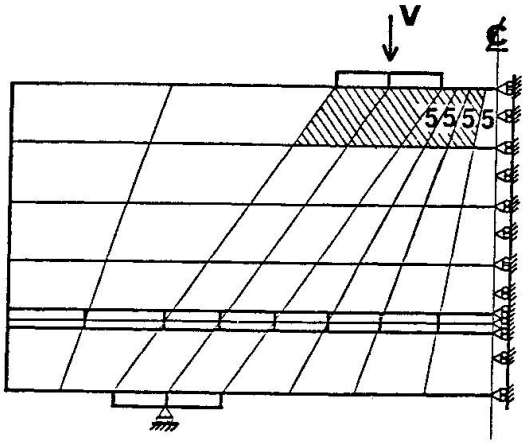

Fig. 5 Idealization of Finite Elements

Eight nodes isoparametric elements were used taking into account that the strain distribution in the beam is more or less linear. Two by two stress evaluation points, or Gauss points, were arranged in each element. This number of Gauss points may ordinarily be sufficient. However, five by five Gauss points were arranged in four elements where strains have the possibility of changing from a very small magnitude to softening level within the element. The elements are marked with character 5 in Fig.5. For this kind of element, two by two points were insufficient for the evaluation of stresses.

Totally, 40 concrete and 12 steel elements with 174 nodes and 292 Gauss points were used. The CPU time to calculate ten steps with two iterations in each step was about 70 seconds using a HITAC M-200H system at the computer center of University of Tokyo, and the computation fee for one case was about 500 yen ($ 2.50).

A perfect bond of steel and concrete was assumed at the selected nodes and no bond was assumed in other places. In order to effect this particular bond behavior, the nodes of steel elements were connected to the nodes of concrete elements that were located at the same level as the center of steel elements.

5. EVALUATION OF THE ANALYTICAL RESULTS

5.1. Failure Mode and Ultimate Load

Failure modes predicted by the analysis, when the shear stiffness along the cracks is assumed to be zero, otherwize shear transfer across the cracks is ignored, are classified into three types : (a) diagonal compression failure of concrete above the support, (b) flexural compression failure of concrete at the section in the center of the span, and (c) flexural failure due to yielding of main reinforcing steel.

Four beams classified in diagonal compression failure have small shear span-depth ratios equal to 0.30 and 0.39 . Analytical results of these cases showed that the principal compressive stresses in the elements above the support were maximum among all elements. Stresses increased with applied enforced displacements and the elements gradually became plastic and softened. As a result, stress redistribution occurred. Stresses in adjacent elements increased and stress distribution became more uniform and the load carrying capacity of the beam became the maximum. When strains of softened elements above the support became very large

and stresses decreased extremely, stresses of other elements that had not yet been plastic began to decrease.

In the experiment, four beams, T2,T4,T5 and T6, which belonged to case (a) indeed failed in diagonal compression above the support. Observed failed portions of the specimen T5 is shown by shadow in Fig.6(a). Predicted results are very similar to observed results in failure mode and failed portions.

Analytical results of case (b) showed that the most critical stress state existed in the element of the top surface and at the span center where the moment is maximum. With an increase of applied displacement, stresses of the element increased and the element became plastic and softened. On the other hand, adjacent elements of top surface, which have the higher strength, nor the elements above the support did not become plastic.

In the experiments, three beams, T1,T3 and T7, which belonged to case (b), did not fail at the sections in the maximum moment region. Observed failed portions of the specimen T7 is shown by shadow in Fig.6(b). When cracks possessing an angle steeper than already existing diagonal cracks developed towards the edges of the bearing plate, slip occurred along this crack and the beam failed. This type of slip failure mode was not predicted by this analysis. This was considered to be due to the ignorance of the shear transfer. Therefore, trial calculations were executed on the assumption that the shear stiffness along the crack is made half of the uncracked one(α = 0.5 in equation 11). The results of calculations for T1 and T7 conformed that the secondary crack occurred in the point above the support at lower load than the ultimate load predicted by the analysis without shear transfer.

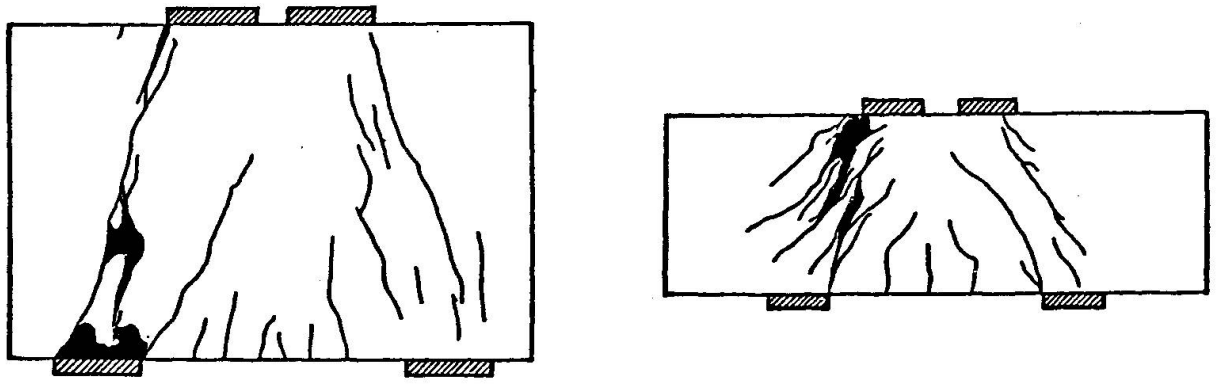

(a) T5, predicted to be failed in diagonal compression

(b) T7, predicted to be failed in flexural compression

Fig. 6 Crack Formation and Failed Portions

This will suggest that the proper modeling for shear transfer is extremely important for the analysis of this type of beams.

Results of analysis of case (c) showed that the beam failed in flexural mode governed by yielding of steel. The observed failure of T8, which belonged to case (c), was also in flexural mode.

Predicted failure modes and loads are given in Table 2 in comparison with the experimental values. The average ratio of the experimental ultimate load to the analytical one is 0.96 with the coefficient of variation of 0.18.

Table 2 Failure Mode and Ultimate Load

Beam	Failure Mode		Ultimate Load (KN)		
	expt.	anal.	expt.	anal.	expt./anal.
T1	SL	FC	629	506	1.24
T2	DC	DC	1028	1373	0.75
T3	SL	FC	228	235	0.97
T4	DC	DC	425	484	0.88
T5	DC	DC	1763	1930	0.91
T6	DC	DC	1155	996	1.16
T7	SL	FC	892	1221	0.73
T8	FT	FT	941	888	1.06

DC:Diagonal Compression
SL:Slip
FC:Flexural Compression
FT:Flexural Tension

5.2 Diagonal Cracking

According to the analysis two types of diagonal cracking mode was recognized. Four specimens, which had small a/d and belonged to case (a), and the rest, which had large a/d and belonged to case (b), showed different tendencies.

The analysis of small a/d specimens predicted that diagonal cracks developed dominantly while the development of flexural cracks was limited. On the other hand, in the analysis of large a/d specimens, diagonal cracks were distributed and developed uniformly in larger areas. Further, flexural cracks developed extensively. In Fig.7, predicted crack development of T5 as an example of small a/d specimens and T7 as an example of large a/d specimens are shown by broken lines. The load level in these figures is about 70% of analytical maximum load.

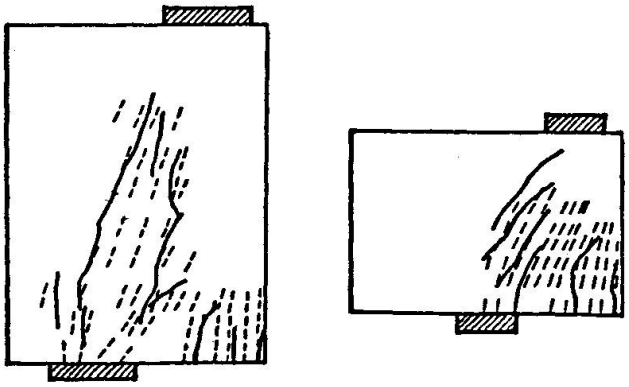

(a) T5 (b) T7

Fig. 7 Predicted and Observed Crack Pattern

In the experiments, development of dominant and long diagonal cracks were indeed characteristic of all small a/d beams and distributed diagonal cracks characterized large a/d beams. In Fig. 7,

development of observed cracks are superposed by bold lines. In both small and large a/d beams, positions of predicted and observed diagonal cracks are not necessarily coincident to each other. However, in consideration of the fact that crack evaluation points are discrete, the locations of cracks may be said to be similar. Moreover, directions of diagonal cracks are similar both in the prediction and in the observation. Therefore, it is deduced that this analysis can predict the actual behaviors reasonably accurately with regard to positions and directions of diagonal crack development for all the specimens.

5.3. Displacement and Strains of Concrete

The displacement of beam was satisfactorily predicted by the analysis. Fig.8 shows an example of the relationship between applied shear forces and the relative displacements of T5 specimen with the experimental values.

Fig.9 shows an example of the relationship between applied shear forces and the compressive principal strains of concrete just above the support. The tested values were obtained from the gauges attached to the surfaces of specimen T5. Fig.10 shows examples of strain distributions of Gauss points located at the same level of the concrete strut. These figures clearly show that strains of concrete and the displacement can be satisfactorily predicted by the analysis for the beams failed in diagonal compression mode.

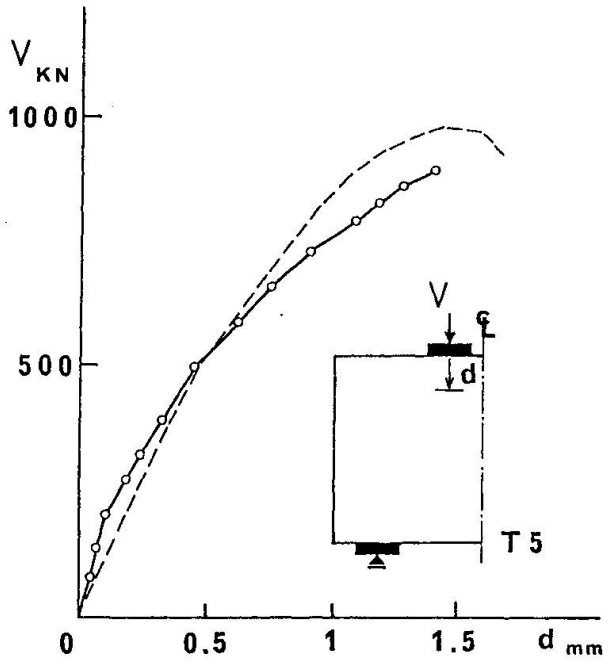

Fig.8 Shear-Displacement

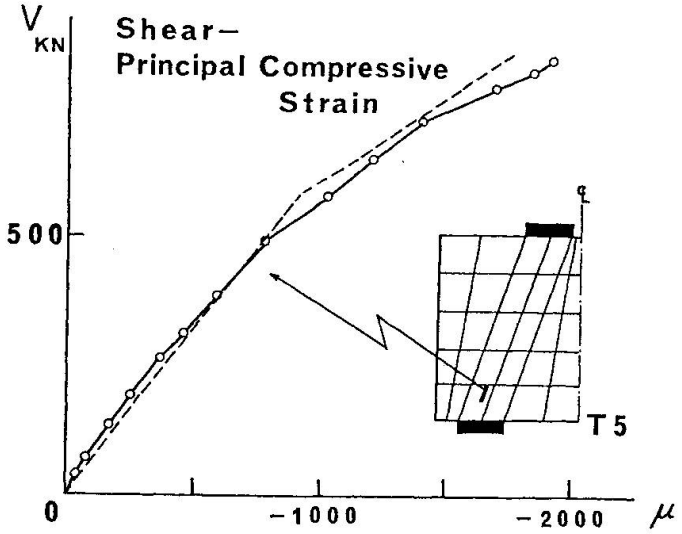

Fig.9 Shear-Compressive Strain

5.4. Evaluation of the Finite Element Analysis

Three types of failure mode were predicted by this analysis. In case (a), that is, diagonal compression failure mode of concrete above the support, the observed diagonal cracking pattern, stress distribution and failure mode were predicted reasonably accurately. Therefore, it is admitted that this analysis can estimate the actual behavior, on the whole, of this type of failure mode.

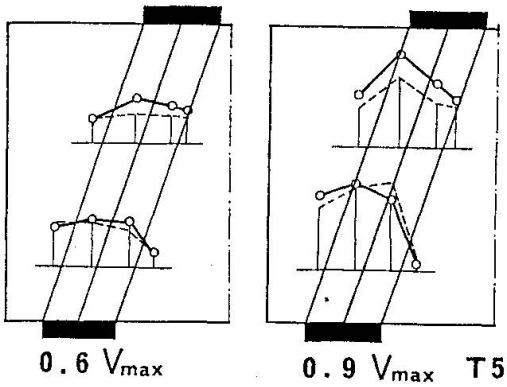

Fig.10 Strain Distribution in Concrete Strut

Secondly, in case (b), that is, flexural compression failure mode of concrete at the center span, the observed diagonal cracking pattern was predicted reasonably accurately but the variation of crack directions with load and failure mode could not be predicted by ignoring the shear stiffness along inclined cracks. Without shear transfer along the inclined crack surfaces, the stress condition in diagonal concrete struts bordered with diagonal cracks is almost uniaxial compression. When the shear stiffness is considered, there are additional shear stresses along the cracks and the resulting stress condition is severer (provided the existing compressive stress remains constant). Hence, the additional shear stress at crack surface results in undesirable stress condition in the diagonal concrete struts. The estimation of shear transfer along cracks is an important problem in order to predict the slip failure mode along a new surface inclined to the earlier cracks.

In case (c), that is, yielding of main reinforcement, the observed behaviors were adequately predicted.

6. CONCLUDING REMARKS

The behavior of reinforced concrete deep beams under increasing load was analyzed by a non-linear finite element method of analysis and the results were compared with experimental observations. For the loading tests of reinforced concrete deep beams the influencial parameters such as geometrical configuration, concrete strength and reinforcement ratio were varied so that various load carrying mechanisms can be observed. The bi-axial stress-strain relationship of concrete was expressed by a relation between stress and strain invariants developed herein. The following remarks appear to be relevant regarding the

techniques for non-linear method of analysis and capability of behavior prediction of deep beams.

(1). A step-iterative procedure of imposed displacement analysis was effective for solution of the behavior of structures where the portions were in strain softening region.

(2). The three failure modes observed on deep beam test specimens were, (a) crushing near the bottom of diagonal concrete struts, (b) slip along diagonal crack and (c) yielding of main reinforcement. The analysis was capable of predicting the two failure modes (a) and (c) described in (2). However, the failure mode (b), the slip along diagonal crack, was not predicted by the analysis. This may be due to the finite element idealization where the shear transfer resistance along the cracks was not assumed correctly, and thus resulting in different stress conditions in the diagonal struts which are vital load carrying member.

ACKNOWLEDGEMENTS

Dr. Jun Yamazaki, Associate Professor of Tokyo Metropolitan University, joined the discussions and gave valuable suggestions. Yutaka Ishikawa and Shin-ichi Inoue, undergraduate of our department, helped in executing the calculations. The program used in this analysis were developed from the program called FEMN (Finite Element Method of analysis for Non-linear problems) developed by the Non-linear Analysis Program Research Association. The authors express their gratitude for the warm and devoted cooperations.

REFERENCES

1. J.Eibl, "Application and Experimental Verification of Advanced Mechanics in Reinforced Concrete", Introductory Report IABSE Colloquium Delft 1981
2. H.Kupfer, H.K.Hilsdorf and H.Rusch, "Behavior of Concrete under Biaxial stresses", ACI Journal, Proceedings Vol. 66, No. 8, August 1969, pp.656-666
3. M.E.Tasuji, A.H.Nilson and F.O.Slate, "Biaxial Stress-Strain relationships for concrete", Magazine of Concrete Research, Vol. 31, No. 109, December 1979, pp217-224
4. H.Onuma and Y.Aoyagi, "Experimental Study on Ultimate Strength and Strain Behavior of Concrete under Biaxial Compressive Stresses, (in Japanese)", Report No.375016, Central Research Institute of Electric Power Industry, July 1976
5. M.D.Kotsovos and J.B.Newman, "A Mathematical description of the deformational behaviour of concrete under complex loading", Magazine of Concrete Research, Vol. 31, No. 107, June 1979, pp77-90

Nonlinear Finite Elements Analysis of Reinforced Concrete Beam-Column Joints

Analyse non-linéaire par éléments finis de la liaison entre poutre et colonne en béton armé.

Nichtlineare Finite-Elemente-Berechnung von Träger-Stützen-Verbindungen

H. NOGUCHI
Associate Professor
Dep. of Arch. Eng., Fac. of Eng.
Chiba University
Chiba, Japan

SUMMARY
The nonlinear behavior of reinforced concrete beam-column joints is analyzed by the finite element model combining the individual material properties with emphasis on the effect of the different bond characteristics of beam bars through the joint. Comparisons are presented with tests for deflection behavior, crack propagation, strain distributions of beam and column longitudinal bars, strain of ties and bond slips of beam bars through the joint. The effects of the truss mechnism and loss of bond on the strain distribution of beam bars and the shear resistance mechnism of the joint are discussed.

RÉSUMÉ
Le comportement non-linéaire de jonctions colonne-poutre en béton armé est analysé par éléments finis. L'analyse tient compte tant des propriétés individuelles des matériaux que des effets des différentes caractéristiques d'adhésion entre armatures et béton. La comparaison est faite avec des essais mésurant le comportement à la flexion, à la fissuration, à la distribution des déformations des armatures longitudinales de la poutre et de la colonne, à la déformation des étriers et le glissement des armatures principales au niveau de le jonction. L'effet du mécanisme de treillis et de la perte d'adhésion sur la distribution des déformations des armatures et sur le mécanisme de résistance au cisaillement de la jonction est discuté.

ZUSAMMENFASSUNG
Das nichtlineare Verhalten von Träger-Stützen-Verbindungen aus Stahlbeton wurde mit finiten Elementen untersucht, wobei der Nachdruck auf die Verbundeigenschaften gelegt wurde. Versuchsergebnisse wurden in Bezug auf Durchbiegung, Rissbildung, Dehnungsverteilung und Relativverschiebung zwischen Bewehrung und Beton verglichen. Fachwerkwirkung und Verbundversagen werden diskutiert.

1. INTRODUCTION

The stress level recently becomes very severe in the reinforced concrete (RC) beam-column joints subjected to earthquakes for the following backgrounds. The high strength and large-sized deformed bar was developed and the dimension of sections in beams or columns is getting smaller. As the shear strength of beams and columns is getting reinforced according to the revised building code in Japan, the beam-column joint is getting a relatively weak point.

The mechanical characteristics of the RC beam-column joint are mainly composed of the following two elements:

1. The shear resistance mechanism after inclined cracks initiate in the joint.
2. The bond slip mechanism of beam longitudinal bars through the joint.

Especially the bond slip of beam longitudinal bars through the joint for the bond deterioration has great influences on the story deflection and the restoring force characteristics of overall structures.

There are many active experimental studies for the beam-column joints. Recently the effects of lateral beams [1], eccentric beams [2] and biaxial loading [3] are discussed. As for analytical studies, the works of Shimohira [4], Will [5], Mirza [6], Ohtsuki [7], Ohwada [8], Ichinose [9] and Tada [10] are listed, but the nonlinear behavior after the initiation of the inclined crack in the joint has been scarcely discussed.

In this study the modeling of material properties is carried out in accordance with the previous experimental studies and the analytical results obtained by the finite element method are compared with the test results.

2. ANALYTICAL MODELS

2.1 General

The effects of lateral beams, eccentric beams and the confinement of ties are originally three-dimensional problems. In this study the subject of analysis is limited to the joint without the lateral beams or the eccentric beams, and the plane stress state is assumed.

2.2 Concrete

Concrete is represented by the linearly varying strain triangular element with six nodal points which was originally developed by Felippa [11], as shown in Fig.1. In this element the current stress-strain matrices are decided at corner points and midpoints. The element is subdivided into 4 subtriangles. Inside each subtriangle the entries of the stress-strain matrix are assumed to vary linearly.

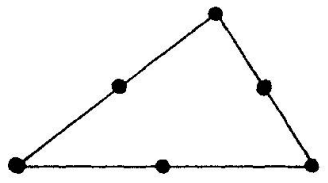

Fig.1 Triangular Element for Concrete and Longitudinal Bar

The analytical model used to represent the behavior of concrete under biaxial stresses in this study was originally developed by Darwin [12], [13], [14]. The author [15], [16] compared a model based on the theory of plasticity and using Drucker-Prager's yield criterion, which had been used by many investigators, and four other models with the test results of Kupfer [17] and Nelissen [18]. He concluded that the plasticity model could not represent the behavior of concrete adequately, especially at higher stress levels, and that the

orthotropic model of Darwin [12 - 14] gave the best results in both principal directions for the models that he considered.

In Darwin's model concrete is assumed to be an orthotropic material in the two principal stress directions. The incremental constitutive relationship referred to the two principal axes are written as follows:

$$\begin{Bmatrix} d\sigma_1 \\ d\sigma_2 \\ d\tau_{12} \end{Bmatrix} = \frac{1}{1-\upsilon^2} \begin{bmatrix} E_1 & \upsilon\sqrt{E_1E_2} & 0 \\ & E_2 & 0 \\ (\text{symm.}) & & \frac{1}{4}(E_1+E_2-2\upsilon\sqrt{E_1E_2}) \end{bmatrix} \begin{Bmatrix} d\varepsilon_1 \\ d\varepsilon_2 \\ d\gamma_{12} \end{Bmatrix} \quad (1)$$

In Eq.(1) both the shear modulus and Poisson's ratio, υ, are assumed to be independent of orientation.

Darwin developed the concept of "equivalent uniaxial strain," ε_{iu}, which is obtained when only the Poisson's effect is removed from the biaxial strains. The total equivalent uniaxial strain at any point is obtained as follows:

$$\varepsilon_{iu} = \Sigma\, d\varepsilon_{iu} = \Sigma \frac{d\varepsilon_i}{(1-\upsilon\alpha n)} = \Sigma \frac{d\sigma_i}{E_i} \quad (2)$$

where $\alpha = \sigma_1/\sigma_2$ = biaxial stress ratio
$n = E_2/E_1$ = modular ratio.

The "equivalent uniaxial" stress-strain curves for compressive loading are based on the following equation suggested by Saenz [19].

$$\sigma_i = \frac{E_0\varepsilon_{iu}}{1+\left(\frac{E_0}{E_s}-2\right)\frac{\varepsilon_{iu}}{\varepsilon_{ic}}+\left(\frac{\varepsilon_{iu}}{\varepsilon_{ic}}\right)^2} \quad (3)$$

where E_0 = initial uniaxial tangent modulus
$E_s = \sigma_{ic}/\varepsilon_{ic}$ = secant modulus
$\sigma_{ic}, \varepsilon_{ic}$ = maximum compressive stress and corresponding equivalent uniaxial strain in principal direction, i.

As the crack pattern is predicted from the test results in this study, the elasticity is assumed for tension.

$$\sigma_i = E_0\varepsilon_{iu} \quad (4)$$

The values of the maximum stresses in the two principal directions, σ_{1c}, σ_{2c}, are obtained from the modified biaxial strength envelope of Kupfer and Gerstle [17] which is shown in Fig.2.

For values of strength greater than f'_c in absolute magnitude, a relatively large strain at the maximum stress, was indicated by Kupfer [20].

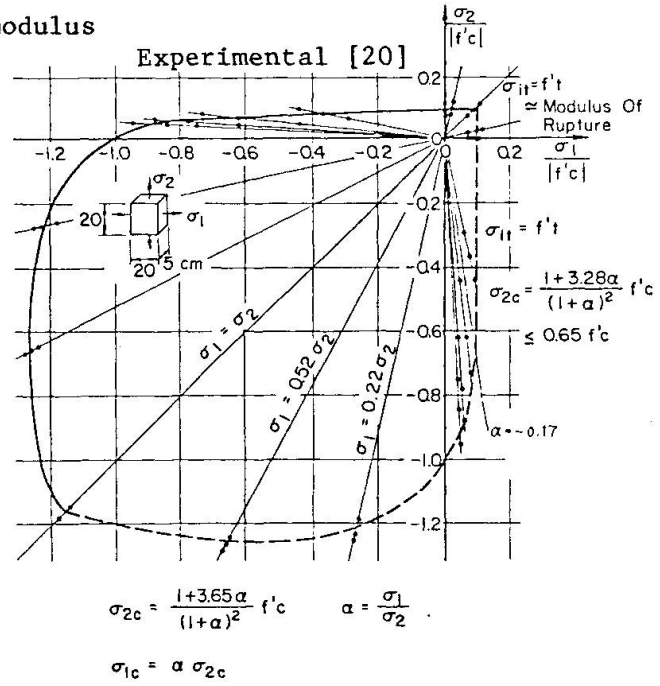

Fig.2 Biaxial Strength Envelope Used in the Present Study

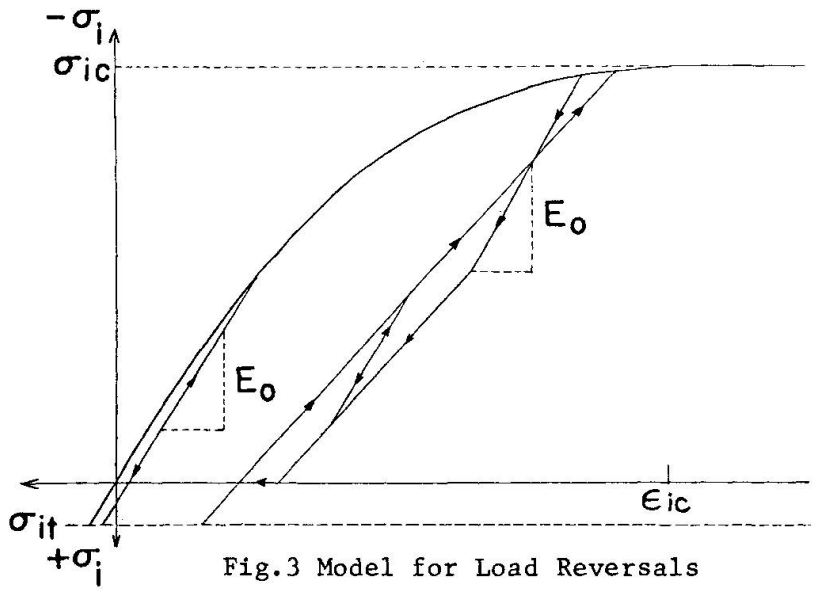

Fig.3 Model for Load Reversals

To include this behavior in the model, the variation of ϵ_{ic} at the maximum compressive stress, σ_{ic}, is determined from the experimental stress-strain curve and it is given in Refs. [12], [14].

The variation of Poisson's ratio is assumed as follows:

$$\upsilon = 0.2 \qquad \text{for tension-tension and compression-compression} \qquad (5)$$

$$\upsilon = 0.2 + 0.6\left(\frac{\sigma_2}{f'_c}\right)^4 + 0.4\left(\frac{\sigma_1}{\sigma_{1t}}\right)^4$$

$$\upsilon \leq 0.99 \qquad \text{for uniaxial compression and tension-compression} \qquad (6)$$

where

f'_c = uniaxial compressive strength

σ_{1t} = uniaxial tensile strength

Also for the unloading and reloading curves, Darwin's model is adopted, as shown in Fig. 3. Beyond the maximum compressive strength the strength is kept constant in this study.

2.3 Longitudinal Bar

The linearly varying strain triangular element is used also for the longitudinal bar to represent the dowel action. The constitutive law under biaxial stresses is based on the theory of plasticity using Von Mises's yield criterion. For this study a simplified bilinear model is used for the equivalent stress-strain curve and the rate of strain hardening is set to $0.01E_s$, where E_s is the Young's modulus.

2.4 Stirrup and Tie

The stirrup and tie are represented by the bar elements. A simplified bilinear model is used for the stress-strain curve and the rate of strain hardening is set to $0.05E_{st}$, where E_{st} is the Young's modulus. When the stirrup or tie is a round bar, its anchorage to longitudinal bars is assumed to be carried out at only the exterior nodal points of the londitudinal bar elements.

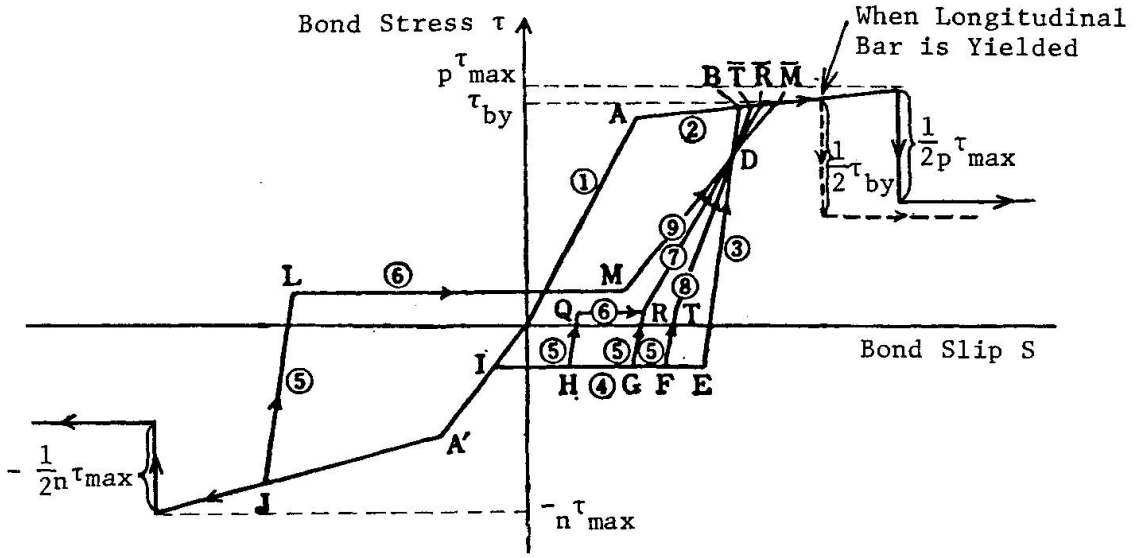

Fig.4 Idealized Bond Stress-Slip Relationships

2.5 Bond Slip

Bond slip is modeled by the bond-link element which was first developed by Ngo and Scordelis [21]. The discussion on the applicability of the bond-link element was made by the author in Refs. [22], [23]. Though there are some problems in the bond-link element, it is rather appropriate to use such a simple model as the bond-link element for the large-scale subject like a beam-column joint.

Slip characteristics parallel to the bar axis are obtained from the modified bond stress-slip relations under cycles of load reversal which were originally proposed by Morita and Kaku [24], [25], as shown in Fig.4. As a modified point for Morita's model, when the bond stress yields the maximum bond strength or the longitudinal bar is yielded, half of the bond stress is released and the bond stiffness is set to zero, as shown in Fig. 4. [26]

For the spring stiffness of the bond-link element perpendicular to the bar axis, about the same relations as those of spring stiffness parallel to the bar axis are used as the first step to represent the sinking or separating of the longitudinal bar which is subjected to the dowel forces.

2.6 Concrete Cracking

The author discussed the modeling of crack initiation and propagation in Refs. [16], [27]. In this study, as the crack pattern is predicted from the previous test results, the crack-link element, as shown in Fig. 5, is put in between two nodes on both faces of the crack. When the principal stress of a node on the predicted cracking surface exceeds the modulus of rupture, a crack occurs along the particular grid line. The crack initiation is represented by setting the spring stiffness both vertical and parallel to the crack surface from the initial large values to zero, and cracking release

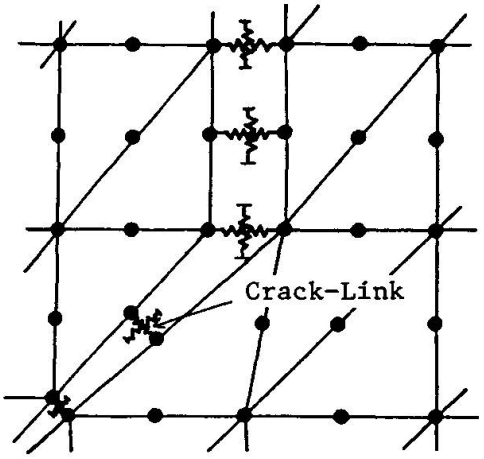

Fig.5 Crack-Link Elements

nodal forces are applied to two nodes on the crack surface at the next iterative step. Therefore, the aggregate interlock on the crack surface is not considered.

The closing or reopening of a crack is judged on the crack width. When a crack is closed, the only vertical spring stiffness to the crack surface is set to the initial large value.

3. NONLINEAR ANALYTICAL METHOD

The load incremental method using the tangent modulus is adopted for the nonlinear analysis [28], [29], [30]. At each loading stage, crack initiation and propagation are checked. The number of the iteration steps at which only cracking release nodal forces are applied is limited to one, and the next crack propagation is treated at the next loading stage.

The frontal method is used for the solution of the simultaneous, linear algebraic equations [28], [29].

4. SPECIMENS FOR SUBJECTS OF ANALYSIS

The beam-column joint specimens tested by Kamimura and Hamada [31] are selected for the subjects of analysis, because there were three specimens with different bond characteristics on beam bars within a joint and the detailed measurements on deformations, strains and bond slips were carried out in their tests. The detailed reinforcement of Kamimura's specimens is shown in Fig. 6. In this study the test results of two specimens, No.1 and No.3 are compared to the analytical results. The specimen No.1 had normal bond and specimen No.3 had almost no bond on beam bars within a joint by applying paraffin on the surface of the beam bar with a thickness of 1 - 2 mm above the rib of the bar.

The finite element idealization of Kamimura's specimen is shown in Fig. 7. Only half of the whole specimen is analyzed due to symmetry around a point. The crack pattern was set up using crack-link elements in general accord with the test results. Steel nodal points on both edges of a longitudinal bar were connected with the corresponding concrete nodal points by bond-link elements. Two bond-link elements were introduced on both faces of a crack. Ties and stirrups were

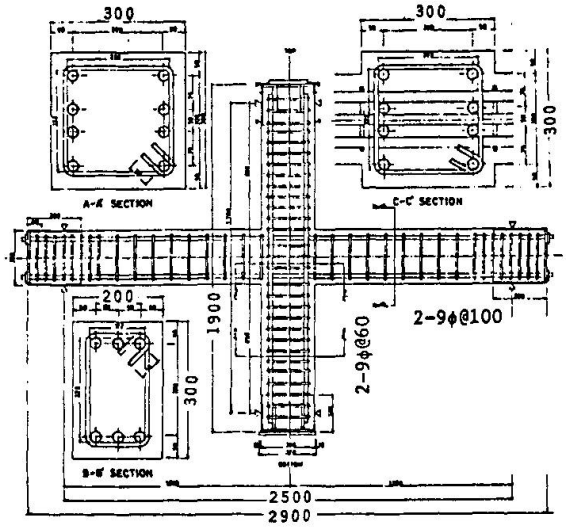

Fig.6 Specimens Tested by Kamimura et al. [31]

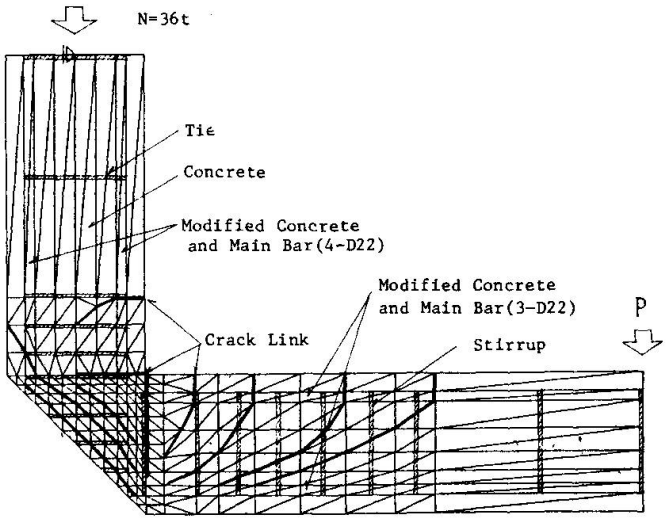

Fig.7 Finite Element Idealization

set up in well accord with those of the test specimen. As they were round bars, their anchorage to longitudinal bars was assumed to be carried out at the exterior nodal points of the longitudinal bar elements.

Test results of local bond stress-slip relations of beam longitudinal bars within a joint are shown for specimen No.1 in Fig. 8. From Fig. 8 it can be stated that the initial bond stiffness and the bond yielding stress are higher in the compression zone of the joint than in the tension zone. These phenomena were shown in tests by other researchers; Tada et al. [32]. In this study, for specimen No.1, bond characteristics of beam longitudinal bars within a joint are given separately in the compression and tension zones, as shown in Fig. 8. Bond characteristics of column longitudinal bars within a joint are given in accordance with those of the beam bars within the joint. Bond characteristics of longitudinal bars in the beam and column are given with reference to the test results of strain distributions, as shown in Fig. 8.

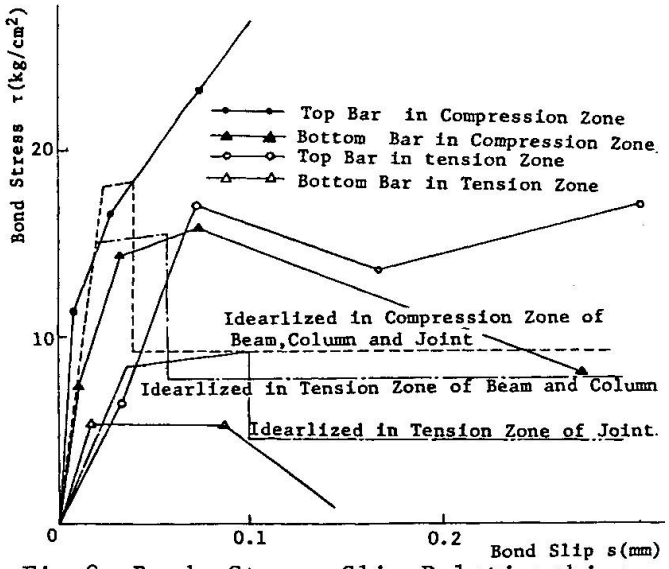

Fig.8 Bond Stress-Slip Relationships

In this study four specimens including specimen No.1 were analyzed as shown in Table 1. They had different bond characteristics on beam bars within a joint.

For specimen No.2 with almost perfect bond , the effect of the truss mechanism after the propagation of the inclined crack in a joint on the strain distribution of beam bars is studied.

For specimen No.3 with almost no bond, the effect of the loss of bond and the truss mechanism on the strain distribution of beam bars and the shear resistance mechanism of the joint is studied from the comparison of the analytical results with the test results.

Table 1. Material Properties Used for the Analysis

Specimen	No.1	No.2	No.3	No.4
Bond Characteristics	Normal Bond	Perfect Bond Truss Mechanism	No Bond	No Bond No Inclined Crack in Joint
Initial Bond Stiffness in Joint (kgf/cm^3)	Tension: 2640 Compression: 8100	2×10^8	20	20
Concrete	$E_0 = 2.54 \times 10^5$kgf/cm^2, $f'_c = -197$kgf/cm^2, $\varepsilon_{cu} = -0.23\%$, $f'_t = 29.6$kgf/cm^2, $_c\upsilon_0 = 0.2$			
Longitudinal Bar SD 35, D22	$E_s = 1.94 \times 10^6$kgf/cm^2, $_y\sigma_s = 3633$kgf/cm^2, $_s\upsilon_0 = 0.3$			
Stirrup and Tie SR 24, 9ϕ	$E_{st} = 1.98 \times 10^6$kgf/cm^2, $_y\sigma_{st} = 3300$kgf/cm^2			

For specimen No.4, in which the initiation of the inclined crack was prohibited and almost no bond was assumed for beams within the joint, only the effect of the loss of bond on the strain distribution of beam bars and shear resistance mechanism is studied.

The variables used to define material models are given in Table 1.

5. PROGRESS OF FAILURE

The analytical results on the condition of deformation and crack propagation for specimen No.1 are shown in Figs. 9 and 10. The comparisons of various analytical cracking and yielding loads with the test results are shown in Table 2.

In the analyses the flexural cracks initiated near the beam joint at the loading stage, P = 1t. These are corresponding to the test results. Then they propagated in the center of the beam span as the load increased. The flexural cracks of the column initiated at the column joint at P = 4t and the cracking load is a little higher than the test results.

The conditions of deformation of the joint and its vicinities at P = 5t are shown in Fig. 11 for No.1, No.2, No.3. From Fig. 11 it can be stated that the effects of bond characteristics are appeared in the flexural crack width at the beam joint. For No.3 the flexural crack at the beam joint propagated very quickly and the crack width amounted to about 1.0mm. For No.1 and No.2 the propagation of the flexural crack was rather slow and the crack width was only 0.15mm for No.2. Meanwhile the propagation of the flexural crack at the column joint was a little quick for No.2 as compared with No.3.

The inclined crack in the joint initiated near the corner of the joint most quickly at P = 2t for No.2. Thereafter the inclined cracks occurred near the center of the joint, but the crack width was not so large and about 0.1mm. For No.1 the propagation of the inclined crack was about the same as for No.2 except that it was a little slow and the crack width was relatively large and about 0.2mm. The inclined crack initiated most slowly at P = 4t for No.3 and thereafter propagated from the center to the compression corner. Analytical results on the initial inclined cracking load gave good agreements with test results.

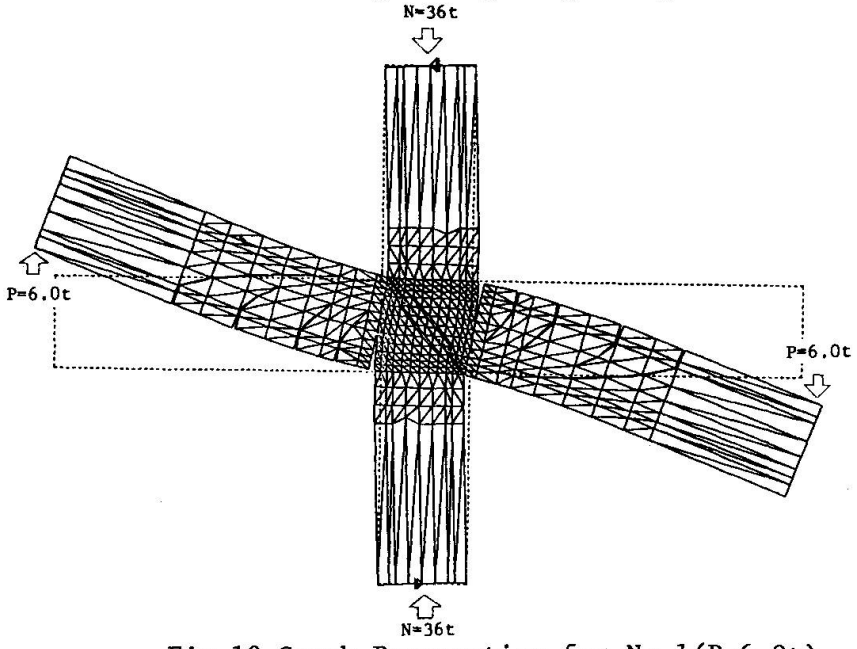

Fig.10 Crack Propagation for No.1(P=6.0t)

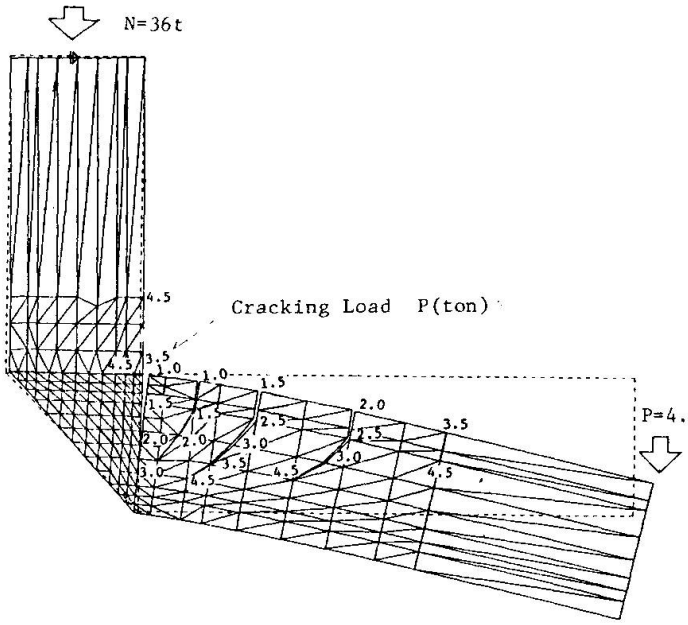

Fig.9 Crack Propagation for No.1(P=4.5t)

Table 2. Comparisons of Analytical Results with Test Results

	Calculated	No.1	No.2	No.3	No.4
Beam Flexural Crack	1.0	1.0 (1.3)	1.0 (1.0)	1.0 (1.0)	1.0
Column Flexural Crack	3.3	3.5 (3.0)	4.0 (2.5)	4.0 (3.0)	4.0
Joint Inclined Crack	2.8	3.0 (3.0)	2.0 (2.5)	4.0 (4.0)	-
Beam Shear Crack	3.3	3.0 (3.5)	3.5 (3.5)	3.0 (3.5)	3.0
Beam Bar Yielding	7.9	9.5 (6.5)	9.6 (6.0)	- (-)	-
Yielding in P-δ Curve of Test		(7.3)	(6.3)	(6.0)*	

Note: ( ):Test Result. Unit(ton)
Calculated: obtained by the theoretical or experimental equation.
* :Compression Failure of Concrete

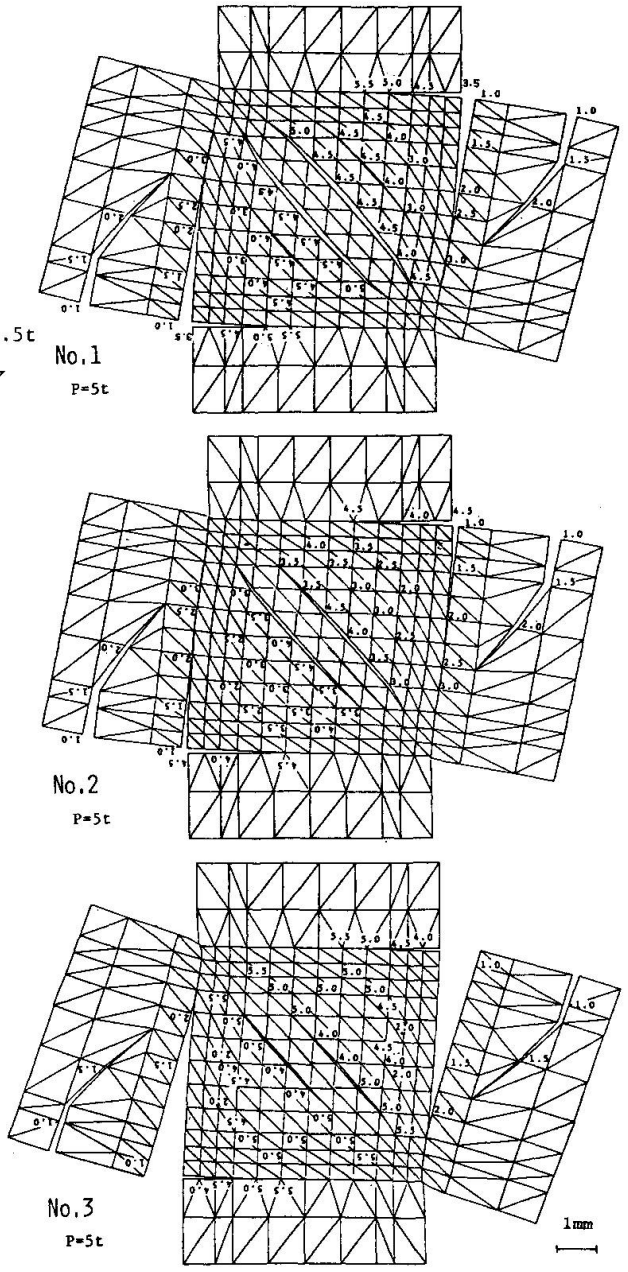

Fig.11 Deformation of Joints and Their Vicinities

The flexural yielding of the beam occurred at P = 9.5t, 9.6t respectively for No. 1, No.2. The analytical result, P = 9.5t is rather higher than the test results, P = 7.3t for No.1. For No.3 the flexural yielding did not occur. This is corresponding to the test result.

The local compressive failure of concrete occurred at the beam joint at P = 6 - 7t and thereafter began to occur in the center of the joint for No.1 and No.3.

6. LOAD-DEFLECTION RELATIONSHIPS

The load-deflection curves for the test and the analytical model are shown in Figs. 12 through 15. The analytical results were obtained in accordance with

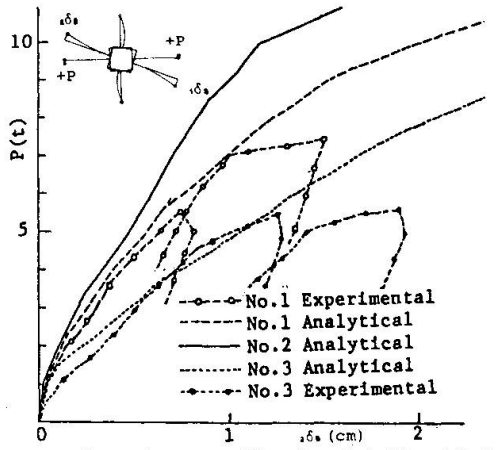

Fig.12 Load-Beam Deflection Relationships

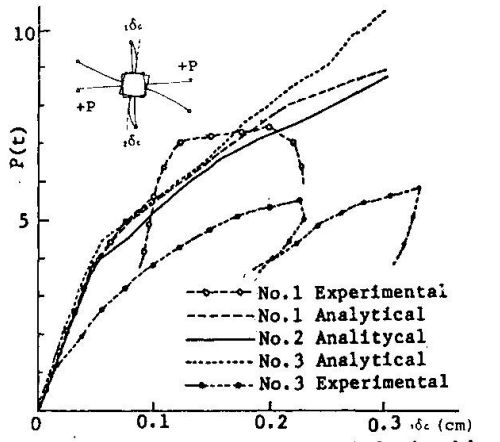

Fig.13 Load-Column Deflection Relationships

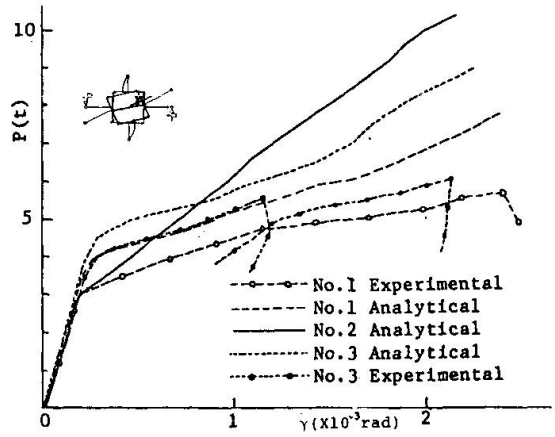

Fig.14 Load-Joint Distortion Relationships

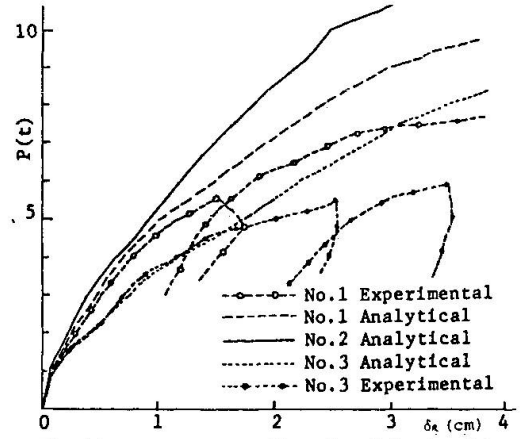

Fig.15 Load-Story Deflection Relationships

the measuring method in the tests as well as possible.

For No.1 the analytical model predicted a higher yield strength than was actually obtained, but gave a good match with the load-deflection behavior to the yield strength obtained in the test except that the analytical joint distortion proved to be a little stiff.

For No.3 the analytical model also obtained a good agreement with test results to P = 5.5t except that the analytical column deflection proved to be stiff.

The beam deflection increased as the bond chracteristics became poorer. These phenomena are considered to be based on the effect of bond slip of beam bars through the joint.

The column deflections were almost the same for all specimens to P = 4t, but thereafter No.3 proved to be slightly stiff and an opposite tendency was developed as compared with the beam deflection.

The initial stiffness of the joint distortion was almost the same for all specimens, but No.2 proved to be rather stiff even after the initiation of the inclined crack as compared with No.1 and No.3.

The story deflection of each specimen was subjected to the great influence of the beam deflection.

7. STRAIN AND BOND SLIP OF BEAM LONGITUDINAL BARS

The strain distributions of beam longitudinal bars for the test and the analytical model are shown in Fig. 16.

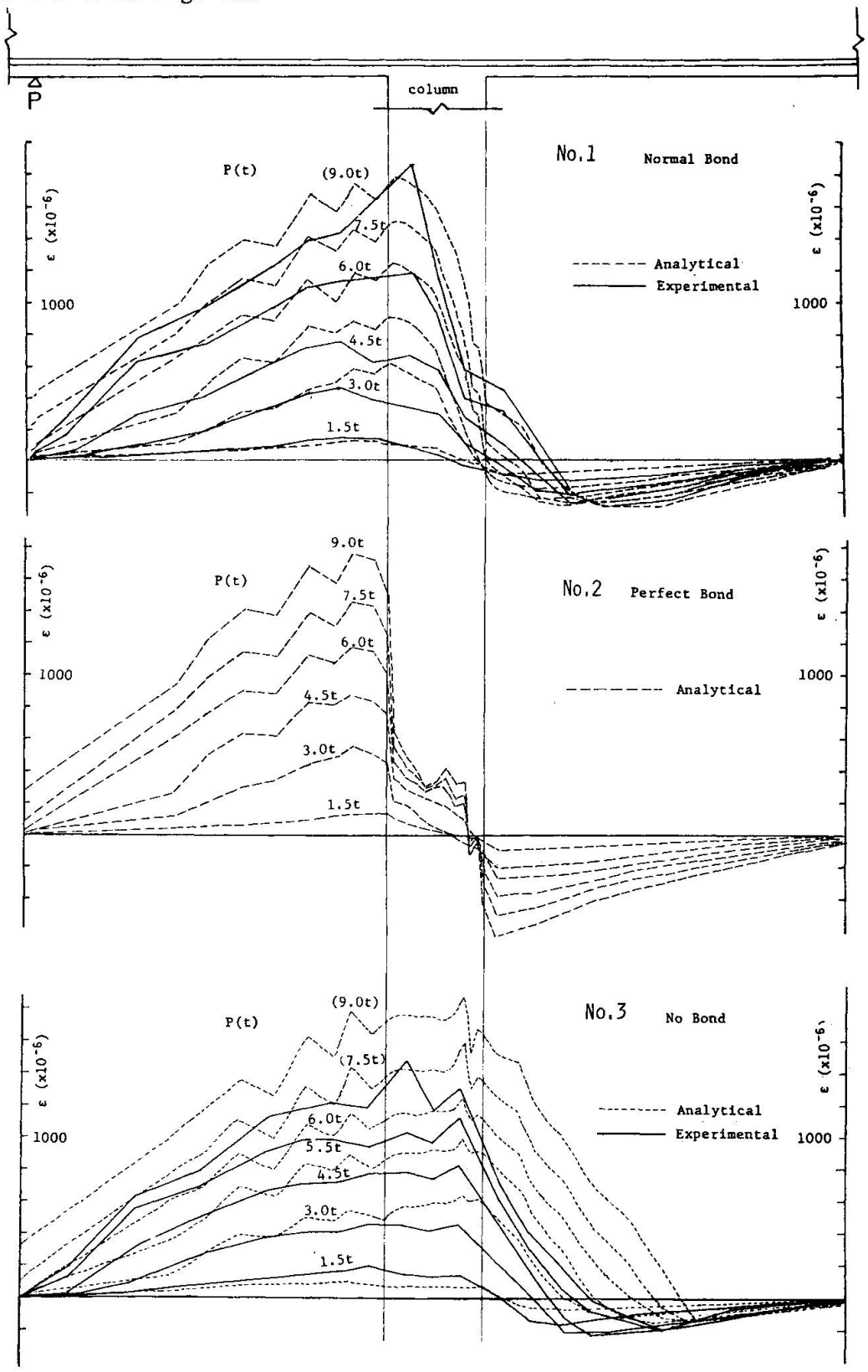

Fig.16 Strain Distributions of Beam Bottom Bars

The bond slips of beam longitudinal bars through the joint for the test and the analytical model are shown in Fig. 17.

The analytical results obtained a good agreement with test results for No.1, except the transformation of the compressive strain of beam longitudinal bars to tensile strain appeared a little later near the joint than test results and the sinking of beam bar into the joint proved to be a little smaller than test results.

From the analytical results for No.2 with almost perfect bond, it can be stated that the tensile strain of beam bars decreases greatly inside the joint and the transformation of the compressive strain of beam bars to tensile strain did not appear very conspicuously even inside the joint. This phenomenon indicated that the truss mechanism after the initiation of the inclined crack had not so great influence on the strain distribution of beam bars through the joint with the tie ratio, p_w = 0.7 %.

Meanwhile analytical results for No.3 obtained a good agreement with test results and show that the bond slips of beam bars through the joint increased remarkably and the tensile stress of beam bars at the beam joint was transferred directly to the compression zone through the joint. As the result the transformation of the compressive strain of beam bars to tensile strain was very noticeable.

As there was no great difference between the analytical results for No.3 and No.4, the effect of the loss of bond on the strain distribution of beam bars through the joint appeared to be much greater than that of the truss mechanism which was developed by the inclined crack.

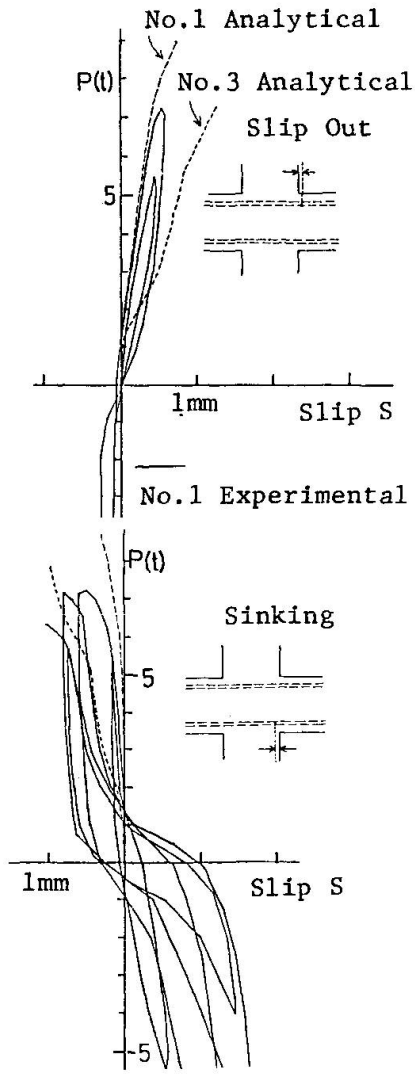

Fig.17 Bond Slip of Beam Bars through Joints

8. STRAIN OF COLUMN LONGITUDINAL BARS

The analytical results of strain distribution of column longitudinal bars showed almost the same tendencies for No.1, No.2 and No.3.

Fig. 18 shows the strain distribution of column bars for No.1. The transformation of the compressive strain to tesile strain appeared at about P = 6t, and this phenomenon is corresponding to the test result.

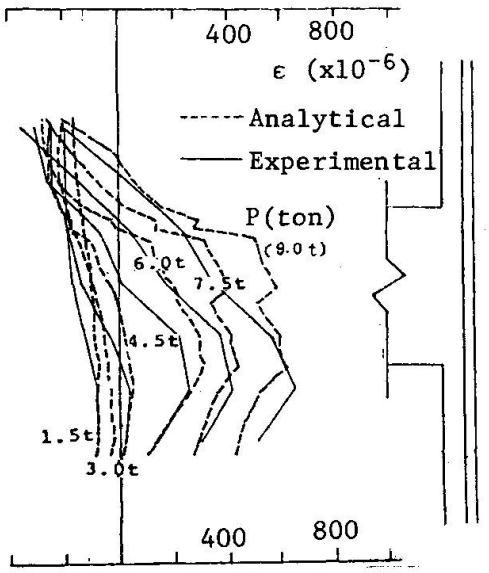

Fig.18 Strain Distributions of Column Longitudinal Bars

9. STRAIN OF TIES

Fig. 19 shows the strain of ties inside the joint for the test and the analytical models. The analytical strain of ties began to increase after the inclined crack initiated.

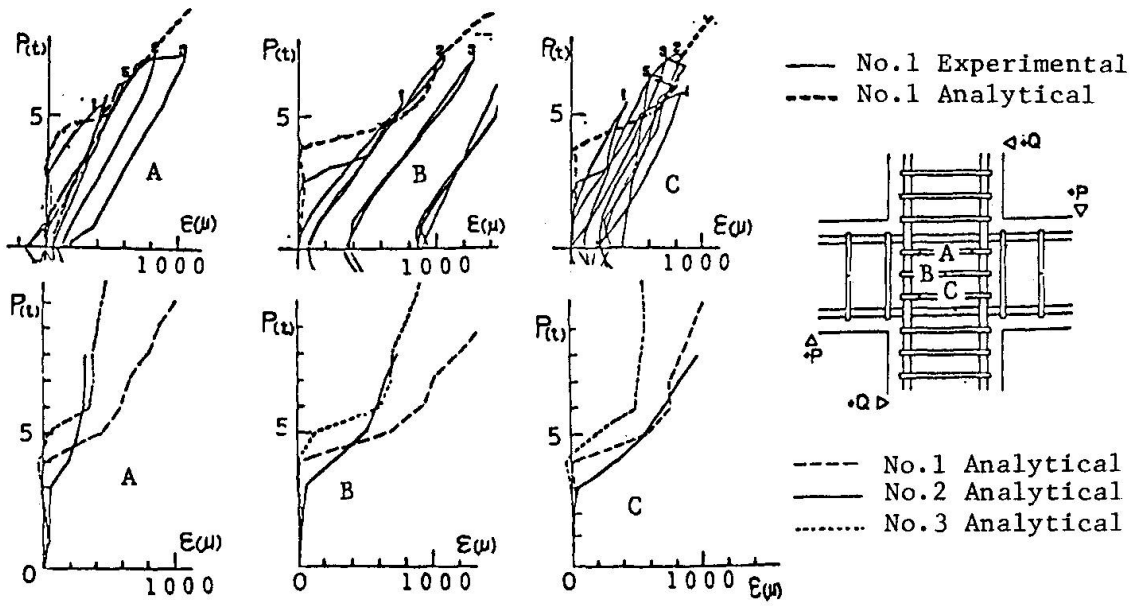

Fig.19 Relationships between Load and Strain of Ties

These phenomena were also observed a little later in the test results.

The strain of ties for No.3 appeared to be relatively smaller than that for No.1, but the effect of bond characteristics of beam bars on the strain of ties was not so remarkable.

10. TRUSS MECHANISM AND LOSS OF BOND

Fig. 20 shows the analytical stress distribution in the joint for No.2 and No.4. For No.2 with almost perfect bond for beam bars only the effect of the truss mechanism was designed to appear after the inclined crack initiated. For No.4, in which the initiation of inclined cracks were prohibited and almost no bond was assumed for beam bars, only the effect of the loss of bond was designed to appear.

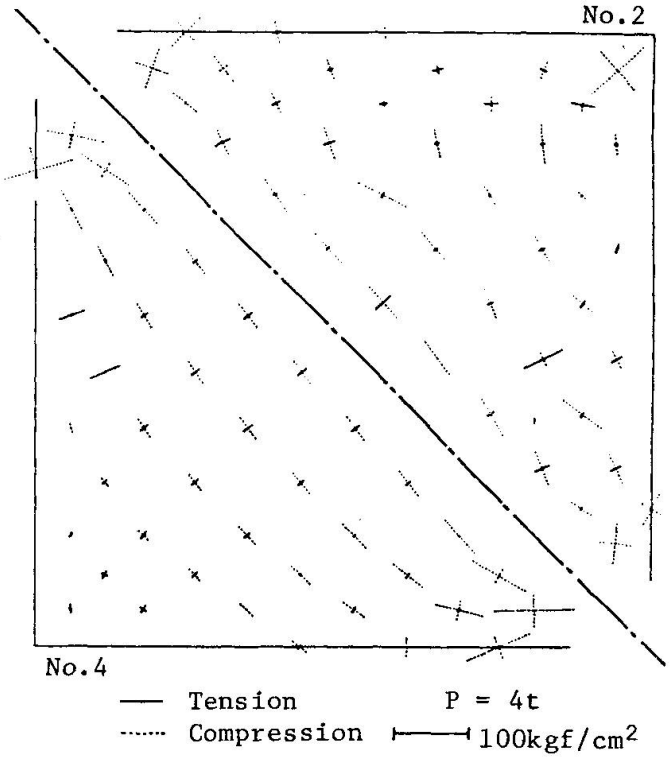

Fig.20 Stress Distributions of Joints

In No.2 the truss mechanism was observed and the higher compressive stresses were concentrated upon the center strut of the joint. But the stresses were dispersed by the bond near the end of the joint and the concentration of stresses upon the compression corner was not so marked.

In No.4 the flow of stress had a wide range in the center of the joint, but the compressive stress concentration was conspicuous at the compression corner from the loss of bond. The local compression failure of concrete at the beam joint was considered to be caused primarily by this phenomenon.

11. CONCLUSIONS

The nonlinear behaviors of reinforced concrete beam-column joints, such as the transformation of strain distribution of beam bars or the bond slip of beam bars through the joint, were analyzed by the finite element model combining the individual material properties.

From the comparison of analytical results for the normal bond (No.1) and almost no bond (no.3) for beam bars through the joint, it could be stated that analytical model predicted a higher yield strength of the beam for No.1, but the analytical load-deflection behavior after the initiation of the inclined crack, various cracking load and the strain distribution of beam bars gave a good match with test results.

The principal cause of higher yield strength of the beam obtained in the analysis was to be sought in not considering the downward sloping portion of the stress-strain curve of concrete after the compressive strength in the analytical model. Really in the test the transformation of the compressive strain of beam bars to tensile strain and the compressive stress concentration near the beam joint from the bond deterioration caused the local compression failure of concrete. It will be necessary to add the modeling of the downward sloping portion of the stress-strain curve to this model.

From the comparison of the truss mechanism model, No.2, with the loss of bond model, No.4, it could be stated that the transformation of strain distribution of beam bars, which had a great influence on the shear resistance mechanism of the joint, was more seriously affected by the loss of bond than by the truss mechanism.

It was recognized from this study that the bond slip through the joint from the bond deterioration not only increased the story deflection, but also changed the stress distribution of concrete and beam bars in the joint and brought about the transformation of compressive strain of beam bars to tensile strain and the local compression failure of concrete. These phenomena will be a primary factor to decrease the flexural yield strength of beams and deteriorate the restoring force characteristics of the overall structures.

It was known that the bond deterioration was severer in the case of cyclic loading [24], [25], [26], [33]. In the further work it will be necessary to study the effect of bond deterioration under load cycles on the behavior of the beam-column joint.

ACKNOWLEDGEMENTS

This study was supported by the Kohzoh Keikaku Engineering. The autor wishes to express his sincere gratitude to Professor Emiritus H. Umemura and Professor H. Aoyama at the University of Tokyo for their warmhearted guidance and encouragement.

REFERENCES

1. Jirsa, J.O., Aleman, M.A. and Meinheit, D.F., "Influence of Lateral Beams on the Behavior of Beam-Column Joints," 6th World Conf. on Earthquake Engrg., New Delhi, Jan. 1977.
2. Umemura, H., Hamada, D., Kamimura, T. and Takada, M., "Experimental Study on Reinforced Concrete Beam-Column Joints with Eccentric Wallgarder Beams," Proc. Annual Conv., Architectural Institute of Japan (AIJ), Sep. 1980, pp.1517-1520.
3. Burguiers, S.T., Jirsa, J.O. and Longwell, J.E., "The Behavior of Beam-Column Joints under Bidirectional Load Reversals," Bulletin D'information, No.132, AICAP - CEB Symposium, Rome, May 1979, pp.221-228.
4. Shimohira, F. and Higashi, Y., "Analysis of Reinforced Concrete Beam-Column Joint by Finite Element Method," Proc. Annual Conv., AIJ, Nov. 1971, pp.843-844.
5. Will, G.T., Uzumeri, S.M. and Sinha, S.K., "Application of the Finite Element Method to the Analysis of Reinforced Concrete Beam-Column Joints," Proc. of the Speciality Conf. on FEM in Civil Engrg., CSCE, EIC, Canada, Jun. 1972, pp.745-766.
6. Mirza, M.S. and Mufti, A.A., "Nonlinear Finite Element Analysis of Reinforced Concrete Structures," Proc. of the 1974 International Conf. on FEM in Engrg., Univ. of New South Wales, Australia, 1974, pp.403-417.
7. Ohtsuki, K. and Obata, M., "Elasic Plastic Analysis of Infinitely Uniform Frames by Finite Element Method," Proc. Annual Cov., AIJ, Oct. 1975, pp.771-772.
8. Ohwada, Y., "Stress Analysis of Reinforced Concrete Beam-Column Joint Subjected to Seismic Stress: Three-Dimensional Elastic Analysis by FEM," Proc. Kanto Dist. Symp., AIJ, Jul. 1979, pp.185-188.
9. Ichinose, T. and Aoyama, H., et al., "Nonlinear Analysis of Reinforced Concrete Rectangular Frame Considering the Continuity of Reinforcement," Proc. Kanto Dist. Symp., AIJ, Jul. 1980, pp.137-140.
10. Tada, T. and Takeda, T., "Analytical Study on Deformation Characteristics of Plastic Hinge at the End of RC Memeber and Process of Bond Deterioration in Neighbouring Anchorage Zone," Proc. Kanto Dist. Symp., AIJ, Jul. 1980, pp.125-132.
11. Felippa, C.A., "Refined Finite Element Analysis of Linear and Nonlinear Two-Dimensional Structures," SESM Report, No.66-22, Univ. of California, Berkeley, Oct. 1966.
12. Darwin, D. and Pecknold, D.A., "Nonlinear Biaxial Stress-Strain Law for Concrete," Jour. Engr. Mech. Div., ASCE, vol.103, No.EM2, Apr. 1977, pp.229-241.
13. Darwin, D. and Pecknold, D.A., "Analysis of R.C. Shear Panels Under Cyclic Loading," Jour. Struct. Div., ASCE, Vol.102, No.ST2, Feb. 1976, pp.355-369.
14. Darwin, D. and Pecknold, D.A., "Inelastic Model for Cyclic Biaxial Loading of Reinforced Concrete," SRS No.409, Univ. of Illinois at Urbana-Champaign, Jul. 1974.
15. Noguchi, H., "Finite Element Nonlinear Analysis of Reinforced Concrete: Part 1: Stress-Strain Relationships of Concrete under Biaxial Stresses," Trans. of AIJ, No.252, Feb. 1977, pp.1-11.
16. Aoyama, H. and Noguchi, H., "Mechanical Properties of Concrete under Load Cycles Idealizing Seismic Actions," Bulletin D'information, No.131, AICAP - CEB Symposium, Rome, May 1979, pp.31-63.
17. Kupfer, H.B. and Grstle, K.H., "Behavior of Concrete under Biaxial Stresses," Jour. Engr. Mech. Div., ASCE, Vol.99, No.EM4, Aug. 1973, pp.853-866.
18. Nelissen, L.J.M., "Biaxial Testing of Normal Concrete," Heron, Delft, Vol.18, No.1, 1972.
19. Saenz, L.P., Disc. of "Equation for the Stress-Strain Curve of Concrete," by Desayi and Krishnan, ACI J., Proc. Vol.61, No.9, Sep. 1964, pp.1229-1235.

20. Kupfer, H.B., Hilsdorf, H.K. and Rüsch, H., "Behavior of Concrete under Biaxial Stresses," ACI J., Proc. Vol.66, No.8, Aug. 1969, pp.656-666.
21. Ngo, D. and Scordelis, A.C., "Finite Element Analysis of Reinforced Concrete Beams," ACI J., Proc. Vol.64, No.3, Mar. 1967, pp.152-163.
22. Noguchi, H., "Finite Element Nonlinear Analysis of Reinforced Concrete: Part 2: Mechanics of Bond and Slip of Deformed Bars in Concrete," Trans. of AIJ, No.258, Aug. 1977, pp.27-37.
23. AIJ Structural Standard Committee and R.C. Structural Subcommittee, "Bond Characteristics: Part 2," Series 12, Materials for Ultimate Strength Design of R.C., Jour. of Arch. and Building Science, AIJ, Vol.95, Jan. 1980, pp.61-62.
24. Morita, S. and Kaku, T., "Local Bond Stress-Slip Relationship under Repeated Loading," Proc. IABSE Symp., Lisbon, Portugal, Sep. 1973.
25. Morita, S. and Kaku, T., "Bond-Slip Relationship under Repeated Loading," Trans. of AIJ, No.229, Mar. 1975, pp.15-24.
26. Tassios, T.P., "Properties of Bond between Concrete and Steel under Load Cycles Idealizing Seismic Actions," Bulletin D'information, No.131, AICAP - CEB Symposium, Rome, May 1979, pp.65-122.
27. Noguchi, H., "Finite Element Nonlinear Analysis of Reinforced Concrete: Part 4: Crack Initiation and Propagation," Trans. of AIJ, No.262, Dec. 1977, pp.43-52.
28. Zienkiewicz, O.C., "The Finite Element Method in Engineering Science," Second Edition, McGraw-Hill, 1971.
29. Zienkiewicz, O.C., "The Finite Element Method," Third Edition, McGraw-Hill, 1977.
30. Yamada, Y., "Plasticity and Visco-elasticity," Baifuhkan, 1972.
31. Kamimura, T. and Hamada, D., et al., "Experimental Study on Reinforced Concrete Beam-Column Joints: Part 1 - 3," Proc. Annual Conv., AIJ, Sep. 1978, pp.1673-1674, Sep. 1979, pp.1303-1306.
32. Tada, T., Takeda,T. and Takemoto, Y., "Tests on Bond Characteristics of Deformed Bars: Process of Bond Deterioration in the Beam-Column Joints," Proc. Kanto Dist. Symp., Jul. 1977, pp.229-232.
33. Gerstle, K.H., "Material Modeling of Reinforced Concrete," Inductory Report of IABSE Colloquium, Delft 1981, IABSE - AIPC - IVBH, Oct. 1980, pp.41-61.

Finite Element Analysis of Reinforced Concrete Beams with Special Regard to Bond Behaviour

Calcul des poutres en béton armé par la methode des éléments finis en tenant compte de l'adhérence entre le béton et l'armature

Die Berechnung von Stahlbetonbalken nach der Methode der finiten Elemente unter besonderer Berücksichtigung des Verbundes

GÜNTHER PLAUK
Dr.-Ing.
Federal Institute for Materials Testing (BAM)
Berlin (West), Germany

GEBHARD HEES
Prof. Dr.-Ing.
Technical University Berlin
Berlin (West), Germany

SUMMARY
A nonlinear finite element method has been developed and used to study the behaviour of reinforced concrete beams. The mechanical model takes into account the nonlinear properties of material, progressive cracking and local failure. For the first time realistic bond-slip relations were used in a finite element model. The validity of the method was studied by comparing analytical and experimental results which show an excellent agreement.

RÉSUMÉ
Une méthode de calcul par les éléments finis a été développée pour déterminer le comportement des poutres en béton armé. Le modèle mécanique a tenu compte de la fissuration progressive, des propriétés non-linéaires du matériau, de l'adhérence et de la rupture locale. Les examens effectués ont montré que dû à l'utilisation des relations réalistes relatives à l'adhérence on a obtenu une conformité excellente entre les résultats d'essais et les résultats de calcul.

ZUSAMMENFASSUNG
Ein Rechenverfahren nach der Methode der finiten Elemente wurde entwickelt und auf die Untersuchung des Verhaltens von Stahlbetonbalken angewendet. In das mechanische Modell einbezogen wurde die Rissbildung, das nichtlineare Werkstoffverhalten, der Verbund sowie das örtliche Beton- und Verbundversagen. Die durchgeführten Untersuchungen haben gezeigt, dass insbesondere durch Verwendung wirklichkeitsnaher Gesetze für den Verbund eine ausgezeichnete Übereinstimmung von Rechen- und Versuchsergebnissen erreicht wird.

1. INTRODUCTION

Recent development of the finite element method permits study of reinforced concrete structural member behaviour in the full range of loading. An excellent summarized presentation of existing finite element models used for analysing reinforced concrete is given in [1,2].

A critical review of published analytical solutions for reinforced concrete beams subjected to static loading [3,4,5,6] such as load-deflection curves, stress and strain distributions and crack patterns show only little agreement with experimental results. In finite element analysis of reinforced concrete it has become customary to assume that steel bars are ridgidly attached to concrete nodes. This treatment, however, is unrealistic and physically unjustified. The reason for the discrepancy in analytical and experimental results must therefore be seen in the fact that bond between concrete and reinforcement in mechanical models which are applied to study the structural response has mostly been neglected.

The finite element method presented in this paper permits to determine the internal stress and strain distribution as well as the crack patterns and deflections of reinforced concrete beams incrementally loaded from zero load to ultimate load. The proposed model used for analysis takes into consideration nonlinear material properties, progressive cracking, and bond between concrete and reinforcement. Included is also local crushing of concrete and bond failure. To fully account for the profound influence of bond on cracking and on the internal stress distribution different bond-stress slip relations for bond intervals near cracks, respectively in some distance from cracks, were implied into the finite element model.

2. FINITE ELEMENT APPROXIMATION

The finite element idealization of a reinforced concrete beam for two-dimensional analysis is shown in Fig. 1. To account for the varied material properties the beam is divided into concrete and steel elements. For both, concrete and steel reinforcement, conventional two-dimensional quatrilateral plane stress elements are used. Each element consists of four triangular sublements with

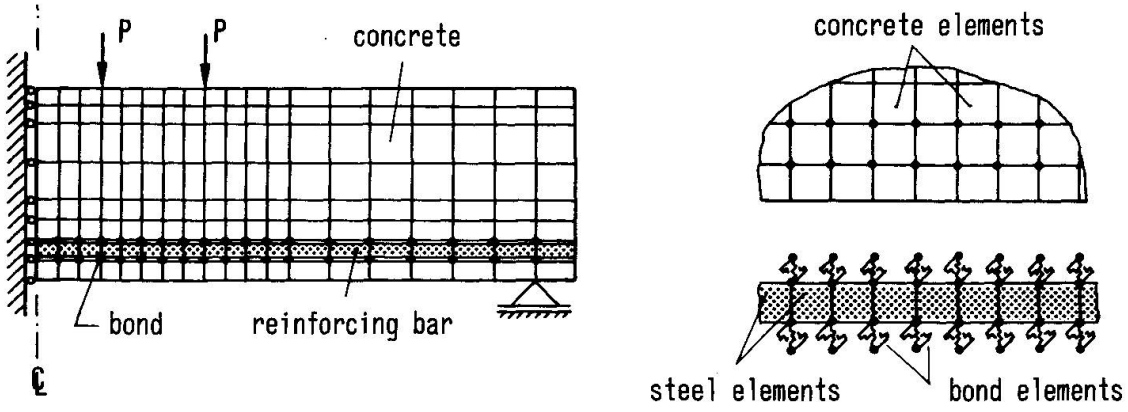

Fig. 1 Finite Element Idealization of a Reinforced Concrete Beam

constant stress and strain distribution. The unloaded central node of this type of element is eliminated which reduces the degrees of freedom.

The finite element model contains separate nodes for concrete and reinforcing elements crossing each other. Bond between concrete and steel bars is represented by special bond-elements first created by Nilson [7]. Each bond element contains two springs, one acting parallel to the axis of the steel bar, the other acting perpendicular to it. The overlapping nodes of concrete and steel elements are directly connected by these linkage elements.

In regions of the beam where intensive crack propagation is expected a finer element mesh is used so that in the tension zone between the cracks a number of concrete elements remain uncracked. In connection with establishing a realistic model for bond behaviour this simple but necessary treatment permits to analize the true state of stress and strain between cracks so that the influence of bond on beam deflections is fully accounted in the model.

3. MATERIAL IDEALIZATION

3.1 Modelling of Concrete

The stress-strain relationship for concrete under biaxial state of stress used here for analysis are given in Fig. 2. The uncracked concrete is assumed to be a homogeneous material with properties differing in two directions perpendicular to each other. The axes of anisotropy are identical to the axes of the principle stresses. Furthermore, isotropic behaviour is assumed for the concrete element due to uniaxial loading σ_1 or σ_2, respectively shear loading τ as shown in Fig. 2. It should be noted that the four material properties E_1, E_2, ν_1, and ν_2 are not independent and could only be determined if test data were available. Neglecting the non-diagonal terms of the stress-strain relationship the values of the material properties E_1 and E_2 can be obtained from uniaxial stress-strain curve as a function of strains in the principle directions. The uniaxial stress-strain curve used for analysis is shown in Fig. 3.

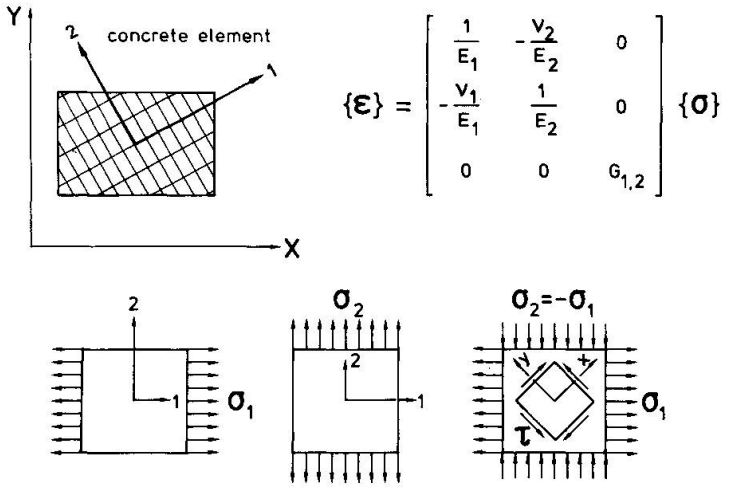

Fig. 2 Stress-Strain Relationship for Concrete under Biaxial State of Stress

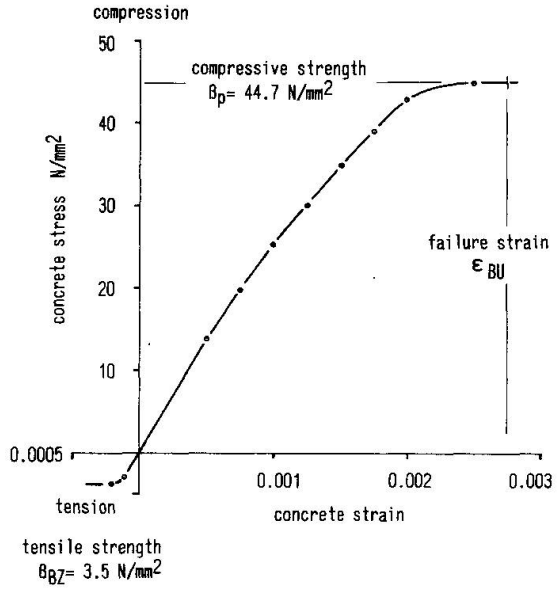

Fig. 3 Uniaxial Stress-Strain Curve for Concrete

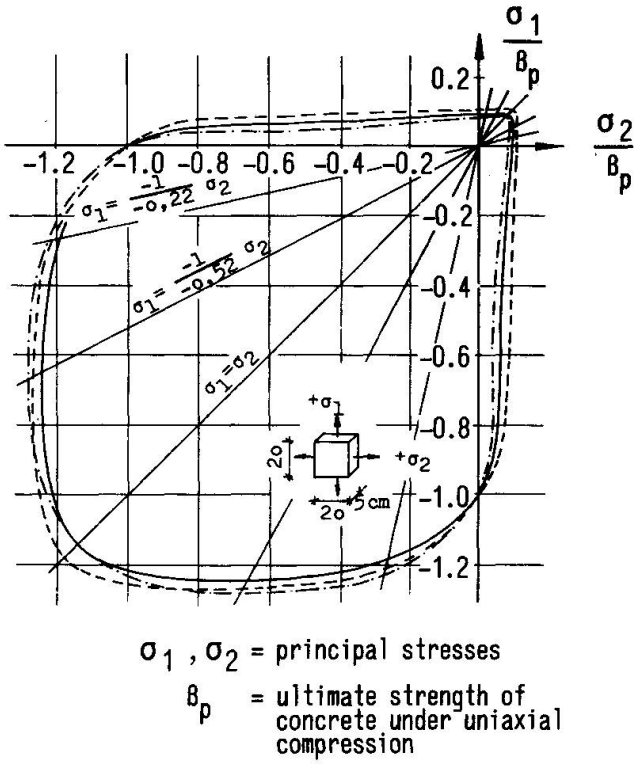

σ_1 , σ_2 = principal stresses

β_p = ultimate strength of concrete under uniaxial compression

Fig. 4 Strength Envelopes for Concrete under Biaxial State of Stress [8]

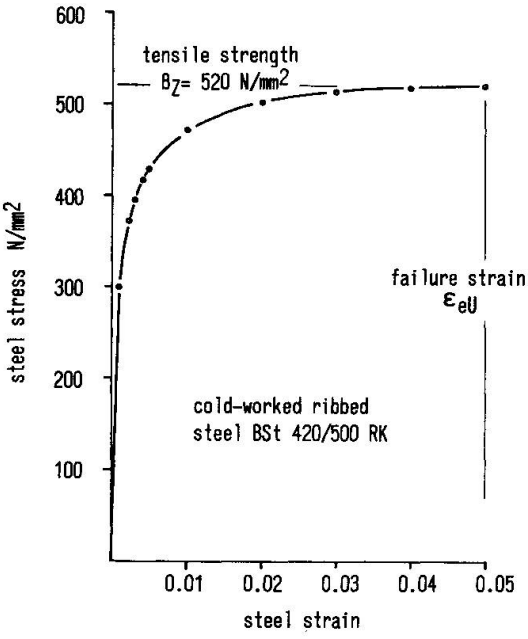

Fig. 5 Uniaxial Stress-Strain Curve for Reinforcing Steel

To take into account the failure of concrete elements under a combined state of stress a biaxial failure envelope (Fig. 4) derived from test data by Kupfer [8] is implied in the material model. Cracks are established in concrete elements when in one of the principle directions concrete strains exceed the maximum strain value obtained from the uniaxial stress-strain curve of Fig. 3.

3.2 Modelling of Steel

Similar treatment as for concrete is proposed for steel. The reinforcing bars of a beam are essentially in a state of uniaxial stress. Therefore, an uncoupling of the stress-strain matrix given in Fig. 2 is justifiable. Neglecting the influence of Poisson's ratio on element stresses which can be done without any loss of accuracy, the values of material properties E_1 and E_2 can be taken directly from the nonlinear stress-strain diagram of Fig. 5. The shown curve is valid for a particular reinforcing steel and was obtained from uniaxial tests. This steel was used for a test beam [10] which is selected here for analysis.

To determine failure of steel elements a maximum strain criterion was used. Failure occurs if the principle strains exceed the maximum value of strains corresponding to peak stress in tension given in Fig. 5.

3.3 Modelling of Bond

An intensive experimental study of bond between steel reinforcement and concrete was done for the last years by Eifler [9]. For the present analysis realistic bond-slip relations were obtained from these test results.

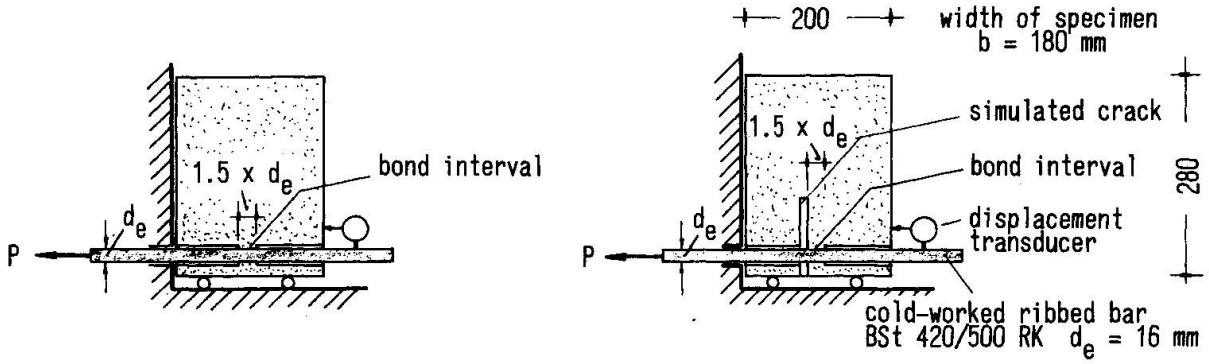

Fig. 6 Test Specimens for Bond Investigation Ref. 9

The specimens used for bond investigations are shown in Fig. 6. It is important to recognize that the midsection of the test specimens are very similar to beam sections of a short length. The steel bar is only over a short length of approximately 1.6 x bar diameter in connection with the surrounding concrete, so that in this case a uniform distribution of bond stresses could be assumed. It should be noted that this means a full correspondence between bond intervals in the test specimen and the bond idealization proposed in the finite element model. To study the influence of cracking on bond behaviour, a modified test specimen was developed and used with a simulated crack in front of the bond interval (Fig. 6b).

Furthermore, the influence of a plastic steel strain on bond behaviour was investigated. Therefore, before carrying out pull-out-tests the casted steel bar in bond with the concrete of the test specimen was stretched to a certain amount of plastic steel strain by applying tension to the projecting ends of the bar.

The bond-slip curves obtained from first test results are shown for bond in uncracked regions of a beam or in some distance of cracks in Fig. 7 and for bond near crack faces in Fig. 8.

Several points are of interest to observe in the bond-slip-curves presented. In general, a significant influence of plastic steel strain on bond stiffness and peak bond stress is obvious. Comparing the two sets of bond-slip-curves it can be clearly seen that bond stiffness and bond stresses near cracks are significantly lower than in some distance from the crack face or in uncracked regions for equal values of bond slip.

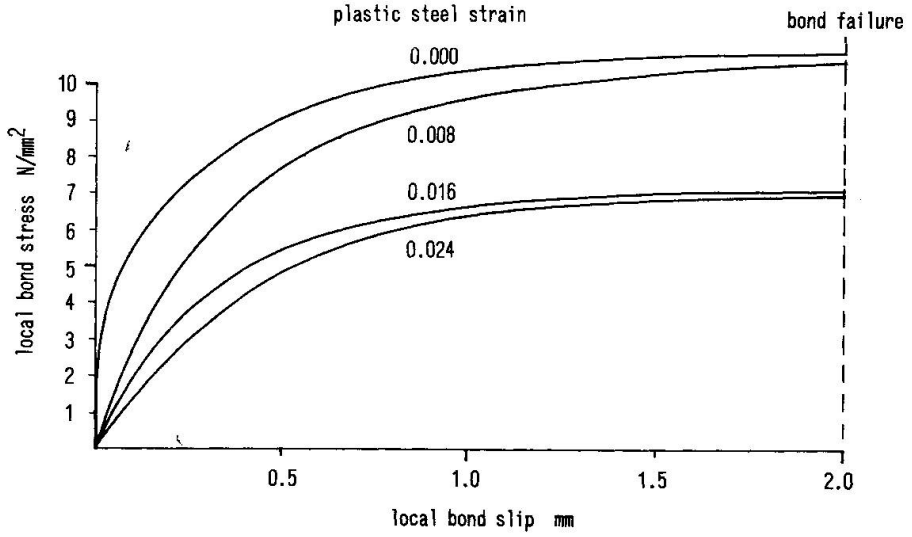

Fig. 7 Bond Stress-Slip Relations for Bond in Uncracked Regions or in some Distance from Cracks

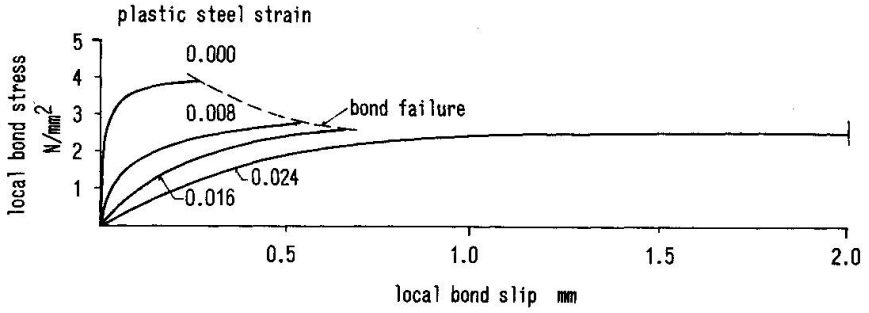

Fig. 8 Bond Stress-Slip Relations for Bond near Cracks

The different bond properties near cracks and between cracks can be easily incorporated into the finite element model as shown in Fig. 9.

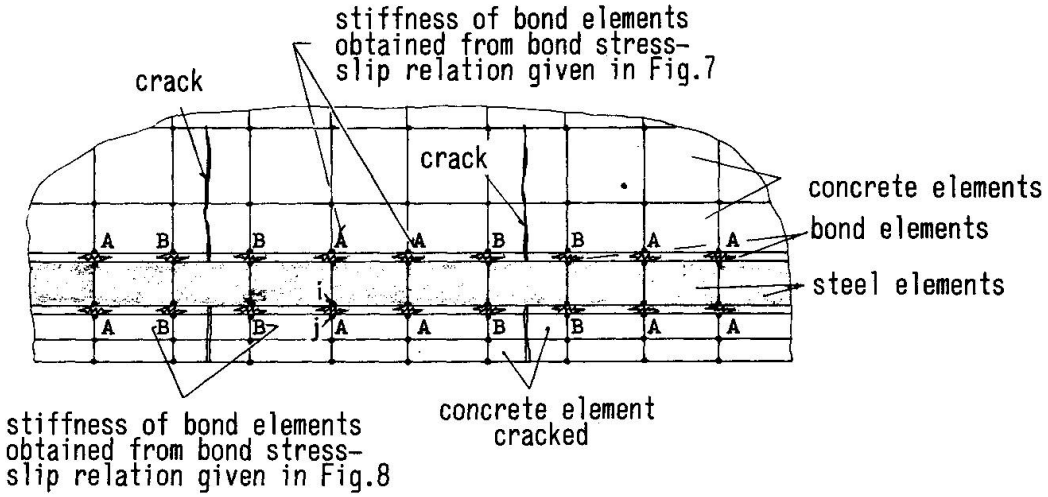

Fig. 9 Representation of Bond in a Cracked Reinforced Concrete Beam

4. NONLINEAR ANALYSIS AND COMPUTATIONAL ASPECTS

A nonlinear analysis of reinforced concrete beams accounting for all important effects on internal stress distribution, crack propagation and external deformations can only be realized by a step-by-step solution procedure. Therefore, the finite element method proposed involves an incremental loading and two different iteration procedures to satisfy equilibrium and constitutive relations within each load increment.

The solution process starts with incrementation of external loads. In each load increment the increments of nodal deflections and internal stresses are first obtained by using a global stiffness matrix containing tangential values of beam stiffness reached in the previous load step. After computing the resulting stress and

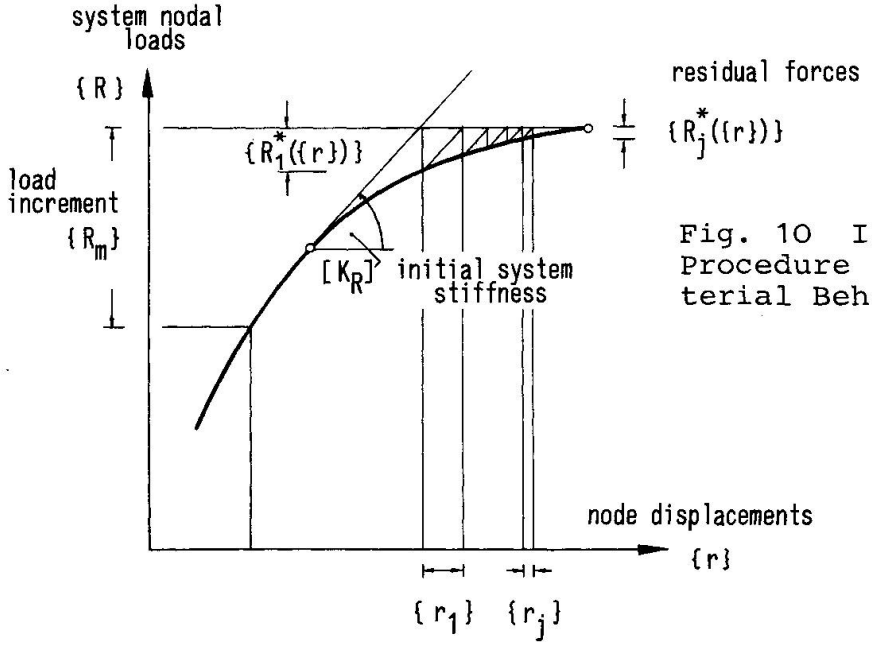

Fig. 10 Iterative Solution Procedure for Nonlinear Material Behaviour

strain increments the total stresses of elements are not corresponding to the stress state obtained from constitutive relations for total strains. The "unbalanced" stresses are now integrated to receive "unbalanced" nodal forces which are applied to the element nodes in the next iteration step. To fully account for nonlinear material behaviour to structural stiffness an iteration process is now started as shown in Fig. 10 until constitutive relations are satisfied. It should be noted that the global stiffness matrix remains unchanged in this case.

Cracking of concrete causes a sudden change of element stiffness and needs, therefore, a modified treatment. In a system with a compatible state of stress and strain the proposed failure criterion for concrete in tension is satisfied in a more or less greater number of adjacent concrete elements or possibly in the total area of tension zone. To help the system adjust in the correct manner only in elements with a maximum value of tensile stresses in principal directions - exceeding tensile strength - cracks are established as shown in Fig. 11. The stiffness of cracked elements satisfying this criterion is now modified and reduced to zero in a direction perpendicular to cracks.

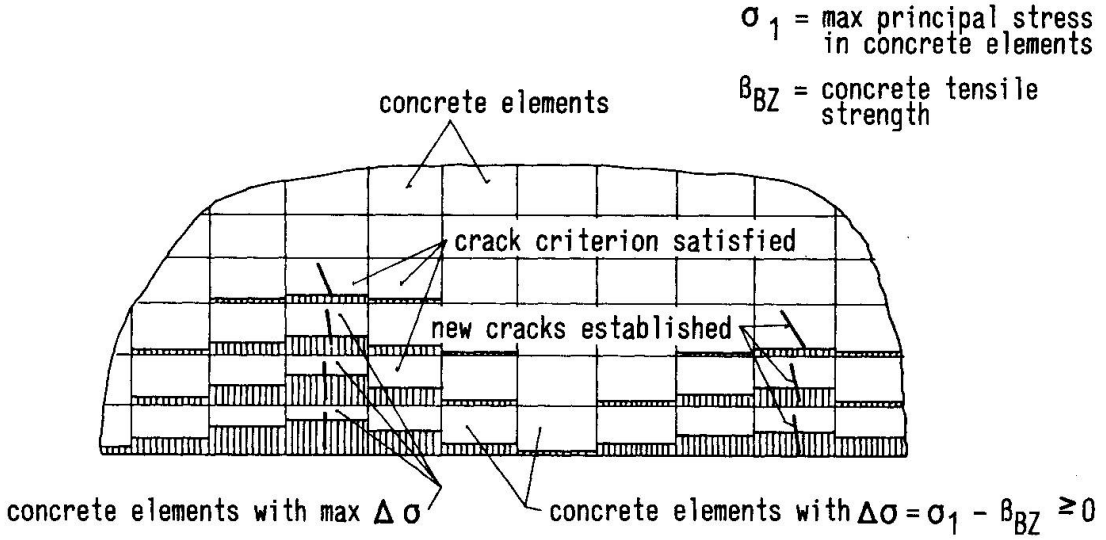

Fig. 11 Crack Propagation in a Seperate Step of Iteration

Tension stresses causing cracks are removed and transferred to adjacent uncracked concrete elements. This is done by sets of nodal forces as illustrated in Fig. 12. To simulate the process of successive cracking a similar iteration process as shown in Fig. 10 is proposed, but with a global stiffness matrix changing in each iteration step. This iteration is stopped if the constitutive relations of materials are violated. In this case iterations corresponding to Fig. 10 are performed until the equilibrium of the system is re-established.

All load increments are treated in the same manner until the ultimate load has been reached and failure in concrete or steel occurs.

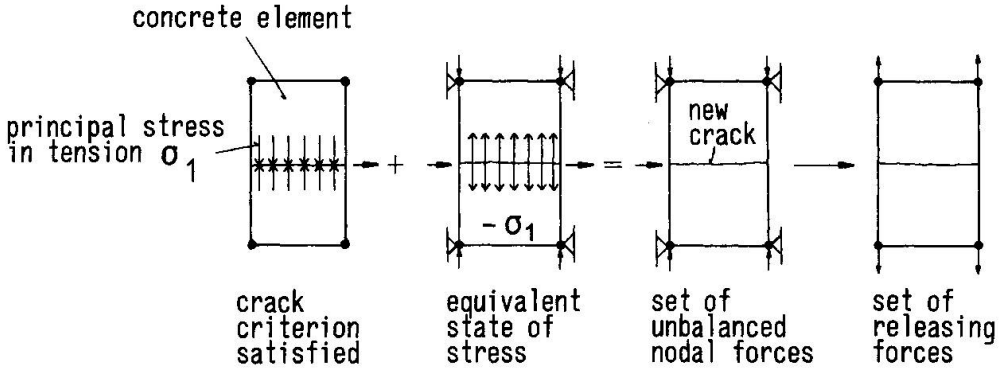

Fig. 12 Removing of Tension Stress in a Cracked Concrete Element

5. RESULTS

5.1 Analysis of a Reinforced Concrete Beam

The method is applied to study the behaviour of a reinforced concrete beam previously tested by Eifler [10]. Crack propagation, internal stress and strain distribution and load deformation response due to vertical single loads were traced through the elastic and inelastic ranges. The test beam and the finite element idealization used for analysis is shown in Fig. 13. One half of the symmetrically loaded beam was divided into a finite element mesh with a total number of 514 elements and 1056 degrees of freedom. In the region of proposed progressive cracking finer grid dimensions were chosen.

In the following the analytical solutions are presented and compared if possible with the experimental results.

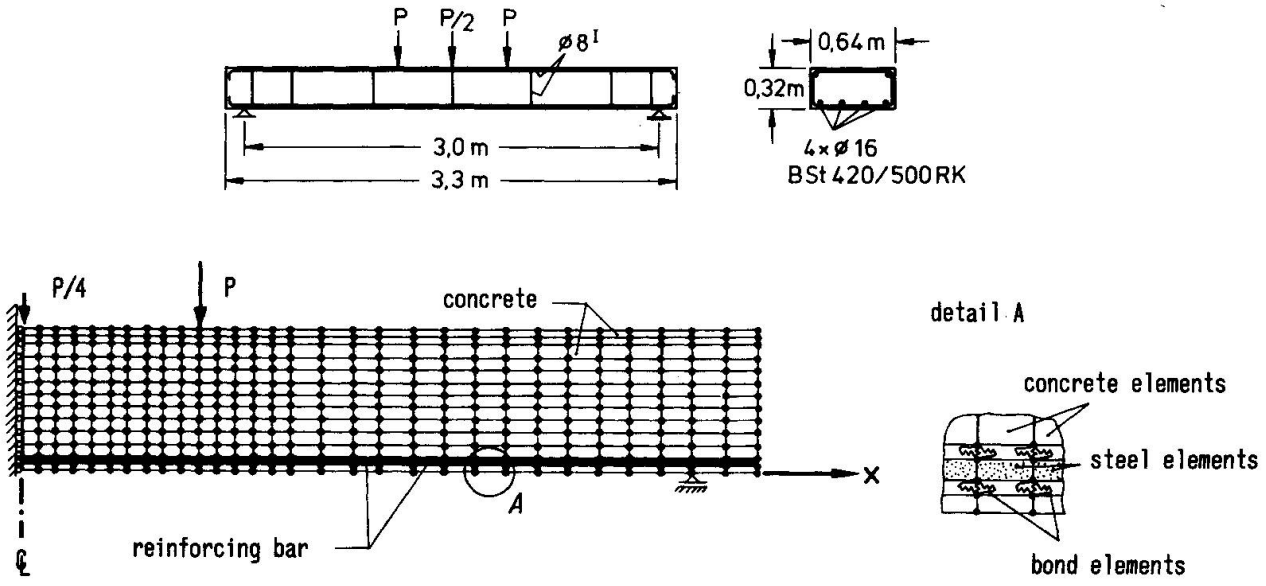

Fig. 13 Test specimen [10] and Analytical Beam Mesh Layout

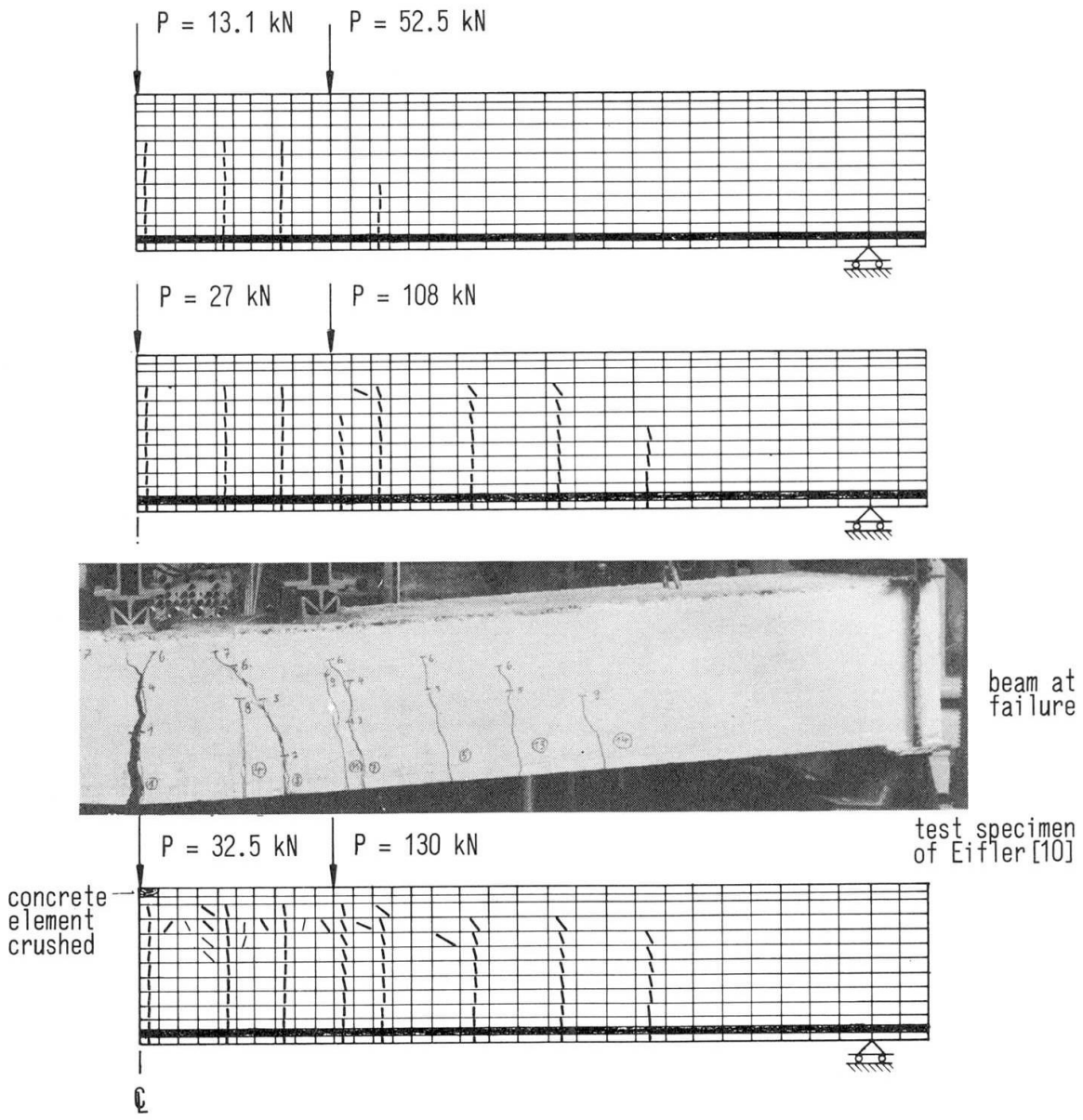

Fig. 14 Comparison of Analytical and Experimental Crack Patterns

The extent of concrete cracking at various stages in the loading history of the beam is shown in Fig. 14. The crack patterns, e.g., number, direction, and distance of cracks obtained from analytical solution agree with the experimental results. The analytical failure consisted in a crushing of concrete elements in the midspan cross section of the beam. It occured at a bending moment of M = 124 kNm which corresponds to the experimental values. It may now be observed in Fig. 14 that in the tension zone between cracks a number of concrete elements remained uncracked which shows the validity of the bond model.

For each load increment the internal stresses and strains of the beam were calculated. To demonstrate the influence of cracking and bond the distribution of concrete stresses in the cover of reinforcement, the steel stresses along the bar and the bond stresses between concrete and steel for the analytical ultimate load are given in Fig. 15. It may be of some interest to show the

steel stresses along the bar for this case. Peak steel stresses were found in the cracked cross sections. Between cracks the decrease of steel stresses is obviously caused by bond and indicates the force transfer between concrete and reinforcement.

The bond stress curve is characterized by an antisymmetric stress distribution between cracks with peak bond stress near to crack surfaces and zero bond stress approximately in the middle of the concrete blocks. At ultimate load bond failure occured only adjacent to the first crack near the midspan section of the beam.

To show the stress and strain distribution at each cross section of the beam which can also easily be obtained from analytical results a concrete block between two cracks is regarded in Fig. 16.

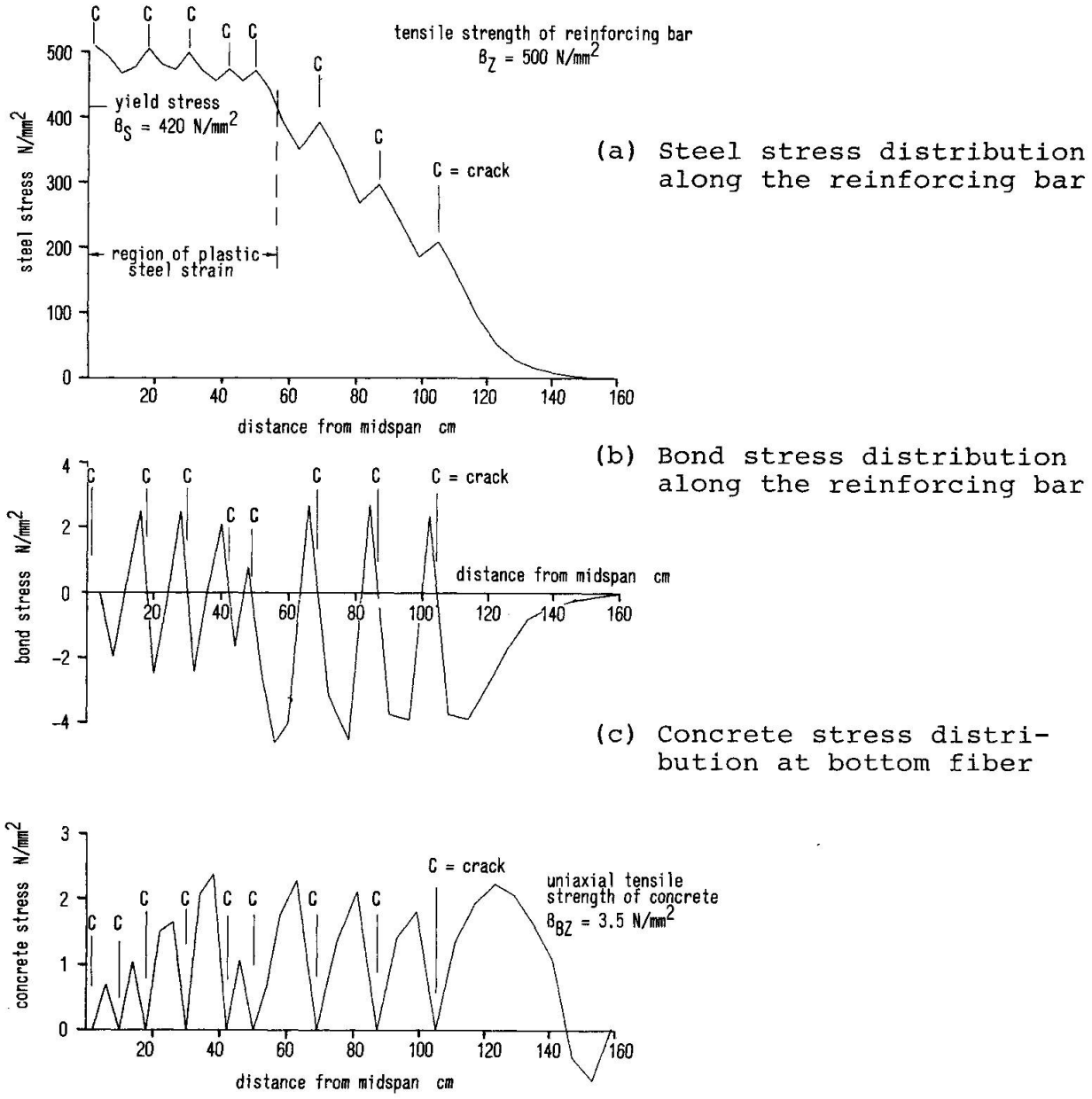

Fig. 15 Longitudinal Variation of Stresses at Ultimate Load

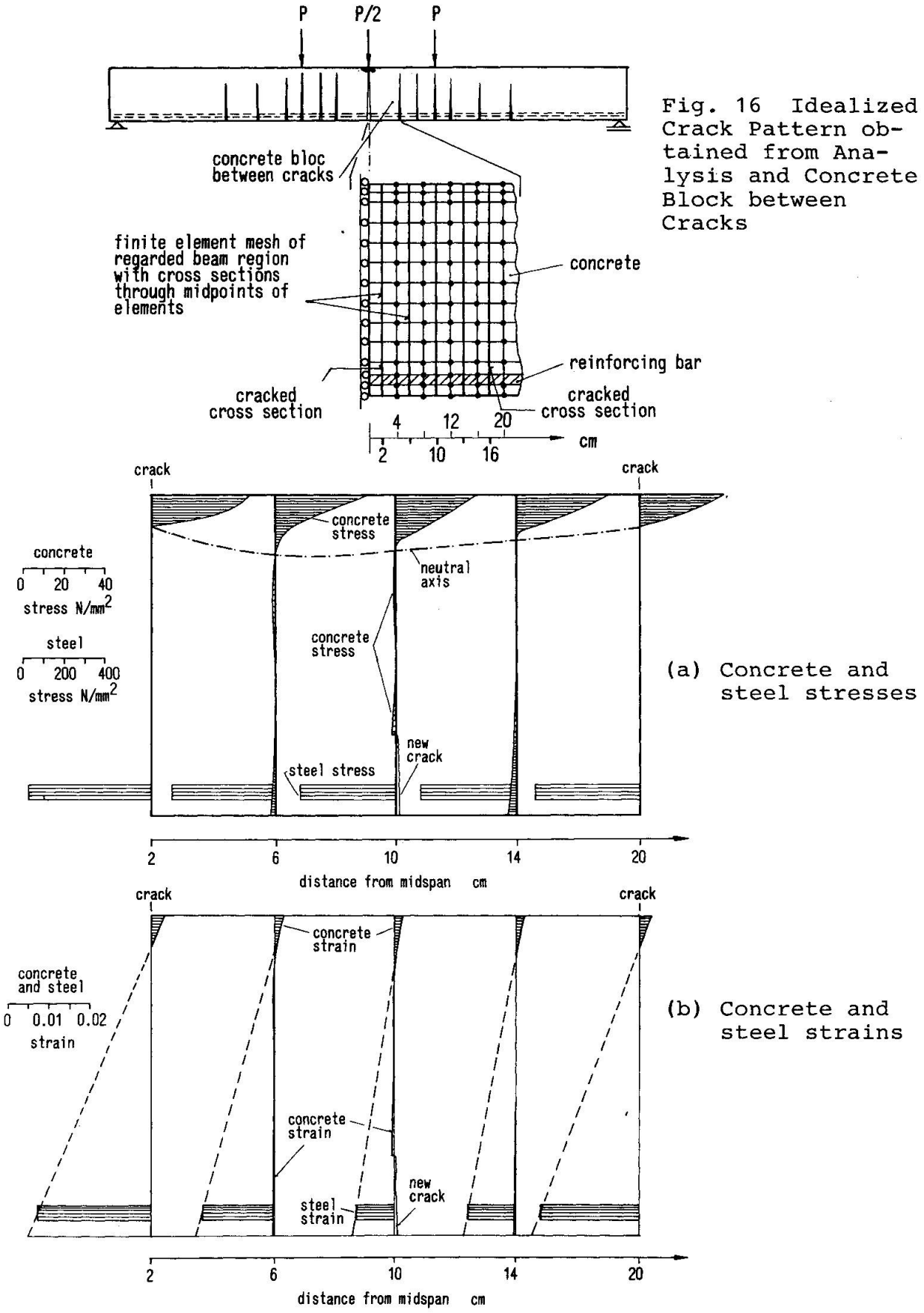

Fig. 16 Idealized Crack Pattern obtained from Analysis and Concrete Block between Cracks

(a) Concrete and steel stresses

(b) Concrete and steel strains

Fig. 17 Longitudinal Stress and Strain Distribution at Cross Sections between Cracks at Ultimate Load

The concrete and steel stresses due to ultimate load for cross sections through the midpoints of concrete and steel elements are given in Fig. 17. The longitudinal concrete stress distribution at any cross section is almost nonlinear. It should be noted that the concentration of concrete stresses above cracks causes a fluctuation of the neutral axis position. The variation of steel stresses along the reinforcing bar is nonlinear as mentioned before with peak steel stresses at both ends of the block. The resulting strain distribution is shown in Fig. 17 b. It may now be observed from Fig. 17 b that cross sections of cracked reinforced concrete members do not remain plane as normally assumed in simplified analysis.

The load-deflection curves (which are not shown here) obtained for each load increment permit to determine approximately a moment-rotation relation for the plastic hinge forming in the middle of the beam. The moment-rotation curve in Fig. 18 shows a sufficient agreement with the test results.

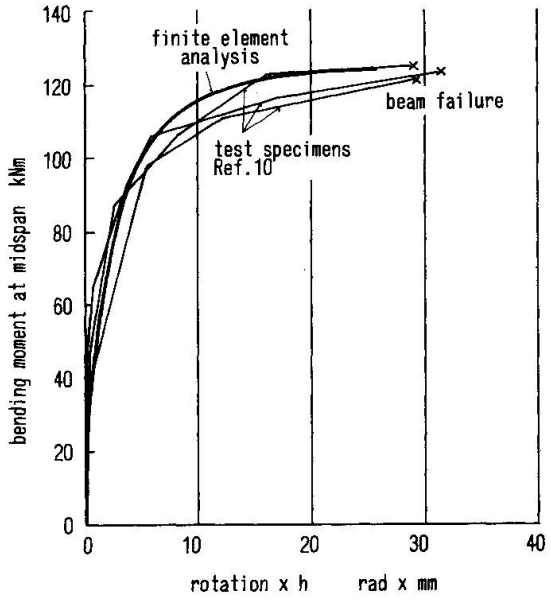

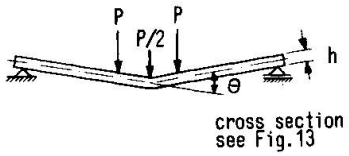

Fig. 18
Comparison of Analytical and Experimental Moment-Rotation Curves

5.2 Moment-Curvature Relation

The analytical results also permit to establish a realistic moment-curvature relation for the beam. Therefore, the concrete block of Fig.16 between two cracks is regarded again. For this block the strain distribution at one cracked cross section and at the midsection between both cracks is given for selected load increments in Fig. 19. It can be easily seen in Fig. 17 b and Fig. 19 that the slope of a line connecting the maximum concrete strain with the steel strain represents the rotation of a "plane" cross section. As indicated in Fig. 17 b the rotation of cross sections is decreasing with increasing distance from the crack surface which clearly reflects the influence of bond.

If a constant moment region is assumed between two cracks a mean value of curvature can be calculated approximately by integrating the rotations of the individual cross sections.

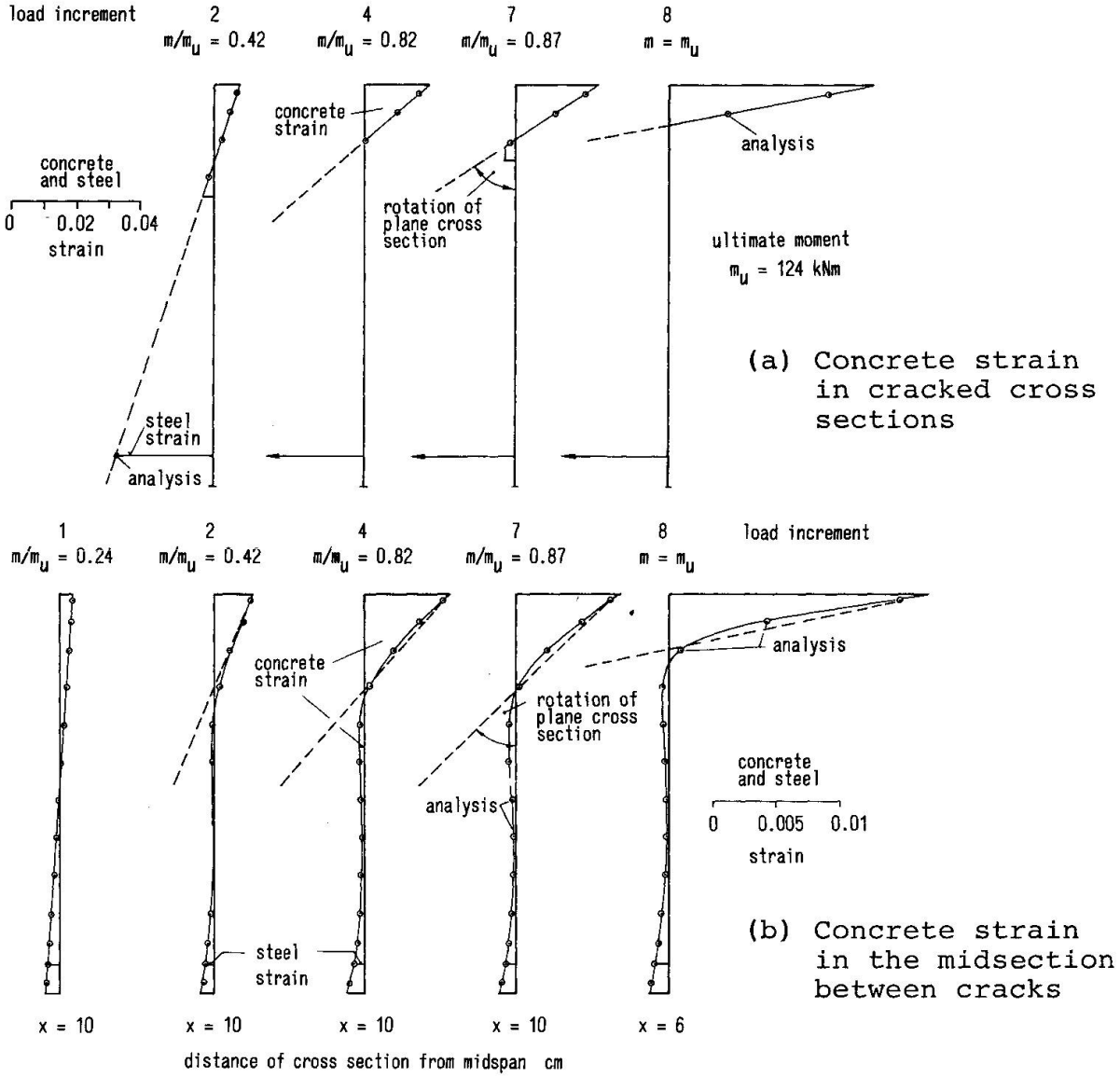

Fig. 19 Longitudinal Strain Distribution at Cross Sections for Several Load Increments

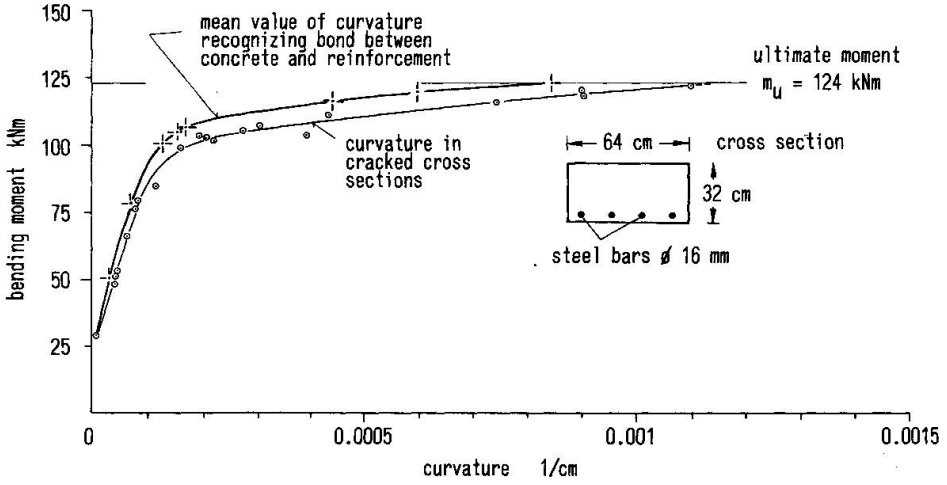

Fig. 20 Analytical Moment-Curvature Relation for the Reinforced Concrete Beam [10]

The mean value of curvature versus bending moment is shown in Fig. 20 and is compared with the moment-curvature curve resulting alone from the rotation of the cracked sections. It may be of some interest to realize that for equal bending moments the mean curvature is less than the curvature of cracked sections. The difference between both curves is growing with increasing plastic steel strains at cross sections.

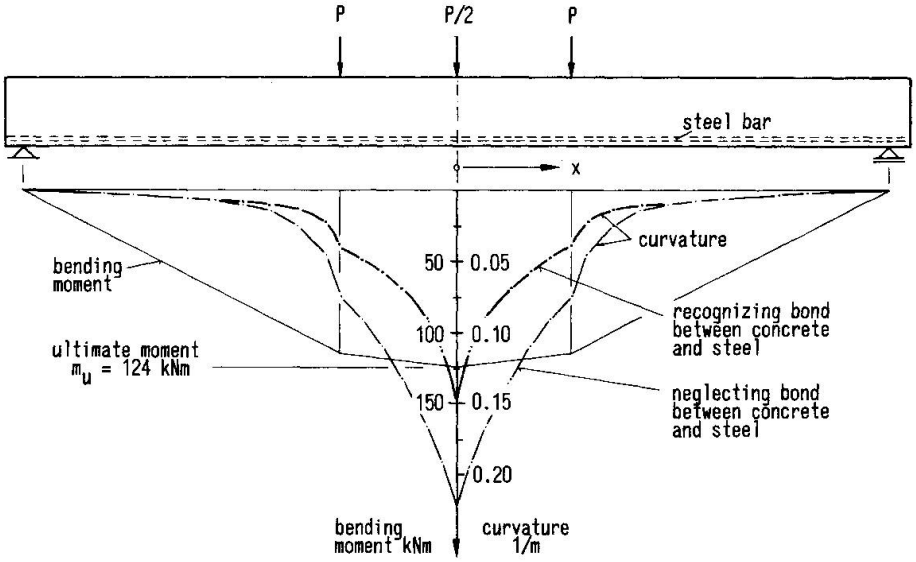

Fig. 21 Variation of Curvature along Beam Axis for Ultimate Load

The variation of curvature along the beam axis for the ultimate loading stage using both moment-curvature relations given in Fig. 20 is presented in Fig. 21. It can be seen by comparing both curves that the mean curvature which is recognizing the influence of bond on steel deformations gives a much more realistic basis for the calculation of beam deflections than the commonly for cracked sections used relation (deeper curve) which is neglecting this effect.

6. CONCLUSIONS

The finite element concept has been used for the development of an analytical method for reinforced concrete beams due to static loading which permits a simulation of beam behaviour through the entire range of loading. The accuracy of results show the validity of the proposed mechanical model which includes all important effects. It can be concluded from the results given in this paper that the true state of stress and strain as well as the actual crack pattern and deflections of a reinforced concrete beam can only be obtained from analysis if a realistic concept for bond is used recognizing a different bond-slip behaviour near cracks and in some distance from cracks respectively in uncracked regions of the beam. The moment-curvature relation obtained from analytical results shows furthermore the significant influence of bond on internal deformations which cannot be neglected without essential loss of accuracy if such a relation is used as a basis for simplified calculation of beam deflections.

REFERENCES

1. EIBL, J., IVÂNYI, G.: Studie zum Trag- und Verformungsverhalten von Stahlbeton, Deutscher Ausschuß für Stahlbeton Heft 260 (1976)

2. PLAUK, G.: Ermittlung der Verformungen biegebeanspruchter Stahlbetonbalken mit der Methode der Finiten Elemente unter besonderer Berücksichtigung des Verbundes zwischen Beton und Stahl, Dissertation Berlin TU,Berlin (1977)

3. SAUGY, B.: Contribution à l'étude théorique de comportment non linéaire des structures massives en bêton armé sous charges rapides, Bulletin Technique de la Suisse Romande No. 22, Nov. 1969

4. FRANKLIN, H.A.: Nonlinear Analysis of Reinforced Concrete Frames and Panels, SESM Report No. 70-5, University of California, Berkeley, March 1970

5. LASSKER, A.J.: Nonlinear Behavior of Reinforced Concrete Beams by the Finite Element Method, Ph.D. Thesis, Department of Civil Engineering, Oklahoma, State University, 1972

6. NAM, C.H.: A Finite Element Study on the Nonlinear Behavior of Reinforced Concrete Flexural Members due to Short-Time Loading, Ph.D. Thesis, Civil and Environmental Engineering, University of Wisconsin, 1973

7. NILSON, A.H.: Finite Element Analysis of Reinforced Concrete Ph.D. Thesis, University of California, Berkeley, 1967

8. KUPFER, H.: Verhalten des Betons unter zweiachsiger Beanspruchung - Lehrstuhl für Massivbau TH München, Bericht Nr. 78 (1969)

9. EIFLER, H.: Drehfähigkeit plastischer Gelenke in biegebeanspruchten Stahlbetonkonstruktionen, Bericht Teil C: Verbunduntersuchungen an Rippentorstahl unter bauteilähnlichen Verhältnissen als Grundlage zur theoretischen Ermittlung der Drehfähigkeit plastischer Gelenke in Stahlbetonkonstruktionen, Bundesanstalt für Materialprüfung (BAM), Berlin 1974

10. EIFLER, H.: Bericht über Voruntersuchungen für die Ermittlung des Werkstoff- und Verbundverhaltens im Bereich plastischer Gelenke von Stahlbetonplatten bei statischer Belastung Bundesanstalt für Materialprüfung (BAM), 2.2/119 31 (1969)

Shear Lag Analysis in Reinforced Concrete

Analyse du phénomène de flux du cisaillement (shear lag)

Schubversatz im Stahlbeton

A. GHANI RAZAQPUR
Graduate Student
University of Calgary
Canada

AMIN GHALI
Professor of Civil Engineering
University of Calgary
Canada

SUMMARY
At the intersection of the web of a T-beam or a box girder with the flange or with the top and bottom slabs longitudinal shear and transverse bending stresses occur. The finite element method of analysis is used to study the deformation and strength of reinforced and transversely prestressed concrete flanges under this stress condition. The analytical and experimental results are compared for beams tested in Zurich, Switzerland. The adequacy of the mathematical model to represent the behaviour of cracked reinforced concrete is assessed with particular attention to the shear lag phenomenon.

RÉSUMÉ
A la jonction de l'âme et de la table d'une poutre à caissons, des tensions de cisaillement longitudinal et de flexion transversale apparaissent. La méthode des éléments finis est utilisée pour étudier la déformation et la résistance de ces tables en béton armé à précontrainte transversale, soumises à ces conditions de charges. Les résultats analytiques et expérimentaux sont comparés sur base d'essais exécutés à Zurich (Suisse). La capacité du modèle mathématique de représenter le comportement du béton armé fissuré est analysée avec une attention toute spéciale au phénoméne de flux du cisaillement.

ZUSAMMENFASSUNG
Am Stoss des Steges eines T-Trägers oder eines Kastenträgers mit dem Flansch oder der Bodenplatte entstehen Längsschub- un Querbiegespannungen. Die Finite-Elemente-Methode ist auf diesen Fall angewandt. Theoretische und experimentelle Ergebnisse (aus Zürich) wurden verglichen, wobei gute Übereinsstimmung im Hinblick auf Schubversatz erzielt wurde.

1. INTRODUCTION

The successful application of the finite element method to the analysis of concrete structures depends much upon the development of accurate analytical models that can simulate the complex behaviour of concrete under multiaxial stresses, the initiation and propagation of cracks, bond and slip, and the manner in which stresses are subsequently transferred across cracks. Some of these problems have been successfully dealt with while others remain to be yet fully explored. Perhaps the most complex of these is the formulation of an acceptable shear transfer model.

An exact analysis of shear by finite element is indeed complex since an accurate modelling of most of the aforementioned phenomena is necessary. However, despite the complex nature of the problem, it is possible to obtain a fairly acurate picture of the overall stress condition by a rather simple model in most practical situations. Several investigators [1, 7, 13, 16] have used such simplified models to study the problem of shear in ordinary beams, deep beams, and panels.

In this paper yet another case of shear transfer is considered, namely the longitudinal shear at the web-flange connection of a flanged beam, and the interaction of this shear with transverse bending of the flange. In practice, this stress condition occurs at the connection of floor slabs with their supporting beams, between bridge decks and supporting girders, and at the connection of the webs and top and bottom slabs of box girders. Using a simplified shear model, four reinforced concrete T-beams that have been previously tested [2, 3, 4, 5] are analyzed by the finite element method. The model adopted is equally applicable to box girders but since no sufficiently documented test results are available for comparison with analytical findings, the results for T-beams only are compared here. The limitations of the applied simplified model and a review of some of the other proposed models is presented.

The purpose of comparing experimental and analytical results in this paper is to establish a procedure for the analysis of shear transfer at the web-flange connection which can be reliaby applied to situations not yet tested.

2. FINITE ELEMENT MODELLING

The program FELARC [11, 12] used in this investigation utilizes layered F.E. with an incremental iterative tangent stiffness approach. The concrete and distributed steel are represented by a quadrilateral inplane element QLC3 [18] with twelve nodal degrees of freedom and a quadrilateral plate bending element RBE [21] also with twelve degrees of freedom. The above two elements are combined to develop a shell element. The thickness is divided into a number of concrete and smeared steel layers, or prestressing layers, and the contribution of each is summed up to compute the element stiffness. Individual heavier bars or prestressing tendons are modelled by a so-called element bar which assumes perfect bond between the steel and concrete and which can be located anywhere within an element. The contribution of these bars to the element stiffness is directly superimposed on the element stiffness matrix.

3. CONSTITUTIVE MATERIAL RELATION

Increments of stress $\{\Delta\sigma\}$ and strain $\{\Delta\varepsilon\}$ in principal stress directions 1 and 2 are related by

$$\{\Delta\sigma\} = [D]\ \{\Delta\varepsilon\}$$

where [D] is the constitutive matrix shown in Eq. (1).

$$[D] = \frac{1}{1-\nu 2}\begin{bmatrix} E_1 & \nu\sqrt{E_1E_2} & 0 \\ \nu\sqrt{E_1E_2} & E_2 & 0 \\ 0 & 0 & \frac{1}{4}(E_2 + E_2 - 2\nu\sqrt{E_1E_2}) \end{bmatrix} \quad (1)$$

in which E_1 and E_2 are the uniaxial tangent moduli and ν is the Poisson's ratio. The values of E_1 and E_2 depend upon the ratio of the two principal stresses following the "equivalent uniaxial strain" concept of Darwin and Pecknold [9].

The equivalent stress-strain relationship employed to determine E_1 and E_2 is comprised of two parts, as illustrated in Fig. 1. Part I follows Eq. (2) proposed by Saenz [17],

$$\sigma = \frac{E_o\varepsilon}{(1 + \frac{E_o}{E_{cs}} - 2)(\frac{\varepsilon}{\varepsilon_{cu}}) + (\frac{\varepsilon}{\varepsilon_{cu}})^2} \quad (2)$$

whereas Part II traces the Smith-Young [20] model as described by Eq. (3),

$$\sigma = \sigma_c(\frac{\varepsilon}{\varepsilon_{cu}})\ \exp(1 - \frac{\varepsilon}{\varepsilon_{cu}}) \quad (3)$$

In the above equations, E_o, E_{cs}, σ_c and ε_{cu} are initial elastic modulus, secant modulus, maximum compressive stress, and the strain corresponding to σ_c, respectively (Fig. 1); σ and ε are equivalent uniaxial stress and strain [9].

The maximum compressive strength σ_c is determined from the modified biaxial failure envelope of Kupfer and Gerstle [14], and ε_{cu} is evaluated as a function of σ_c/f'_c, where f'_c is the uniaxial compressive cylinder strength. To avoid numerical difficulties, the value of the tangent modulus for the unloading portion of Fig. 1 is set equal to zero.

Steel and prestressing steel are both modelled as bilinear elastic-strain hardening material, including the Bauschinger effect.

4. CRACKING AND TENSION STIFFENING

In this study the smeared crack approach is adopted. When a principal stress exceeds the uniaxial tensile strength of concrete in a principal direction, cracking is assumed perpendicular to the particular direction. If $\sigma_1 \geq f'_t$, where f'_t is the uniaxial tensile strength of concrete, then the constitutive matrix in the principal directions is given by

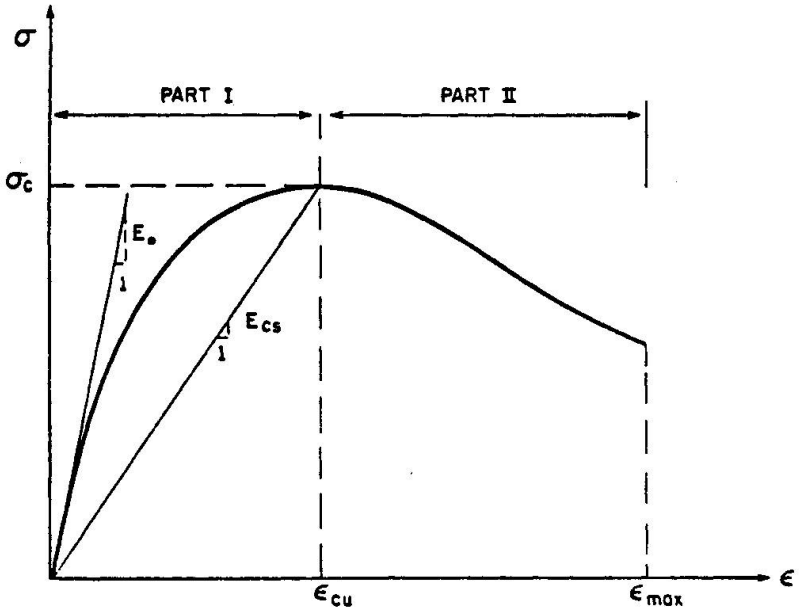

Fig. 1 - Equivalent stress-strain relation for concrete (in case of uniaxial stress $\sigma_c = f'_c$).

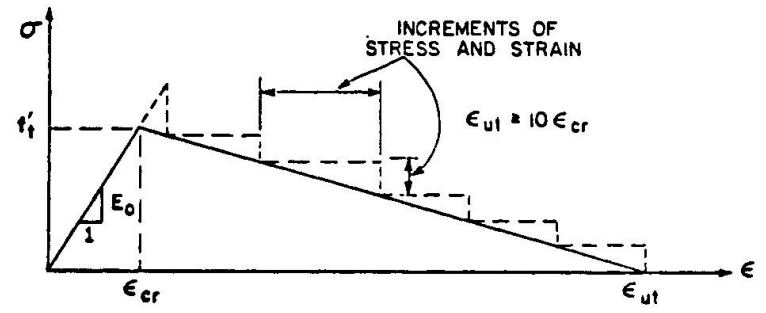

Fig. 2 - Tension stiffening model

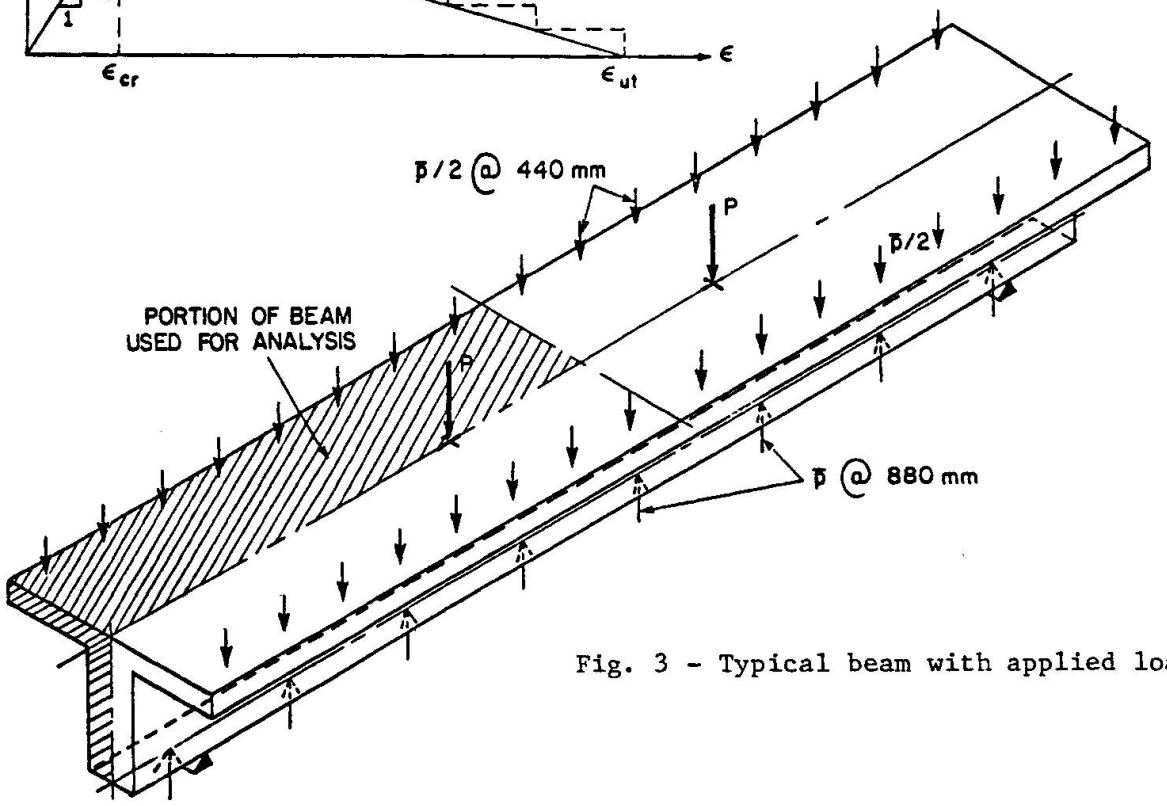

Fig. 3 - Typical beam with applied loads

$$[D] = \begin{bmatrix} 0 & 0 & 0 \\ 0 & E_2 & 0 \\ 0 & 0 & \beta G \end{bmatrix} \qquad (4)$$

while if $\sigma_1 \geq f'_t$ and $\sigma_2 \geq f'_t$, then all elements of the above matrix, except βG, are set equal to zero. In Eq. (4) G is the elastic shear modulus and β is the shear retention, or reduction, factor.

The concept of shear retention factor was first introduced by Suidan and Schnobrich [20] and later with certain modifications adopted by other analysts. In the present analysis, as demonstrated later, it was found out that setting the shear rigidity on the cracked plane equal to 10% of the uncracked concrete shear modulus, i.e. $\beta = 0.1$, and holding it constant renders good results in the case of most of the beams analyzed. In one case, however, this approach did not yield acceptable results. This will be dwelt upon in more detail later.

For accurate modelling of reinforced concrete, one has to account for the tension that is resisted by the concrete in between the cracks. This phenomenon known as "tension stiffening" is allowed for in FELARC by the use of the stress-strain relationship for concrete in tension shown in Fig. 2.

5. EXPERIMENTAL BEAMS AND THEIR ANALYTICAL MODELS

To investigate the action of longitudinal shear alone and longitudinal shear plus transverse bending at the junction of compression flange and web in reinforced concrete T-beams, Bachmann et al. [2, 3, 4, 5] carried out tests on seven beams, Fig. 3, whose transverse flange reinforcements were designed on the basis of different analyses.

Four of the above beams, namely Beams 1, 2, 4 and 7 are selected as representative. Beams 1 and 2 are intended to investigate the action of longitudinal shear alone, hence, the beam webs are loaded with two concentrated loads P at the third points of the span (Fig. 3). The amount of reinforcement running in the transverse direction in Beam 1 is determined by Bachmann et al by considering the principal stress in a longitudinal section at the intersection of the flange with the web. In Beam 2 the transverse reinforcement is designed using a spatial truss model [3, 4].

The flanges in Beams 4 and 7 are subjected to longitudinal shear and transverse bending. In addition to the concentrated loads P, a downward distributed load of $1.136\bar{p}$ per meter length is applied to the outer edges of flange. Equal and opposite forces are applied on the bottom of the web as shown in Fig. 3. The transverse flange reinforcement is obtained by superposition of required steel from the truss model for shear alone plus the steel needed for transverse bending. Beam 7 is similar to Beam 4 except that the flange is partially prestressed with a transverse prestressing of 58 kN/m. The dimensions and web reinforcement for all the beams are identical, as illustrated in Fig. 4.

Tables (1) and (2) give the concrete and steel properties data used in the analysis and were taken to comply as far as possible with data reported by Bachmann et al.

Due to symmetry about two vertical planes, only one quarter of the beams, i.e. the cross-hatched portion in Fig. 3, is analyzed. The finite element idealization of the quarter beam is shown in Fig. 5.

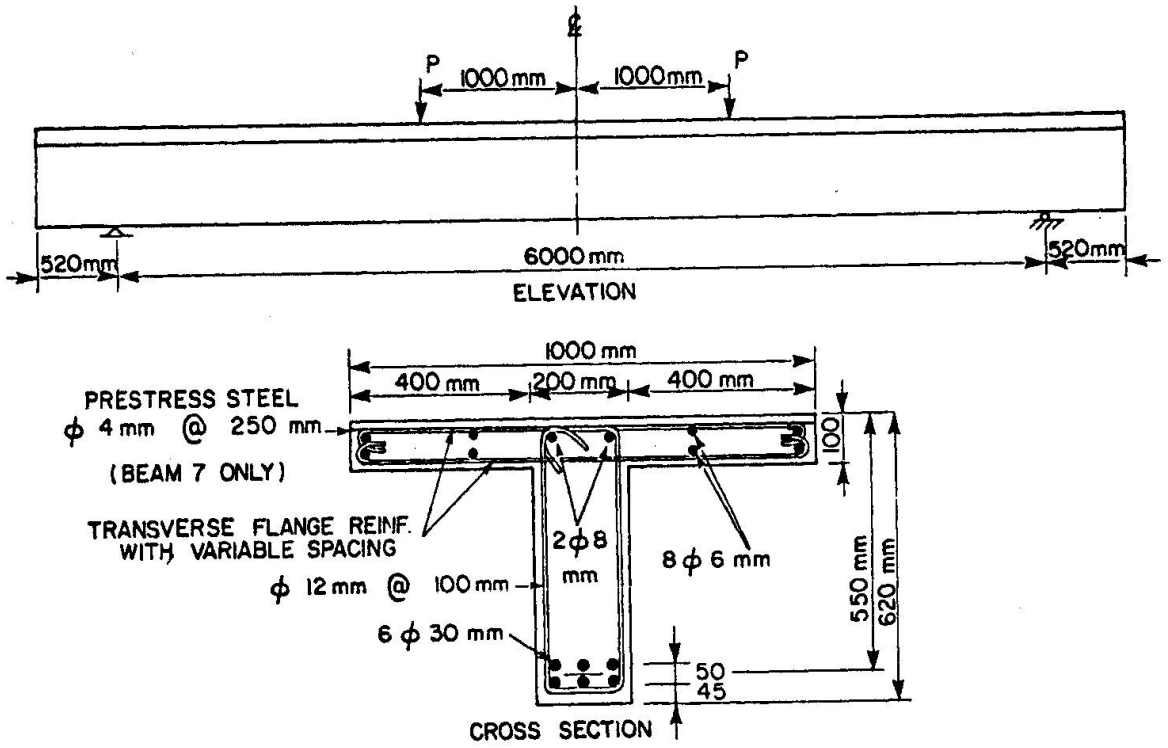

Transverse reinforcement in the flange:

Beam 1: 18 ϕ 6 mm at 85-285 mm top and bottom
Beam 2: 28 ϕ 6 mm at 125 mm top and bottom
Beam 4: 49 ϕ 6 mm at 55-100 mm top and
21 ϕ 6 mm at 125-275 mm bottom
Beam 7: 27 ϕ 6 mm at 82-250 mm top and
14 ϕ 6 mm at 275-285 mm bottom

Fig. 4 - Typical beam dimensions and reinforcement

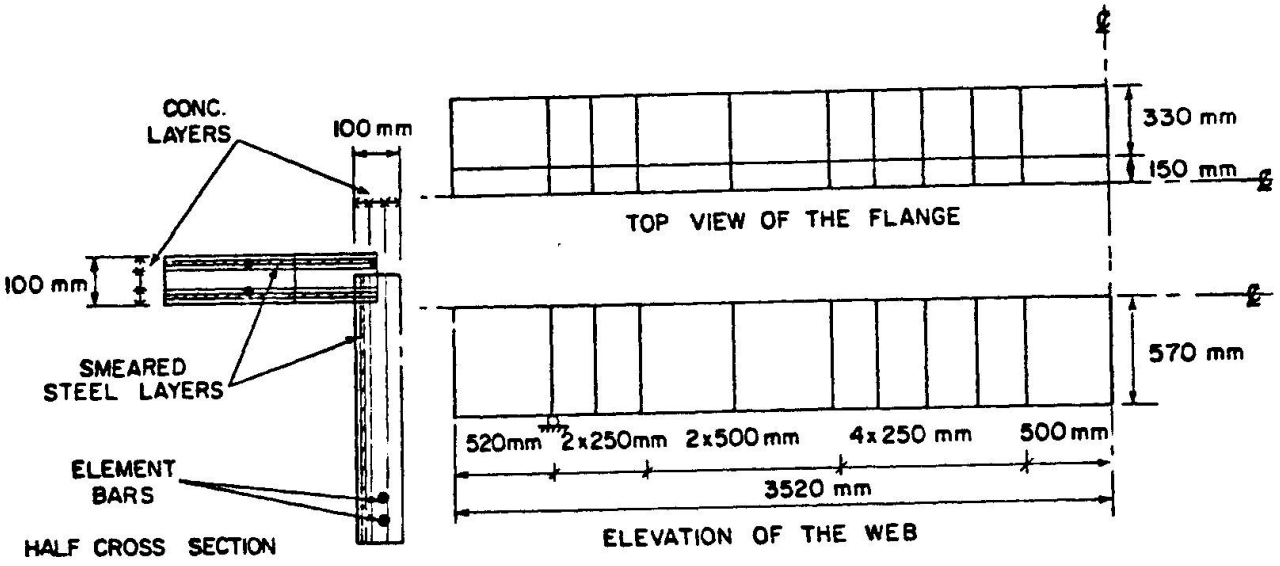

Fig. 5 - Typical finite element idealization

Table 1. Concrete strength data(1) based on 120 x 120 x 360 mm prisms

Beam No.	f'_c MPa	f'_t MPa	ε_{cu}	ε_{max}	E_o(2) GPa
1	23.40	2.16	0.00165	0.00375	31.38
2	27.22	2.45	0.00182	0.00225	34.53
4	24.71	2.06	0.00170	0.00225	34.90
7	25.57	2.26	0.00170	0.00270	34.70

(1) f'_c is the prism strength, other symbols are defined in Figs. 1 and 2.
(2) Calculated from f'_c.

Table 2. Steel strength data[1]

Bar ϕ mm	Area mm^2	f_y MPa	ε_{smax}	E_s GPa	E_s^* GPa
4	12.6	1686.63	0.037	178.3	5.31
6	28.1	482.45	0.066	196.0	0.94
12	108.0	508.93	0.162	196.0	1.16
30	696.0	567.77	0.138	196.0	1.54

(1) fy = yield stress; ε_{smax} = the strain at failure; E_s = modulus of elasticity (the value 196 MPa was assumed because it was not reported by Bachmann et al.); E_s^* = strain hardening modulus

6. RESULTS AND DISCUSSION

The load deflection curves of Beams 1, 4 and 7 are shown in Fig. 6 a to c. In all three cases analysis indicates good agreement with the load-deflection curves in the experiment but the analytical response seems slightly stiffer, especially for Beam 1. The reason may be the assumption in the analysis of higher initial concrete modulus and/or higher compressive strength. The failure loads in Table (3) corroborate this as the analysis gives 3.5 - 8% higher values. The experimental and analytical deflected shapes of Beam 4 are compared in Fig. 7 for a load of 0.76 P_u, where P_u is the failure load.

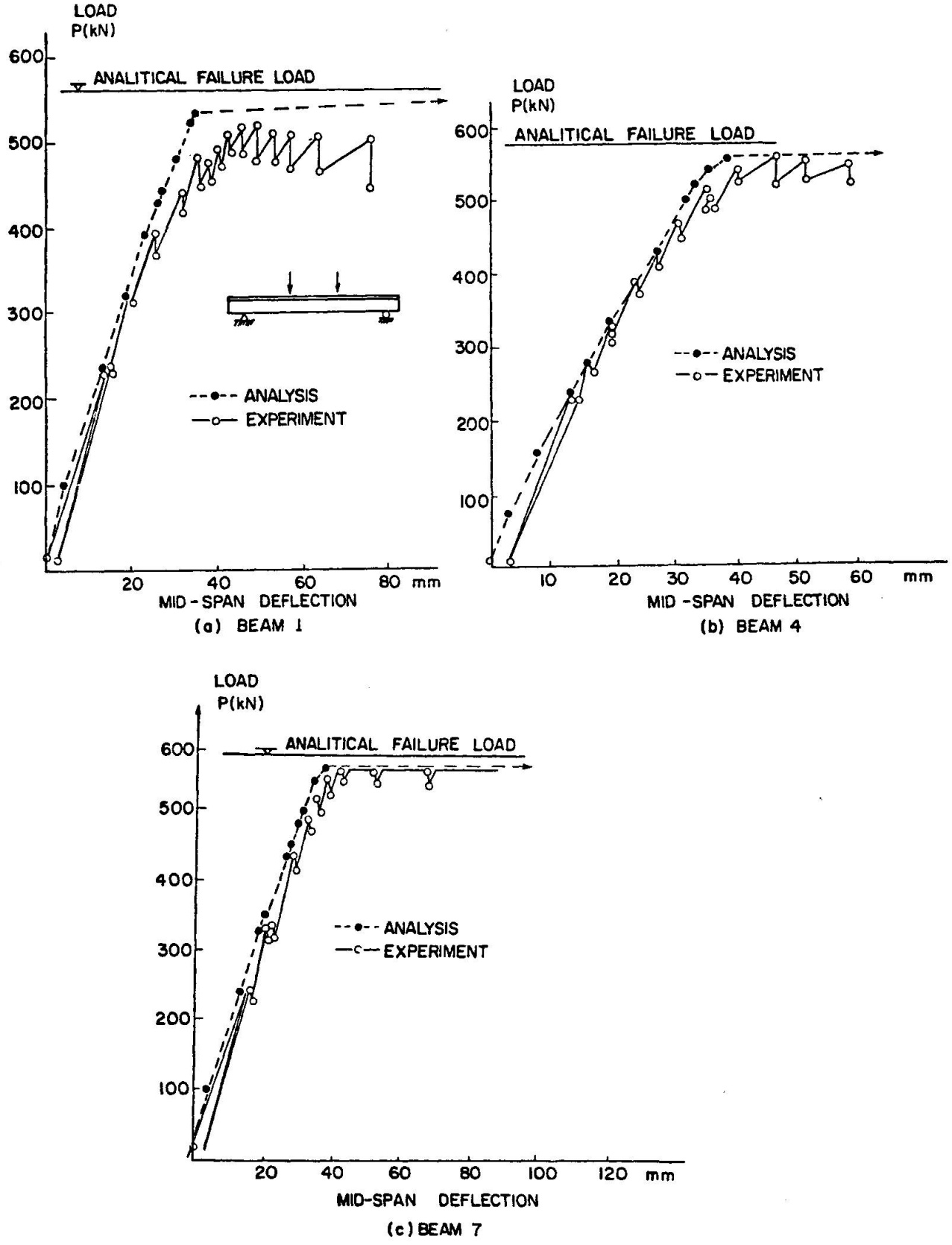

Fig. 6 - Load versus mid-span deflection

Table 3. Failure loads

Beam No.	Failure Load P_u kN		$\frac{P_u \text{ Experiment}}{P_u \text{ Analysis}}$
	Experiment	Analysis	
1	507.95	549.1	1.081
2	550.12	568.7	1.033
4	549.10	568.7	1.036
7	549.10	568.7	1.036

In Fig. 8 the strain variation in the main longitudinal web reinforcement is depicted. In the case of Beam 7, the experimental strain at P = 549.1 kN represent the failure stage, while analysis shows that failure is imminent but has not occurred yet. Therefore, unlike the experimental results, the analytical strains near the failure section are comparatively small, (Fig. 8b).

Another parameter in the analysis is the strain in concrete. Since the experimentally reported concrete strains on the top and bottom faces of the flange along the span represent average values over a base length of the instrument used (200 mm), the analytical results are also averaged from appropriate points where strains are computed. Fig. 9 illustrates the longitudinal concrete strain variation in the flanges at service and ultimate loads. The values indicated are average strains along a line at the center of the overhang. It is worthwhile to mention that since in the analysis the stiffness matrix may become singular at failure, indicating instability in the structure, the results obtained from such a load step are not generally indicative of the actual stress situation. For the analytical strains reported here, the values at 97% of P_u are considered to be the ultimate strains. This may explain the reason for the high measured strains at failure.

It is to be noted that when the flanges are subjected to transverse bending, the longitudinal strain at the top face of the flange is a shortening caused by the longitudinal bending moment of the beam as well as the shortening caused by Poisson's effect from the transverse tensile stress caused by the transverse bending of the slab in Beams 4 and 7. In the analysis Poisson's ratio is assumed constant = 0.15 while some investigators [15] observed much higher values of Poisson's ratio at stresses close to f'_c. This may account for the large discrepancy between measured and calculated strains near the center of the span for case of loading close to P_u.

7. STRAIN IN TRANSVERSE REINFORCEMENT IN THE FLANGES

Figs. 10a and b show the variation along the span of the strain in the top_ transverse steel layer for Beams 4 and 7 which are subjectd to both P and p loadings (see Fig. 3). The strains for Beams 1 and 2 are shown in Figs. 11a and b. Analytical and experimental results are reasonably close except for

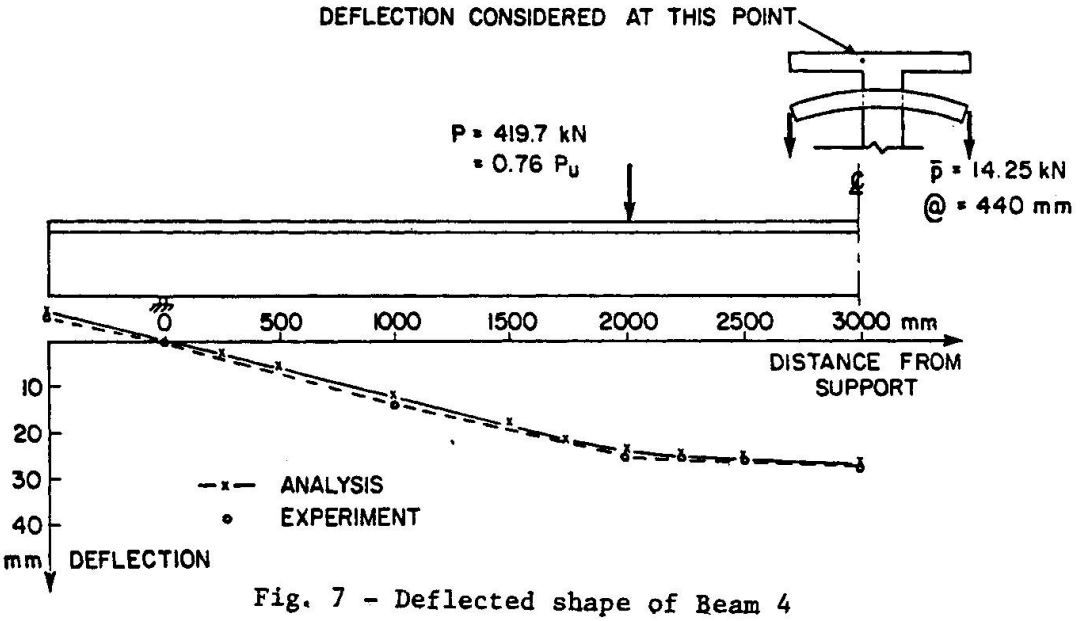

Fig. 7 - Deflected shape of Beam 4

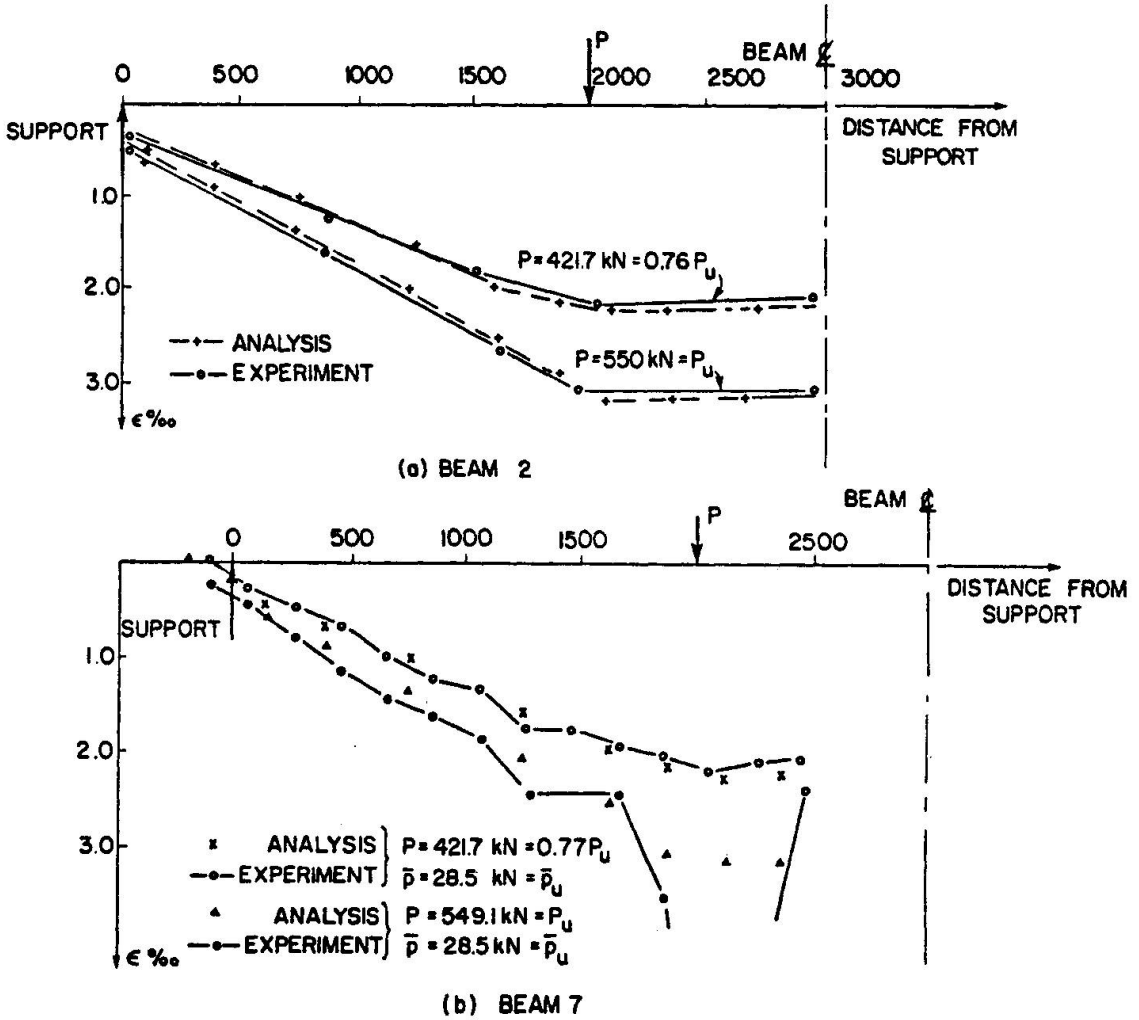

Fig. 8 - Strain in main longitudinal web reinforcement

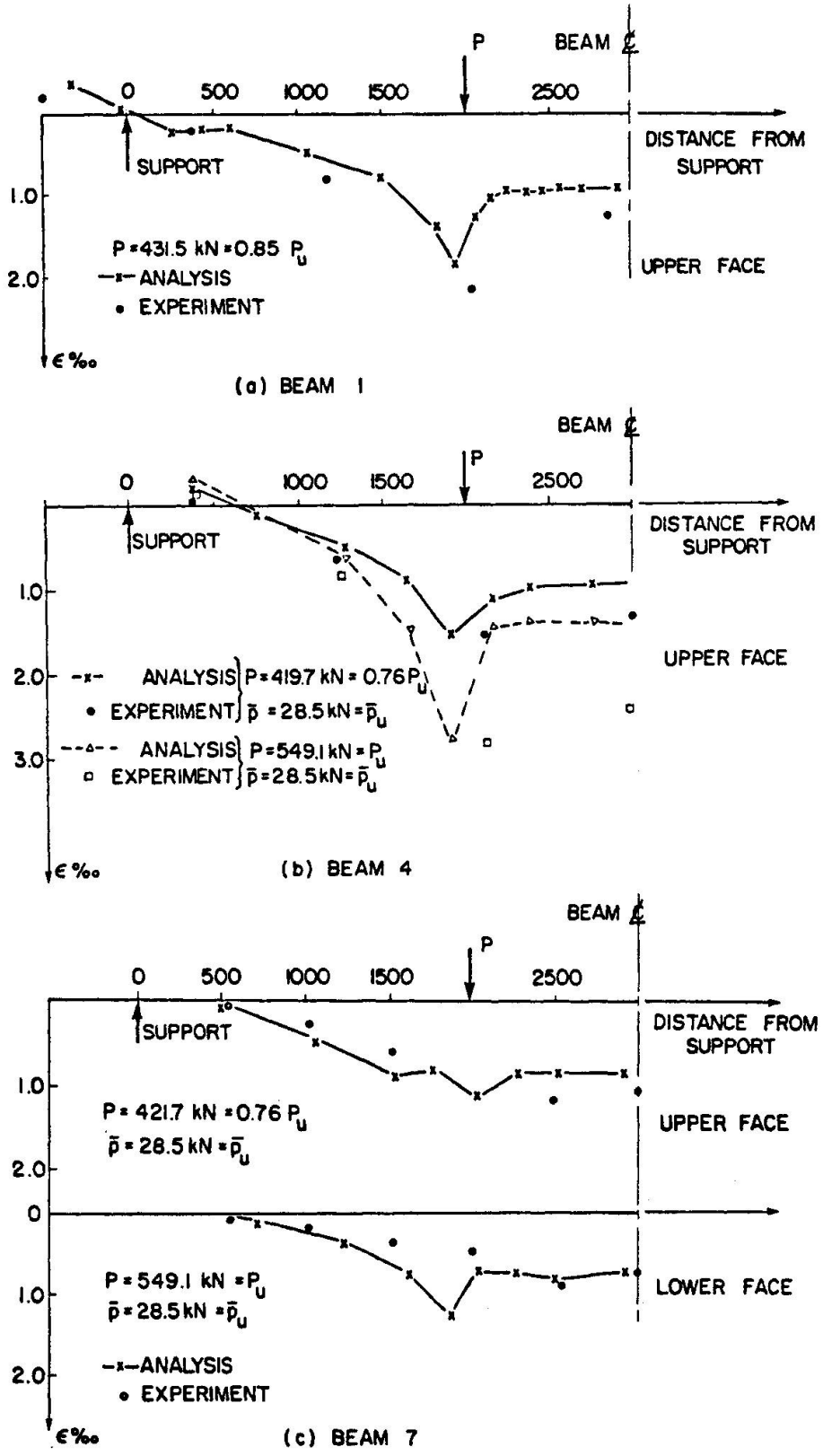

Fig. 9 - Strain in concrete in the direction of the span along centerline of the overhang

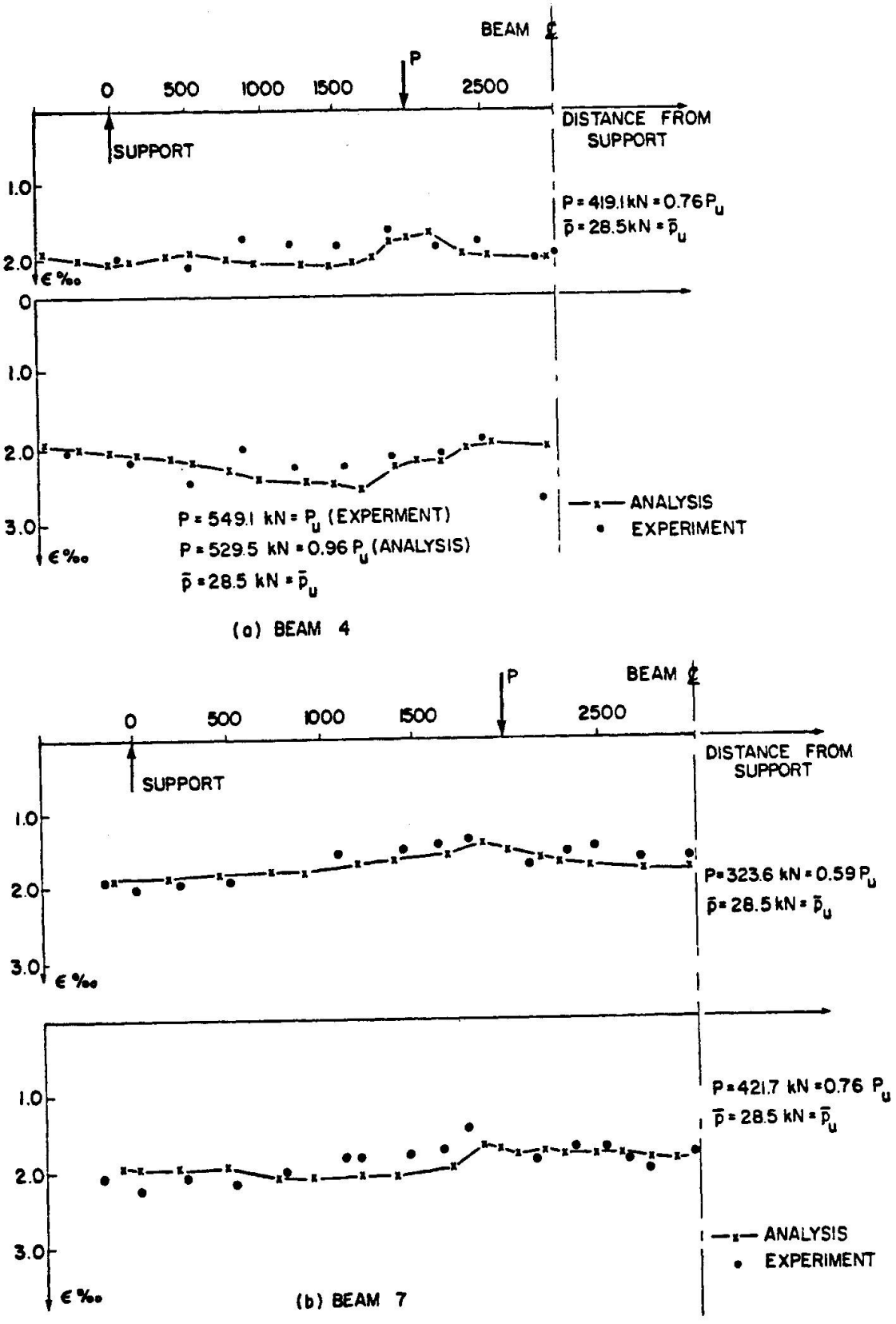

Fig. 10 - Maximum strain in transverse top reinforcement of the flange

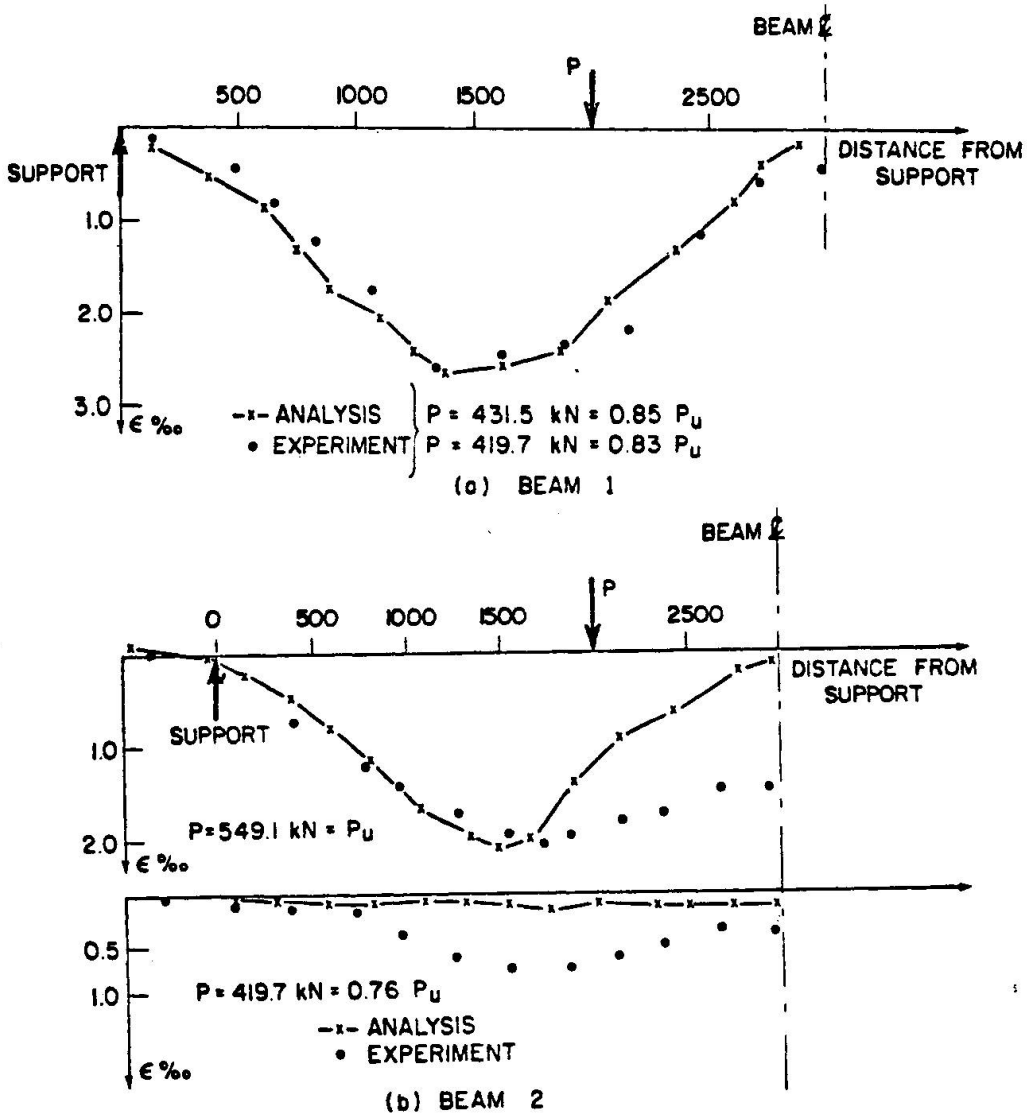

Fig. 11 - Maximum strain in transverse top reinforcement of the flange

Beam 2. This beam is not subjected to transverse bending and thus the stress in the transverse steel is caused by the longitudinal shear. Hence a close look at the way shear is accounted for in the constitutive relation used for cracked reinforced concrete, Eq. 4, is necessary. In particular, the coefficient β which accounts for the shear capacity of cracked concrete has to be examined.

Beam 2 was analyzed using successively decreasing values of β starting from 0.9. At $\beta = 0.01$, the beam failed prematurely at about $0.8\ P_u$, but varying β between these two limits had little effect on either the failure load or stress in the transverse reinforcement.

Some authors have suggested the following expressions for the reduced shear modulus $\bar{G} = \beta G$ for cracked concrete:

$$\bar{G} = 0.1E\left(1 - \frac{\varepsilon}{0.004}\right) \quad \ldots\ (a)$$

$$\bar{G} = \left(\frac{0.4\varepsilon_o}{\varepsilon}\right)G \quad \ldots\ (b)$$

$$\bar{G} = 50\left(\frac{1}{c}\right)^{1.5}\sqrt{\frac{f'_c}{34.6}} \quad \ldots\ (c)$$

$$\bar{G} = \left[\frac{1}{G} + \frac{b}{\ell(K_N + bK_D)}\right] - 1 \quad \ldots\ (d)$$

where

ε = fictitious strain normal to crack
ε_o = cracking strain
c = crack width in mm
f'_c = concrete strength in MPa
b = constant
K_N = extensional stiffness of bars crossing the crack
K_D = dowel stiffness of bars crossing the crack
ℓ = crack spacing
G = shear modulus of uncracked concrete

Expressions (b) and (a) proposed by Al-Mahaidi [1] and Cedolin and Dei Poli [7], respectively were used in the current study to analyze Beam 2 and gave results practically the same as when $\beta = 0.1$ in Eq. 4. Expression (c) suggested by Houde and Mirza [13] cannot be used unless crack widths can be determined accurately. The use of an assumed crack width in this expression will make it equivalent to (a) and (b). It is to be mentioned that expressions (a), (b) and (c) have been used, by their formulators, in conjunction with special linkage elements to account for bond stress-slip and crack opening. Since such elements would involve inclusion of additional unknown parameters they have not been adopted here.

Expression (d) was developed by Fardis and Buyukozturk [10]; and, according to its authors, applies when cracks run in one direction. This again purports knowledge of crack spacing, and gives a value of $\bar{G} = 0$ when K_N and K_D are zero (concrete without reinforcement). Such a value corresponds to $\beta = 0$.

Thus it appears that unless crack spacing is know, the more sophisticated expressions involve the same degree of approximation as the original simple approach of Suidan and Schnobrich (see Eq. 4).

Recently Bazant and Gambarova [6] and Chen and Schnobrich [8] have proposed more comprehensive models which consider crack dilatancy and crack displacement-stress non-linearity. However, while the first model still requires advance knowledge of crack spacing, the latter involves a number of constants to be determined by experiments yet to be done. Moreover both of these models are based on limited experimental data.

8. CONCLUSIONS

Four reinforced concrete T-beams that have been previously tested are analyzed by the finite element method using a non-linear iterative tangent stiffness approach. The main purpose is to study analytically the shear transfer at the web-flange connection and the interaction of this shear with transverse bending. Once an analytical procedure is established, a wide range of conditions not yet tested can be investigated.

From the study presented, it appears that although the constitutive relations for reinforced concrete used in the analytical work described in this paper, give accurate results in most situations, they are still inadequate in predicting the stress in transverse flange reinforcement in some cases. This inadequacy brings forth the exigency of developing suitable mathematical models. Such models have been recently proposed, but they require knowledge of certain parameters that are unknown a priori. Finally, it is not clear what effect geometric nonlinearity may have at later stages of loading.

ACKNOWLEDGEMENTS

The writers would like to thank Professor A. Bachman for prompt response to enquiries concerning his tests. Thanks are also due to Dr. G.A.M. Ghoneim for his assistance in the use of the computer program FELARC and to Professor W.H. Dilger for his useful discussions.

This research was supported by a grant from the Natural Sciences and Engineering Research Council of Canada which is gratefully acknowledged.

REFERENCES

[1] Al-Mahaidi, R.S.H., "Nonlinear Finite Element Analysis of Reinforced Concrete Deep Members", Report No. 79-1, Department of Structural Engineering, Cornell University, January, 1979.

[2] Bacchetta, A. and Bachmann, H., "Versuche zur teilweisen Vorspannung fur Langsschub and Querbiegung in Druckplatten von Betontragern", (Tests Concerning Partial Prestress to Resist Longitudinal Shear and Transverse Bending in Compression Flanges of Concrete Girders), Report No. 6504-9, Swiss Federal Institute of Technology, Zurich, July 1977.

[3] Bachmann, H., "Langsschub and Querbiegung in Druckplatten von Betontragern", (Longitudinal Shear and Transverse Bending in Compression Flanges of Concrete Girders), Beton-und Stahlbetonbau, Vol. 3, S. 57-63, 1978.

[4] Bachmann, H. and Bacchetta, A., "Teilweise Vorspannung fur Langsschub und Querbiegung in Druckplatten von Betontragern", (Partial Prestress to Resist Longitudinal Shear and Transverse Bending in Compression Flanges of Concrete Girders), Beton-und Stahlbetonbau, Vol. 5, S. 116-120, 1978.

[5] Badawy, M. and Bachmann, H., "Versuche uber Langsschub und Querbiegung in Druckplatten von Betontragern", (Tests Concerning longitudinal Shear and Transverse Bending in Compression Flanges of Concrete Girders), Report No. 6504-8, Swiss Federal Institute of Technology, Zurich, June 1977.
[6] Bazant, Z.P. and Gambarova, P., "Rough Cracks in Reinforced Concrete", Proceedings, ASCE, Vol. 106, No. ST4, April 1980.
[7] Cedolin, L. and Dei Poli, S., "Finite Element Studies of Shear-Critical R/C Beams", Proceedings, ASCE, Vol. 103, No. EM3, June 1977.
[8] Chen, E.Y. and Schnobrich, W., "Models for the Post-Cracking Behavior of Plain Concrete under Short Term Montonic Loading", Proc. NASA Conf. on Research in Nonlinear Structural and Solid Mechanics, Washington D.C., October 1980.
[9] Darwin, D. and Pecknold, D.A., "Nonlinear Biaxial Stress-Strain Law for Concrete", Proceedings, ASCE, Vol. 103, No. EM4, April 1977
[10] Fardis, N.M. and Buyukozturk, O., "Shear Stiffness of Concrete by Finite Elements", Proceedings, ASCE, Vol. 106, No. St6, June 1980.
[11] Ghoneim, G.A.M., "Nonlinear Analysis of Concrete Structures", Ph.D. Thesis, Department of Civil Engineering, The University of Calgary, Canada, August 1978.
[12] Ghoneim, G.A.M. and Ghali, A., "Users Manual for Computer Program FELARC (Finite Element Layered Analysis of Reinforced Concrete), Report No. CE78-15, Department of Civil Engineering, The University of Calgary, Canada, May 1979.
[13] Houde, J. and Mirza, M.S., "A Finite Element Analysis of Shear Strenth of Reinforced Concrete Beams", ACI, SP 42, 1974.
[14] Kupfer, H.B. and Gerstle, K.H., "Behavior of Concrete under Biaxial Stresses", Proceedings, Vol. 99, No. EM4, August 1973.
[15] Kupfer, H., Hilsdorf, H.K. and Rusch, H., "Behavior of Concrete under Biaxial Stresses", ACI Journal, Proc. Vol. 66, No. 8, August 1969.
[16] Ngo, D. and Scordelis, A.C., "Finite Element Analysis of Reinforced Concrete Beams", ACI Journal, Proc. Vol. 64, No. 3, March 1967.
[17] Saenz, L.D., Disc. of "Equation for the Stress-Strain Curve of Concrete, by Desayi and Krishnan, ACI Journal, Proc. No. 61, No. 9, September 1964.
[18] Sisodiya, R.G. and Ghali, A., "Analysis of Box Girder Bridges of Arbitrary Shape", Publications, IABSE, Vol. 33-I, 1973, pp. 203-218.
[19] Smith, G.M. and Young, L.E., "Ultimate Theory in Flexure by Exponential Function", ACI Journal, Vol. 52, No. 3, November 1955.
[20] Suidan, M. and Schnobrich, W.C., "Finite Element Analysis of Reinforced Concrete", Proceedings, ASCE, Vol. 99, No. ST10, October 1973
[21] Zienkiewiez, O.C., "The Finite Element Method", 3rd Ed. McGraw-Hill, London, 1977, (pp. 234-241).

Inelastic Analysis of Reinforced Concrete Shear Wall Structures - Applications and Experimental Verifications -

Analyse inélastique de la structure asismique des refends en béton armé - Ses applications et vérifications expérimentales -

Inelastische Berechnung von erdbebenfesten Stahlbetonwandkonstruktionen - Anwendungen und experimentelle Bestätigung -

NOBUAKI SHIRAI
Assistant

TOSHIO SATO
Professor

Department of Architecture, College of Science and Technology, Nihon University, Tokyo, Japan

SUMMARY

The purpose of this study is to verify the validity and applicability of the material modelling of reinforced concrete proposed by the authors and also to clarify inelastic behavior of reinforced concrete structures.
Numerical examples on tensile bond specimens, reinforced conrete panels and reinforced concrete shear wall-frame structures are given and some numerical results, such as load-deflection curves, internal stress transfer and crack propagation are compared with experimental results.

RÉSUMÉ

Le but de cette étude est de vérifier une validité et une applicabilité de la formule mathématique pour les matériaux de béton armé proposée par les auteurs, ainsi que d'éclaircir les comportements inélastiques de la structure asismique du mur en béton armé. Les exemples numériques sont donnés sur les échantillons d'adhérence à la traction, les panneaux en béton armé, et la structure asismique des refends en béton armé et de l'armature; ensuite, quelques résultats numériques tels que des courbes charge-déflexion, du transfert de contrainte interne et de la propagation des fissures sont comparés avec les résultats expérimentaux.

ZUSAMMENFASSUNG

Der Zweck dieser Forschung besteht darin, die Wirksamkeit und Anwendbarkeiut der von den Autoren vorgeschlagenen Modellierung von Stahlbetonmaterialien zu bestätigen und das inelastische Verhalten von Stahlbetonkonstruktionen zu klären.
Es werden numerische Beispiele für Zughaftproben, Stahlbetonplatten und erdbebenfeste Stahlbetonrahmenkonstruktionen gegeben. Numerische Ergebnisse für Lastverformungskurven, interne Spannungsübertragung, Rissausbreitung usw. werden mit experimentellen Ergebnissen verglichen.

1. INTRODUCTION

The finite element model of reinforced concrete for inelastic effects due to tensile cracking of concrete, nonlinear stress-strain response of concrete and steel, bond between steel and concrete, aggregate interlock between cracked concrete surfaces and dowel action of reinforcing bar was proposed by the authors in the reference[1] in order to investigate inelastic behaviors of reinforced concrete shear wall-frame structures under monotonic and cyclic loading.

The purpose of this paper is to verify a validity and an applicability of the proposed analytical model through several numerical applications.
First of all, tensile bond specimen of Fig.1 are analyzed by both the proposed and the linkage model, and then bond behaviors are compared with experimental ones and a stress transfer process due to cracking is investigated.

Secondly, concrete panels contained by a square grid of equal reinforcing bars ,which were tested under uniaxial tension, are analyzed by the proposed model, and an influence of inelastic effects; bond, aggregate interlock and dowel action, on several behaviors is studied.

Finally, in order to understand monotonic and cyclic behaviors of reinforced concrete shear walls analytically, two different types of shear walls are analyzed by the proposed model. Specimen of the first type, Fig.15, is the reinforced concrete shear wall-frame structure with one bay and three stories under the combined stresses of axial force, bending moment and shear force, and solutions under monotonic horizontal loading such as load-deflection curve, crack propagation and stress transfer are compared with experimental results. Specimens of the second type, Fig.26, are reinforced concrete shear wall-frame structures tested under concentrated loading of simply supported beam's type, and cyclic behaviors and an influence of inelastic effects on them are studied.

2. TENSILE BOND SPECIMEN

It is an important subject to make an analytical model being capable of representing bond behaviors between reinforcing bar and concrete accurately, and to incorporate it into an analytical procedure in clarifying static hysteresis of reinforced concrete structures. In order to verify a validity of the bond model proposed by the authors in the reference[1], numerical solutions on the tensile bond specimens tested by Morita[2], as indicated in Fig.1, are compared with experimental results. Furthermore, finite element solution by the linkage element proposed by Ngo and Scordelis[3] which idealizes the bond stress (u) - relative slip(S) relation proposed by Morita et al.[4] as shown in Fig.2 are also presented with a view to investigating stress transfer process due to cracking minutely.

The linkage element is a spring element being composed of the bi-directional springs as shown in Fig.3 which has spring stiffnesses $K_{\bar{X}}$ and $K_{\bar{Y}}$ in the orthogonal directions $\bar{X},\bar{Y}$ and letting an angle between the local coordinates $\bar{X},\bar{Y}$ and the global coordinates X,Y be ${}_s\theta$, then the relation between the incremental displacements $\Delta\{\delta\}= \{\Delta\delta_1, \Delta\delta_2, \Delta\delta_3, \Delta\delta_4\}$ and the incremental nodal forces $\Delta p\{\bar{p}\}= \Delta p\{ \bar{p}_1, \bar{p}_2, \bar{p}_3, \bar{p}_4\}$ in the global coordinate system is given as follows,

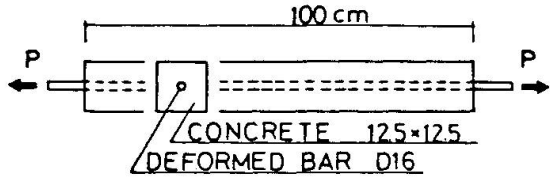

Fig.1 Tensile Bond Specimen

$$\Delta p\{\bar{p}\} = [k]\Delta\{\delta\}$$

in which

$$[k]=\begin{pmatrix} K_{\bar{x}}\cos^2_s\theta+K_{\bar{y}}\sin^2_s\theta & (K_{\bar{x}}-K_{\bar{y}})\cos_s\theta\sin_s\theta & -K_{\bar{x}}\cos^2_s\theta-K_{\bar{y}}\sin^2_s\theta & (K_{\bar{y}}-K_{\bar{x}})\sin_s\theta\cos_s\theta \\ & K_{\bar{x}}\sin^2_s\theta+K_{\bar{y}}\cos^2_s\theta & (K_{\bar{y}}-K_{\bar{x}})\sin_s\theta\cos_s\theta & -K_{\bar{x}}\sin^2_s\theta-K_{\bar{y}}\cos^2_s\theta \\ & & K_{\bar{x}}\cos^2_s\theta+K_{\bar{y}}\sin^2_s\theta & (K_{\bar{x}}-K_{\bar{y}})\sin_s\theta\cos_s\theta \\ \text{SYM.} & & & K_{\bar{x}}\sin^2_s\theta+K_{\bar{y}}\cos^2_s\theta \end{pmatrix}$$

and $K_{\bar{x}} = K_i \pi D l_b$ with k=1, 2 and 3 , $\Delta u = K_i \Delta S$

The spring stiffness $K_{\bar{x}}$ parallel to reinforcing bar is calcualted by multiplying slopes K_1, K_2 and K_3 of bond stress-relative slip curve of Fig.2 by the artificial bond area over which one spring governs. On the other hand, since a physical meaning of stiffness $K_{\bar{y}}$ perpendicular to reinforcing bar is not obvious so far, it is set equal to zero value. Cracks are also idealized by the linkage element and the stiffnesses $K_{\bar{x}}$, $K_{\bar{y}}$ are set equal to big values before crack formation or after the closing of cracks, and they are set equal to zero values when cracks open.

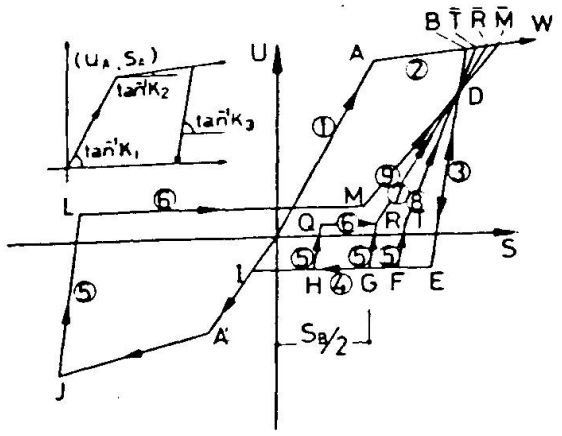

Fig.2 Cyclic Bond Stress-Relative Slip Relation

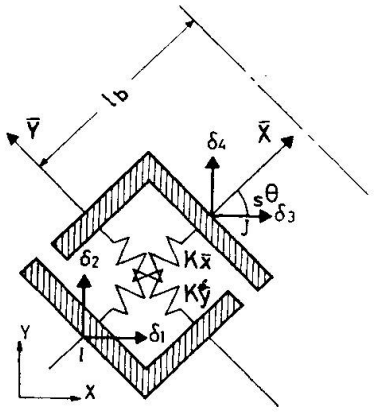

Fig.3 Linkage Element

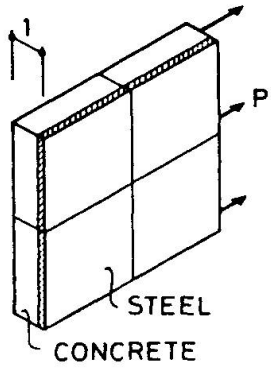

Fig.4 Finite Element Idealization by Proposed Model

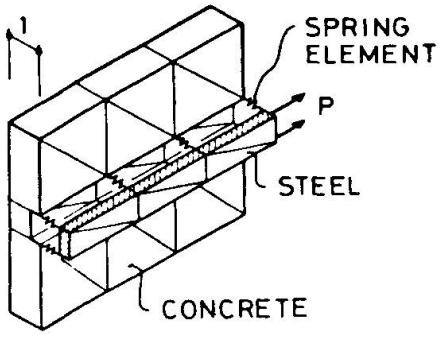

Fig.5 Finite Element Idealization by Linkage Model

Table 1. Material Properties of Bond Specimen

Material		Young's Modulus E (kg/cm^2)	Poisson's Ratio υ	Tensile Strength f_t (kg/cm^2)
Reinforcing Bar		2.0×10^6	0.3	———
Concrete	Specimen of Type 1 (Monotonic)	2.8×10^5	0.167	24.0
	Specimen of Type 2 (Cyclic)	2.8×10^5	0.167	21.5

Table 2. Characteristic Values for Linkage Model

Loading Direction	u_A (kg/cm^2)	S_A (cm)	K_1 (kg/cm^3)	K_2 (kg/cm^3)	K_3 (kg/cm^3)
Positive	46.875	0.00525	8929	687	17858
Negative	-46.875	-0.00525	8929	687	17858

The assigned finite elements are shown in " Figs.4 and 5 " respectively. " Tables 1 and 2" indicate material properties used in the analysis. " Fig.6" shows load-average strain curves for both the models on the tensile specimen under monotonic loading. " Fig.7" shows equivalent stress-average strain curves non-dimensionized by the cracking strength of concrete. " Fig.8" shows distributions of bond stresses and steel stresses at the loads of 4, 5 and 8 tons obtained by the linkage model.

It is found from Figs.7 and 8 that analytical results for both the models relatively agree with experimental ones and thus the assumptions made in the bond modelling may be reasonable. The reason why the initial stiffness of the proposed model is higher than the experimental one perhaps may be due to the assumption of perfect bond before cracking. The equivalent stresses of the linkage model suddenly increase against strains over about 0.0013 and this is considered to be attributable to the fact that the cracking positions are fixed to two sections on the basis of the experimental cracking pattern and thus internal cracks are not considered in the analysis.

Analyzing the process from results of Fig.8 in which the equivalent stress decreases with an increase of average strain, it can be seen that while bond stress changes with an increase in number of cracks as shown in the figure, concrete stress at the cracking parts is transfered to reinforcement and a resistance of concrete gradually deteriorates.

" Figs.9 and 10" show two cycles of load-average strain curves for both the models in which unloading was carried out at the strains of 0.0012 and 0.002. " Fig.11" shows the equivalent stress-average strain curve non-dimensionized by the cracking strength of concrete. The area of hysteresis loop for the proposed model is somewhat smaller than that of the experiment, but their correlation is satisfactory and particularly the slope of a line connecting a unloading point and a reloading point relatively agrees with the experimental one.

3. REINFORCED CONCRETE PANEL

In order to investigate a validity of the modelling of bond effect, aggregate

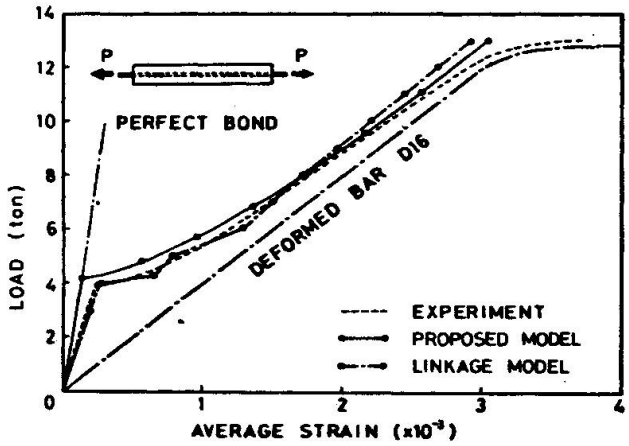

Fig.6 Load-Average Strain Curve under Monotonic Loading

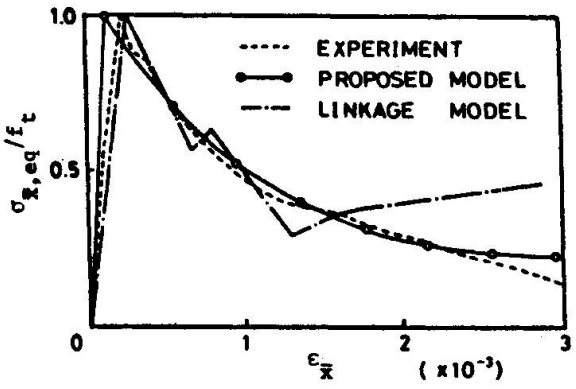

Fig.7 Non-Dimensionized Equivalent Stress-Average Strain Relation

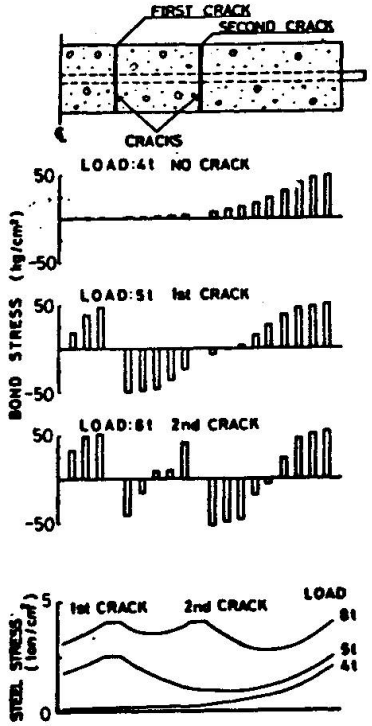

Fig.8 Distributions of Bond Stresses and Steel Stresses by Linkage Model

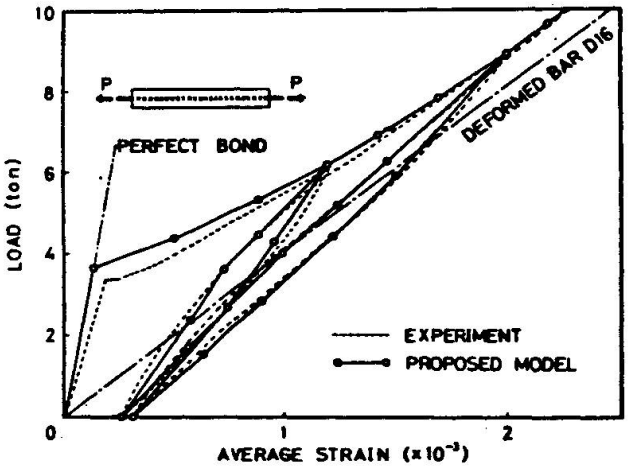

Fig.9 Load-Average Strain Curve by Proposed Model under Cyclic Loading

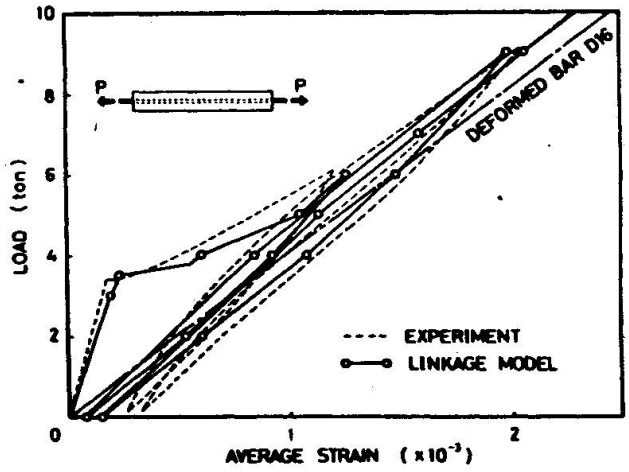

Fig.10 Load-Average Strain Curve by Linkage Model

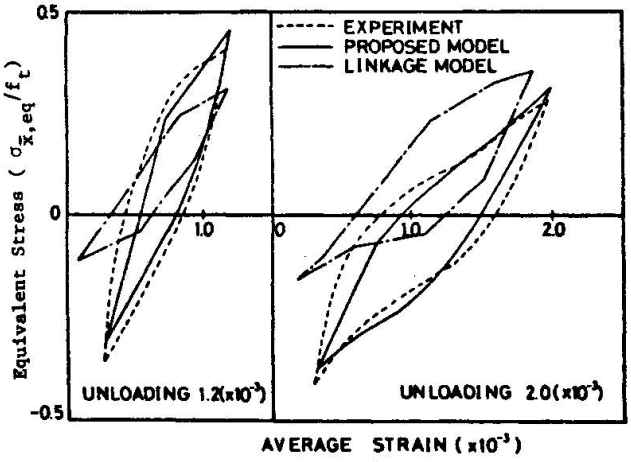

Fig.11 Non-Dimensionized Equivalent Stress-Average Strain Curve

interlock and dowel action formulated in the reference[1], numerical results by the proposed model are compared with Peter's experimental results[5] on reinforced concrete panels tested under uniaxial tension and theoretical values by Cervenka et al [6]. The test specimens were square concrete panels subjected to uniaxial tension as shown in " Fig.12" and they contained a square grid of equal reinforcing bars. The variable factor of this experiment is an angle θ between the reinforcing direction and the loading direction, and here five specimens with $\theta = 0^0$, 10^0, 20^0, 30^0 and 40^0 are comparatively studied. " Table 3" indicates material properties and note that in order to obtain predicting cracking loads consistent with experimental ones, tensile strengthes linearly interpolated from principal stresses by the elastic analysis are used in the analysis instead of those determined from the material test.

"Figs.13(a), (b), (c), (d) and (e)" compare load-extension curves predicted by the proposed model with those observed by the experiment and they also contain theoretical values by Cervenka et al. which do not take bond, aggregate interlock and dowel action into consideration. The numerical result of the proposed model for $\theta = 10^0$ (Type 2) which considers bond but no aggregate interlock and dowel action is given in Fig.13 (b).

Numerical results by the proposed model relatively agree with experimental ones except the case of $\theta = 40^0$ and it may be known that a effect of bond, aggregate interlock and dowel action on stiffness after crack formation is serious.
It is seen from Fig.13(b) that an influence of aggregate interlock and dowel action on predicted loads is from 3 to 8 percents and thus it is relatively

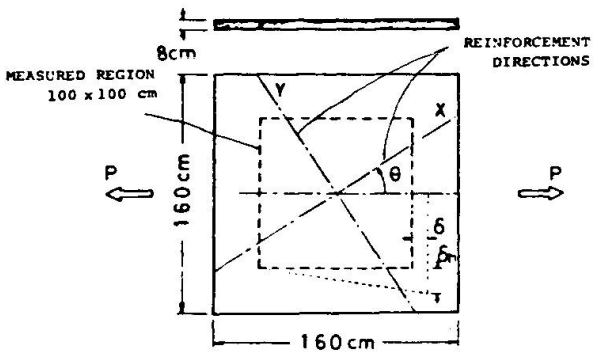

Fig.12 Reinforced Concrete Panel subjected to Uniaxial Tension

Table 3. Material Properties of Reinforced Concrete Panels

Specimen	Reinforcement (ϕ 8)					Concrete		
	p_x (%)	p_y (%)	$_sE$ (kg/cm^2)	$_sE_{sh}$ (kg/cm^2)	θ	f_c (kg/cm^3)	f_c^* (kg/cm^2)	E(kg/cm^2)
S 2r 0	0.6625	0.6625	2.08 x 10^6	6.6 x 10^4	0	18.5	14.56	2.5 x 10^5
S 2r10	0.6625	0.6625	2.08 x 10^6	6.6 x 10^4	10	23.4	14.93	2.5 x 10^5
S 2r20	0.6625	0.6625	2.08 x 10^6	6.6 x 10^4	20	23.1	12.78	2.5 x 10^5
S 2r30	0.6625	0.6625	2.08 x 10^6	6.6 x 10^4	30	20.9	15.24	2.5 x 10^5
S 2r40	0.6625	0.6625	2.08 x 10^6	6.6 x 10^4	40	27.6	15.70	2.5 x 10^5

* the tensile strength used in the analysis

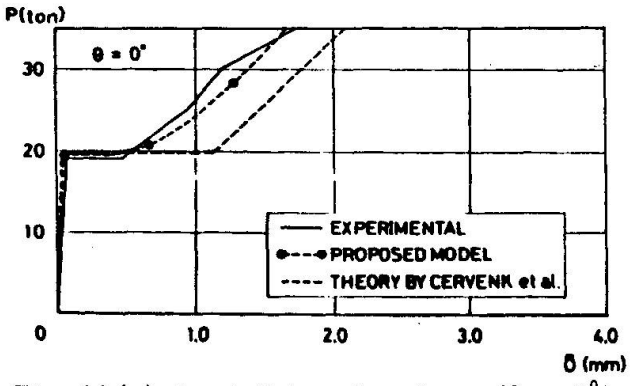

Fig.13(a) Load-Extension Curve($\theta = 0^0$)

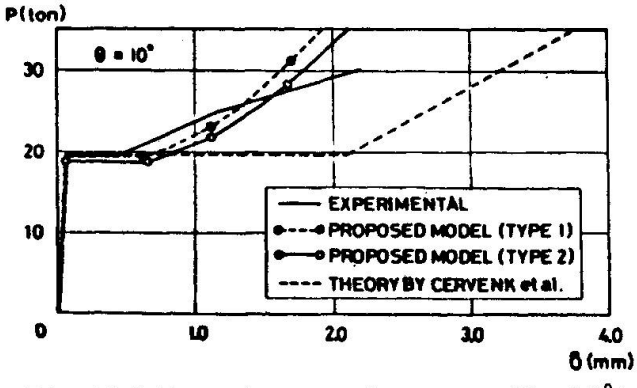

Fig.13(b) Load-Extension Curve($\theta = 10^0$)

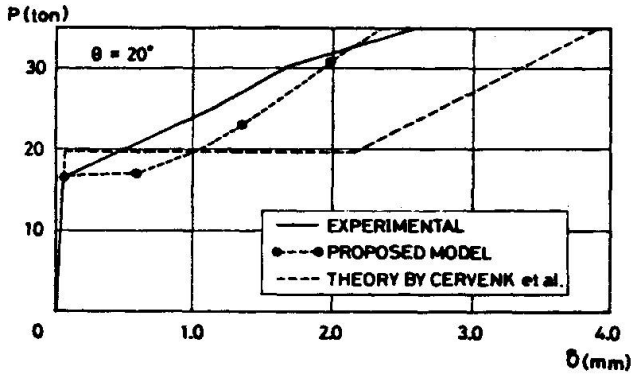

Fig.13(c) Load-Extension Curve($\theta = 20^0$)

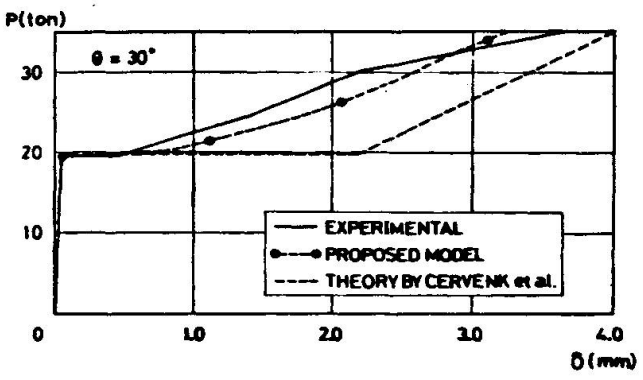

Fig.13(d) Load-Extension Curve($\theta = 30^0$)

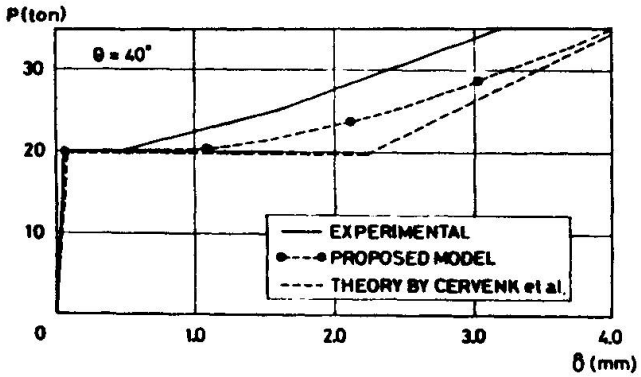

Fig.13(e) Load-Extension Curve($\theta = 40^0$)

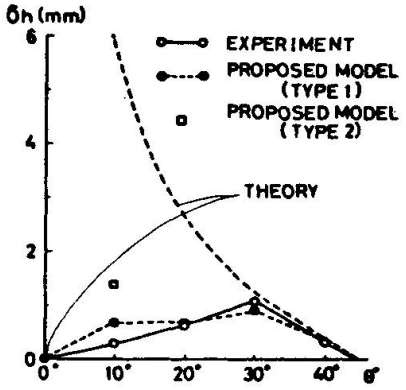

Fig.14 Effect of Reinforcing Direction on Transverse Displacement

small in the case of this specimen and loading condition.

In the next place, " Fig.14" shows plots of transverse displacements δ_h at the load p = 35 tons ($\theta = 0^0$, 20^0, 30^0 and 40^0) and at p = 30 tons ($\theta = 10^0$) against the reinforcing direction θ along with theoretical values by Cervenka et al. , where δ_h means the shear displacement of Fig.12 induced by uniaxial tension. Results of the proposed model and the experiment give a good correlation and as it is seen from theoretical values, an analysis which ignores bond, aggregate interlock and dowel action leads to a big discrepancy in results for specimens with reinforcing angles less than 30^0.
It is found that a contribution of aggregate interlock and dowel action to shear displacements is big to be about 50 percents unlike the contribution of these to predicted loads.

4. REINFORCED CONCRETE SHEAR WALL - FRAME STRUCTURE

4.1 Behavior under Monotonic Loading

In order to investigate behaviors of reinforced concrete shear wall-frame structures, the authors et al.[7] conducted a large number of cycles of alternative loading tests on eighteen reinforced concrete shear wall-frame specimens of about one-fifth of actual size with I-shaped cross section of three stories and one bay

which simulated lower portions of buildings.
" Fig.15" shows the detail of bar arrangement of specimen, that is, one among eighteen specimens and " Table 4" indicates structural dimensions of specimen, and here analytical results such as load-deflection curve, crack propagation, stress transfer, etc. are compared with experimental ones minutely.
The cantilever beam system for loading was adopted as shown in " Fig.16" and the foundation part of specimen was fixed to the test floor by using six prestressed concrete steel bars and introducing 25 tons of prestress a bar. Concentrated horizontal loads were applied to the center line of uppermost story's beam from either the left or the right hand side with an application of constant vertical load of 13.5 tons to tops of surrounding columns equally.

The failure progression of this specimen was as follows(see Fig.22). Shear cracks at the corner of wall, flexural cracks at the bottom of column in the tension side and major shear cracks at the center of wall in the first story occured in order respectively, and thereafter minor shear cracks occured in the wall panels of each story. Main reinforcement at the bottom of column in the tension side yielded in the member rotation angle $R = 4.32 \times 10^{-3}$ rad.(horizontal deflection $\delta = 7.45$mm). The maximum loading capacity was attained in the first cycle of $R = 10.0 \times 10^{-3}$ rad.($\delta = 17.25$mm) and diagonal cracks of column in the compression side was observed on the way to the subsequent cycles of $R = 10.0 \times 10^{-3}$ rad. and thereafter the splitting along main reinforcement of column in the compression side and the protrusion of cover concrete followed by the buckling of main reinforcement were observed on the way to $R = 20.0 \times 10^{-3}$ rad. ($\delta = 34.5$ mm) and then the specimen reduced its strength largely along with the progression of concrete crushing at the corner of wall in $R = 14.7 \times 10^{-3}$ rad. ($\delta = 25.36$ mm).

"Tables 4 and 5" indicate material properties obtained from the material test of reinforcing bar and concrete, and "Table 6" indicates material properties adopted in the analysis. The specimen is seperated into 93 super elements, that is, 372 finite elements as shown in "Fig.17". The specimen was analyzed by the initial stress approach. First equal axial loads of 3.375 tons were vertically applied to nodes of 1, 2, 7 and 8 respectively and then 23 incremental displacements up to $R = 15.2 \times 10^{-3}$ rad.($\delta = 26.0$ mm) were given in the horizontal direction of the node 1, and note that at the same time relatively big axial loads were vertically applied to upper nodes of foundation elements in

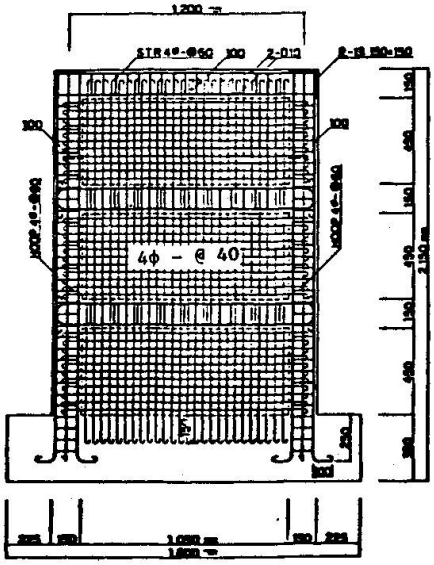

Fig.15 Detail of Reinforced Concrete Shear Wall Specimen

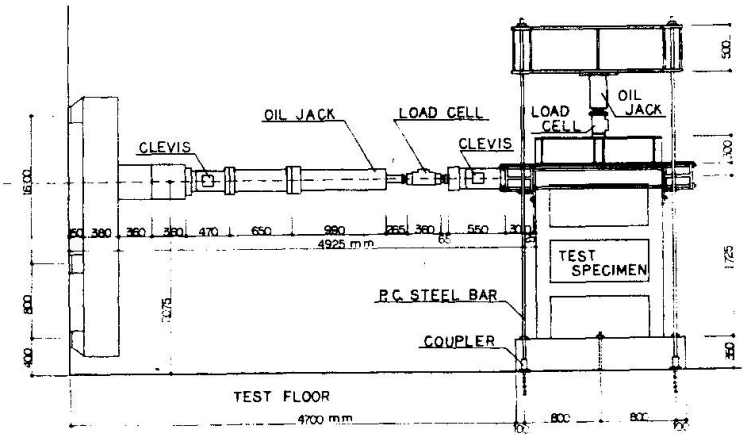

Fig.16 Loading Setup

order to simulate a settlement of foundation. Von-Mises's yield criterion was used for plastification of concrete in compression in this analysis.

"Fig.18" shows load-deflection curve of the proposed model(Type 1) calculated by considering all inelastic effects and that(Type 2) by neglecting bond, aggregate interlock and dowel action along with the experimental one.
Both analytical results fairely coincide with the experimental one, but predicted loads of Type 2 give a some what smaller estimation than the experiment after flexural yielding.

"Fig.19" shows plots of ratios of differences between predicted loads of Type 1 and Type 2 at the same deflection levels to predicted loads of Type 1 against horizontal deflections, and these quantities mean a contribution of bond, aggregate interlock and dowel action to the load-carrying capacity.
An influence of these inelastic effects is relatively big to be about 8-18 percents before the yielding loads(P = 20.85 tons) and on the other hand it is small to be about 2-10 percents after the yielding load though there are some scatters.

"Fig.20" shows the principal stress distribution of Type 1 at the elastic stage (P = 4.49 tons and δ = 0.45 mm). The compression field extending from the loading point toward the bottom of column in the compression side is formed and it is considered that the principal stress distribution at the elastic stage roughly determines crack formation and angles of concrete.

"Fig.21" shows the predicted cracking pattern of Type 1 at the load P = 27.26 tons the horizontal deflection δ = 24.0 mm, where the single line indicates the cracked element and its inclination indicates the crack angle, the shaded portion indicates the strain-softening element, and the black solid indicates the crushing element. "Fig.22" shows the final cracking pattern observed by the experiment. The cracking pattern predicted by the analysis fairely agrees with the experimental one and it is understood that the crushing of concrete at the corner of wall and at the bottom of column in the compression side in the first story is a direct cause of a failure.

"Figs.23(a) and (b)" show shear stress distributions of Type 1 along several horizontal cross sections of specimen at P = 4.49 tons,δ = 0.45 mm and at P = 27.26 tons, δ = 24.0 mm respectively. The shear stress distribution of Fig. 23(a) except that for the third story is close to that of I-shaped cross section being assumed in the conventional elastic theory and therefore shear stresses near the center of wall panel are maximum. On the other hand, as it is known from Fig.21, noting that shear stresses near the bottom of column in the compression side at the first story are zero since the crushing has been occured in the corresponding elements, shear stresses near the diagonal line connecting the loading point and the bottom of column in the compression side at the first story are maximum.

"Fig.24" shows the load-strain curve of Type 1 for the main reinforcement at the bottom of column in the tension side. The analysis gives a little bit higher yielding load than that of the experiment, but it is considered that this prediction is sufficiently accurate in spite of the assumption that the area of reinforcement distributes uniformly within any concrete element.

"Figs.25(a) and (b)" show a comparison between crack widths predicted by the analysis of Type 1 and measured crack widths at the center of wall panels in the first and second story. Measured widths are wider than predicted ones, but here it should be noted that widths of the experiment were measured on the concrete surface and on the other hand widths of the analysis were evaluated on the

Table 4. Structural Dimensions of Specimen

Shear Span Ratio	Column Section (cm x cm)	Beam Section (cm x cm)	Wall Thickness (cm)	Main Bar in Column (p %)	Main Bar in Beam (p %)	Hoop in Column (p %)	Wall Reinforcement (p_x %)	(p_y %)
1.28	15 x 15	15 x 15	4.5	8 - D10 (2.53)	4 - D10 (1.46)	4φ - a 60 (0.28)	4φ - a 40 (0.72)	4φ - a 40 (0.72)

Table 5. Material Properties of Reinforcement

Steel	$_sA$ (cm^2)	$_s\sigma_y$ (kg/cm^2)	$_s\varepsilon_y$ ($\times 10^{-6}$)	$_s\sigma_B$ (kg/cm^2)	$_sE$ ($\times 10^6$ kg/cm^2)
D10	0.71	3761	1896	5279	1.96
4φ	0.127	5398	4559	5784	2.11

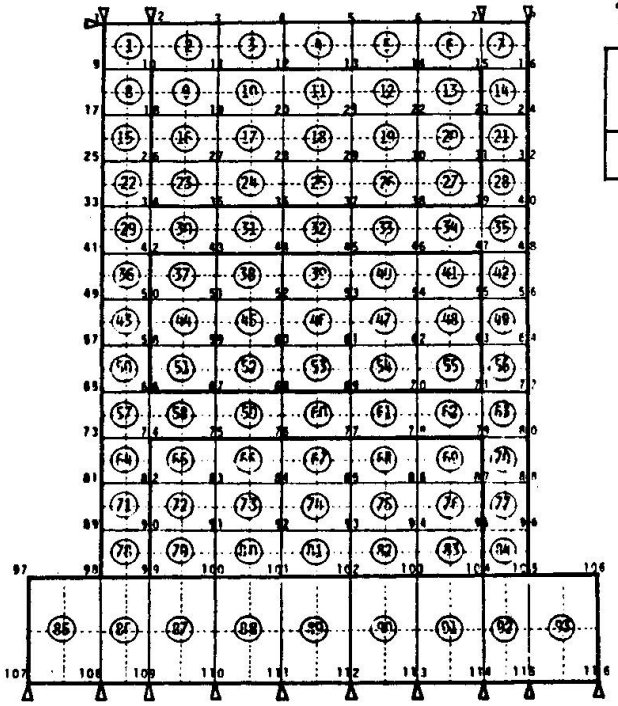

Fig.17 Finite Element Discretization

Table 6. Material Properties of Concrete

E (kg/cm^2)	υ	σ_B (kg/cm^2)	ε_B (kg/cm^2)	f_t (kg/cm^2)
2.25×10^5	0.196	226	2240×10^{-6}	27.9

σ_B : the compressive strength

ε_B : the strain at the compressive strength

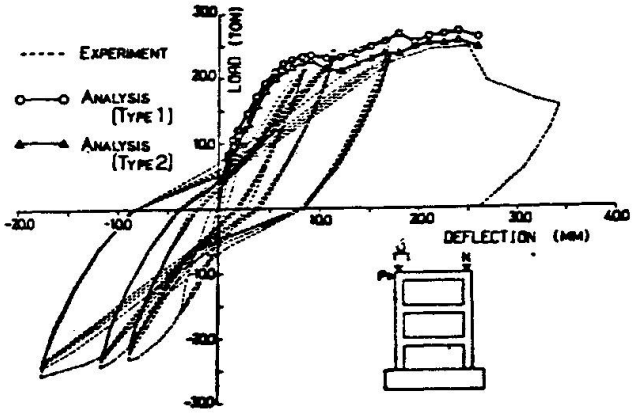

Fig.18 Horizontal Load-Deflection Curve

Table 7. Material Properties used in the Analysis

Material		Young's Modulus (kg/cm^2)	Yield Stress (kg/cm^2)	Poisson's Ratio υ
Concrete		$E = 2.25 \times 10^5$	$\sigma_{y1} = 162$	0.196
		$E_{t1} = 0.323 \times 10^5$	$\sigma_{y2} = 226$	
		$E_{t2} = -0.613 \times 10^5$	———	
Steel	D10	$_sE = 1.96 \times 10^6$	$\sigma_y = 3761$	———
		$_sE_{sh} = 1.49 \times 10^4$	———	
	4φ	$_sE = 2.11 \times 10^6$	$\sigma_y = 5398$	———
		$_sE_{sh} = 1.99 \times 10^6$	———	

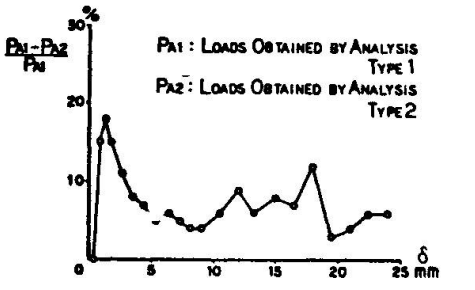

Fig.19 Contribution of Bond, Aggregate Interlock and Dowel Action to Loads

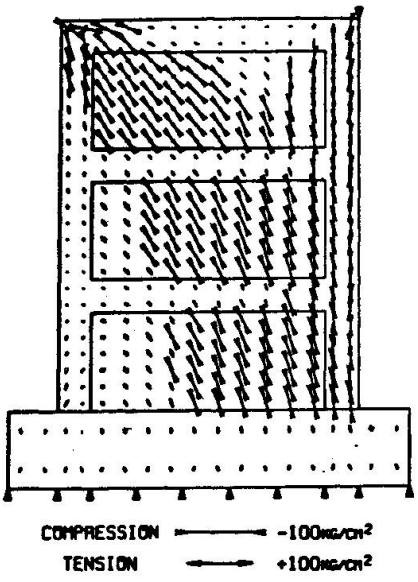

Fig.20 Principal Stress Distribution at P=4.49(t)

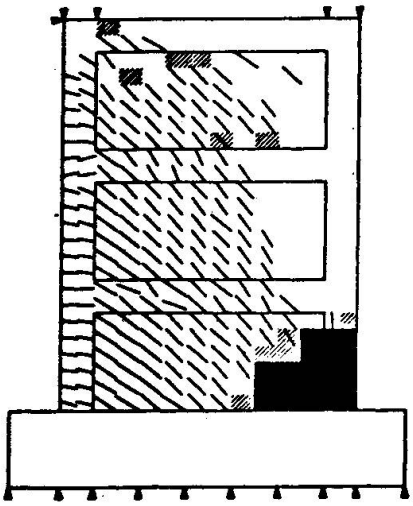

Fig.21 Predicted Cracking Pattern at P=27.26 (t)

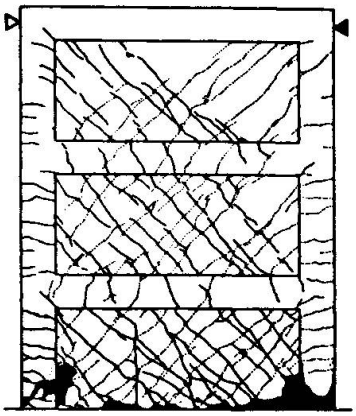

Fig.22 Final Cracking Pattern of Experiment

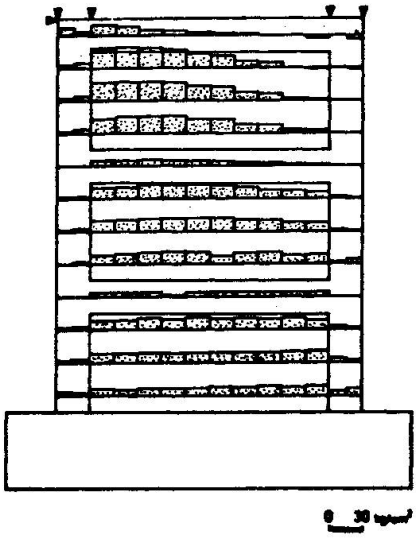

Fig.23(a) Shear Stress Distribution at P = 4.49 (t)

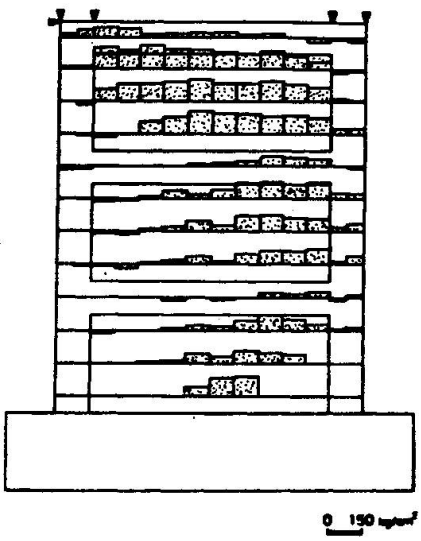

Fig.23(b) Shear Stress Distribution at P = 27.26 (t)

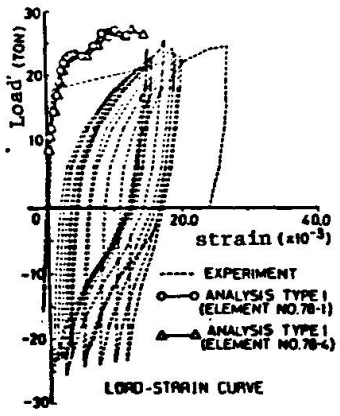

Fig.24 Load-Strain curve for Main Reinforcement

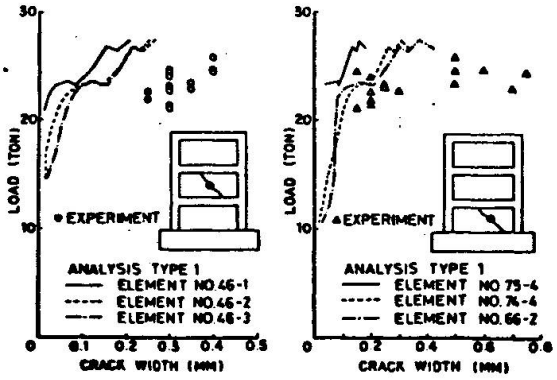

Figs.25(a),(b) Load-Crack Width Relation

exposed surface of reinforcement. Judging from the experimental result[8] on tensile bond specimen in which ratios of widths on the exposed surface of reinforcement to those on the concrete surface are from 75 to 80 percents in the case of smooth round bars, it is thought that predicted crack widths are nearly satisfactory estimation.

4.2 Behaviors under Cyclic Loading

In order to examine a validity of the proposed model, an analysis is conducted on two reinforced concrete shear wall-frame specimens[9] with the same configurations and details, where the detail of specimen is shown in "Fig.26", but different wall thicknesses, where the thickness of Type 1 is 7.8 cm and that of Type 2 is 7.5 cm, and loading excursions, and a comparison with experimental results is made. The specimen was composed of two symmetrical structural systems and they were tested as a simply supported beam.
"Tables 7 and 8" indicate material properties of steel and concrete.

The specimen was seperated into 30 super elements as shown in "Fig.27" and it was analyzed by the self-correcting approach. Von-Mises's yield criterion was adopted for plastification of concrete in compression in this analysis.

"Fig.28(a)" shows the load-deflection curve for the specimen of Type 1 in which unloading was done at the deflection of about 1.0 mm and then reloading was done from zero-load level. "Fig.28(b)" shows the load-deflection curve for the specimen of Type 1 without a consideration of bond effect.
Analytical results by Schnobrich et al.[10] and Darwin et al.[11] are also included in Fig.28(a), where the former considers no bond effect but aggregate interlock and dowel action as one-quarter of the elastic shear stiffness G for the cracked concrete and the latter does not consider bond effect, aggregate interlock and dowel action. The analytical result by the proposed model gives a somewhat smaller area of hysteresis loop than that of the experiment, but it gives a fairely good agreement with the experiment as a whole.

If bond effect is not considered, it is found that the analysis not only underestimates loads in the region of relatively small deflections, but also results in a big discrepancy in cyclic behaviors.
Furthermore, it is possible to correspond the anatytical load-deflection curve in the early stage to the experimental one by assuming appropriate constant values as the shear stiffness after crack formation, but such assumption leads

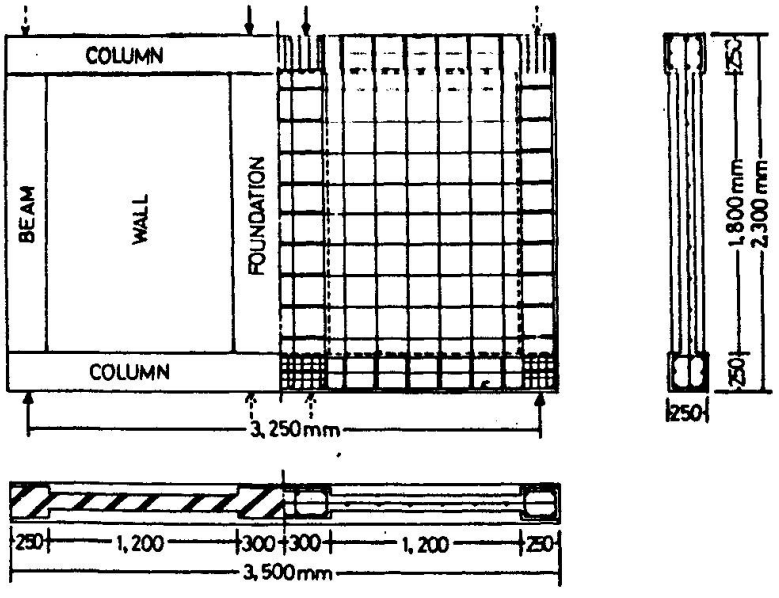

Fig.26 Detail of Reinforced Concrete Shear Wall Specimen

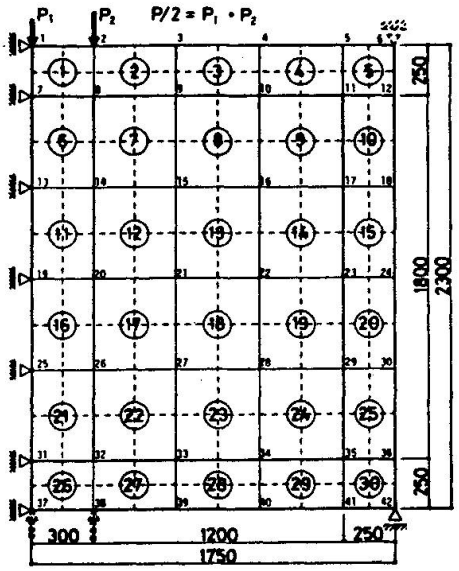

Fig.27 Finite Element Discretization

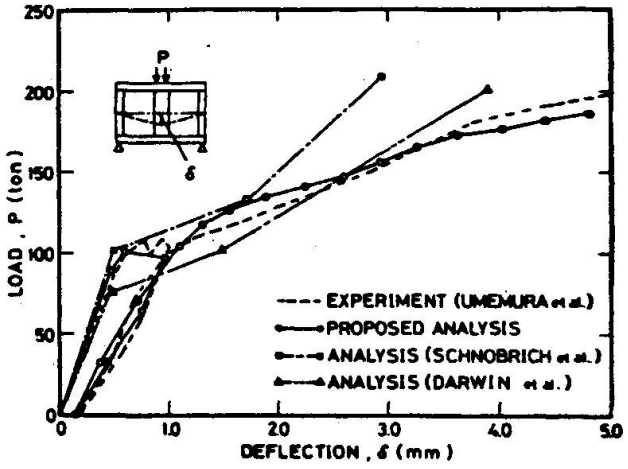

Fig.28(a) Load-Deflection Curve for Specimen of Type 1

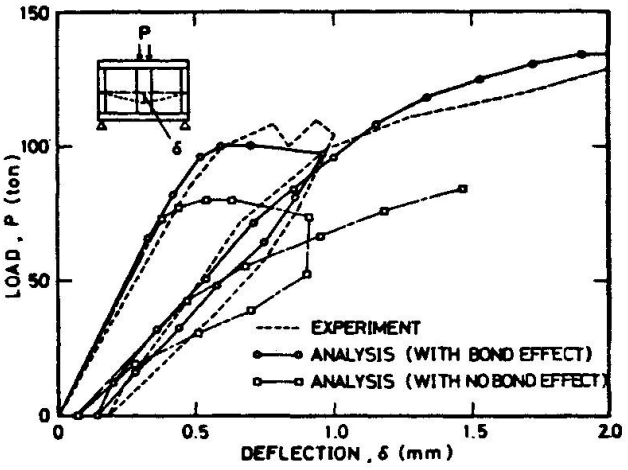

Fig.28(b) Load-Deflection Curve for Specimen of Type 1

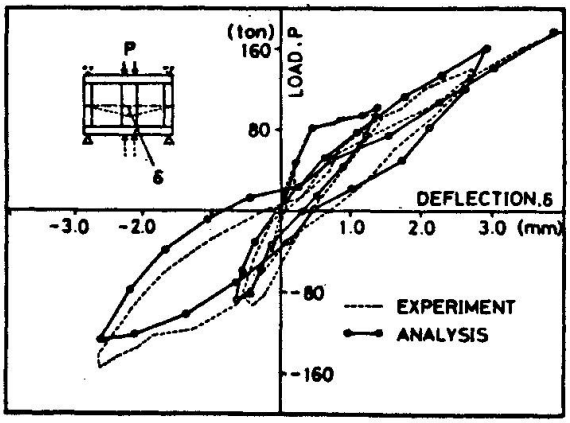

Fig.29 Load-Deflection Curve for Specimen of Type 2 under Alternative Cyclic Loading

to an overestimation of loads as deflections become larger.

"Fig.29" shows two cycles of load-deflection curve for the specimen of Type 2 in which unloading was conducted at the deflections of + 1.4 , - 0.6 , + 2.7 and - 2.6 mm respectively.
The analytical load-deflection relation has a tendency that a recovery of strength is late and deflections become larger in the negative loading cycles, but the configuration of hysteresis loop is similar to the experimental one and also the analytical result relatively agrees with the experimental one as a whole.

5. CONCLUSION

The following conclusions were obtained from an evaluation of the proposed model described in the reference[1] and a comparison between analytical results and experimental ones,

- It is necessary for pursuing hysteresis behaviors of reinforced concrete structures to consider bond effect and the proposed bond model is effective in

such a sense that its accuracy is high and an incorporation it into the analytical procedure is easy. However, the furtherdevelopment of bond model is required to consider the different type of bar surface(smooth round bar or deformed bar) and the effect of transverse pressure field as observed in wall panels on bond behaviors.

- Aggregate interlock and dowel action could be idealized as the equivalent shear stiffness depending upon static hysteresis by considering crack spacing and width. Although the effect of these inelastic effects on behaviors is different depending upon the type of structures and loading conditions, an influence of these effects on deflections,that is, shear displacements is greater than that of these on loads and particularly the new model of aggregate interlock gives a reasonable result, for example as indicated in Fig.28(a).

- The predicted failure pattern nearly corresponds to that observed by the experiment.

- The analysis tends to underestimate crack widths and furthermore it is considered that the judgement of crack closing in the cyclic analysis is the remaining question.

- The incremental self-correcting approach is valuable to reduce the computational time and also gives satisfactory results. However, it must note that the effect of incremental size of load factor on behaviors is serious.

REFERENCE

1. N.Shirai and T.Sato,"Inelastic Analysis of Reinforced Concrete Shear Wall Structures : Material Modelling of Reinforced Concrete," IABSE Colloquium, Delft, 1981.
2. S.Morita et al.,"Bond-Slip Relationship under Repeated Loading," Transactions of Architectural Institute of Japan, No.229, 1975 (in Japanese).
3. Ngo,D., and A.C.Scordelis,"Finite Element Analysis of Reinforced Concrete Beams," Journal of ACI, Vol.64, No.3, March 1967.
4. S.Morita,"Study on Bond Effect of Reinforced Concrete Members by Tensile Tests ," The Annual Report of Cement Engineering, Vol.XVII, 1963 (in Japanese).
5. Peter,J.,"Zur Bewehrung von Scheiben und Schalen für Hauptspannungen schiefwinklig zur Bewehrungsrichtung," Dr.-Ing. Dissertation, T.H. Stuttgart, 1964.
6. V.Cervenka and K.H.Gerstle,"Inelastic Analysis of Reinforced Concrete Panels, Part I : Theory," IABSE Publications, Vol.31-II, 1971.
7. T.Sato, A.Ono, H.Adachi, N.Shirai and M.Nakanishi,"Experimental Study on Elast-Plastic Behavior of Reinforced Concrete Shear Wall Structures," Journal of the Research Institute of Science and Technology, Nihon University, No.53, July 1980 (in Japanese).
8. Y.Goto et al.,"Investigation on Tension Cracks in Reinforced Concrete Member : An Experiment by Tensile Bond Specimen," The 2nd Symposium on Deformed Bars , Concrete Library, No.14, 1965 (in Japanese).
9. H.Umemura et al.,"Studies on Reinforced Concrete Shear Wall and Framed Masonry Shear Walls," Research Report, University of Tokyo, 1964.
10. W.C.Schnobrich et al.,"A Numerical Procedure for the Determination of the Behavior of Shear Wall Frame System," Journal of ACI, 1973.
11. D.Darwin et al.,"Inelastic Model for Cyclic Biaxial Loading of Reinforced Concrete," Civil Engineering Studies, SRS-No.409, University of Illinois, 1974.

Ultimate Strength of Reinforced Concrete Members under Combined Loading

La résistance à la rupture d'éléments en béton armé sous charges combinées.

Traglast von Stahlbetonbauteilen unter kombinierten Belastung

RYOICHI SHOHARA
Research Engineer
Shimuzu Construction Co., Ltd.
Tokyo, Japan

BEN KATO
Prof. Dr.-Eng.
University of Tokyo
Tokyo, Japan

SUMMARY

The ultimate strength of reinforced concrete members is analyzed based on the concept of a diagonal compression field. In this analysis, the interaction among bending moment, axial force and shear force is evaluated using a simple mathematical model. This theory is very simple but can explain the resisting mechanisms of reinforced concrete beam-columns and of precast concrete connections by a unified theory. The theoretical predictions obtained here are compared with the test results of many beam-column specimens and with those of push-off specimens; a satisfactory agreement was found.

RÉSUMÉ

La résistance à la rupture d'éléments en béton armé est analysée sur base du principe de champs de compression diagonale. Dans cette étude, l'interaction entre moments de flexion, effort axial et effort de cisaillement est évaluée par un modèle mathématique simple. Bien que simple, cette théorie est capable d'expliquer conjointement les mécanismes de liaisons entre poutres et colonnes en béton armé et entre éléments préfabriqués. Les prédictions théoriques obtenues ici sont comparées aux résultats expérimentaux de jonctions poutres-colonnes et de joints entre éléments préfabriqués.

ZUSAMMENFASSUNG

Die Traglast von Stahlbetonbauteilen ist mithilfe des Konzepts des Diagonaldruckfeldes berechnet. Kombinationen von Biegemoment, Normalkraft und Querkraft wurden mit einem einfachen mathematischen Modell behandelt.
Ortbeton- und Fertigteilkonstruktionen können damit behandelt werden. Befriedigende Übereinstimmung zwischen Theorie und Versuch wurde gefunden.

1. INTRODUCTION

In the conventional evaluation of the ultimate strength of beam-columns subject to combined axial thrust, bending moment and shear, the moment capacity is evaluated considering the interaction with axial force firstly, and then the shear force is calculated from the moment diagram at ultimate state depending on the end condition of the members, and this shear force is compared with the maximum shear capacity of the members which is evaluated on the basis of failure modes of the member. In this procedure of estimating shear capacity, different mechanisms of shear transfer through a section are assumed corresponding to the observed failure modes such as diagonal shear failures and shear bond failure, where the interaction of the shear with axial force and/or beinding stress is not taken into account. Since the observation of ultimate strength and failure mode in shear is made on the limited number of test specimens and thus of the limited varieties of parameters, there is a vulnerability of overlooking other possible modes of failure unless the assessment should be made on the basis of a comprehensive resisting mechanism of the member against axial force, bending moment and shear force.

Herein, a structural model is developed on the basis of the compression field concept. And the ultimate strengths of various types of reinforced concrete members such as beam-columns, beams and precast concrete connections are analyzed in the unified theoretical approach, taking the full interaction among performances of shear, bending and axial force into account.

The theoretical predictions obtained herein are compared with the test results consisting of many beam-column specimens and push-off specimens to show a satisfactory agreement each other.

2. ANALYSIS

The ultimate load carrying capacities of reinforced concrete members are analyzed. In this structural model, the equilibrium is secured through the entire member and the stresses in any constituent elements do not exceed their ultimate stresses, but the compatibility of strains and deformation is not necessarily satisfied. Therefore the lower bound solution will be obtained from this analysis. The stress-strain relationship of steel is assumed to be elastic-perfectly plastic ignoring the effect of strain-hardening. As for that of concrete, it is assumed that the concrete has no resistance against tension and that it can develop some extent of plastic deformation keeping its maximum stress against compression.

2.1. Ultimate Strength of Reinforced Concrete Beam-column Subject to Anti-symmetrical Bending

In this paragraph the ultimate loading capacity of a reinforced concrete beam-column subject to anti-symmetrical bending at its ends under constant axial force is analyzed.

A reinforced concrete beam-column in this model is fictitiously divided into two systems, namely web reinforcement and the diagonal compression field system, and the consisting materials are allocated into these systems without overlapping.

The loading condition and the dimensions of various parts of the reinforced concrete column to be analyzed are shown in Fig.1, where the symbols are;

N = constant axial force
M = bending moment
Q = shearing force
ℓ = length of the member
D = depth of the section
b = width of the section
$_rd$ = distance between the center of gravities of reinforcing bars at each side

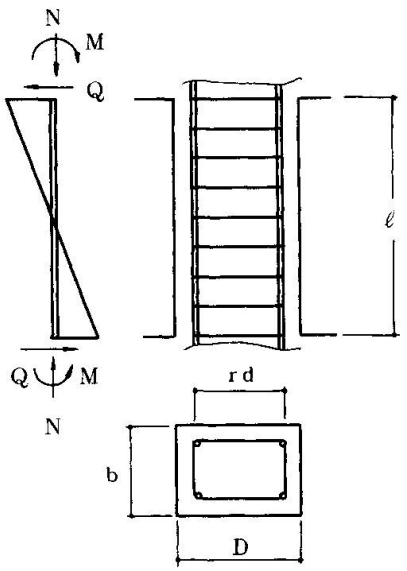

Fig.1 Reinforced Concrete Member and Loading Condition

2.1.1. Bending Moment and Shear Force Carried by the Web Reinforcement System

A kind of truss mechanism consisting of web reinforcement, main reinforcement and concrete which resists compression force are assumed as a load carrying mechanism. The concrete is divided into virtual discreet elements with their inclinations $\varphi = 45°$, their stresses Fc, and imaginary width of the concrete βb in equilibrium with the stresses of the reinforcements.

Assuming the stress of main reinforcing bars at each end of the member $T = \alpha Ty$ when the web reinforcing bars have yielded, the following equations are derived from the equilibrium of the system. Where $Ty = {}_ra \cdot {}_r\sigma_y$ is the yield strength of the reinforcing bars at one side of the section.

$$ {}_wQ = P_w \cdot {}_w\sigma_y \cdot b \cdot {}_rd \qquad (1) $$

$$ {}_wM = \alpha Ty \cdot {}_rd \qquad (2) $$

$$ {}_wN = {}_wQ \qquad (3) $$

$$ \alpha = \frac{P_w \cdot {}_w\sigma_y \cdot b \cdot \ell}{2Ty} $$

$$ \beta = \frac{2P_w \cdot {}_w\sigma_y}{F_c} \qquad (0 \leq \alpha, \beta \leq 1) $$

where;

$_wa$ = sectional area of a set of web reinforcing bars

$_ra$ = total sectional area of main reinforcing bars allocated on either side of the section with respect to the bending axis

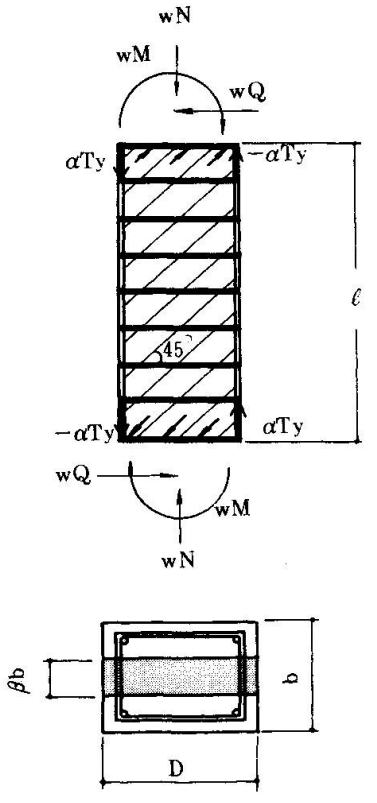

Fig.2 Equilibrium of Web Reinforcement System

P_w = web reinforcement ratio $\frac{w a}{b x}$

X = pitch of web reinforcing bars
$r\sigma y$ = yield point of main reinforcement
$w\sigma y$ = yield point of web reinforcement
F_c = maximum compressive stress of concrete

Putting $\alpha = 1$ in the above equations, it can be observed that the yielding of web reinforcement and that of main reinforcement will take place simultaneously when the condition that

$$\bar{P}_w = \frac{2_r a \cdot r\sigma y}{b\ell \cdot w\sigma y}$$

is satisfied. And it will be seen that the moment capacity of this system will be saturated at this state, and does not increase further even if one provides more amount of web reinforcement than that defined by the critical value of $\bar{P}w$.

In general, the main reinforcements have reserve strength of $(1-\alpha)Ty$ before yielding.

2.1.2. Bending Moment and Shear Force Carried by the Compression Field

At this step of the analysis, the materials in the member which can be utilized as load carrying elements are $(1-\alpha)_r a$ of the main reinforcement and the concrete. Compression field which consists of these materials are assumed as shown Fig.3(a), where c corresponds a steel chord member consisting of $(1-\alpha)_r a$, and d is a fictitious compressive diagonal member made of concrete.

In Fig.3(a), dashed lines which define the fictitious diagonal compression member d are drawn from the corners of the opposite column ends with a inclination θ which is the function of $_tM$ and $_tN$, and the width of the horizontal intersection of this diagonal member is $X = D - \ell \tan\theta$.

Denoting the compressive stress in this diagonal member σ_c, the compressive force in this member N_c can be written as

$$N_c = \sigma_c\, b' \cdot X \cdot \cos\theta$$
$$= (D - \ell \tan\theta) b' \cdot \sigma_c \cdot \cos\theta \qquad (4)$$

where $b' = (1-\beta)b$ is fictitious width of diagonal compression field.

The equilibrium of the axial force, the bending moment and the shear at each end of the member can be written as follows.

$$_tN + 2S = N_c \cdot \cos\theta \qquad (5)$$

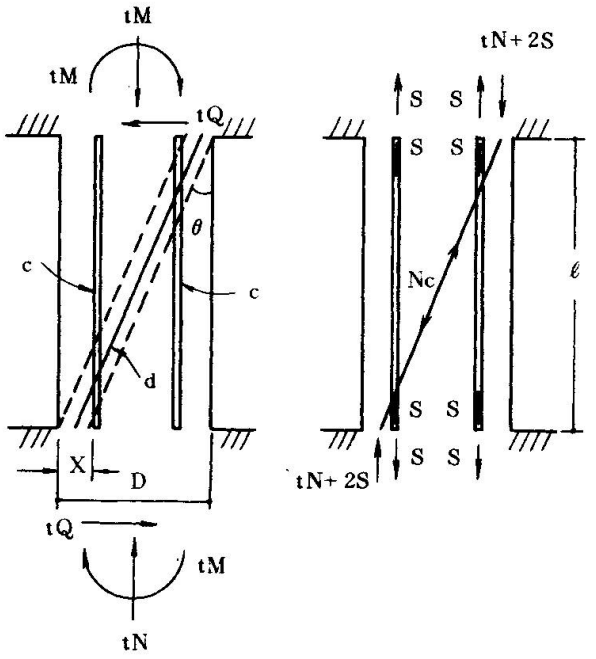

(a) (b)

Fig.3 Compression Field Model Subject to Anti-symmetrical Bending

$$ {}_tM = \frac{\ell \cdot \tan\theta \cdot N_C \cdot \cos\theta}{2} = \frac{N_C \cdot \ell \cdot \sin\theta}{2} \qquad (6) $$

$$ {}_tQ = N_C \cdot \sin\theta \qquad (7) $$

Where ${}_tN = N - {}_wN$ is the axial force carried by this compression field system and is positive for compression, ${}_tM$ is the bending moment at each end of the member and is positive for clockwise direction, ${}_tQ$ is the shear force, and the cords forces S are positive for tension. Substituting Eq.(4) into Eq.(5), the inclination of the diagonal compression field $\tan\theta$ is found to be

$$ \tan\theta = \frac{\lambda}{2}\left(\frac{b'D\cdot\sigma_C}{2S+{}_tN}\right)\left\{\sqrt{1+\frac{4}{\lambda^2}\left(\frac{2S+{}_tN}{b'D\cdot\sigma_C}\right)\left(1-\frac{2S+{}_tN}{b'D\cdot\sigma_C}\right)}-1\right\}. \qquad (8) $$

where $\lambda = \ell/D$, and substituting Eqs.(4) and (8) into Eq.(6), the end moment ${}_tM$ is found to be

$$ {}_tM = \frac{b'D\cdot\sigma_C\lambda\ell}{4}\left\{\sqrt{1+\frac{4}{\lambda^2}\left(\frac{2S+{}_tN}{b'D\cdot\sigma_C}\right)\left(1-\frac{2S+{}_tN}{b'D\cdot\sigma_C}\right)}-1\right\}. \qquad (9) $$

Eq.(9) shows that ${}_tM$ increases when σ_C increases, and ${}_tM$ becomes maximum when σ_C becomes its maximum value F_C, and if $2S + {}_tN \leq \frac{bD\cdot\sigma_C}{2}$, ${}_tM$ becomes maximum when the chords forces S reach their yield value S_O, namely

$$ S = S_O = (1-\alpha)T_y . $$

Region I ${}_tN < N_1$, $N_1 = \frac{N_O}{2} - 2S$.

Substituting F_C into Eq.(9) for σ_C, and S_O for S, the maximum bending moment at column ends is found to be

$$ {}_tM = \frac{N_O\lambda\ell}{4}\left\{\sqrt{1+\frac{4}{\lambda^2}\left(\frac{2S_O+{}_tN}{N_O}\right)\left(1-\frac{2S_O+{}_tN}{N_O}\right)}-1\right\}. \qquad (10) $$

Where; $N_O = b'DF_C$ = maximum compressive capacity of the concrete section used in compression field system. And the corresponding shear force ${}_tQ$ is

$$ {}_tQ = \frac{2\,{}_tM}{\ell} = \frac{N_O\lambda}{2}\left\{\sqrt{1+\frac{4}{\lambda^2}\left(\frac{2S_O+{}_tN}{N_O}\right)\left(1-\frac{2S_O+{}_tN}{N_O}\right)}-1\right\}. \qquad (11) $$

Looking into the effect of the axial force ${}_tN$ on the moment capacity through Eq.(10), it can be seen that ${}_tM$ takes its maximum when ${}_tN$ reaches $N_1 = (N_O/2) - 2S_O$, and until ${}_tN$ reaches this critical value of N_1, ${}_tM$ increases with the increase of ${}_tN$. Substituting $N_1 = (N_O/2) - 2S_O$ into Eqs. (10) and (11) for ${}_tN$, the bending moment and shear force under this critical axial force are found to be

$$ {}_tM_1 = \frac{1}{4}N_O\ell\left(\sqrt{\lambda^2+1}-\lambda\right) \qquad (12) $$

$$ {}_tQ_1 = \frac{1}{2}N_O\left(\sqrt{\lambda^2+1}-\lambda\right). \qquad (13) $$

And the inclination of the diagonal at this state is

$$\tan\theta_1 = \sqrt{\lambda^2 + 1} - \lambda \,. \qquad (14)$$

When the axial force is not larger than this critical value N_1, both steels and concrete develop their full capacity at the ultimate state, and this mode of failure can be defined as the flexural failure in a broad sense.

Region II. $N_1 < {}_tN < N_2 \qquad N_2 = \frac{N_O}{2} + 2S_O$

According to Eq.(10), the bending moment reaches the maximum value at the critical axial force N_1, and then decreases for the larger axial force, and correspondingly the inclination θ starts to decrease as can be seen from Eq.(8). However this is not the only way of excurtion. As Eq.(8) and (9) are the function of (2S+N) and not the independent function of S or N, both ${}_tM$ and θ can remain unchanged for the axial force which is larger than N_1 if S decreases and goes back into the elastic region. And since the member should develop its maximum resistance against given external forces according to the lower bound theorem, this behavior must be the actual one. N-S relationship for this transitive region can be written as

$$2S + {}_tN = 2S_O + {}_tN = \frac{N_O}{2} \,. \qquad (15)$$

From this equation, it can be seen that S becomes zero at the axial force $N_O/2$, and the chord stress will change its sign into compression when the axial force exceeds this value, and finally the chords will yield by compression when the axial force reaches

$$N_2 = \frac{N_O}{2} + 2S_O \,. \qquad (16)$$

Thus it can be concluded that, for the region of $N_1 < {}_tN < N_2$, the ultimate strength of the member is governed by the compressive failure of the concrete diagonal, while the chord members remain elastic. For the range of this axial force, ${}_tM_1$, ${}_tQ_1$ and θ_1 keep constant values, and they are given by Eqs.(12), (13) and (14) respectively. This mode of failure can be defined as the shear failure.

Region III. $N_2 \leq {}_tN \leq N_3, \quad N_3 = N_O + 2S_O$

Since the only difference of equilibrium conditions between Region I and Region III is that S_O in the former becomes $-S_O$ in the latter, ${}_tM$ and ${}_tQ$ for Region III can be obtained by replacing S_O in Eqs(10) and (11) by $-S_O$ as

$${}_tM = \frac{1}{4} N_O \lambda \ell \left\{ \sqrt{1 + \frac{4}{\lambda^2} \left(\frac{{}_tN - 2S_O}{N_O} \right) \left(1 - \frac{{}_tN - 2S_O}{N_O} \right)} - 1 \right\} \qquad (17)$$

$${}_tQ = \frac{2\,{}_tM}{\ell} = \frac{1}{2} N_O \lambda \left\{ \sqrt{1 + \frac{4}{\lambda^2} \left(\frac{{}_tN - 2S_O}{N_O} \right) \left(1 - \frac{{}_tN - 2S_O}{N_O} \right)} - 1 \right\} . \qquad (18)$$

Eq.(17) shows that ${}_tM$ decreases with increasing value of ${}_tN$. As the extreme, ${}_tM$ becomes zero when the axial force reaches the following value

$$N_3 = N_O + 2S_O \,. \qquad (19)$$

N_3 is the sum of the axial yield force of concrete and that of steel chord parts. The failure mode in this region can also be defined as the flexural failure.

The case for $\alpha = 1$

This case corresponds to the situation of S=0 in the preceding section. Since the description for the Region I in the preceding section is independent of the value of S or S_o, the moment and shear capacities for this region can be obtained by introducing $S_o=0$ into Eqs.(10) and (11) as

$$ {}_tM = \frac{1}{4} N_o \lambda \ell \left\{ \sqrt{1 + \frac{4}{\lambda^2} \left(\frac{{}_tN}{N_o}\right)\left(1 - \frac{{}_tN}{N_o}\right)} - 1 \right\} \tag{20} $$

$$ {}_tQ = \frac{1}{2} N_o \lambda \left\{ \sqrt{1 + \frac{4}{\lambda^2} \left(\frac{{}_tN}{N_o}\right)\left(1 - \frac{{}_tN}{N_o}\right)} - 1 \right\} . \tag{21} $$

The critical axial force which makes the moment maximum also can be found by placing $S_o=0$ in the expression of N_1 as

$$ N_1' = \frac{N_o}{2} . $$

The maximum values of ${}_tM$ and ${}_tQ$ for this critical axial force are independent of the value of S_o and are given by Eqs.(12) and (13) of the preceding section.

When S=0, from Eqs.(20) and (21), it can be seen that it is impossible to keep ${}_tM$ and ${}_tQ$ unchanged for the increasing value of ${}_tN$. Therefore, the Region II does not exist, namely the shear failure does not occur in this case. And therefore, Eqs.(20) and (21) are valid even for the larger axial force than N_1', and eventually ${}_tM$ becomes zero when the axial force reaches $N_3' = N_o$.

2.1.3. Total Capacity

The total bending capacity of a member is obtained by summing up those of web reinforcement system (section 2.1.1.) and of compression field (section 2.1.2.). The result is summerized in the following;

Region I. $ {}_tN \leq N_1 , \quad N_1 = \frac{N_o}{2} - 2S_o $

$$ M = {}_wM + \frac{1}{4} N_o \lambda \ell \left\{ \sqrt{1 + \frac{4}{\lambda^2} \left(\frac{2S_o + {}_tN}{N_o}\right)\left(1 - \frac{2S_o + {}_tN}{N_o}\right)} - 1 \right\} \tag{22} $$

$ {}_wM = \alpha \cdot {}_ra \cdot {}_r\sigma_y \cdot rd , \quad \alpha = (P_w \cdot \sigma_y \cdot b\ell)/(2 {}_ra \cdot {}_r\sigma_y) \leq 1 $

$ {}_tN = N - {}_wN , \quad {}_wN = {}_wQ . $

Region II. $ N_1 < {}_tN < N_2 , \quad N_2 = \frac{N_o}{2} + 2S_o . $

$$ M = {}_wM + \frac{1}{4} N_o \ell \left(\sqrt{\lambda^2 + 1} - \lambda\right) . \tag{23} $$

Region III. $N_2 \leq {}_tN \leq N_3$, $N_3 = N_O + 2S_O$

$$M = {}_wM + \frac{1}{4} N_O \lambda \ell \left\{ \sqrt{1 + \frac{4}{\lambda^2} \left(\frac{{}_tN - 2S_O}{N_O} \right) \left(1 - \frac{{}_tN - 2S_O}{N_O} \right)} - 1 \right\}. \quad (24)$$

2.2. Ultimate Strength of Reinforced Concrete Beam-column Subject to Simple Beam Type Loading

Considerable number of specimens have been tested under simple beam type loading, and according to these experimental results[1] the strength of a simple-beam type specimen differs considerably from that of the specimen subject to anti-symmetrical bending. For these reasons, the ultimate strength of a reinforced concrete beam-column subject to simple-beam type loading is analyzed here. Of cource, equations obtained here can directly be applied to symple-beam or cantilever type structures.

To begin with, characteristics of these two loading systems are discussed qualitatively referring to Fig.4.

As for the specimen subject to anti-symmetrical bending, the imaginary diagonal compression field could touch point A to carry larger shear force. On the other hand, as for a simple beam type specimen, it is impossible the diagonal compression field to touch the point A unless sufficient main reinforcing bars are provided to counterbalance the bending moment produced by the compression stress of the diagonal member, because at point A the boundary condition of bending moment is $M = 0$.

On this reason, if the lengths of the members and other dimensions are equal, ultimate shear strength of the specimen subject to anti-symmetrical bending is larger than that of the specimen subject to simple-beam type loading unless main reinforcing bars are not sufficiently provided to the specimen.

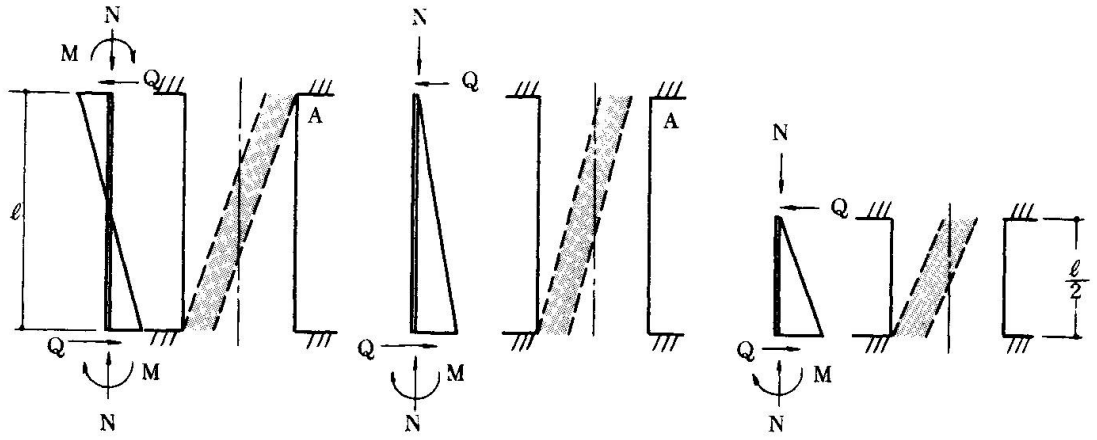

(a) Beam-column under Anti-symmetrical Bending (b) Beam-column under Simple Beam Type Loading (c) Simple Beam Type Specimen with Same Parameter M/QD to Fig.4(a)

Fig.4 Predicted Inclinations of the Diagonal Compression Fields Corresponding to the Various Loading Systems

Figs.4(a) and (c) show the differences of models under the same condition of the parameter M/QD. Under this condition a simple beam type specimen carry larger shear than that of the specimen subject to anti-symmetrical bending with equal dimensions, because the compression field of the former can be drawn nearer to the edge of the section at point M = 0 corresponding to the amount of the main reinforcing bars, while that of the latter always remains at the center of the section.

2.2.1. Bending Moment and Shear Force Carried by Web Reinforcement System

According to the same method descrived in section 2.1.1., the ultimate loading capacity of a web reinforcement system is deduced with the same equations (1), (2) and (3), though under this loading condition $\alpha = P_W \cdot {}_W\sigma_y \cdot b\ell/T_y$. Because the relationship ${}_WM = \ell \cdot {}_WQ$ exists while in section 2.1.1. ${}_WM = \ell \cdot {}_WQ/2$.

2.2.2. Bending Moment and Shear Force Carried by the Compression Field

Based on the boundary condition M = 0 at point A and the equilibrium of forces, referring to Fig. 5(a), the bending moment at point B can be derived as follows.

$$ {}_tM = \lambda N_O \cdot \ell \left\{ \sqrt{1 + \frac{({}_tN + S + S')N_O + \gamma(S - S')N_O - ({}_tN + S + S')^2}{(\lambda N_O)^2}} - 1 \right\} \qquad (25) $$

and the corresponding shear force across the section is

$$ {}_tQ = {}_tM/\ell \ . $$

where; $\gamma = {}_rd/D$

According to the lower bound theorem, chord forces S and S' which maximize the moment ${}_tM$ should be obtained. The derived equations are as follows.

Region I	${}_tN \leq \frac{1-\gamma}{2} N_O - 2S_O$	$S = S_O,\ S' = S_O$
Region II	$\frac{1-\gamma}{2} N_O - 2S_O < {}_tN \leq \frac{1-\gamma}{2} N_O$	$S = S_O,\ S' = \frac{1-\gamma}{2} N_O - S_O - {}_tN$
Region III	$\frac{1-\gamma}{2} N_O < {}_tN \leq \frac{1+\gamma}{2} N_O$	$S = S_O,\ S' = -S_O$
Region IV	$\frac{1+\gamma}{2} N_O < {}_tN \leq \frac{1+\gamma}{2} N_O + 2S_O$	$S = \frac{1+\gamma}{2} N_O + S_O - {}_tN,\ S' = -S_O$
Region V	$\frac{1+\gamma}{2} N_O + 2S_O < {}_tN$	$S = -S_O,\ S' = -S_O$

As the compression field can not protrude beyond member width, following condition must be satisfied.

$$ {}_tN^2 - [N_O - 2(S+S')]\ {}_tN - (S+S')N_O + (S-S')\gamma N_O + \frac{(S-S')^2}{\lambda'^2} + (S+S')^2 \leq 0 \qquad (26) $$

where; $\lambda' = \ell/{}_rd$

If this condition is not satisfied, a model where the compression field touches point A is supposed as shown in Fig.5(b). Satisfying the boundary condition and the equilibrium of forces of this model, the bending moment at point B ${}_tM$ is derived as follows.

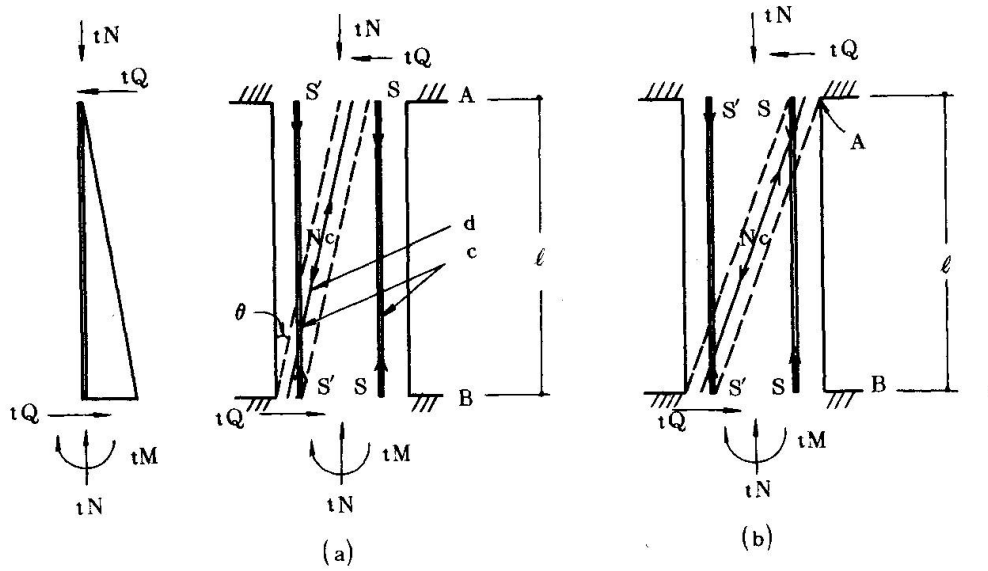

Fig.5 Equilibrium of Compression Field Model Subject to Simple Beam Type Loading

$$ {}_tM = N_O \cdot \ell \frac{\tan\theta}{1+\tan^2\theta}(1-\lambda\tan\theta) \tag{27} $$

The inclination of the diagonal compression field $\tan\theta$ which maximize ${}_tM$ can be obtained by the following equations.

Region VI $\quad {}_tN \leq \frac{N_O}{2}[1+\lambda'(\sqrt{\lambda^2+1}-\lambda)] - 2S_O$.

$$ \tan\theta = \frac{N_O(\lambda'-\lambda)}{2(N_O\lambda\lambda'+2S_O+{}_tN)}\left\{\sqrt{1+\frac{4(N_O\lambda\lambda'+2S_O+{}_tN)(N_O-2S_O-{}_tN)}{N_O^2(\lambda-\lambda')^2}}+1\right\} \tag{28} $$

Region VII $\quad \frac{N_O}{2}[1+\lambda'(\sqrt{\lambda^2+1}-\lambda)] - 2S_O < {}_tN < \frac{N_O}{2}[1-\lambda'(\sqrt{\lambda^2+1}-\lambda)] + 2S_O$

$$ \tan\theta = \sqrt{\lambda^2+1}-\lambda \tag{29} $$

Region VIII $\quad {}_tN \geq \frac{N_O}{2}[1-\lambda'(\sqrt{\lambda^2+1}-\lambda)] + 2S_O$

$$ \tan\theta = \frac{N_O(\lambda'+\lambda)}{2(N_O\lambda\lambda'+2S_O-{}_tN)}\left\{-\sqrt{1-\frac{4(N_O\lambda\lambda'+2S_O-{}_tN)(N_O+2S_O-{}_tN)}{N_O^2(\lambda+\lambda')^2}}+1\right\} \tag{30} $$

Loading capacities on these regions are obtained substituting above descrived values for $\tan\theta$ into Eq.(27).

In region VII the ultimate strength of the member is governed by the compressive failure of the concrete diagonal, while the chord members remain elastic. This mode of failure can be difined as the shear failure. For the range of axial force in region VII ${}_tM$ and ${}_tQ$ keep constant values as follows.

$$ {}_tM = \frac{N_O \cdot \ell}{2} (\sqrt{\lambda^2 + 1} - \lambda) \qquad (31) $$

$$ {}_tQ = \frac{N_O}{2} (\sqrt{\lambda^2 + 1} - \lambda) \qquad (32) $$

This region corresponds to region II in section 2.1.2.

2.2.4. Example

M - N interactions and Q - N interactions of reinforced concrete beam-columns with the section as shown in Fig.6(a) are shown in Figs.6(b) and (c) respectively evaluated according to the foregoing analysis.

According to this analysis, as parameter ℓ/D increases, the ultimate end moment M increases and "shear failure" region where moment capacity keep a constant value for the change of axial force N decreases. Referring to Fig.6(c), it can be understood that the ultimate shear capacity of the specimen subject to anti-symmetrical bending is larger than that subject to simple beam type loading with equal values of $\lambda(\ell/D)$.

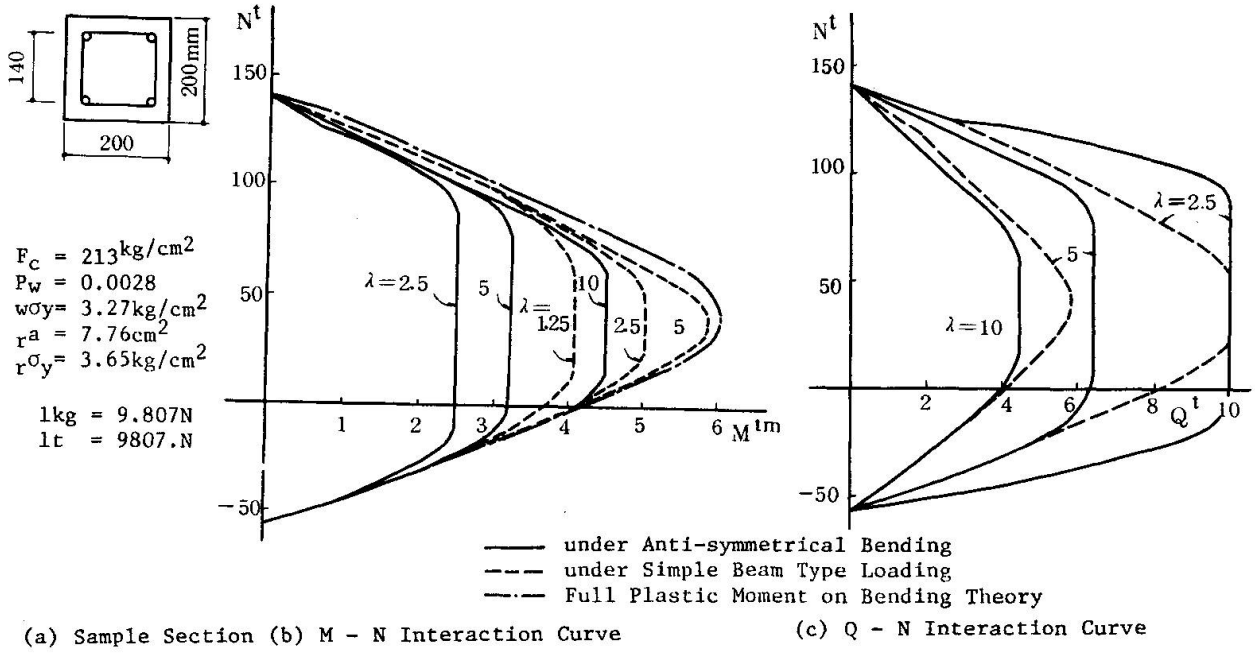

(a) Sample Section (b) M - N Interaction Curve (c) Q - N Interaction Curve

Fig.6 Example

2.3. Ultimate Strength of a Reinforced Concrete Member Subject to Shear and Axial Force without Bending

Mattock et.al.[2] investigated the shear transfer strength of push-off specimens shown in Fig.7 supposing the shear transfer mechanism of precast concrete connections. The shear strength of such a reinforced concrete member subject to shear and axial force without bending is analyzed here making use of the analogical concept of diagonal compression field model for a beam-column descrived in section 2.1.2.

The specimen shown in Fig.7(a) corresponds to the beam-column shown in Fig.3 making the length of it sufficiently small. X - X′ axis in Fig.7 corresponds to the longitidinal axis of the beam-column shown in Fig.3. The main reinforcing bars in Fig.3 correspond to the shear reinforcing bars shown in Fig.7.

The equations (11), (13) and (18) can be transformed into (33), (34) and (35) substituting $N_O = bD \cdot F_C$, ${}_tN = bD\sigma_O$, ${}_tQ = \tau_u bD$, and $2S_O = P_S \cdot \sigma_y \cdot bD$ and also replacing $\lambda = \ell/D$ by 0. Where;

- σ_O : mean value of compressive stress on the shear plane
- τ_u : mean value of ultimate shear stress on the shear plane
- P_S : shear reinforcement ratio
- σ_y : yield point of reinforcement

Eqs.(33), (34) and (35) are thus derived equations to calculate the ultimate shear strength and the corresponding inclination of the diagonal for reinforced concrete member subject to shear and axial force without bending.

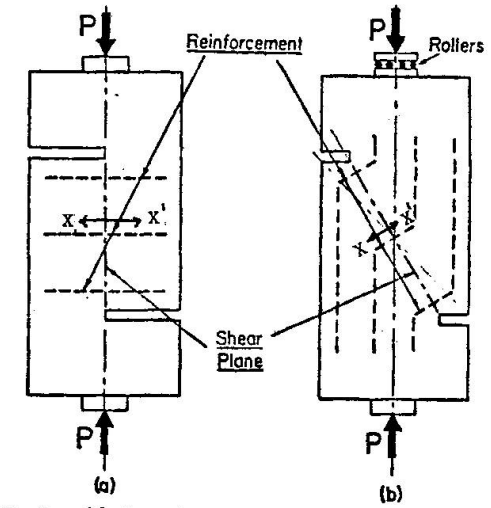

Fig.7 Loading Systems

Region I $\quad \sigma_O \leq \dfrac{F_C}{2} - P_S \cdot \sigma_y$

$$\tau_u = (P_S \cdot \sigma_y + \sigma_O) \cdot \sqrt{\frac{F_C}{P_S \cdot \sigma_y + \sigma_O} - 1} \qquad (33)$$

$$\tan\theta = \sqrt{\frac{F_C}{P_S \cdot \sigma_y + \sigma_O}}$$

Region II $\quad \dfrac{F_C}{2} - P_S \cdot \sigma_y < \sigma_O \leq \dfrac{F_C}{2} + P_S \cdot \sigma_y$

$$\tau_u = \frac{F_C}{2} \qquad (34)$$

$$\tan\theta = 1$$

Region III $\quad \sigma_O > \dfrac{F_C}{2} + P_S \cdot \sigma_y$

$$\tau_u = (-P_S \cdot \sigma_y + \sigma_O) \cdot \sqrt{\frac{F_C}{-P_S \cdot \sigma_y + \sigma_O} - 1} \qquad (35)$$

$$\tan\theta = \sqrt{\frac{F_C}{-P_S \cdot \sigma_y + \sigma_O} - 1}$$

As shown in Fig.3 main reinforcing bars of the beam-column are located at each side of the section, while in the specimen shown in Fig.7 reinforcing bars are uniformly distributed. Yet, the strength is not affected with the locations of reinforcements as can be understood in Eq.(9). For this reason the substitution $2S_O = P_S \cdot \sigma_y \cdot bD$ is capable.

As mentioned in section 2.1.2. reinforcements yield by tension in region I, by compression in region III while they remain elastic in region II.

3. EXPERIMENTAL VERIFICATIONS

3.1. Strength of Reinforced Concrete Beam-columns

The prediction on this analysis are compared with experimental results of 877 beam-column specimens tested recently in Japan[1]

The experimental results of the specimens subject to anti-symmetrical bending in region II are compared with the prediction in Fig.8. As the vertical axis of Fig.8 shows the strength of the diagonal compression field, the modified experimental value Q_e' is computed by substructing the value ${}_wQ$ calculated with Eq.(1) from the experimental value Q_e. The experimental results agree satisfactory with the predicted tendency that the shear strength increases, as the paramater ℓ/D decrease.

All the specimens in region II are reported as shear failure from the experimentalists, though all the reported shear failure specimens are not in region II, but also scattered in the neighbourhood of region II. Main reason of this fact is supposed that they call it shear failure even if main reinforcing bars have yielded.

The ratios of experimental values Q_e to theoretical values Q_c are shown in Fig.9 ~ Fig.14 as to all the beam-column specimens, with the parameters ℓ/D and F_c. In table 1, mean values m and coefficients of variation σ/m concerning Q_e/Q_c are shown. Also in table 1 these values of empirical equations (36) and (37) for shear failure specimens, and Eq.(38) for flexure failure specimens are shown. These equations are commonly used in Japan[3].

$$Q_u = \left\{ \left(0.9 + \frac{\sigma_o}{250}\right) \frac{0.23 k_u k_p (F_c+180)}{h_o/d + 0.23} + 2.7\sqrt{P_w \cdot w\sigma_y} \right\} \cdot bj \qquad (36)$$

$$Q_u = \left\{ \frac{0.23 k_u k_p (F_c+180)}{h_o/d + 0.23} + 0.1\sigma_o + 2.7\sqrt{P_w \cdot w\sigma_y} \right\} \cdot bj \qquad (37)$$

Table 1 Comparison between Culculated and Experimental values

Beam-columns subject to Anti-symmetrical Bending

1 Shear Failure Specimens				
	Beam(112)		Column(57)	
	m	σ/m	m	σ/m
Writers	0.941	0.155	1.057	0.178
Eq.(36)	1.083	0.165	0.994	0.199
Eq.(37)	0.975	0.165	0.949	0.160
2 Flexure Failure Specimens				
	Beam(35)		Column(231)	
	m	σ/m	m	σ/m
Writers	1.149	0.121	1.096	0.118
Eq.(38)	1.099	0.131	1.008	0.104
3 Bond Failure Specimens (32)				
	m	σ/m		
Writers	0.938	0.099		
Eq.(36)	0.862	0.145		
Eq.(38)	0.857	0.113		

m ; mean value
σ/m ; coefficient of variation

Simple Beam Type Specimens

1 Shear Failure Specimens				
	Beam(45)		Column(119)	
	m	σ/m	m	σ/m
Writers	0.858	0.150	1.069	0.133
Eq.(36)	0.944	0.160	0.840	0.137
Eq.(37)	0.850	0.160	0.860	0.110
2 Flexure Failure Specimens				
	Beam(94)		Column(152)	
	m	σ/m	m	σ/m
Writers	1.178	0.146	1.179	0.128
Eq.(38)	1.202	0.183	1.081	0.152

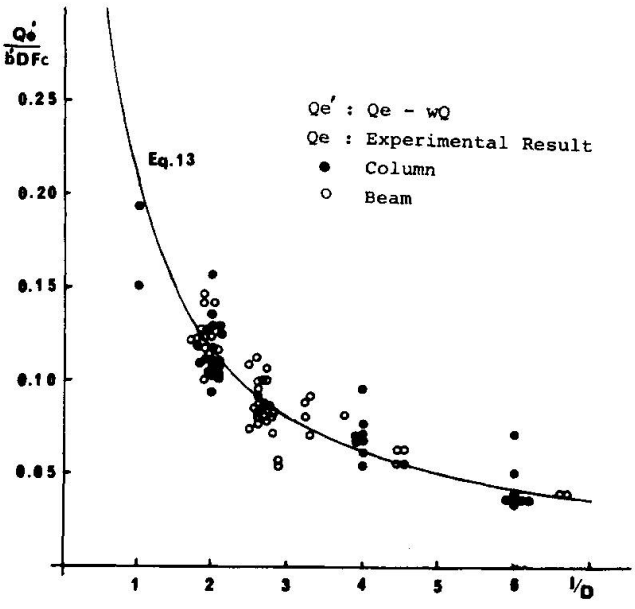

Fig.8 Comparison between Tests and Theory on Specimens Subject to Anti-symmetrical Bending in Region II

$$M_u = 0.8_r a \cdot {}_r\sigma_y \cdot D + 0.5\sigma_o \cdot bD^2 (1 - \frac{\sigma_o}{F_c}) \quad (38)$$

Where;

ku, kp = coefficients depending on the size of section and tensile reinforcement ratio respectively

h_o = shear span

d = distance from extreme compression fiber to centroid of tension reinforcement

j = distance between the centroid of compression and tension stress

In this section a shear failure specimen is defined as the specimen reported as shear failure from the experimentalist and of which ultimate strength does not reach its ultimate flexure strength calculated by Eq.(38).

Seeing the above mentioned comparisons between experimental and theoretical values following facts are evident.

1) This analysis predicts the ultimate strength of shear failure specimens with equal accuracy as those of the empirical equations (36) and (37), and predicts the ultimate strength of flexure failure specimen a little conservatively, however coefficients of variation σ/m of this analysis for Q_e/Q_c are almost equal with those of Eq.(38).
2) This analysis predicts the ultimate strength of the specimens subject to anti-symmetrical bending and simple beam type loading with almost equal accuracy. Therefore the modelings on this theory as to the characteristics of each loading systems are supposed to be appropriate.

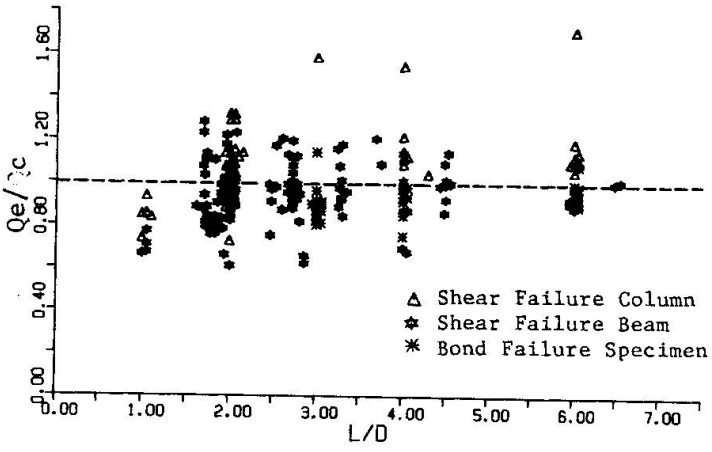

Fig.9 Shear and Bond Failure Specimens Subject to Anti-symmetrical Bending

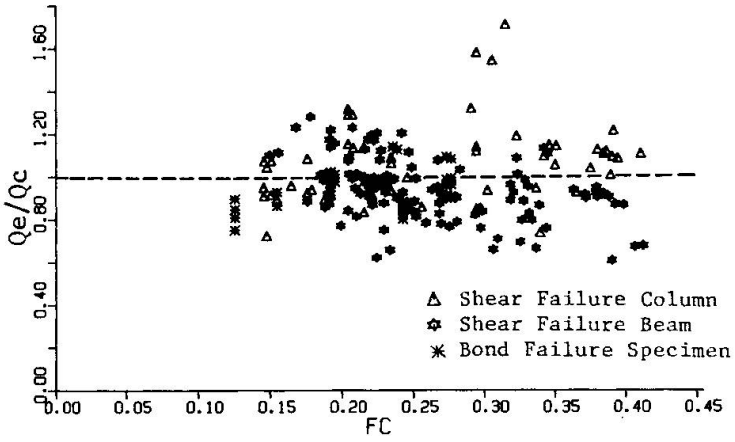

Fig.10 Shear and Bond Failure Specimens Subject to Anti-symmetrical Bending

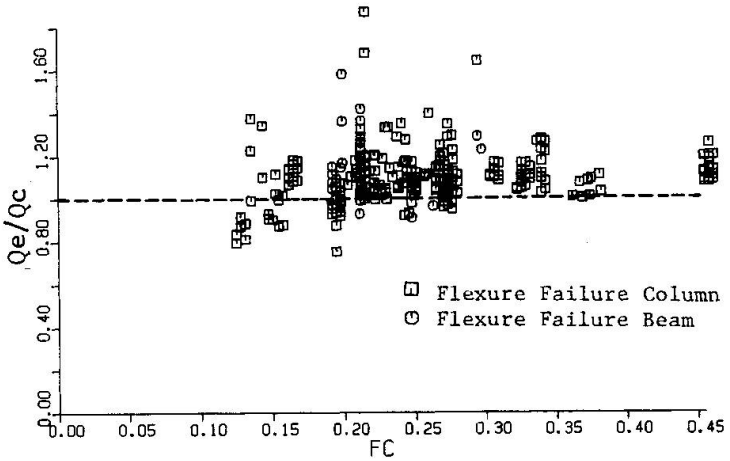

Fig.11 Flexure Failure Specimens Subject to Anti-symmetrical Bending

3) The strength of shear failure beams in experiments are generally a little smaller than that of the theoretical one.
4) Though the diagonal compression field is supposed to be formed only in a "short" beam-column intuitively, this theory predicts the ultimate strength fairly well without affected with the change of the parameter ℓ/D.
5) The accuracy of the theory is not also affected with parameter F_c, though it is often considered that the shear strength is the function of $\sqrt{F_c}$ and not F_c.
6) Though this analysis over-estimates the resistance of a shear bond failure specimen a little, coefficient of variation σ/m for Q_e/Q_c is small. small.

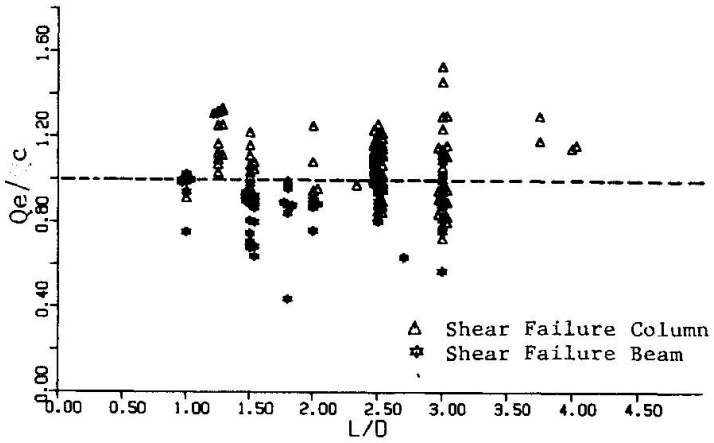

Fig.12 Shear Failure Specimens Subject to Simple beam type Loading

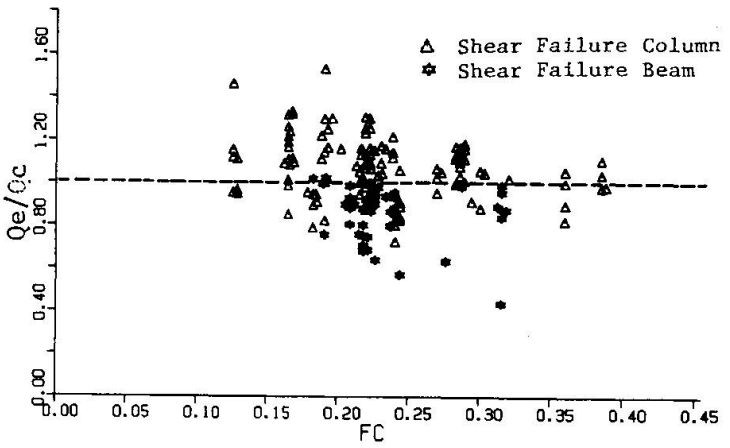

Fig.13 Shear Failure Specimens Subject to Simple Beam Type Loading

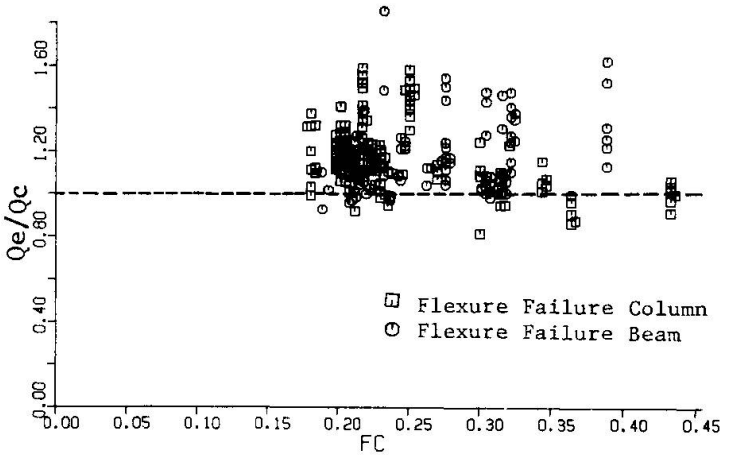

Fig.14 Flexure Failure Specimens Subject to Symple Beam Type Loading

3.2. Ultimate Strength of Reinforced Concrete Member Subject to Shear and Axial Force without Bending

The Experimental results tested using the loading apparatus shown in Fig.7 and writers' prediction by Eq.33 are shown in Fig.15.

Marks ○● show the test results by Mattock et.al.[2] and marks △ show the test results by Aoyagi[4] et. al.

Though the theoretical prediction by Eq.33 show a fairly good correlation to the test results, it overestimates the resistance perhaps due to the fact that the plastic stress can not be sufficiently redistributed in such an extremely short length of specimen. A reduction factor of 0.78 may be applied to Eq. 33 to obtain the modified semi-empirical formula which is shown by dashed line in Fig.15.

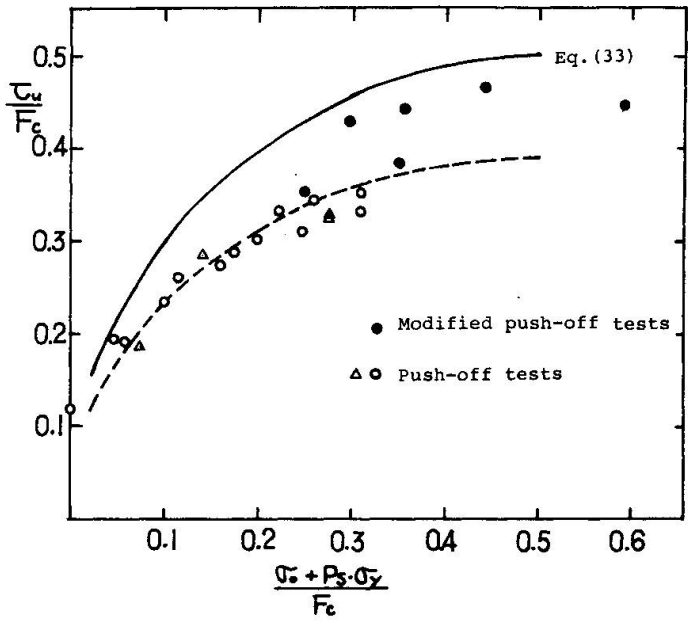

Fig.15 Comparison Between Test Results and Calculated Values

4. CONCLUSION

The ultimate strength of reinforced concrete members was analyzed based on the concept of compression field. In this analysis, the interaction among bending moment, axial force and shear force was evaluated using a simple mathematical model. Though proposed theory is simple, it can explain the test results of reinforced concrete beam-columns and precast concrete connections fairly well on a unified theory.

REFERENCES

[1] Hirosawa "Strength and Ductility of Reinforced Concrete Members", Report of the Building Research Institute No.76 (in Japanese)

[2] Mattock, Hawkins, "Shear Transfer in Reinforced Concrete Recent Research" PCI Journal/ March-April 1972

[3] Architectural Institute of Japan, AIJ Standard for Structural Calculation of Reinforced Concrete Structures, 1971 (in Japanese)

[4] Aoyagi et.al., "Full Scale Model Push-off Test of Reinforced Concrete Block with 51 mm dia. Deformed Steel Bars", Trans. of the 6th International Conference on Smirt J/4/7 1981

Bridging the Gaps: an Intermezzo[1])

Une nouvelle approche dans la recherche

Ueberbrückung von Gräben: ein Intermezzo

JOHAN BLAAUWENDRAAD
Professor of Civil Engineering
Delft University of Technology, Delft
Rijkswaterstaat - Bouwresearch, Utrecht, The Netherlands

SUMMARY
There often exist serious communication gaps between researchers and designers and even between researchers themselves.
The Dutch experience in this field confirms this statement, and it is supported by the general discussion during the colloquium.
To bridge these gaps, a new approach in research is needed, which is explained here.

RÉSUMÉ
Il y a souvent des abîmes de communication entre les chercheurs et les auteurs de projets et même entre les chercheurs eux-mêmes.
L'expérience néerlandaise dans ce domaine confirme cette affirmation qui est confirmée par la discussion générale de ce séminaire.
Pour jeter un pont entre les chercheurs et les auteurs de projets, une nouvelle façon d'aborder la recherche est nécessaire, qui fait l'objet de cet article.

ZUSAMMENFASSUNG
Es bestehen oft breite Kommunikationsgräben zwischen Forschern und entwerfenden Ingenieuren, ja sogar selbst zwischen Forschern.
Diese Behauptung wird bestätigt durch die einschlägige niederländische Erfahrung, als auch durch die allgemeinen Diskussionen an diesem Kolloquium.
Um diese Gräben zu überbrücken, ist ein neuer Ansatzpunkt für die Forschung nötig, welcher hier kurz erörtert wird.

[1]) Lecture presented to fill the gap caused by the cancellation of the lecture by Prof. Valente, Italy, who was prevented to come.

1. ON PLATEAUS, GAPS AND LONELY PEOPLE

The general discussions during this colloquium concentrated among others on the relation between scientific people in the research field and designers in the engineering society. Many interesting remarks were heart, which made us remember in what way we discussed similar points in The Netherlands. A series of pictures will be shown to illuminate this, providing plenty of opportunity to draw the attention to corresponding comments raised by attendents of this colloquium.
It is a manyfoldly heart complaint that only a poor interaction exists between the research society and design practice. Both parties are living on their own plateau and have their own language (Fig. 1); the researcher will formulate his work and results in mathematical terms, but the designer needs information on structures to be erected.

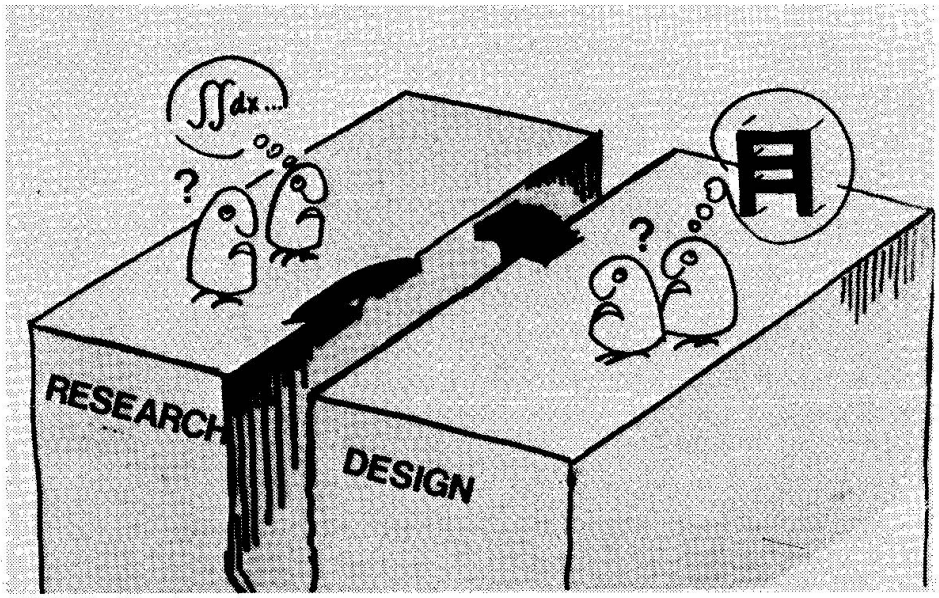

Fig. 1. A deep gap exists between research and design practice. Well-intentioned trials to bridge the gap often fail.

A deep gap proves to exist between the two plateaus. To do justice it must be said that individuals are found on both plateaus that seriously try to bridge this gap. However, each is doing so starting from his own point of view and the erected bridge parts do not meet each other properly .
This is also displayed in Fig. 1.
It may even be worse. In many cases research people hardly understand each other! Within the research society gaps can exist also. A particular research discipline may develop a so specialistic jargon, that colleagues in an adjacent discipline cannot communicate with them at all. It was felt in The Netherlands that such a situation can initiate between the research in reinforced concrete structures and the research in applied and structural mechanics. Fig. 2 shows the separate plateaus for the concrete people and the mechanics people.
This figure now displays the three different plateaus which have been mentioned earlier in the symposium by prof. Scordelis and prof. Van der Vlugt.

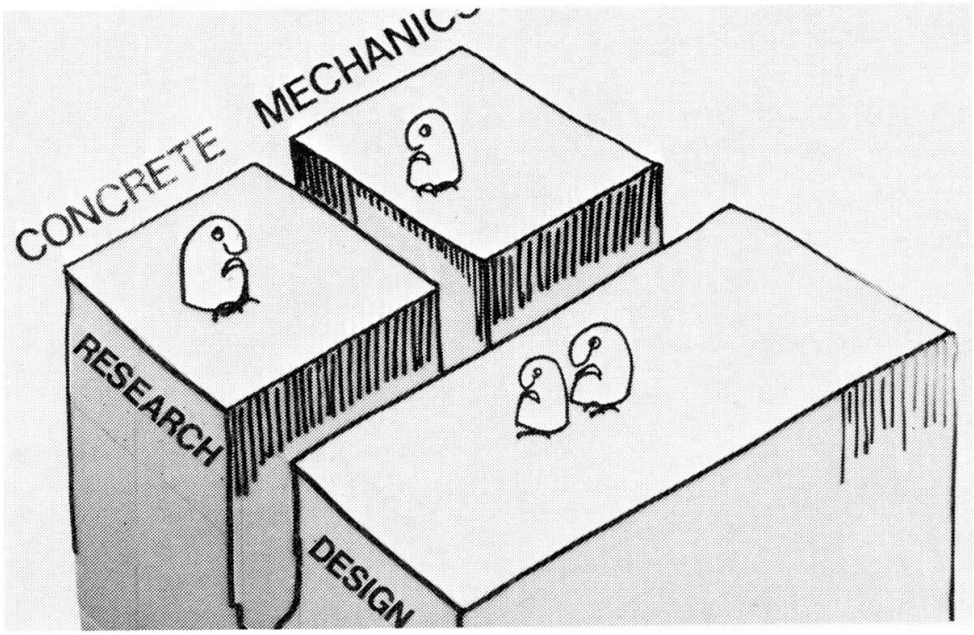

Fig. 2. In some research disciplines such a jargon may develop, that colleagues in an adjacent discipline hardly can communicate any more. Another gap.

Let us consider which experience has been gained in the two research disciplines mentioned above. The concrete research (see Fig. 3) has mainly concentrated on small scale model tests in the laboratory and has indeed done a good job in the past. We might entitle the way in which the concrete doctor examines his patient 'surface view'. Deflections, crack patterns and average strains can be recorded, but one still needs quite a bit of nerve to derive from such data what exactly is happening internally in the structure.

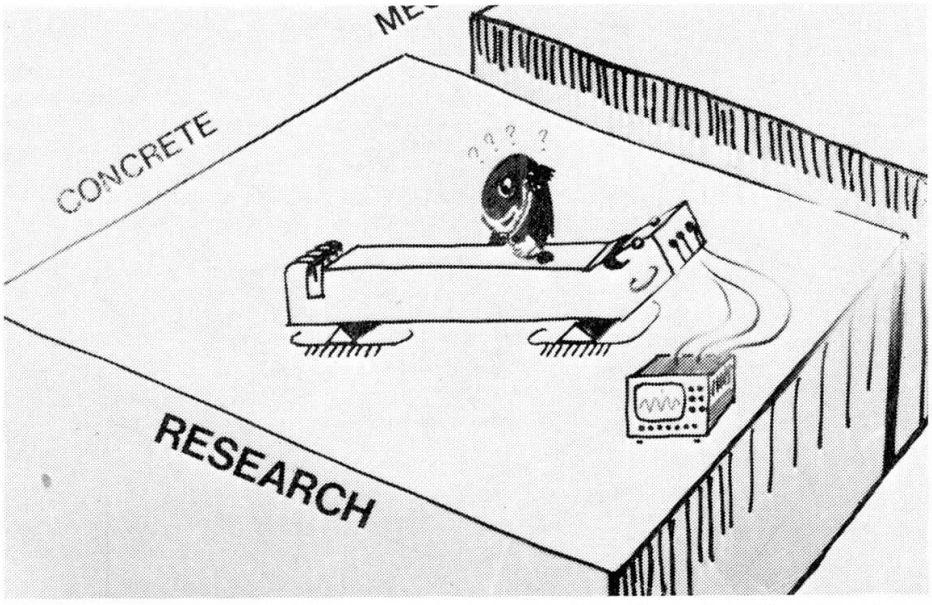

Fig. 3. In conventional concrete research a total structure is investigated. The concrete specialist is very capable for 'surface view'.

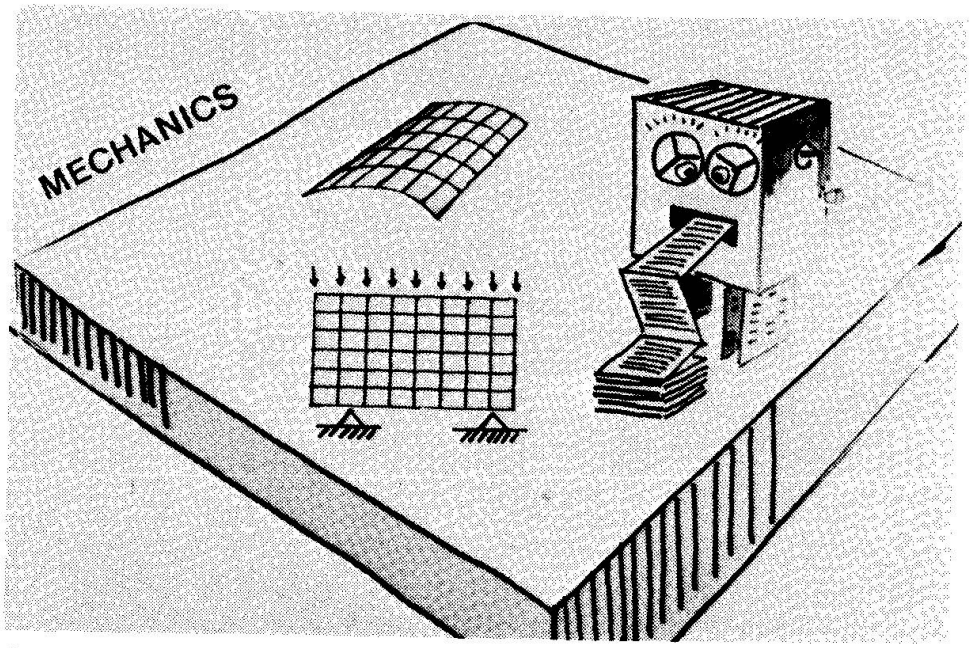

Fig. 4. Nowadays the mechanics doctor uses a dissecting-knife for his observations. The patient is firstly splitted in small separate basic components, the elements, which then are processed.

Let us now visit the mechanics plateau (Fig. 4). The old-day methods of differential equations have been replaced by analytical procedures of which the finite element method is the most familiar one. The mechanics doctor now handles a dissecting-knife in his observations and splits his patient in small separate parts, the elements. He is more like a specialist for internal diseases, and therefore clearly differs in his method from the surface view of his colleague in the concrete society.

The initiators of the Dutch joint project 'betonmechanica' (Concrete Mechanics) are aiming for bridging the gap between the two research plateaus (Fig. 5). The intention is to combine the advantages of both plateaus and to eliminate the disadvantages. How to achieve that?

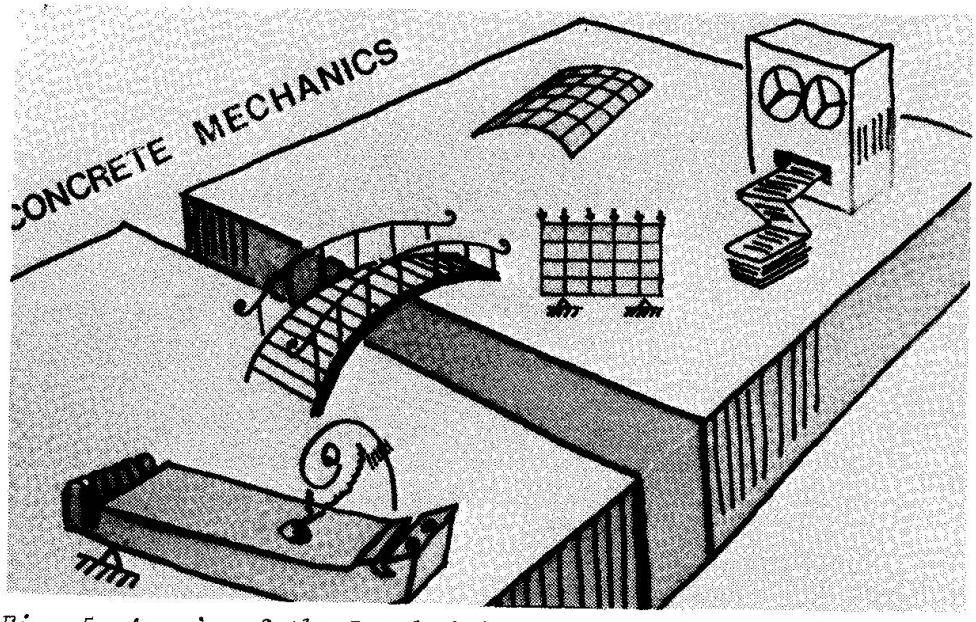

Fig. 5. An aim of the Dutch joint project 'betonmechanica' is to bridge the gap between the two research plateaus for concrete and mechanics.

2. A NEW APPROACH IN RESEARCH IS NEEDED

To answer the question at the end of the previous chapter we more seriously examine the two procedures again. The study of the real world of structures in a (small scale) laboratory model typically refers to a total structure, or a total structural member (beam, column). In this approach we have a prompt registration of the total behaviour, see Fig. 6. The advantages are clear. The ultimate aim is reached directly and design recommandations may be induced immediately. However, also disadvantages exist. Problems arise of unique interpretation, having normally only few signals but a lot of parameters to be solved. Above that, we lack detailed information and therefore do not get basic understanding.

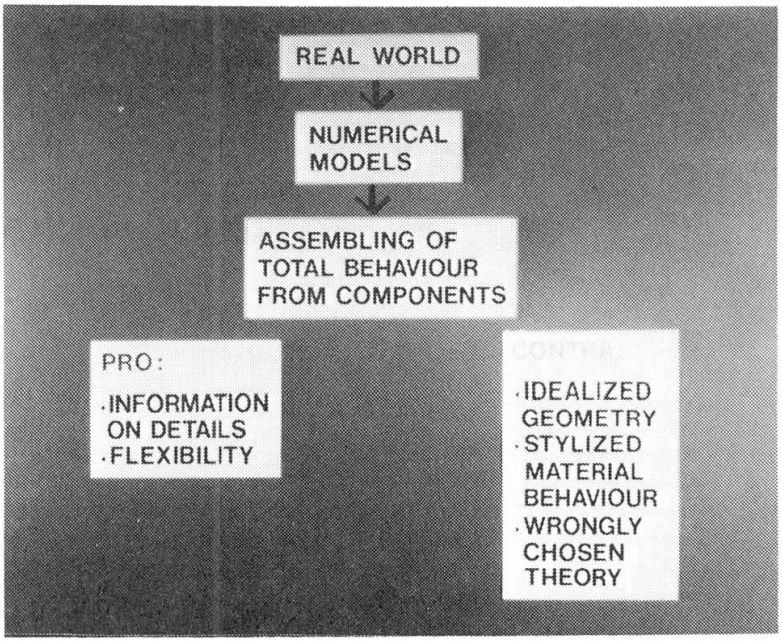

Fig. 6. Typical aspects of conventional model scale tests in a laboratory.

When we study the real world of structures by numerical models, we use the behaviour of many small separate components and assemble the behaviour of a total structure or structural member from these components (Fig. 7). The advantage of this approach is that we get information on details. In a flexible way also structures of other shapes can be examined. But some severe drawbacks exist as well. You have to idealize the geometry and to stylize the material behaviour. In cases where you have to choose some theory, you may choose the wrong one.

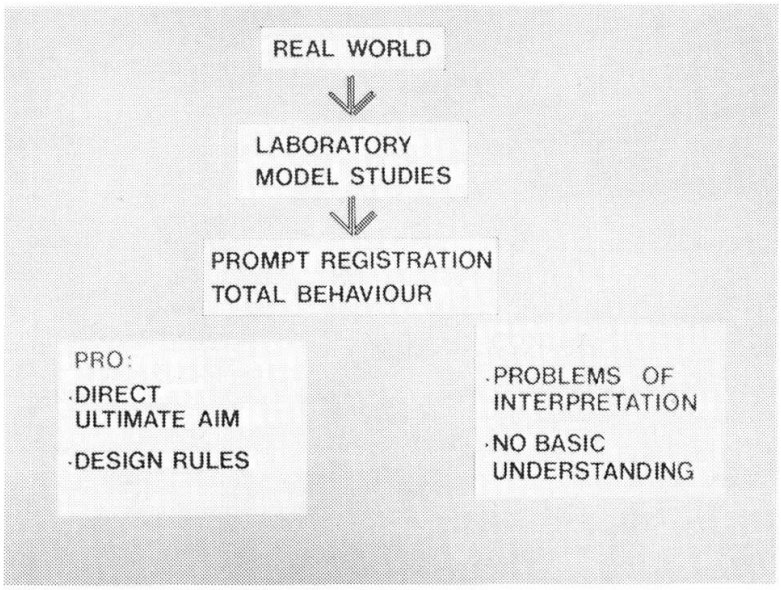

Fig. 7. Typical aspects of the nowadays use of numerical models.

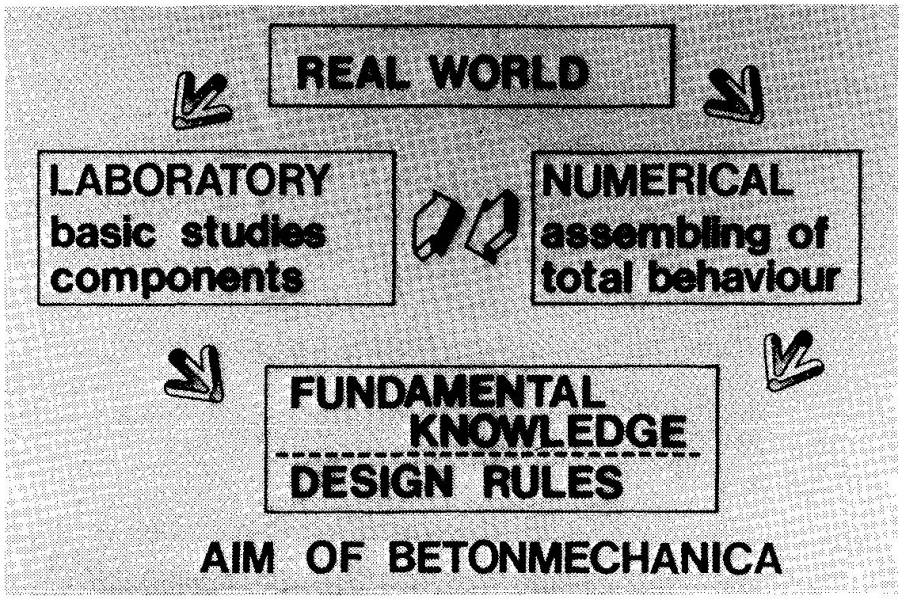

Fig. 8. Goal of 'betonmechanica': interaction and co-operation of the modern concrete research and the new possibilities of the numerical methods in structural mechanics.

When you compare the two approaches of laboratory models and numerical models it can be concluded that they are complementary to each other. The aim of the Dutch project 'betonmechanica' is to combine the advantages and to eliminate the drawbacks. So, the specialists in concrete matters and the specialists in mechanics shake hands (Fig. 8). You can do so by concentrating on basic studies for small component behaviour in the laboratory and by exploring the analytical techniques to assemble the total behaviour. Along these lines one can hope to increase fundamental knowledge. Later on, the new knowledge may form a firm basis to derive design rules for practizing engineers.
It is important to realize that the concrete specialists not just do another type of research, but that they must present their results in a different way as well. Prof. Kerstle already focussed attention on this point. The concrete researcher must be aware of the way in which his results are used by the structural analyst. This will influence the set up of his experiments and will mean a way of presentation of results which was not familiar to him in the past.

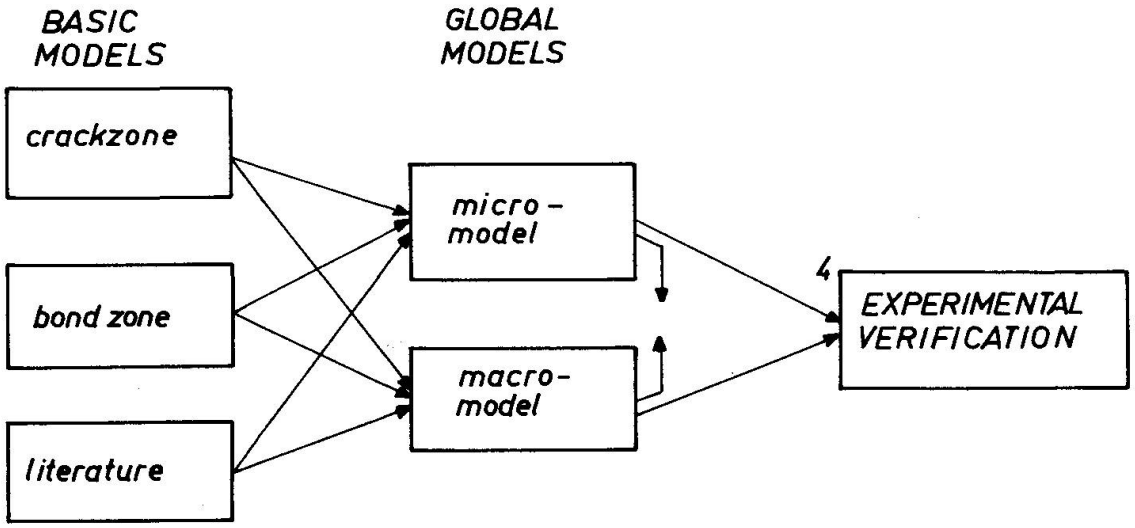

Fig. 9. The results of material basic model studies (1st colloquium day) are fed in the analytical global models (2nd colloquium day). The global models must be varified using experimental investigations (3rd colloquium day).

The studies on *basic models* concentrate on the behaviour of the crack zone and the bond zone, see the left part of Fig. 9. This was more or less the topic of the first day of the colloquium. Other basic studies are found in the literature as well, for instance on the anchoring zone. The numerical models, in which we assemble the total behaviour of a structure from its basic models, can be called *global models*. In this colloquium we noticed that a lot of people distinguish between Micromodels and Macromodels, see mid part of Fig. 9. This we also did in The Netherlands. In a Micromodel we really take in account all possible basic models. In this colloquium such Micromodels provide for single sharp crack analysis or discrete crack analysis. In a Macromodel, on the contrary, a smeared out approach for cracks is used. This area of interest was covered more or less in the second day of the present-day colloquium.
Finally we want to confront our global models with the results of *experimental investigations*, see the right hand part of Fig. 9. In the colloquium this was the subject-matter of the third day.

3. ON ORGANIZATION, FINANCES AND EXPECTATIONS

In many countries some type of coordination on the advanced mechanics of reinforced concrete structures has been achieved. A working commission of the American Society of Civil Engineers is well-known in this respect.
From the working papers of this colloquium and the explanation of prof. Okamura we can know that Japanese firms and universities joint together as well in Napra, a non-linear program research association. In The Netherlands a number of institutes , universities and organizations joint together in the project 'betonmechanica'. Other countries have similar modes of co-operation.
Such efforts clearly cost a lot of money.
In The Netherlands more than 8 million guilders (about 4 million dollars) will be spent in 8 years. Fig. 10 shows how the several partners contribute in these funds.

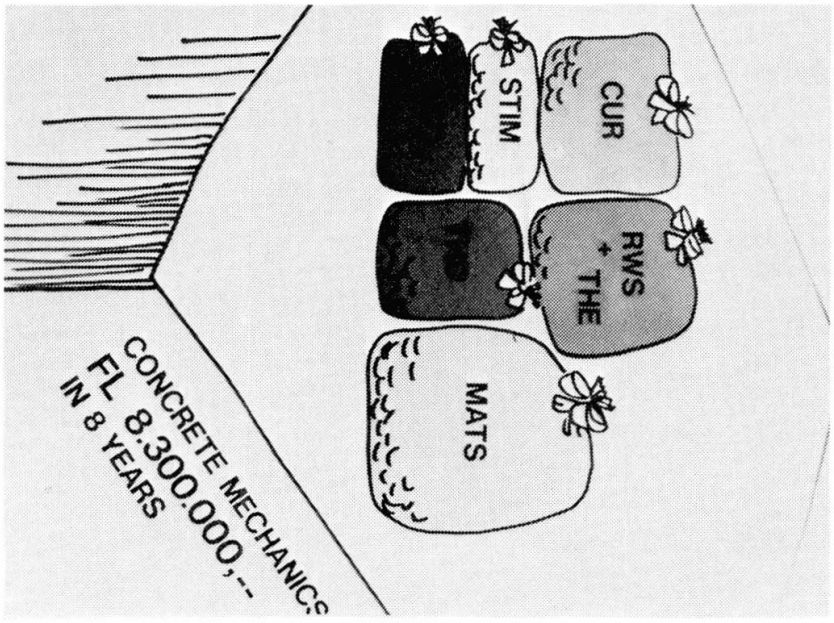

Fig. 10. To finance the joint project each contribution is welcomed.

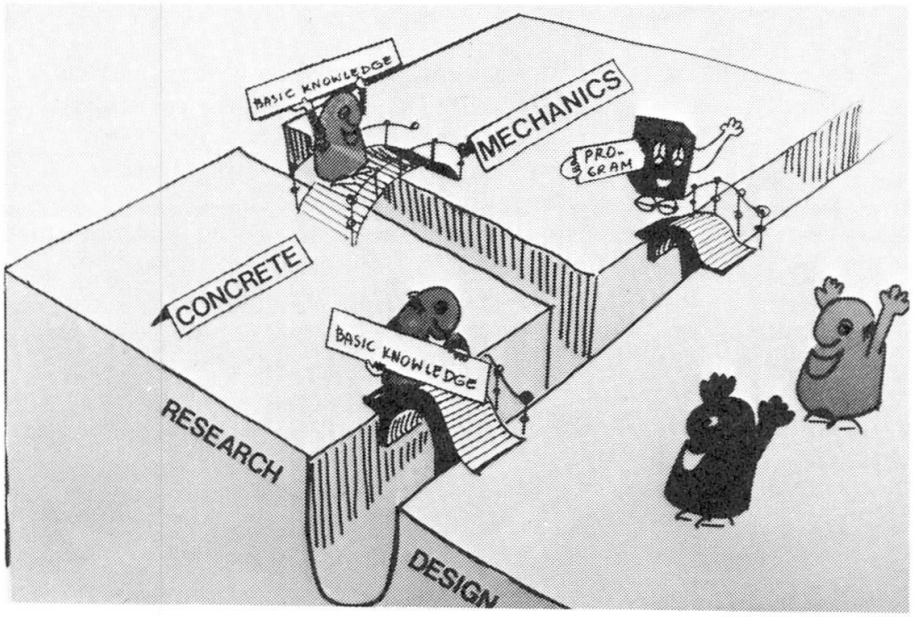

Fig. 11. The design practice looks forward to a positive final result. The newly gained knowledge will not fail of its effect on futural codes and can become available in the same time in computer programs for designing engineers.

Coming back to the plateaus and gaps at the beginning of this intermezzo, we give expression to good hopes on better communication in future between researchers, and on an improved interaction between research and design (Fig. 11). If the job is well done, the concrete research will result in much basic knowledge which immediately can be fed in numerical models. Such basic knowledge can also be made available to the design society in course of time, when it influences codes and specifications. The written programs can be placed at the disposal of designers likewise. We nourish great hopes that the sombreness of the persons at the several plateaus will change in joy in the future. And that intensive crossing of the newly built bridges may be seen.

Session 3, part 1: Applications and Experimental Verifications

Introduction by A.C. Scordelis, Chairman.

On Tuesday and Wednesday our speakers told us about the basic problems involved in material modelling and structural modelling, and perhaps they raised more questions than we have answered for the present time.

However, the ultimate aim of our work is its application to real structures that must be designed to have sufficient strength, stiffness and stability to meet the design requirements with respect to deflection and cracking under service load and time-dependent effects, and as well they must have a specified ultimate strength under design loads.

Those are our objectives.

If I may I would like to make a few historical comments about the finite element method; some of you may have heard some of these remarks from me before, but I am sure many have not.

Being from Berkeley, which has sometimes been referred to as the "birthplace of the finite-element method", my interest in the finite-element method goes back some 27 years, when my colleague, prof: Clough, returned to Berkeley after a summer working with the Boeing Airplane Company in Seattle, and set out talking about a new method for analyzing complex structures.

The method was ideally suited to the then newly available digital computers and to the matrix methods of analysis which were being developed.

In 1960, in a paper by Clough, he first gave the method the name "the finite element method" (f.e.m.)

The peal of the method to many of us at Berkeley, involved in structural analysis and design, was that the f.e.m. could be thought of in terms of a physical model, familiar to a structural engineer.

Of course, since that time tremendous developments have taken place in the application of the method to all kinds of problems, as well as to the establishment of a firm mathematical basis for the method.

It might be of interest to you, historically, that some of the earliest important applications of the method by the Berkeley group in the late fifties and early sixties was an analysis of cracking in many of the large, mass concrete dams, which were being built in the U.S. at the time. These were unreinforced, plain concrete structures.

On the other hand, while some of us thought that it could be applied to modelling a reinforced concrete structure, including cracking, it was not till about 1967 that the first paper, to my knowledge, was published on this type of application.

Since that time there has been a tremendous interest in the development in the field culminating in our colloquium here in Delft this week.

As I listened to the papers here during the last two days, I thought back to the first general conference on this subject, held in Montreal in 1972, almost ten years ago.

At that time I gave a state-of-the-art report and showed a table of problems to be solved. These problems are still with us: the composite material, cracking of the concrete, non-linear constitutive relationship, failure

We recognized these problems ten years ago and at that time I indicated that I thought that what was really needed was experimental research, so that we could get the necessary input to put into this computer program.

That was ten years ago. Well, much progress has been made in this area since the Montreal conference in 1972, as evidenced by the papers presented at this Colloquium.

Finally, I like to emphasize again, if I may, that our objective is really to be able to make these methods to design complex structures, such as the following example.
This happened to be a project I was a consultant on by 1968; it is a large hyperbolic shell in Portorico, spans 82 m, it is 4 in. thick and has edge beams.

At the time we used f.e.m. to design this structure and to analyse it, and we used linear-elastic solutions, and I was concerned about what happens if it cracks, if it creeps and what can go on in ten years later. Will we have the tools then?

And I think that I am still interested in the total structure. I think also that I hope very shortly I will be able to trace the total response of such a structure through its elastic and cracking, its inealastic and ultimate ranges, including material and geometric non-linearities, as well as the timedependent effects.

I think we are getting there. And this conference has taken us in that direction and I think we will continue to go.

DISCUSSION

Session 3, part 1: Applications and Experimental Verifications

Introductory Report by White/Gergeley, U.S.A.

Scordelis (U.S.A.): Professor White has shown to us the wide range of topics he covers and given us his impression as to what the future should hold for us. I should like to hear comments from the audience as to what should be the future direction of our efforts in the field of finite elements and concrete mechanics.

Gerstle (U.S.A.): I wonder how to incorporate micro-effects such as bond-slip and crack behaviour in a global analysis. As an example he refers to the approach of Prof. Collins and to the approach of Prof. Sarja which seems to be appropriate in a global model.

Hsu (U.S.A.): As the chairman, Prof. Scordelis, suggested to discuss about the development and use of the finite element method in the future, Prof. Hsu states that, rather than using the finite element method to predict experiments in advance (see also Collin's suggestion in the discussion of Session 2, part 2), the finite element method should be used to explain and understand the behaviour of the experimental results.

Blaauwendraad (The Netherlands): comments on the future use of the non-linear finite element method. He states that it is to be expected that the use of it will develop in the same way as the use of the linear (elastic) finite element method. That will be in two directions:
On one side, structures can be better understood which enables later on to develop simple design rules.
On the other side, the engineer becomes more familar with this type of analysis and so we will see an increased use of it. Moreover, because of better and cheaper hardware, the accessibility will increase and the use of more advanced methods will be stimulated.

Paper by Van den Beukel/Blaauwendraad/Merks/Monnier, The Netherlands

Braestrup (Denmark): Do you expect that the results from the beam specimens (plane stress) are representative for what is going on in a tunnel (plane strain)?

Monnier: We started with a simple approach and we realize that the behaviour of a beam is not the same as the behaviour of a slab.

Marti (Switzerland): I would like to suggest to give some additional information about the experimental details in the final report of this colloquium.

Monnier: I will do my best to fulfill your wishes.

Paper by Niwa/Maekawa/Okamura, Japan

Bazant (U.S.A.): If the concrete is uncracked, you have an isotropic stiffness matrix, yet your relationship between equivalent stress and strain corresponds to the total stress-strain relationship. If that is differentiated fully, you get a completely anisotropic form. Equations 17 and 6 do not seem to be compatible.

Maekawa: The reported stiffness matrix of uncracked concrete is not derived from this total strain formulation directly. It is difficult to differentiate the reported stress-strain relationship by analytical form. Therefore we defined the stiffness matrix so as to agree with the results which were calculated from the reported stress-strain relationship by numerical differentiation with reasonable accuracy. However, there exists the difference between the real stiffness and the assumed one. This difference is corrected by iterative calculation with rapid convergence.

Blaauwendraad (The Netherlands): Could Prof. Okamura explain what is meant by NAPRA (Non-linear Analysis Program Research Association)?

Okamura: NAPRA is a small group dealing with non-linear finite element method and concrete. It started about two years ago.

Abdel Rahman (U.K.): Is it not better to use a finer mesh instead of 5 by 5 Gauss points?

Niwa: Using 5 by 5 Gauss points, an underestimation of stress is avoided; also less computer time is needed.

Paper by Plauk/Hees, F.R.G.

Mehlhorn (F.R.G.): Did you compare your bond-slip test results to the test results of Doerr as presented in 1978 in Darmstadt?

Plauk: No, I did not. The bond investigations were done by Mr. Eifler who had compared the results of his bond slip tests with experimental observations obtained from 50 cm long excentrically reinforced tension members with the steel bar extending through the concrete without interruption. The agreement was excellent.

Macchi (Italy): Can you get with your approach plastic rotation in one section of the beam in the case of a constant moment?

Plauk: For this particular case I have no analytical results up to now, but if between single loads a constant moment area exists, you will get with the finite element approach a concentration of tensile stresses under the single loads, which causes cracks and plastic deformations in these cross sections. This is the reason why the proposed method will also work here.

Bergan (Norway): How can you model the S-shaped shear transfer with only one element between the cracks?

Plauk: Only if ultimate load is reached, it is possible to have one concrete element between two cracks, but also in this case our super-element, which actually consists of 4 single elements, continues to work properly.

Paper by Minami/Wakabayashi, Japan:

Braestrup (Denmark): A question to the paper of Minami and Wakabayashi. With a normal amount of shear reinforcement, the maximum strut angle is not 45°, it is lower. What are your comments?

Minami: Our paper mainly deals with a method for design and we intended to make simple equations. The problem of the angle of the compression strut is treated in detail in the paper of Shohara and Kato.

General discussion

Comments on future developments, as suggested by the chairman, Prof. Scordelis.

Elfgren (Sweden): Multinational structural design companies will quickly incorporate international codes, e.g. the CEB-FIP Model Code for concrete, in their programs for computer aided design. Furtheron they will design standard structures at prices that are very competitive at the expense of medium size national companies. To prevent such a development we must take care that the engineering society becomes familiar with the new methods. All companies and countries should have a possibility to take advantage of advanced computerized methods for design and analysis of reinforced concrete.

Saouma (U.S.A.): Structures where a few cracks are descisive, must be analysed with the discrete crack approach. If more cracks govern the behaviour, the smeared crack approach should be recommended.

Kotsovos (U.K.): Concrete is very sensitive to constraints. This results in higher strengths of the concrete in the constrained regions. Nobody has mentioned the contribution that these regions make to the overall strength of the structural member. If one is considering this contribution it would be found that probably e.g. aggregate interlock and dowel forces are not as important as is believed at the moment.

Meyer (U.S.A.): Referring to earlier remarks of Profs. White and Blaauwendraad, I am also looking forward to the moment when design engineers have their own personal computers, but at the same time I am aware of the danger of misuse of general analysis and design programs. Those familiar with computation know how often ordinary linear analysis programs are misused. Now imagine, releasing fully non-linear dynamic finite element programs for common use! We should use this kind of sophisticated technology only for very unusual structures, but mostly as a tool to educate ourselves, to learn how concrete behaves in order to develop simple methods suitable for design offices. These complicated programs that we have been discussing here will never be used in ordinary design offices.

Braestrup (Denmark): Cracks can occur even under pure compressive stresses. However in the finite element methods, as discussed in this colloquium, cracks are assumed to occur when the principal stress reaches a certain positive value, which is then interpreted as the tensile strength. How can that be?

Session 3, part 2: Applications and Experimental Verifications

Introduction by B.W. van der Vlugt, chairman (The Netherlands)

The first two days of this conference we have listened to the specialists on modelling of material properties, structures, mathematics. Now we are focussing on the questions of how this modelling can be interpreted and verified by experiments. A bridge is constructed over the gap between numerical specialism and the specialism on materials and structures; I think that it is one of the great successes of this conference that this gap between the two groups is bridged more and more. There is, however, another gap between the scientists on one side and the group of normal designers, who need simple rules, on the other side. The concern about this was this morning already expressed by Prof. Gerstle.
The designers rely fully on the rules, provided by the scientists. However, a common characteristic of scientists is that they are never sure of anything. Nevertheless they should provide simple and sound design rules, and suggestions for detailing, basing themselves on the tools that we have at the moment even for complicated fields of earthquakes, impact and cyclic loading, fire resistance. What happens if the scientists disregard this aspect of their task is illustrated by the following figure, respresenting the applications as a function of scientific effort. As you see, I have copied the stress-strain diagram, quite familiar to us.

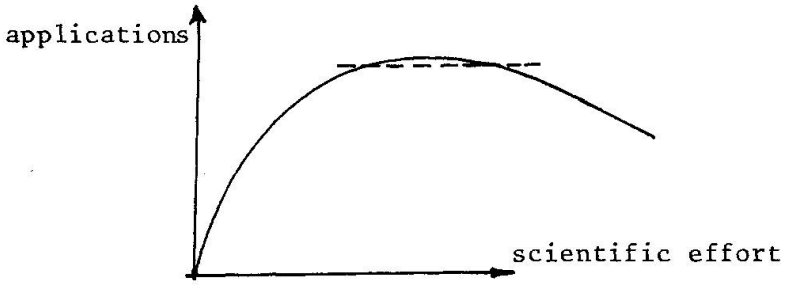

As it is seen we can reach a situation in which an increment of scientific effort may not any more result in more applications and can even have a negative effect on these applications. Although making codes is primarily the task of institutes like CEB or ACI, rather than IABSE, we should not forget that we can all contribute to an amelioration of this situation.

Abstract on a practical application of the subject of Session 3

Non-Linear Behaviour of a Large Highway Superstructure in Berlin

Horst Falkner, Dr.-Ing., Partner
Ulf Hinke, Dipl.-Ing.
Leonhardt und Andrä, Consulting Engineers
Stuttgart, Federal Republic of Germany

1. General

In West-Berlin a 15-storey appartment building with two Autobahn tunnels passing through about 600 m suffered large deformations due to unexpected settlements (Fig. 1).
The structure consists of 77 three-legged stiff wall-frames placed in a distance of 6,4 m, carrying a total load of35.000 kN (Fig. 2).

2. Analysis of the structure

In order to get the most realistic and economical design value for the structure, it was decided to make a precheck by using three different approaches of analysis on the structure:
- Finite-Element approach (Fig. 3);
- Frame analysis by linear theory;
- Model analysis on a plexiglas model (Fig. 4).

The most important result of the different approaches was the governing influence of the different elastic soil behaviour between the inner and outer supports.

Having absolutely stiff supports of the three-legged frame we obtain a support moment -23 MNm. Due to the elastic behaviour of the soil we obtain a moment of +23 MNm corresponding to a differential settlement of 7 mm. Hence only 7 mm produce a variation of the support-moment of 46 MNm, which corresponds to about 200% of the initial value (Fig. 5).

With this analysis, the fundamental question for the structure and its design was solved. Measurements and observations showed that the structure over a length of 85% corresponds to the design values.

However, in a local area of 70 m length sudden differential settlements between the inner and the outer supports have been observed.
The irregular settlements led to final values which exceeded the initial design values by a factor 4 to 6. From this the main question arose: "What will happen to the stiff structure designed for a differential settlement of 7 mm, but being subjected in reality to a value up to 40 mm?"

3. Non-linear behaviour of the wall frame

Because it was not possible to reinforce the structure, there was the responsibility of checking the structure using refined methods of analysis considering the following conditions:
- The amount of restraint actions depends substantially on the time sequence and the absolute values of differential settlements.
- The change of the structure from the uncracked State I into cracked State II depending on the tensile strength of the concrete was observed.
- A substantial contribution to the deformation of wall structures is the contribution due to shear in State I, but even more in State II.
- Material data such as moduli of elasticity, and tensile and compression strength were checked.

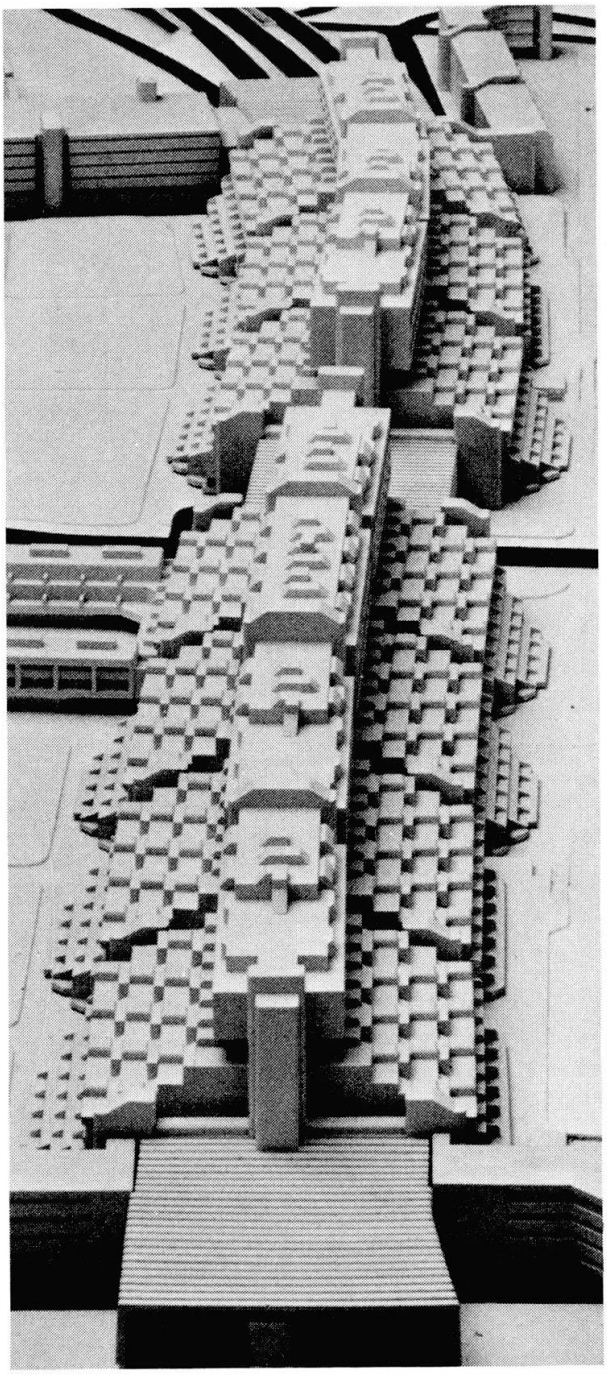

Fig. 1 Model of the SAB-Project

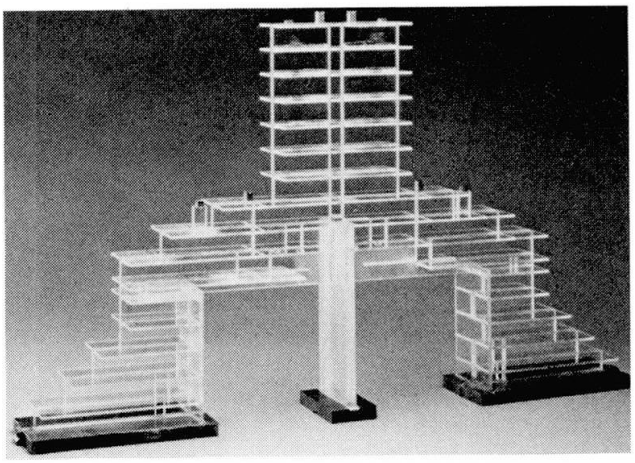

Fig. 4 Plexiglas model

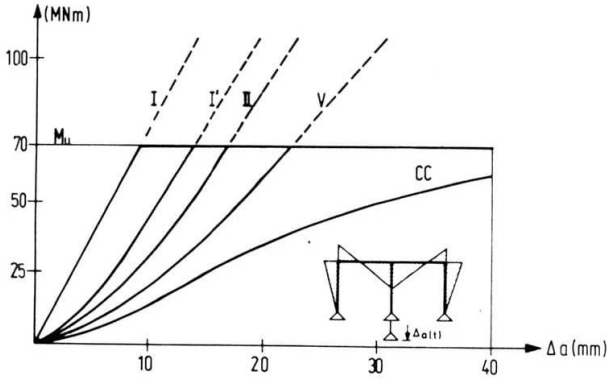

Fig. 6 Structure responses to differential settlements

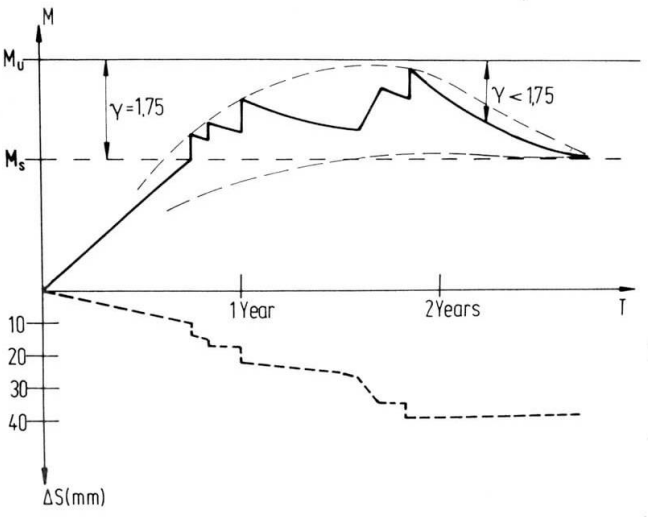

Fig. 7 Time depending restraint actions due to settlements

- In order to define the restraint actions of one year old concrete, it was important to know the creep and the relaxation behaviour. Therefore laboratory investigations were executed.
- Definitely one of the main tasks of the analysis was to define the existing factor of safety against ultimate strength behaviour.

In Fig. 6 the distribution of the actions of a relevant section of the structure is shown as a function of the differential settlements under consideration of the various influences as mentioned above.

With alle these data it was possible to prove that the structure would be able to deform by a factor 4 to 6 times bigger compared to values established by elastic analysis. It could be shown theoretically as well as by practical observations at the structure that these large deformations could be carried by the structure without permanent damages.

The actions in the structure might possibly have led to the development as shown in Fig. 7. This means that in certain stages of settlement the structure was subjected to such high restraint actions, that it came close to its ultimate carrying capacity.

Today, however, after it was possible to stabilize the settlements by cement injections into the ground it can be stated definitely that the stiff wall frame structure could withstand differential settlements of 40 mm. After grouting some large cracks the structure now behaves perfectly under service conditions.

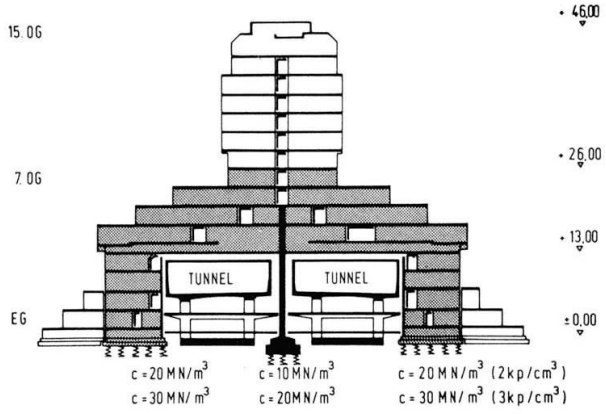

Fig. 2 Cross section of the wall frame structure, foundation moduli

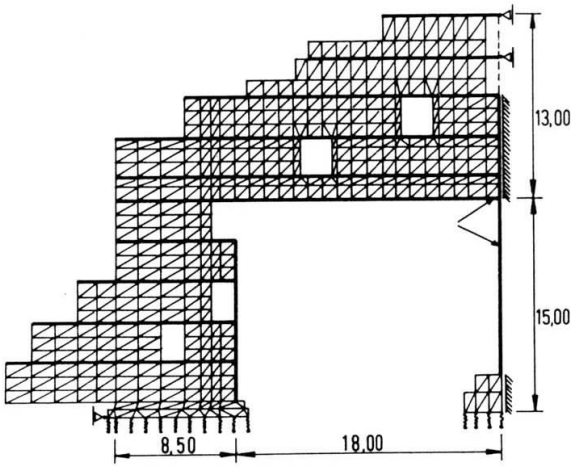

Fig. 3 Layout of the Finite-Elements.

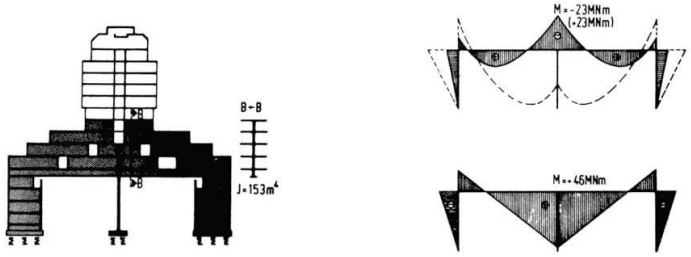

Fig. 5 Variation of the support-moment due to elastic supports.

DISCUSSION

Session 3, part 2: Applications and Experimental Verifications

Paper by Ketchum/Scordelis, U.S.A.

Jávor (Czechoslovakia): In section 4.6 of the presentation it is seen that the results of the calculation are in general agreement with the observed behaviour. If we consider however structures, which are not of a classical shape, as analysed here by Prof. Scordelis, but for instance prefabricated cantilevered box girders, we can meet differences between theory and practice. Whereas a finite element analysis displays equal strains for all corners of the cross-section, in reality measurements show that there are considerable differences, which can be well observed after stabilization of the main creep, so after about two years. These differences in strain are caused by the effect of temperature gradients on creep, shrinkage, prestressing losses etc., which is not taken into account by such a computer analysis.

Scordelis: Deformations of such kind can be predicted by this computer program if you know what the input is as far as load history, temperature history etc., are concerned. If you do not know these effects, you have to adopt a lower bound and an upper bound for these values, put it into the computer program and see how it will vary. Furtheron, it is not possible to predict detailed stresses in concrete structures; however, we can predict overall force distributions, and that is what we are primarily interested in.

Van der Vlugt (The Netherlands): In general it is possible to take such temperature effects on box girder bridges into account, but then you need another type of computer program. The program used here can only analyse structures which can be linearized.

Scordelis: As mentioned in the paper, the computer program can perform a non-linear geometric material and time-dependent analysis of reinforced and prestressed concrete planar frames, subjected to any load or temperature history.

Ingvarson (Sweden): What was meant by the statement that the bridge has a 7-fold overload capacity?

Scordelis: It is meant that, if the bridge is designed in such a way that one truck can be resisted (see Fig.), the real capacity is 7 trucks, placed one upon another, so that it is seen that the design is very conservative.

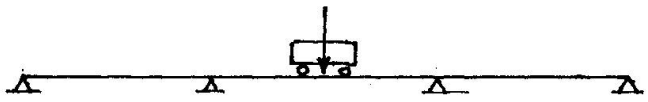

Ingvarson (Sweden): However, from a probabilistic point of view it is possible that a situation occurs in which the bridge is loaded by a combination of trucks, driving one after another along the whole bridge. In that case the safety will not be as high as a factor 7.

Scordelis: The safety of this span will not be violated by what is put on the other spans. So what I meant is really that 7 trucks are placed on top of each other.

Paper by Razaqpur/Ghali, Canada

Walraven (The Netherlands): During his presentation Prof. Ghali raised the question whether it is possible that, at zero crack width, a shear displacement between the crack faces can occur. In this respect I do not agree with the statement of Dr. Gambarova and Prof. Bazant, that the first displacement of the crack faces should also be vertical to the crack. The structure of the utmost part of a crack face, on microlevel, is characterized by particles, which extend for a minor part from the crack faces (Fig. a).

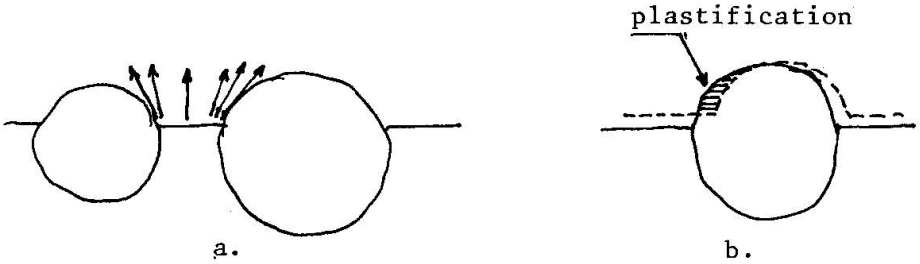

a. b.

So there is a certain range of freedom as far as the crack opening direction is concerned. Only a limited number of particles will be found providing planes of resistance, perfectly perpendicular to the crack plane (Fig. b). In such a case deformation of the relatively soft matrix will occur, so that shear displacement is not prevented. So from a physical point of view we can expect a shear displacement component to occur already at zero-crack width. This was also confirmed by our tests.

Braestrup (Denmark): I would like to support the comment by Walraven. I think also that from a physical point of view there is no reason why the crack displacement could not immediately have a shearing component. If we have a plane strain situation, then, according to the plastic model, the angle ϕ, in the figure, cannot be smaller than the angle of friction; ϕ will be the dilatancy angle. If we consider a plane stress situation, there is no reason why we cannot start immediately with pure shear, but in that case the resistance of the concrete is equal to half the compressive strength, thus pure shearing is very energy consuming. Therefore, the concrete would prefer a deformation which is more perpendicular to the discontinuity.

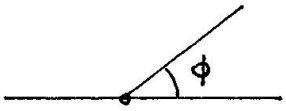

Van der Vlugt (The Netherlands): I think that in the case of smeared-out cracks it will be very difficult to establish this direction, because you have to combine the displacements of an unknown number of cracks and the deformation of the sound concrete between the cracks.

Ghali: Aggregate interlock can be important in some cases, but in many cases it is not. A shear displacement parallel to the crack sould occur in order to get aggregate interlock, but in many, so-called shear loading conditions, it actually ends up by having a crack in the principal direction, and the movement in the crack will be just simply widening without producing any aggregate interlock at all, so that the smeared-crack approach still can do the job perfectly.

Discussion on non-orally presented papers

Paper by Lorrain/Pinglot/Suhud, France

Van der Vlugt (The Netherlands): It is mentioned that the cracking moment of prestressed concrete is influenced by the reduction of the tensile strength of the concrete due to creep. Is this correct or a misprint?

Lorrain: Indeed, it should be the reduction of the concrete compressive strength by creep.

CLOSURE OF THE COLLOQUIUM

Prof.Dr.-Ing. H.W. Reinhardt
Delft University of Technology, Delft, The Netherlands

At the end of the colloquium we should try to balance accounts, i.e. we should look at the aims of the colloquium and compare the expectations with the results. May I cite some statements of the preliminary invitation to this colloquium:

"Structural theories have been based on experimental research without any full understanding of the internal force transfer. There is a need for more generality in the outcome of research. This can be reached by concentrating on elementary basic models which describe the characteristic properties of the materials involved."

Further:

"The modern high speed computer has stimulated new numerical techniques of which the finite element method proves to be the most promising one.... For a complicated load history the method provides the desired detailed information on the internal force transfer. However, this numerical approach relies upon the proper material behaviour being available."

Now the main statement:

"It is the aim of the colloquium to stimulate the synthesis of experimental investigation and numerical analysis of reinforced concrete structures."

Experimental investigation can have different meanings: the investigation of materials with subsequent deduction of material laws - constitutive relations - or the investigation of structures with subsequent verification of numerical models. Both aspects have been treated in the last three days. On the first day we heard about modelling of material behaviour. It was emphasized that micro-aspects should be taken into account in order to describe concrete behaviour properly. Micro-aspects are the process zone around the crack tip, the strain softening, the crack dilatancy. As fracture criteria, it was proposed, methods should be preferred which are based on strain or fracture energy rather than on stress or strength. We learned also that plain concrete does not exhibit the typical feature of a plastic material, namely a yield plateau, and that therefore the application of plasticity theory on concrete should be done with care.

Later on there have been other models presented which use tensile strength as a failure criterion or critical stress intensity factors which may not be exceeded. A whole palet of material models for concrete has been presented, and all of them pretend to be suitable.
An engineer who is no real specialist, must become crazy having the choice of so many possibilities because he must ask, why this variety?
There are various explanations possible: it may not be so important what material model is used or, for special cases a special model has to be established. What Hooke's law has made so powerful was the fact that it could be applied to any material, any structure under arbitrary conditions.

Let us keep in mind that human beings need to have not too many philosophies, and that applies also to engineers. Professor Gerstle said it in a condensed form: "If you don't need the complications, don't use them". I got the impression that we are in a rapidly and immensely growing jungle which should be cultivated, even if in the future much more powerful computers will be available.
The only difficulty is that the cultivators do not yet agree together.

I wonder whether agreement can be achieved as long as basic experimental results are missing which should be inserted into the models: realistic bond slip behaviour, shear resistance, fracture mechanics of concrete in compression and shear, strain rate effects on mechanical properties. On the other hand, there are so many experiments carried out and documented in the literature, that more experiments are perhaps superfluous. But if experiments should be done, they should be done after thorough theoretical examination and the results should be worked out in a way that they can be used by the analyst.
From this, you could prove a kind of predominance of the analyst over the material scientist. We think that the analyst who likes to refine his methods, must take care that he does not loose the contact with building practice. Today, we use high quality concrete, but couldn't we be forced to use waste material or garbage as aggregate for making concrete, and how useful are then our refined material models?
This brings me to another point which has been mentioned during the colloquium, but as I think, in a low voice. That is the scatter of the mechanical properties of material. We are discussing the problem where the first crack will occur in a beam with equal shrinkage stresses.
According to the theory, at a certain instant at any point an equal crack should occur, and that would mean that the tensile zone must crumble into a thousand pieces in one instant. Concrete knows better because all parts of the concrete are a little bit different.
In normal practice it is even worse, as Prof. Eibl pointed out; if you order a certain concrete quality, the mixing plant guarantees a certain minimum value which may well be exceeded.
This value is tested on 28 days age, but what about further hydration.
The same is true for reinforcing steel which may have higher yield stress and fracture strength. These facts imply that we have to think carefully and critically about all sophisticated models. More research should be done in order to cultivate the jungle - which as such is very nice but a little impractical - and to establish appropriate tools for the necessary tasks.

The question arises: "What is appropriate?" I agree with Professor Meyer who stated that the best technology should be used - I understand material and numerical models and high speed computers - if the public has to be protected against severe danger.
For instance, against dynamic effects from earthquakes, tornados, missile impacts, air blasts.
On the other hand, daily work of a structural engineer is to design structures in such a way that they can carry dead loads and normal live loads. I think that also for these engineers advanced mechanics is an appropriate tool, only in a somewhat different way. Modern regulations and standards which he has to use, can be based on finite element sensitivity analyses rather than on limited experimental data. Tables, plots and graphs will

also in the future be normal tools of daily practice and educational aids because engineers are highly sensitive to visual perception.
We are dealing with an applied science, that means applied to concrete problems which arise in the technical world. Or, expressed somewhat differently, this science serves the society and the topics of the science are derivatives of the demands of the people. From that, the best method is that which provides the best results within the least time for the least cost.
Let us come back to the aim of the colloquium; namely: to stimulate the synthesis of experimental investigation and numerical analysis of reinforced concrete structures. Did we reach the goal? I am sure we did, and for several reasons:

- outstanding personalities in the fields of materials and numerical methods have exchanged knowledge and ideas about the way to treat difficult problems;
- many papers have dealt with both aspects: materials and analysis;
- a great number of participants has learned a lot about current developments;
- research needs have been formulated by different disciplines;
- it was shown that there is a lot of material knowledge which should be prepared in such a way that the analyst can use it;
- different parties agreed to have a check of their capabilities. I strongly support the proposal by Professor Collins of a blind test and I am looking forward to know the "Mike Collins Award Winner" for the best prediction.

Ladies and Gentlemen,

On behalf of the organizing committee I would like to thank all of you for your attendance at this colloquium. We had very good speakers who have presented their papers with enthusiasm. Thanks to all of them.
I think the invited reporters have done a very good job, not only during these three days, but also in preparing the introductory report which has served as a guideline for the authors. Thank you very much for your effort which has stimulated so many authors and which has inspired the audience. I am also very grateful to the chairmen of the technical sessions for introducing the speakers, for leading the discussion and watching the time schedule. We have appreciated all contributions to the discussions.

We are proud of this colloquium and we wish that all of you have the idea that you have attended an interesting and useful meeting.

By this, I close the scientific part of the colloquium.

Leere Seite
Blank page
Page vide